Création d'Atlas des Réseaux Cérébraux Sous-tendant les Fonctions Cognitives Latéralisées : Application à l'Étude de la Variabilité Inter-individuelle du Langage

Loïc Labache

THÈSE PRÉSENTÉE

POUR OBTENIR LE GRADE DE

DOCTEUR DE L'UNIVERSITÉ DE BORDEAUX

ÉCOLE DOCTORALE : Mathématiques et Informatique

SPÉCIALITÉ : Mathématiques Appliquées et Calcul Scientifique

Par Loïc LABACHE

CRÉATION D'ATLAS DES RÉSEAUX CÉRÉBRAUX SOUS-TENDANT LES FONCTIONS COGNITIVES LATÉRALISÉES

APPLICATION À L'ÉTUDE DE LA VARIABILITÉ INTER-INDIVIDUELLE DU LANGAGE

Sous la codirection de :
Marc JOLIOT & Jérôme SARACCO
Directrice CEA : Nathalie TZOURIO-MAZOYER

Soutenue le 23 Octobre 2020

Membres du jury :

Mme BACIU, Monica	Pr.	Université de Grenoble	Présidente
M. JACQUES, Julien	Pr.	Université de Lyon	Rapporteur
Mme GENON, Sarah	Dr.	Heinrich Heine University Düsseldorf	Examinatrice
Mme TZOURIO-MAZOYER, Nathalie	Dr.	Université de Bordeaux	Examinatrice
M. JOLIOT, Marc	Dr.	Université de Bordeaux	Codirecteur
M. SARACCO, Jérôme	Pr.	Université de Bordeaux	Codirecteur

CRÉATION D'ATLAS DES RÉSEAUX CÉRÉBRAUX SOUS-TENDANT LES FONCTIONS COGNITIVES LATÉRALISÉES

—

Application à l'Étude de la Variabilité Inter-individuelle du Langage

Loïc Labache

Thèse déposée conformément aux exigences pour l'obtention du diplôme de doctorat.

Université de Bordeaux
Mathématiques et Informatique

Septembre 2017 - Octobre 2020

Groupe d'Imagerie Neurofonctionnelle – CEA, Université de Bordeaux, CNRS – IMN
CQFD Team – INRIA Bordeaux Sud-Ouest – IMB
3300 Bordeaux, France

Jury de soutenance

DIRECTRICE CEA :
Dr. Nathalie Tzourio-Mazoyer – Université de Bordeaux, CEA, IMN, UMR 5293, Bordeaux, France

CO-DIRECTEURS :
Pr. Jérôme Saracco – Bordeaux INP, INRIA, IMB, UMR 5251, Talence, France
Dr. Marc Joliot – Université de Bordeaux, CEA, IMN, UMR 5293, Bordeaux, France

RAPPORTEUR·E·S :
Pr. Monica Baciu – Université Grenoble Alpes, Université Savoie Mont Blanc, CNRS, LPNC, Grenoble, France
Pr. Julien Jacques – Université de Lyon, Lyon 2, ERIC EA 3083, Lyon, France

EXAMINATRICE :
Dr. Sarah Genon – INM, Research Centre Jülich, Jülich & ISN, Heinrich Heine University Düsseldorf, Düsseldorf, Germany

PRÉSIDENTE DU JURY :
Pr. Monica Baciu – Université Grenoble Alpes, Université Savoie Mont Blanc, CNRS, LPNC, Grenoble, France

Cette thèse a été préparée au sein du Groupe d'Imagerie Neurofonctionnelle, à l'Institut des Maladies Neurodégénératives, en collaboration avec l'équipe Contrôle de Qualité et Fiabilité Dynamique, à l'Institut National de Recherche en Informatique et en Automatique Bordeaux Sud-Ouest, de septembre 2017 à octobre 2020. Elle a été financée par une bourse CFR du Commissariat à l'Énergie Atomique et aux Énergies Alternatives.

Titre : Création d'Atlas des Réseaux Cérébraux Sous-tendant les Fonctions Cognitives Latéralisées, Application à l'Étude de la Variabilité Inter-individuelle du Langage

Résumé :

Mon travail de thèse s'inscrit dans une approche d'intégration multimodale et multi-échelle qui a conduit à l'émergence de la neuroimagerie cognitive et de population. Il repose sur deux modalités de cartes fonctionnelles tridimensionnelles cérébrales obtenues en IRMf : les cartes d'activation permettant de visualiser les régions dont l'activité est évoquée par un processus cognitif et les cartes de connectivité intrinsèque mesurant la synchronisation entre des régions spatialement distantes, mais connectées fonctionnellement. J'ai appliqué à ces deux types de cartes de nouvelles méthodologies statistiques permettant de traiter à la fois les dimensions individuelles et spatiales. Dans une première partie, j'ai conçu des atlas de régions cérébrales dédiées à des fonctions cognitives spécifiques, basés sur leur latéralisation hémisphérique et ciblant une population sélectionnée pour sa faible variabilité. Je présente ici les deux premiers atlas du langage. En effet, bien qu'il existe de nombreuses approches pour cartographier les régions du langage chez les patients, il n'existait pas d'atlas des réseaux langagiers chez les individus sains. J'ai tout d'abord identifié les régions activées dans l'hémisphère gauche et asymétriques gauche, à la fois pendant la production, l'écoute et la lecture de phrases, chez 137 individus sains droitiers. L'analyse de la connectivité intrinsèque entre les 32 régions identifiées a permis de mettre en évidence qu'elles faisaient partie de 3 réseaux fonctionnels distincts. Le tout constituant ainsi l'atlas cérébral SENSAAS (SENtence Supramodal Areas AtlaS). Parmi ces réseaux, l'un comprenant 18 régions contient les zones essentielles du langage (SENT_CORE), c'est-à-dire les aires cérébrales dont la lésion entraînerait une déficience dans l'intégration du sens de la parole. Plus particulièrement, SENT_CORE contient 3 régions clés (hubs) de l'intégration et de la diffusion de l'information situées au niveau de l'aire de Broca et de Wernicke. J'ai ensuite appliqué cette méthodologie à l'élaboration d'un atlas des réseaux du traitement du mot. J'ai ainsi identifié 21 régions cérébrales organisées en 2 réseaux distincts, dont un réseau phonologique incluant la boucle audio-motrice. Pour la première fois, une

forte connectivité intrinsèque entre la boucle audio-motrice de l'hémisphère gauche et le traitement prosodique situé au niveau du sillon temporal supérieur de l'hémisphère droit a été mis en évidence. Enfin, j'ai développé une nouvelle méthode d'étude de la variabilité de données tridimensionnelles. Cette nouvelle méthode comporte deux outils mathématiques différents se basant sur un algorithme de classification ascendante hiérarchique. Le premier permet d'identifier les variables conduisant à une instabilité des partitions, le second permet d'extraire des sous-populations stables d'une population de départ. Les applications de l'ensemble de ce travail sont nombreuses : j'ai par exemple utilisé le réseau SENT_CORE pour étudier la variabilité interindividuelle de la latéralisation hémisphérique des aires supramodales de la phrase. J'ai ainsi identifié deux groupes de sujets typiques asymétriques gauche pour le langage, avec une forte connectivité intra-hémisphérique gauche et une faible connectivité inter-hémisphérique, ainsi qu'un groupe de sujets atypiques : asymétriques droit pour le langage, présentant une forte connectivité intrinsèque des réseaux du langage dans les deux hémisphères et une forte connectivité inter-hémisphérique. SENSAAS a également été utilisé afin d'étudier le support génétique de l'atypicalité du langage, ainsi que pour la caractérisation topologique des réseaux mnésiques et linguistiques des individus souffrant d'épilepsie temporale. La nouvelle méthode d'évaluation de la variabilité interindividuelle a, elle, été utilisée afin d'évaluer la stabilité des réseaux intrinsèques d'un nouvel atlas fonctionnel adapté aux individus de plus de 55 ans.

Mots clés : Neurosciences Cognitives, Apprentissage Statistique, Théorie des Réseaux, IRMf, Neuroimagerie, Langage, Connectivité Intrinsèque, Spécialisation Hémisphérique

---

Title: Elaboration Of Brain Network Atlases Underpinning Lateralized Cognitive Functions, Application To The Study Of Inter-individual Variability Of Language

Abstract:

My thesis work is part of a multi-modal and multi-scale integration approach which has led to the emergence of cognitive and population neuroimaging. More specifically, fMRI provides two types of three-dimensional functional brain maps: activation maps allowing for visualizing brain regions directly involved in a cognitive process, and intrinsic connectivity maps measuring the synchronization between spatially distant but functionally connected regions. I have applied new statistical methodologies to these two types of maps, allowing me to deal with both the individual and the spatial dimensions. In the first part, I designed atlases of brain regions dedicated to specific cognitive functions, based on their hemispheric lateralization and targeting a population selected for its low variability. I present here the first two language atlases. Indeed, although there are many approaches to map language areas in patients, there was no atlas of networks supporting language functions in healthy individuals so far. I first identified left activated and left asymmetrical regions, both during sentence production, listening and reading, in 137 healthy right-handed individuals. Analysis of the intrinsic connectivity between the 32 identified regions reveals that they are part of 3 distinct functional networks, which constitute the SENSAAS (SENtence Supramodal Areas AtlaS) brain atlas. Among these networks, one with 18 regions contains the essential language areas (SENT_CORE), *i.e.* the brain areas whose lesion leads to an impairment in the integration of the meaning of speech. Specifically, SENT_CORE contains 3 hubs supporting the information integration and dissemination, localized in the Broca and Wernicke area. I then applied this methodology to the elaboration of an atlas of word processing networks. I identified 21 brain regions organized into 2 distinct networks, one of which is a phonological network including the audio-motor loop. For the first time, a strong intrinsic connectivity between the left audio-motor loop and the prosodic processing, located in the upper temporal sulcus of the right hemisphere, is evidenced. Finally, I developed a new method for studying the variability of three-dimensional data. This

new method includes two different mathematical tools based on hierarchical agglomerative clustering algorithms. The first one makes it possible to identify variables leading to partition instability, the second one allows for extracting stable sub-populations from a starting population. The applications of all of this work are numerous: for example, I used the SENT_CORE network to study the inter-individual variability of hemispheric lateralization of the sentence supramodal areas. I have thus identified two groups of typical asymmetric left language individuals, with high left intra-hemispheric intrinsic connectivity and low inter-hemispheric connectivity, and a group of atypical individuals: rightward asymmetrical for language, with high intrinsic connectivity of language networks in both hemispheres and high inter-hemispheric connectivity. SENSAAS has also been used to study the genetic support of language atypicality, as well as for the topological characterization of the memory and language networks of individuals with mesial temporal lobe epilepsy. The new method for assessing inter-individual variability was used to evaluate the stability of the intrinsic networks of a new functional atlas adapted for late adulthood.

Keywords: Cognitive Neuroscience, Machine Learning, Network Theory, fMRI, Neuroimaging, Language, Intrinsic Connectivity, Hemispheric Specialization

---

Unités de recherche

Groupe d'Imagerie Neurofonctionnelle – CEA & Institut des Maladies Neurodégénératives de Bordeaux, UMR 5293 - Centre Broca Nouvelle-Aquitaine, 146 rue Léo Saignat, 33000 Bordeaux, France

Contrôle de Qualité et Fiabilité Dynamique – INRIA Bordeaux Sud Ouest & Institut de Mathématiques de Bordeaux, UMR 5251 – Bordeaux INP, 109 Avenue Roul, 33400 Talence, France

Remerciements

Je tiens à remercier les rapporteurs de ma thèse, Monica Baciu et Julien Jacques, pour avoir accepté d'évaluer mon travail de thèse, ainsi que Sarah Genon pour sa participation au jury de soutenance.

Je remercie également Erwan Bézard et Nicolas Roussel pour m'avoir respectivement accueilli au sein de l'IMN et de l'INRIA Bordeaux – Sud-Ouest. Je souhaite également remercier le CEA d'avoir financé ma thèse.

Un très grand merci à mes trois directeur·rice·s de thèse : Nathalie Tzourio-Mazoyer, Jérôme Saracco et Marc Joliot, avec qui j'ai pris un réel plaisir à travailler. Merci d'avoir cru en moi, de m'avoir prodigué des conseils avisés et de m'avoir consacré du temps tout au long de ce travail.

Un merci tout particulier à Nathalie pour m'avoir accueilli au sein du GIN, pour m'avoir formée à la recherche depuis mon stage de dernière années d'école, pour sa patience, sa rigueur et surtout pour sa passion de la recherche qu'elle aura su me transmettre.

Je voudrai également remercier Isabelle Hesling pour avoir parcouru ce chemin à mes côtés (en espérant que celui-ci soit encore long) et de m'avoir livré tous les secrets de la psycholinguistique. Un grand merci également à Bernard Mazoyer pour son aide mathématique, son support et ses conseils divers et variés.

Je souhaite également remercier tous les chercheur·e·s, maîtres de conférence et ingénieur·e·s de l'équipe pour leur accueil. Chacun de vous aura contribué, à sa façon, à cette thèse. Merci également à Mathilde et Victor, mes compagnons de route (de stage au départ et de thèse aujourd'hui) pour, entre autre, toutes ces pauses cafés partagées.

J'aimerai enfin remercier mes ami·es : Margot d'être présente depuis si longtemps et d'avoir relu ce manuscrit, Clément de m'avoir soutenu sur tous les plans, Mélody d'avoir été là, Laure et Elodie pour leur soutien à distance et Paul pour m'avoir accueilli lors de mes péripéties parisiennes. Merci Grenoble, d'avoir croisé ton chemin.

Un dernier merci, chaleureux, à mes parents, à Thomas et Marine, à tous les Verniants et à mémère pour leur soutien depuis toutes ces années et nos vies partagées.

Table des Matières

Liste des Figures

Liste des Tableaux

Liste des Acronymes

AAL	**A**utomated **A**natomical **L**abelling
AICHA	**A**tlas of **I**ntrinsic **C**onnectivity of **H**omotopic **A**reas
ALANs	**A**tlas of **L**ateralized **A**ttention **N**etworks
ATP	**A**dénosine **T**ri**P**hosphate
BC	**B**etweenness **C**entrality (sunnexité ou centralité d'intermédiarité)
BIL&GIN	**B**rain **I**maging of **L**ateralization by the **G**roupe d'**I**magerie **F**onctionnelle
BOLD	**B**lood **O**xygen **L**evel **D**ependent
CA	**C**ommissure **A**ntérieure
CAH	**C**lassification **A**scendante **H**iérarchique
CP	**C**ommissure **P**ostérieure
DC	**D**egree **C**entrality (centralité de degré)
DCM	**D**ynamic **C**ausal **M**odelling
DMN	**D**efault **M**ode **N**etwork
FTT	**F**inger-**T**apping **T**est
HAMOTA	**H**and **A**tlas of **MOT**or **A**reas
hROI	**h**omotopic **R**egion **o**f **I**nterest (régions d'intérêts homotopes)
ICA	**I**ndependent **C**omponent **A**nalysis
IRMf	**I**magerie par **R**ésonance **M**agnétique **f**onctionnelle
JBL	**J**ugement de **B**issection de **L**igne
MICCA	**M**ulti-scale **I**ndependent **C**omponent **C**lustering **A**lgorithm
MVPA	**M**ulti**V**oxel **P**attern **A**nalysis
OHBM	**O**rganization for **H**uman **B**rain **M**apping
REST	**R**andom **E**pisodic **S**ilent **T**hinking
RMN	**R**ésonance **M**agnétique **N**ucléaire
RN	**R**esting-state **N**etwork
ROI	**R**egion **O**f **I**nterest (régions d'intérêts)

SENSAAS	**SEN**tence **S**upramodal **A**reas **A**tla**S**
SIMS	**S**imilarity of **I**ndividual **M**atrice**S**
SGV	**S**accades **G**uidées **V**isuellement
SH	**S**pécialisation **H**émisphérique
SPM	**S**tatistical **P**arametric **M**apping
TEP	**T**omographie par **É**mission de **P**ositons
WMCA	**W**ord-list **M**ultimodal **C**ortical **A**tlas

Avant-propos

Le travail de thèse présenté dans ce manuscrit est multidisciplinaire et allie l'étude du fonctionnement cérébral avec la neuroimagerie par Imagerie par Résonance Magnétique (IRM), aux mathématiques appliquées avec l'utilisation de méthodes de classification non supervisée et de théorie des graphes.

A la suite d'un avis favorable de la Commission de Sélection, présidée par le Haut Commissaire à l'Énergie Atomique et aux Énergies Alternatives, j'ai bénéficié d'une bourse de thèse CFR (Contrat de Formation par la Recherche), pour une durée de trois ans, afin d'élaborer un atlas des réseaux cérébraux à large échelle sous-tendant les fonctions cognitives.

Ma thèse s'inscrit dans la dynamique interdisciplinaire engagée par la communauté scientifique de la neuroimagerie depuis plus de 30 ans, et allie l'analyse des bases anatomo-fonctionnelles de la cognition avec le développement de nouvelles méthodologies.

La présentation des mes travaux s'articule en trois parties.

La première, qui suit cet avant-propos, est une synthèse de la littérature scientifique permettant de situer le travail que j'ai effectué. J'y aborde tout d'abord l'histoire de l'IRM fonctionnelle (IRMf) et j'expose sa méthodologie qui permet, chez les mêmes individus, de procéder à la cartographie des régions impliquées dans des tâches cognitives (activité évoquée) et de mettre en évidence des réseaux de régions à l'activité spontanément synchronisée pendant l'état de repos (connectivité fonctionnelle intrinsèque). Ces deux modes d'investigation de la neuroimagerie fonctionnelle du cerveau humain fournissent des cartes d'activité fonctionnelle qui, comme nous le verrons de manière détaillée, apportent des renseignements différents et complémentaires sur l'architecture cérébrale fonctionnelle *in vivo*. Une des problématiques de ma thèse porte sur l'exploration des relations entre les activations mesurées au cours de tâches cognitives et l'activité intrinsèque du support anatomo-fonctionnel de ces mêmes tâches. Je présente ensuite une revue des

principaux atlas de neuroimagerie *in vivo* du cerveau Humain et de leurs caractéristiques, avec un *focus* sur l'atlas AICHA (*Atlas of Intrinsic Connectivity of Homotopic Areas*, [JOL15]) dédié à l'étude des asymétries, et qui a été un des outils important de ce travail. Cette synthèse de la littérature se termine par la présentation des deux principaux outils mathématiques que j'ai utilisés au cours de cette thèse permettant la caractérisation du support anatomo-fonctionnel des fonctions cognitives latéralisées : la classification ascendante hiérarchique et la théorie des réseaux.

Dans la seconde partie de cette thèse je présente les atlas cérébraux à large échelle des réseaux du langage que j'ai mis au point pour deux niveaux d'intégration : la phrase et le mot.

La troisième partie de cette thèse expose le développement d'une nouvelle méthode mathématique de classification ascendante hiérarchique permettant la prise en compte de la variabilité interindividuelle, adaptée à l'analyse de données tridimensionnelles telles que les données d'imageries cérébrales.

Je termine par une synthèse de la contribution à la communauté des travaux réalisés au cours de ces trois années. Travaux marqués par leur intégration dans des publications d'autres domaines, comme l'étude de la génétique des populations. Enfin je présente les perspectives ouvertes par ces travaux, en particulier sur une application du premier atlas à l'étude de la variabilité interindividuelle du réseau du traitement de la phrase chez 287 individus sains, pour moitié gauchers, ainsi que l'élaboration d'un méta-atlas intégrant les différents atlas des fonctions cognitives latéralisées.

Liste des publications et communications

Articles de journaux évalués par les pairs

Labache L., Joliot M., Saracco J., Jobard G., Hesling I., Zago L., Mellet E., Petit L., Crivello F., Mazoyer B., Tzourio-Mazoyer N. (2019). A SENtence Supramodal Areas AtlaS (SENSAAS) based on multiple task-induced activation mapping and graph analysis of intrinsic connectivity in 144 healthy right-handers. *Brain Structure and Function*. *224*: 859-882.

Hesling I., **Labache L.**, Joliot M., Tzourio-Mazoyer N. (2019). Large-Scale plurimodal networks common to listening, production and reading word-lists: an fMRI study combining tasks-induced activation and intrinsic connectivity in 144 right-handers. *Brain Structure and Function*. *224*: 3075-3094.

Labache L., Mazoyer B., Joliot M., Crivello F., Hesling I., Tzourio-Mazoyer N. (2020). Typical and atypical language brain organization according to intrinsic connectivity and multitasks functional asymmetries. *eLife*, sous presse.

Doucet G., **Labache L.**, Joliot M., Frangou S. (2020). Atlas55+: Brain Functional Atlas of Resting-state Networks for Healthy Late Adulthood. *Cerebral Cortex*, sous presse.

Actes de conférences révisés par les pairs avec communication orale

Labache L., Joliot M., Saracco J., Tzourio-Mazoyer N. (2019). Étude de la variabilité interindividuelle de données de connectivité intrinsèque : détection de réseaux instables et de sous-populations dans un tableau tridimensionnel. *51ème Journées de Statistique*, Université de Lorraine.

Articles soumis

Labache L., Joliot M., Doucet G., Saracco J. (2020). Study of inter-individual variability of three-dimensional data table: detection of unstable variables and samples. Submitted to *Computational Statistics*.

Tzourio-Mazoyer N., **Labache L.**, Zago L., Hesling I., Mazoyer B. (2020). Neural support of manual preference based on right and left during right and left finger-tapping induced activations and resting-state connectivity in 287 healthy adults balanced for handedness. Submitted to *Laterality*.

Zago L., **Labache L.**, Tzourio-Mazoyer N., Mazoyer B. (2020). Atlas of Lateralized Attention Networks (ALANs) in right-handers. *BioRxiv*.

Articles en préparation

Hesling H., **Labache L.**, Tzourio-Mazoyer N. (2020). Language atypicality effect on the word list core network.

Labache L., Joliot M., Saracco J. (2020). SIMS: a new package for assessing the instability of intrinsic connectivity data in a three-dimensional table.

Zago L., **Labache L.**, Tzourio-Mazoyer N. (2021). What matters? Handedness or language atypicality on the rightward lateralization of spatial attention networks.

Conférences nationales

Labache, L. (2019). "SENSAAS, un nouvel atlas des aires cérébrales du langage." 10ème Colloque des Jeunes Chercheurs, Ecole Normale Supérieure – Paris.

Labache, L. (2019). "Etude de la variabilité interindividuelle de données de connectivité intrinsèque." 51ème Journée de Statistique, Université de Lorraine – Nancy.

Labache, L. (2019). "Création d'un atlas cérébral évolutif de régions fonctionnelles." 3ème Journée des Doctorants de l'Institut Frédéric Joliot, Neurospin, CEA – Centre de Paris-Saclay.

Présentation nationale et internationale de posters

Hesling, I., **Labache, L.**, Jobard, G., Leroux, G., Tzourio-Mazoyer, N. (2018). "Heteromodal brain areas commonly activated and asymmetrical in production, listening and reading tasks at the word level: an fMRI study of 144 right-handers from the BIL&GIN." North Sea Laterality International Meeting – Dundee.

Tzourio-Mazoyer, N., Joliot, M., **Labache, L.**, Crivello, F., Zago, L., Hesling, I., Mazoyer, B. (2018). "Brain language dominance and hand lateralization relationships: insights from the Brain Imaging Lateralization database (BIL&GIN)." North Sea Laterality International Meeting – Dundee.

Labache, L., Joliot, M., Saracco, J., Mazoyer, B., Tzourio-Mazoyer, N. (2018). "FALCON: a functional atlas of language comprehension networks based on multiple task-induced activation mapping and graph analysis of intrinsic connectivity in 137 healthy right-handers". 2ème Journée des Doctorants de l'Institut Frédéric Joliot, Neurospin, CEA – Centre de Paris-Saclay.

Labache, L., Tzourio-Mazoyer, N., Jobard, G., Crivello, F., Mazoyer, B., Joliot, M. (2017). "Tentative atlas of core language areas from fMRI mapping of 6 language tasks in 144 healthy right-handers". Organization for Human Brain Mapping – Vancouver.

Partie I

Synthèse de la littérature situant le travail de cette thèse

1. Imagerie par Résonance Magnétique fonctionnelle

"A science of the mind must reduce... complexities (of behavior) to their elements. A science of the brain must point out the functions of its elements. A science of the relations of mind and brain must show how the elementary ingredients of the former correspond to the elementary functions of the latter."

[JAM90]

Voici comment, en 1890, William James, l'un des fondateurs de la psychologie, prévoyait l'évolution de son domaine de recherche tout juste naissant. Plus d'un siècle plus tard, au sein des neurosciences, construire de telles correspondances entre l'architecture fonctionnelle cérébrale et l'organisation des fonctions cognitives telles que définies par les modèles théoriques en psychologie, reste l'un des grands défis scientifiques contemporains. En effet, comprendre les mécanismes qui font qu'un kilogramme et demi de tissus mous : *i.e.* le cerveau[1] ou le télencéphale, anatomiquement parlant, permet de réaliser des opérations dépassant de très loin celles des ordinateurs les plus puissants du monde, tout en consommant moins d'énergie qu'une simple ampoule, reste une question ouverte[2].

Mon travail de thèse s'insère dans cette approche d'intégrations multimodales et multi-échelles qu'évoquait William James, et qui a conduit à l'émergence, au cours de la dernière décennie, de la neuroimagerie cognitive. Cette discipline a pour but de comprendre les relations entre le cerveau et la pensée, grâce à l'étude de cartes d'imagerie cérébrales obtenues *in vivo*.

[1] Pour un adulte, le cerveau représente approximativement 2% de sa masse totale corporelle, mais consomme approximativement 20% de son énergie totale [CLA99].

[2] Les ordinateurs sont extrêmement rapides et accomplissent des tâches (lorsque ces dernières peuvent être décomposées en algorithme) bien plus rapidement et précisément qu'un être humain. A l'inverse, les ordinateurs montrent de médiocres performances quand il s'agit de créativité, de capacités langagières, de reconnaissances de formes, etc...

Le cerveau est l'une des structures biologiques les plus complexes connues[3] [SHE88]. Pour chaque région du cerveau, une très grande quantité d'informations de différentes natures est disponible : morphologiques, physiologiques, génétiques, épigénétiques ou encore cytoarchitectoniques. La neuroimagerie qui est une technique non-invasive permet d'acquérir ces données chez des centaines, voire des milliers de personnes volontaires. La UK Biobank par exemple, une base de données lancée en 2014 pour la partie imagerie cérébrale [MIL16], regroupera à l'horizon 2022 plus de 100 000 jeux de données individuels. Pour chaque individu, un très grand nombre de variables a été mesuré : génétiques, socio-démographiques, médicales, capacités cognitives, cartes cérébrales anatomiques incluant des cartes de diffusion et cartes d'imagerie fonctionnelle pour en citer quelques unes. Cette base de données n'est pas la seule au monde regroupant une aussi grande plurimodalité de variables, mais son unicité réside dans le nombre très important d'individus qui la compose et l'homogénéité avec laquelle les données ont été recueillies, permettant ainsi d'étudier finement les contributions respectives des prédispositions génétiques et de l'exposition environnementale au développement des maladies. Citons également, au niveau européen, le *Human Brain Project* [MAR11a], ou bien le consortium ENIGMA (*Enhancing NeuroImaging Genetics through Meta-Analysis*, [THO14]) qui vise à étudier les relations entre génome et caractéristiques anatomo-fonctionnelles de l'organisation cérébrale via la collaboration de 70 centres de recherche de par le monde. Dans ce cadre de coopération internationale, la plupart des outils nécessaires en imagerie au traitement du signal de base et aux analyses qui s'en suivent sont comme en génétique (*The Sequence Alignment/Map tools* [LIH09], *Genome Analysis ToolKit* [MCK10]) en libre accès ; citons par exemple le logiciel SPM : *Statistical Parametric Mapping* [PEN11], la bibliothèque Python *Scikit-learn* [PED11], ou encore la bibliothèque MATLAB *Brain Connectivity Toolbox* [RUB10].

De tels ensembles de données sont aujourd'hui mis à disposition par des équipes de recherche à travers le monde. Parmi les avancées dans le domaine des techniques

[3] Au côté du système nerveux entérique : le système nerveux de l'appareil digestif. Ce dernier est, comme le système nerveux central, composé de millions de neurones sensoriels, d'interneurones et de motoneurones. Il induit des mouvements à l'intestin sans aucune connexions neuronale avec le cerveau ou la moelle épinière [SPE18]. L'activité du système nerveux entérique a récemment été mis en lien avec l'obésité et un large spectre des troubles du système nerveux central [OCH16].

d'analyse de données de ces dernières années, une des plus remarquables concerne les méthodes permettant non plus de travailler sur la moyenne du groupe, ou sur la différence entre les groupes, mais d'étudier la variabilité interindividuelle unique de chaque participant.

Un des aspects de cette variabilité est l'extrême différence de volume et de forme des cerveaux, les femmes, par exemple, ayant un cerveau en moyenne environ 11% moins volumineux que celui des hommes. La solution qui a été trouvée en 1985, a été d'utiliser l'espace stéréotaxique de Talairach. Le concept d'espace stéréotaxique (*cf.* Annexes : 1.) a été inventé au début des années 1940 par le Pr. Jean Talairach (neurochirurgien de l'hôpital Saint-Anne, *cf.* [MAZ08] pour un panégyrique), afin de définir le trajet en 3-dimensions d'une aiguille vers une cible localisée à l'intérieur du cerveau, et ce sans l'aide des techniques d'imagerie du cerveau, inexistantes à l'époque. Pour ce faire, le Pr. Talairach a inventé un système "proportionnel" formé d'un parallélépipède (contenant théoriquement le cerveau) quadrillé dans ses 3 directions, et de points remarquables permettant un positionnement à l'identique des différentes structures de cerveaux humains de tailles variées. En 1947, il applique ce concept à la fabrication d'un cadre chirurgical, permettant ainsi la première électrocoagulation stéréotaxique réussie du noyau postéro-médian ventral chez un patient souffrant de douleur irréductible [TAL49]. Finalement, le Pr. Talairach mets en place un système à double grille[4] en 1949, couplé en 1952 à l'utilisation de la commissure antérieure (CA) et postérieure (CP) comme références pour déterminer le système de coordonnées stéréotaxiques chez chaque individu, et élabore un atlas (ou gabarit) du télencéphale dans l'espace stéréotaxique de Talairach en 1967 [TAL67].

L'application de l'espace stéréotaxique et de son atlas fut un apport majeur à l'imagerie anatomo-fonctionnelle car il a permis l'analyse statistique, la labellisation anatomique des régions activées et la mise en commun de données provenant de modalités différentes. L'espace de Talairach a été le premier espace de référence appliqué à l'analyse des données d'activation. Ces données étaient obtenues par Tomographie par Émission de Positons (TEP) via l'injection d'eau marquée à l'oxygène 15. Le Pr. Peter Fox et ses collègues, en recalant les images TEP de différents

[4] Support attaché au cadre stéréotaxique permettant de guider précisément l'insertion dans le cerveau d'électrodes ou d'aiguilles.

individus dans l'espace stéréotaxique de Talairach, démontrent dans un premier article [FOX85] que cette normalisation permet de calculer une moyenne de leurs activités de débit sanguin cérébral en un même endroit et d'augmenter le faible rapport signal sur bruit inhérent à l'imagerie par TEP. Ces cartes d'activités individuelles peuvent ainsi être moyennées à travers les sujets, après normalisation, ce qui permet de calculer des cartes de différences entre les mesures qui ont été faites pendant différentes tâches : comme par exemple dans le paradigme emboîté de Petersen qui soustrait une tâche de lecture de mots à celle de génération de verbes [PET88]. Ces cartes de différences sont soumises à des traitements statistiques au niveau du voxel dans l'espace stéréotaxique et les zones présentant un débit sanguin cérébral significativement plus important sont rapportées sous forme de pic de coordonnées stéréotaxiques en millimètres. Pour connaître la localisation anatomique de ces pics d'activation, on reporte ces coordonnées dans l'atlas de Talairach [FOX88].

L'espace stéréotaxique commun permet donc une communication précise et efficace au sein du domaine et une alliance entre les disciplines [MAZ01a] nécessaire à l'avancée des connaissances. Cet espace de travail commun permet de ne plus seulement traiter les modalités indépendamment les unes des autres mais bien d'en réaliser l'intégration plurimodale. Un exemple de l'importance de l'intégration multimodale grâce au système stéréotaxique peut être lu dans [ZIL15]. Le Pr. Karl Zilles y démontre que les densités moléculaires (niveau microscopique) dans les aires du langage de 15 neurotransmetteurs différents (mesurées par autoradiographie[5]) sont proches entre elles et diffèrent considérablement d'autres régions cérébrales non impliquées dans les processus langagiers. Les aires du langage sont préalablement définies fonctionnellement par des études réalisées en IRM fonctionnelle (niveau macroscopique). Zilles & al. définissent cette empreinte digitale de récepteurs ("*receptor fingerprint*") comme le support des processus neuronaux sous-jacents aux fonctions langagières.

[5] L'autoradiographie des tissus implique l'administration d'un traceur radioactif d'intérêt. Lorsque le composant atteint l'organe concerné, l'animal utilisé est sacrifié et l'organe est retiré, découpé en tranche et placé sur un film radiographique permettant au chercheur d'évaluer la distribution du traceur radioactif. Après injection, le traceur pénètre dans le cerveau où il est absorbé par les cellules, proportionnellement à leur métabolisme. Une fois dans les cellules, il se retrouve bloqué à l'intérieur (à cause de sa phosphorylation qui a lieu à l'entrée dans la cellule), ce qui rend possible par la suite la détection des cellules impliquées dans le processus ciblé sur le filtre radiographique [RAI09].

De telles perspectives de travail demandent des outils appropriés tant d'un point de vue du recueil des données que de leur analyse statistique. En effet, le choix des techniques d'analyse statistique est essentiel dans la description et l'extraction de connaissances à partir des données multimodales obtenues par neuroimagerie. Le modèle choisi, sa complexité et son interprétabilité sont essentielles. La Pr. Riitta Hari[6] a d'ailleurs rappelé un message important ; "*au cours de cette quête* (d'intégration multimodales), *il ne faut pas oublier que chaque méthode raconte une histoire, et nous ne devons pas laisser ces histoires différentes des nôtres de côté, nous avons au contraire le devoir de les intégrer à notre propre récit afin de l'enrichir et lui permettre de se déployer dans son entièreté*". La neuroimagerie est en effet une méthode qui contient en son sein différentes histoires, dont l'objectif est de comprendre le fonctionnement du cerveau humain.

L'Histoire de l'imagerie fonctionnelle cérébrale remonte à l'invention de la toute première technique de neurophysiologie cognitive en 1880 par le Pr. Angelo Mosso [MOS80]. Il développe une méthode afin de directement mesurer la pulsation sanguine sur le cerveau de Michele Bertino, un de ses patients, à travers un trou dans le crâne de ce dernier causé par la chute d'une tuile. Le Pr. Angelo Mosso découvre alors que lorsque Michele, qui est assis face à un mur blanc pour éviter toute sorte d'autre distraction, entend les cloches de l'église à midi ou bien répond à une question, son pouls cérébral augmente alors que son pouls radial reste stable (Figure 1). Cela conduit de fait le Pr. Angelo Mosso à l'idée que la circulation sanguine cérébrale répond directement à l'activité mentale : le débit cérébral sanguin est pour la première fois associé aux fonctions cérébrales.

[6] *"different methods may well tell different stories, so it's not the issue of how we think the same things but recognizing that in each method that may be a story that will do have to take into account when interpreting our own data"*

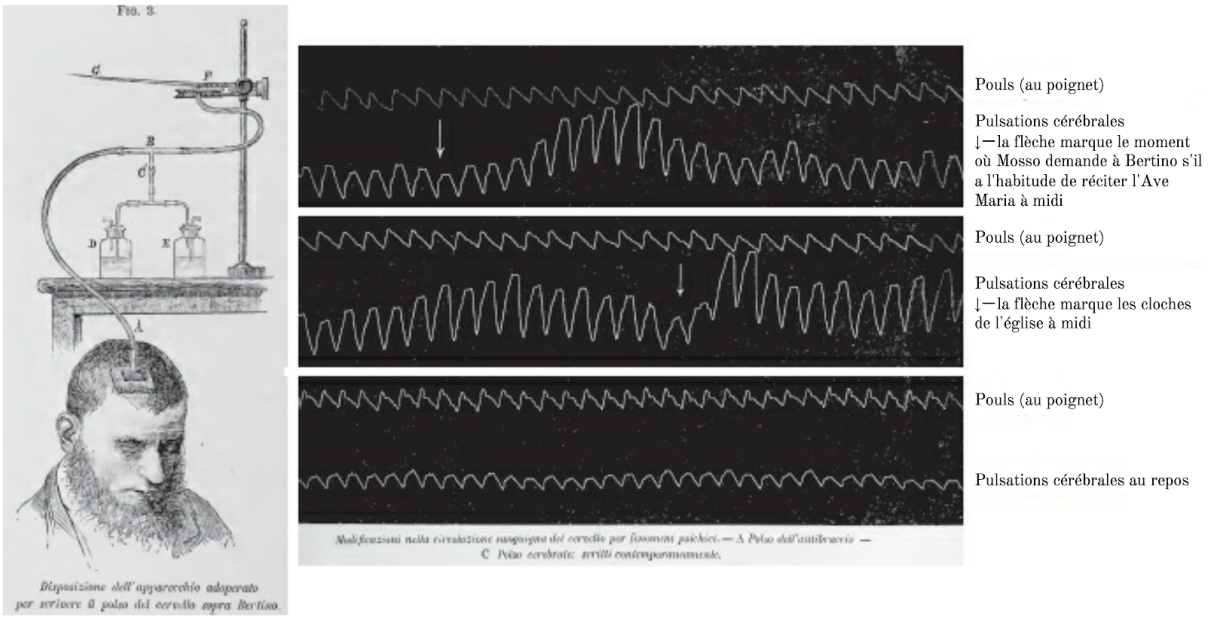

Figure 1 : Mesure du pouls cérébral de Michele Bertino par le Pr. Angelo Mosso. *Figures du livre du Pr. Angelo Mosso [RAI14]. A gauche : schéma d'un pléthysmographe utilisé par le Pr. Angelo Mosso pour mesurer le pouls cérébral de Michele Bertino. A droite : exemples de la façon dont le pouls cérébral de Michele Bertino (la courbe inférieure sur chaque graphique) change en réponse à différents événements, alors que son pouls radial (courbe supérieure) reste constant. La figure est adaptée de [POL18].*

Dix ans plus tard, les Pr. Charles Sherrington[7] et Charles Roy montrent plus rigoureusement l'existence d'un mécanisme automatique par lequel le flux sanguin cérébral est modifié localement en fonction des fluctuations de l'activité chimique sous-tendant l'activité cognitive de cette zone [ROY90]. L'expérience consistait alors à broyer le cerveau d'un chien ayant été saigné, puis à injecter à un autre chien le mélange obtenu afin de comparer les mesures de débit sanguin cérébral et général. Au cours de cette expérience, ils ont constaté que les vaisseaux sanguins cérébraux du chien sain se dilataient après injection du mélange, indiquant une augmentation du flux sanguin cérébral, alors que la pression sanguine générale n'augmentait pas. Ils ont ainsi confirmé leur hypothèse selon laquelle le tissu cérébral en souffrance (du fait d'une hypovolémie) produit des substances chimiques qui sont libérées pour augmenter le volume sanguin.

Dans une perspective plus récente et plus proche de la neuroimagerie moderne que ne le sont les travaux du Pr. Angelo Mosso, la méthodologie développée par l'équipe du Pr. Louis Sokoloff (neuroscientifique au National Health Institute de

[7] Sir Charles Sherrington remporte en 1932, avec le Pr. Edgar Adrian, le prix Nobel de physiologie ou de médecine pour leurs découvertes sur les fonctions des neurones.

Bethesda) conduit, en 1955, aux premières cartes fonctionnelles cérébrales, chez l'animal, à l'aide des techniques d'autoradiographie [LAN55].

Par la suite, les travaux précurseurs en TEP des Pr. Per Roland, Neils Lassen et David Ingvar permettent de réaliser les premières cartes cognitives chez l'Homme ([ING65] et [ROL77]) à l'aide d'injections intra-carotidiennes de Krypton^{85} (et de Xénon^{133}, respectivement) et d'un détecteur de radioactivité disposé comme un casque au-dessus de la tête [LAS63]. Ils démontrent ainsi, pour la première fois chez l'Homme sain, que les fluctuations du débit sanguin, *i.e.* la réponse hémodynamique, changent régionalement en suivant l'activité cérébrale cognitive.

L'étude de l'activité électrique cérébrale se développe également à cette période, puisqu'après 40 ans de travaux solitaires, le Pr. Hens Berger met au point l'électroencéphalographie en 1929 [BER29]. Cette nouvelle méthode consiste en l'enregistrement, sur la surface du cortex cérébral, des potentiels post-synaptiques issus d'un ensemble de neurones.

Il existe plusieurs façons de présenter la suite de l'Histoire de la neuroimagerie, mais j'ai choisi de vous l'exposer en me centrant sur les 25 dernières années et de suivre le développement du consortium OHBM : *Organization for Human Brain Mapping*, qui est le reflet fidèle de l'évolution passée, présente et future, des différentes thématiques du domaine. C'est à l'initiative des Pr. Bernard Mazoyer, Pr. Per Roland et Pr. Rüdiger Seitz qu'est née l'association OHBM quelques années avant sa 1ère assemblée. En 1995, lors de son 1er rassemblement à Paris, 820 scientifiques du monde entier se réunissent pour l'occasion, 25 ans plus tard, en 2019, ce sont plus de 4 000 chercheurs qui se rejoignent à Rome pour évoquer les grandes questions de la neuroimagerie.

404 abstracts sont reçus par les organisateurs en 1995 ; parmi eux 53% traitent du thème de la cognition, 28% abordent le sujet de la méthodologie et 19% des pathologies cérébrales. A cette époque, l'IRM ne représente que 24% des méthodes alors utilisées. En 2019, 3 605 abstracts sont reçus par les organisateurs, soit une augmentation d'un facteur 9 en 25 ans. Mais comme le souligne le Pr. Bernard Mazoyer dans son discours de clôture de cérémonie d'OHBM 2019 : les graines des thèmes de recherche actuels en neuroimagerie sont déjà semées en 1995. En effet, un

article de Peter J. Basser évoque l'IRM de diffusion [BAS95] et un autre de Van Wedeen parle de tractographie et d'exploration des connexions anatomiques entre différentes régions cérébrales à l'aide de l'IRM [WED95]. La neuroimagerie génétique est également présente avec un papier de Berman & al. [BER95]. Finalement, un domaine qui concerne plus particulièrement le sujet de cette thèse : l'étude des bases neurales des fonctions cognitives est également présente, avec la comparaison des activations pendant différentes tâches cognitives [HOR95] et la connectivité fonctionnelle via les corrélations temporelles mesurées à l'état de repos [HYD95]. Enfin, il faut souligner dès 1995 le développement de méthodes permettant de combiner différentes modalités tel que le papier de John George & al. qui vise à combiner les données anatomiques (via l'IRM), d'activation fonctionnelle (IRMf), d'électroencéphalographie (EEG) et de MEG [GEO95]. Par ailleurs, il y a 25 ans, les mots-clés des titres des abstract étaient "*activation*", "*PET*", "*fMRI*", "*mapping*" et "*functional*", en 2019 ce sont les mots "*functional*", "*connectivity*", "*networks*", "*fMRI*" et "*structural*". Ces changements de mot-clés démontrent le passage d'une étude locale de l'activité des régions cérébrales, à l'étude dynamique de l'activité de réseaux de régions cérébrales par les mesures de connectivité fonctionnelle et structurelle.

L'analyse de l'évolution des abstracts soumis à OHBM permet également de constater que la méthodologie reste au coeur de la discipline. En 2019, 50% des abstracts reçus portent sur les questions de méthodologie, alors que la neuroimagerie des fonctions cognitives ne représente plus que 25% des soumissions. La thématique des pathologies quant à elle demeure à 20%, démontrant que les efforts fournis par la communauté en termes de renouveau des technologies, d'analyse de données et de protocoles ont des applications concrètes dans le domaine des maladies neurologiques et psychiatriques.

L'ensemble des avancées historiques présentées en ce début d'introduction n'aurait pu voir le jour sans l'arrivée de l'informatique et des méthodes numériques qui l'accompagnent. En 1973, le CT-scan (*Computer-assisted Tomography* : tomographie axiale calculée par ordinateur) est mis au point par l'ingénieur d'*Electric and Musical*

Industries (EMI, un major de l'industrie musicale) Godfrey Hounsfield[8] [HOU73]. Le CT-scan se base sur la transformée de Radon [RAD17] qui décrit comment reconstruire la géométrie externe ou interne d'un objet à partir d'un ensemble de séries de mesures effectuées depuis son extérieur. Dans notre cas, l'objet en question est le corps humain et les mesures effectuées sont celles de l'absorption des rayons X. Cette technique permet de reconstruire des images 3D des structures anatomiques.

La TEP est développée en 1975 [TER75] : c'est alors la première technique d'imagerie moléculaire, basée sur un traceur radioactif, avec laquelle on calcule, comme nous l'avons vu précédemment, des cartes d'activité cognitive. Grâce aux techniques tomographique utilisées, la TEP permet d'avoir accès à la fois aux fonctions cognitives et aux processus biochimiques des organes les supportant.

Les principes physiques de la Résonance Magnétique Nucléaire (RMN) sont découverts indépendamment en 1946 par les Pr. Felix Bloch et Edward Purcell (*cf.* [KEV97] pour une revue de leurs travaux). Ce n'est qu'en 1980 que la première machine à IRM est utilisée avec succès sur un patient à l'hôpital *Aberdeen Royal Infirmary* en Ecosse. Il aura en effet fallu attendre les travaux du Pr. Paul Lauterbur et sa méthode d'analyse du signal RMN, alors appelé zeugmatographie, afin de reconstruire les premières images 3D d'une orange, à la manière du CT-scan [LAU73]. Tout comme pour le CT-scan, cette technique n'aurait pu voir le jour sans l'analyse numérique et l'avènement de l'informatique dans les années 70 qui l'accompagnent afin de permettre ces reconstructions très complexes.

La co-occurrence du développement des nouvelles méthodes mathématiques et de leur application aux nouvelles techniques d'imagerie, de l'informatique (à travers une puissance de calcul et un stockage de données toujours plus grand) et de la neuroimagerie cognitive a alors été, et est encore, un des moteurs de l'évolution des neurosciences cognitives.

[8] d'après les travaux du Pr. Allan Cormack. G. Hounsfield et A. Cormack reçoivent tous deux le prix Nobel de physiologie ou de médecine en 1979 pour cette découverte.

1.1. Histoire et principe général de l'Imagerie par Résonance Magnétique fonctionnelle

1.1.1. L'IRM comme méthode de référence de neuroimagerie anatomique et fonctionnelle

Jusqu'en 1991, la cartographie des fonctions cognitives est essentiellement réalisée à l'aide de la TEP avec injection d'eau radioactive[9]. Mais en 1991, l'équipe de Bruce Rosen, du *Massachusetts General Hospital* (MGH), publie la première étude fonctionnelle du système visuel en utilisant l'IRM [BEL91] : l'IRM fonctionnelle (IRMf) est née. Pour réaliser cette première, les chercheurs du MGH ont injecté du gadolinium dans la circulation sanguine des participants de l'étude, un traceur paramagnétique dont les variations de concentrations, détectables par IRM, dépendent du flux sanguin cérébral local. En 1992, grâce à deux études pionnières ([KWO92] & [OGA92]), l'IRMf devient réalisable sans qu'il soit nécessaire d'injecter ce produit de contraste, et ce grâce à l'observation par IRM des fluctuations locales de désoxy-hémoglobine (molécule endogène paramagnétique) engendrées par les variations d'activité neuronale : l'IRMf-BOLD[10] (Blood Oxygen Level Dependent) voit ainsi le jour. Cette dernière technique est aujourd'hui considérée comme une méthode de référence [BAN01] pour l'étude des bases neurales des fonctions cognitives.

Contrairement à la TEP qui nécessite l'injection d'un traceur radioactif, et à l'IRMf utilisant le gadolinium, l'IRMf-BOLD est non-invasive et offre donc une capacité d'imagerie en 4 dimensions avec une résolution spatiale entre 1 et 4 millimètres, et un échantillonnage temporel d'environ 1 seconde. La Figure 2 permet d'avoir un aperçu des différentes résolutions spatiales et échantillonnages temporels des techniques d'imagerie cérébrale aujourd'hui disponibles. Les différences d'échantillonnage temporel s'expliquent notamment par la nature même des différents signaux enregistrés : l'EEG ou la MEG s'appuie par exemple sur la réponse électrique

[9] En 1988, la pertinence de l'étude des fonctions cognitives par Tomographie par Émission de Positons (TEP) a été démontrée par le Pr. Michael Posner [POS88].

[10] Par la suite, IRMf fera référence à l'IRMf-BOLD.

des dendrites[11] qui est de l'ordre de 20 millisecondes, alors que l'IRMf repose sur la réponse hémodynamique qui a un temps de réponse physiologique d'environ 1 à 3 secondes après l'activité électrique de l'ensemble neuronal regardé. Les différences de résolutions spatiales s'expliquent quant à elles, par les phénomènes physiques différents utilisés dans chaque méthode.

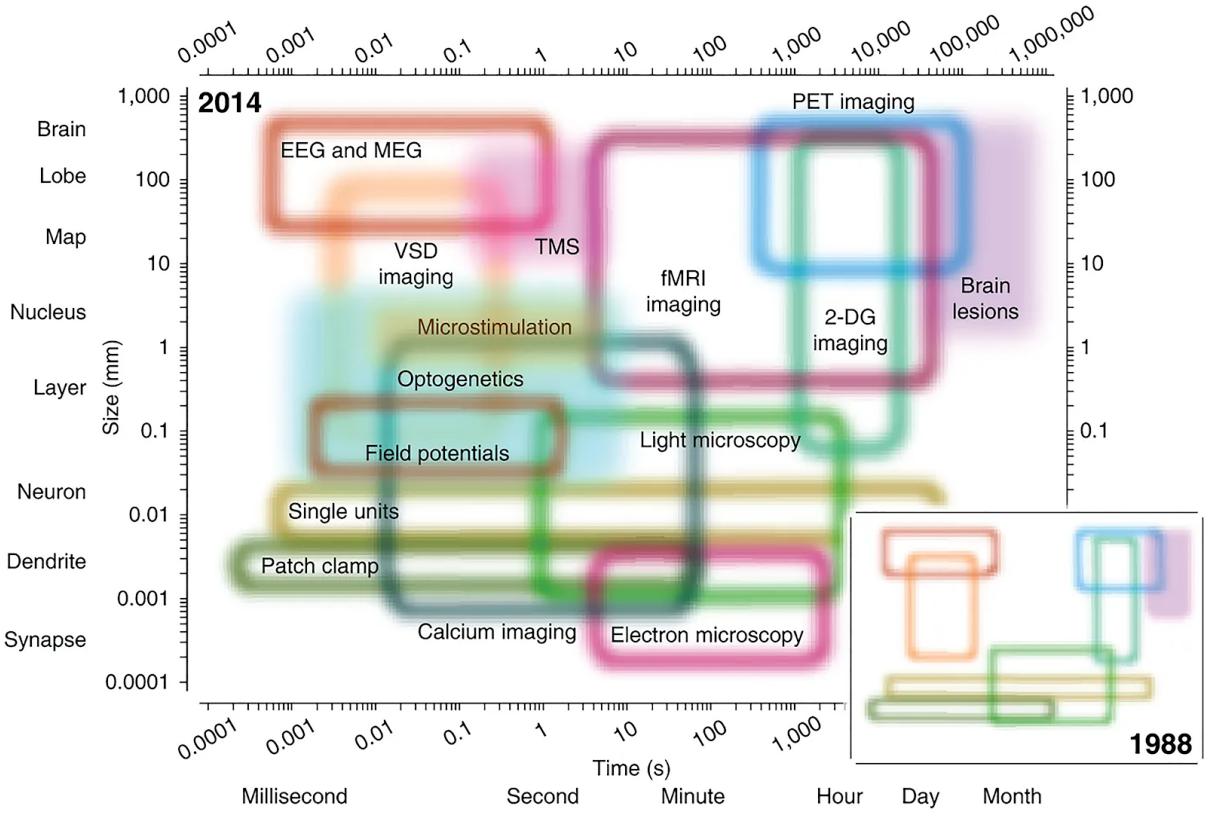

Figure 2 : Résolution spatio-temporelle des principales méthodes utilisées pour mesurer l'activité cérébrale en 2014. *Les rectangles représentent la résolution spatiale et temporelle pour chaque technique. L'encadré en bas à droite permet de comparer les méthodes de 2014 avec les méthodes disponibles en 1988. Il est à noter que le développement de l'IRMf vient combler un manque en termes de résolution méso et macroscopique à l'échelle de la seconde. En général, les techniques à haute résolution spatiale et temporelle sont plus invasives. EEG : électroencéphalographie, IRMf : IRM fonctionnelle, MEG : magnétoencéphalographie, PET : tomographie par émission de positrons, TMS : stimulation magnétique transcrânienne, VSD : colorant sensible au potentiel, 2-DG : 2-désoxyglucose. Figure adaptée de [SEJ14].*

[11] Les dendrites sont des ramifications des corps cellulaires des neurones. Elles propagent les stimulations électrochimiques reçues par les axones d'autres cellules nerveuses, via la synapse, jusqu'au corps cellulaire à partir duquel les dendrites se projettent [KAN13].

Depuis la fin des années 90, l'Imagerie par Résonance Magnétique s'est développée[12] et chaque hôpital possède au moins une machine permettant de faire des acquisitions d'imagerie anatomique et fonctionnelle du cerveau ou d'autres organes. L'IRMf cérébrale en particulier s'est développée et, en 20 ans, les articles d'IRMf sur une année sur PubMed[13] passent de 6 en 1992 à 3 988 en 2011. Avec une augmentation linéaire annuelle d'environ 254 articles supplémentaires (entre 1994 et 2015), la prévision du nombre d'articles pour cette année 2020 est de 6 000 ; conduisant à un total de 64 417 références utilisant l'IRMf comme source de leurs résultats.

1.1.2. Principe de l'IRM fonctionnelle cérébrale pour la cartographie des fonctions cognitives

L'IRM repose sur le principe de Résonance Magnétique Nucléaire (RMN) et utilise les propriétés magnétiques du noyau d'hydrogène constituant la matière organique, et principalement l'eau dont la concentration est très élevée dans le cerveau. En l'absence de champ magnétique, les axes de rotation des noyaux d'hydrogène (*i.e.* leur spin) s'orientent aléatoirement et indépendamment les uns des autres. A contrario, en présence d'un champ magnétique stable, les spins s'orientent parallèlement au champ magnétique : une proportion un peu plus importante de ceux-ci étant orientés dans le sens du champ plutôt qu'en sens inverse, un moment magnétique résultant net est constitué. L'expérience de RMN consiste alors à appliquer un champ magnétique tournant à la fréquence de Larmor des protons, orthogonal au champ stable, pour écarter le moment magnétique initial de l'axe du champ principal et pouvoir ainsi mesurer et observer son retour à l'état initial, phénomène dit de relaxation. Les temps de relaxation sont les mesures centrales en IRM, et permettent notamment de savoir

[12] La Commission Internationale de Protection contre les Radiations Non-Ionisantes (ICNIRP) émet malgré tout certaines recommandations concernant notamment l'effet projectile du champ électromagnétique, l'apparition possible de vertige dû à la susceptibilité magnétique du système vestibulaire et conseille, par principe de précaution, que les femmes enceintes ne s'approchent pas de l'IRM [ICN09]. La loi Jardé (LOI n°2012-300 du 5 mars 2012) est chargée de l'encadrement de ces recommandations dans le cadre de l'instrumentation par IRM et plus généralement encadre les pratiques impliquant la personne humaine. L'IRMf peut être utilisée chez des individus sains, dans le cadre de la précédente loi, qui si besoin, peuvent être scannés à plusieurs reprises si le protocole le justifie et que le comité d'éthique le valide.

[13] Résultats sur Pubmed en avril 2020 de la recherche : ["fMRI" OR "functional MRI" OR "functional magnetic resonance imaging"].

dans quel type de tissu nous sommes (substance blanche, matière grise ou liquide céphalo-rachidien), les temps de relaxation étant différents d'un tissu à l'autre.

Dans le cadre de l'IRMf, une seconde propriété basée sur l'activité hémodynamique cérébrale, résultant d'une cascade d'évènements liés à l'activité électrique et métabolique neuronale, est utilisée afin de mesurer les variations régionales de l'activité cérébrale. L'exécution de processus cognitifs repose en effet sur un ensemble d'activités électriques supporté par les neurones du cerveau : modulation des fréquences ou de la phase des trains de décharge des neurones conduisant à leur synchronisation ou désynchronisation. L'ensemble de ces modulations se traduit par des modifications électrochimiques au niveau des synapses des neurones impliqués dans la tâche. L'énergie nécessaire pour supporter l'activité électrique induite par un processus cognitif est fournie par l'Adénosine TriPhosphate (ATP) qui provient principalement de la dégradation du glucose. Cependant, le cerveau n'a aucune réserve de glucose et sa livraison par les vaisseaux sanguins est donc réalisée en temps réel et à flux-tendu, les dépenses étant constamment compensées par les apports. Le glucose est délivré au cerveau via la circulation sanguine et deux modes de production de l'ATP sont alors possibles. Le premier : la glycolyse, est une voie de production rapide, sans consommation d'oxygène, mais peu efficace en termes d'ATP produit (formation nette de 2 molécules d'ATP[14]) et a essentiellement lieu lors de la réalisation d'une tâche cognitive. Le second mode : la phosphorylation oxydative, est une voie de production deux fois plus lente que la glycolyse [MCG83] et avec consommation d'oxygène, mais très efficace puisque produisant quinze fois plus d'ATP (30 molécules d'ATP produites) que la glycolyse sur laquelle elle s'appuie [GUS01]. Lors d'une activité dirigée, l'activité neurale du réseau de régions cérébrales concernées augmente, induisant un besoin d'ATP plus élevé et plus rapide qui sera produit par glycolyse. Cette activité entraîne une dépense d'énergie assurée par une augmentation de la consommation locale de sucre de l'ordre de 5% (soit 0,1 mg/min, [RAI06a]), sans augmentation de la consommation d'oxygène. En parallèle et dans ces mêmes régions, une augmentation du débit sanguin de l'ordre de 5% a également lieu (soit 1 mL/min) afin de renouveler le sucre dégradé par l'activité cérébrale locale.

[14] Le processus de glycolyse va consommer 2 molécules d'ATP pour en produire 4.

Comment peut-on alors cartographier ces légères fluctuations métaboliques cérébrales déclenchées par des tâches cognitives ?

Lors de l'exécution d'une tâche, l'augmentation local du débit sanguin conduit également à une augmentation locale en oxygène, alors même que la demande métabolique en oxygène reste stable. Ce découplage s'accompagne de fait d'une diminution locale de la concentration en hémoglobine non oxygénée ou désoxyhémoglobine : c'est l'effet BOLD (Blood Oxygen Level Dependent). Cet effet constitue le signal de base enregistré en IRMf. En effet, l'hémoglobine[15] contient un atome de fer, qui lorsque qu'il n'est pas accompagné d'oxygène est paramagnétique : c'est-à-dire qu'il interagit avec le champ magnétique en présence en y créant de petites inhomogénéités locales. Or, la technique d'IRM repose sur l'homogénéité des champs magnétiques afin de mesurer le temps de relaxation des moments magnétiques. L'inadéquation entre l'apport et la consommation d'oxygène [RAI98] conduit de ce fait à une diminution des inhomogénéités des champ magnétiques locaux des régions utilisées pour la tâche en cours de réalisation ; en effet, le sang oxygéné, ou oxyhémoglobine, est par opposition à la désoxyhémoglobine, diamagnétique [PAU36]. La diminution locale des inhomogénéités du champ entraîne alors une augmentation du temps de relaxation transversal (image T2* en IRMf) dans les régions utilisées lors d'une tâche cognitive (Figure 3). Une acquisition en IRMf du signal BOLD permet donc de disposer, en quelques secondes ([LAU73] et [MAN77]), d'une carte du niveau relatif de l'oxygénation sanguine de l'activité cérébrale. Ces cartes mises bout à bout permettent finalement d'obtenir la carte des variations régionales de l'activité cérébrale orientée. Il a par ailleurs été démontré que le signal BOLD est directement corrélé à l'activité électrique régionale des neurones[16] ([LOG01] et [SCH08]), faisant de l'IRMf une méthode fiable et pertinente dans l'étude des mécanismes cognitifs. Il est à noter que l'amplitude du signal BOLD varie au maximum de 5% pour les aires somatosensorielles primaires et de l'ordre de 0.1 à 0.5% pour les régions d'intérêts dans les études cognitives [POL11].

[15] L'hémoglobine est une protéine ayant pour fonction de transporter l'oxygène des poumons vers le reste de l'organisme.

[16] C'est-à-dire les décharges neuronales et les potentiels de champ local.

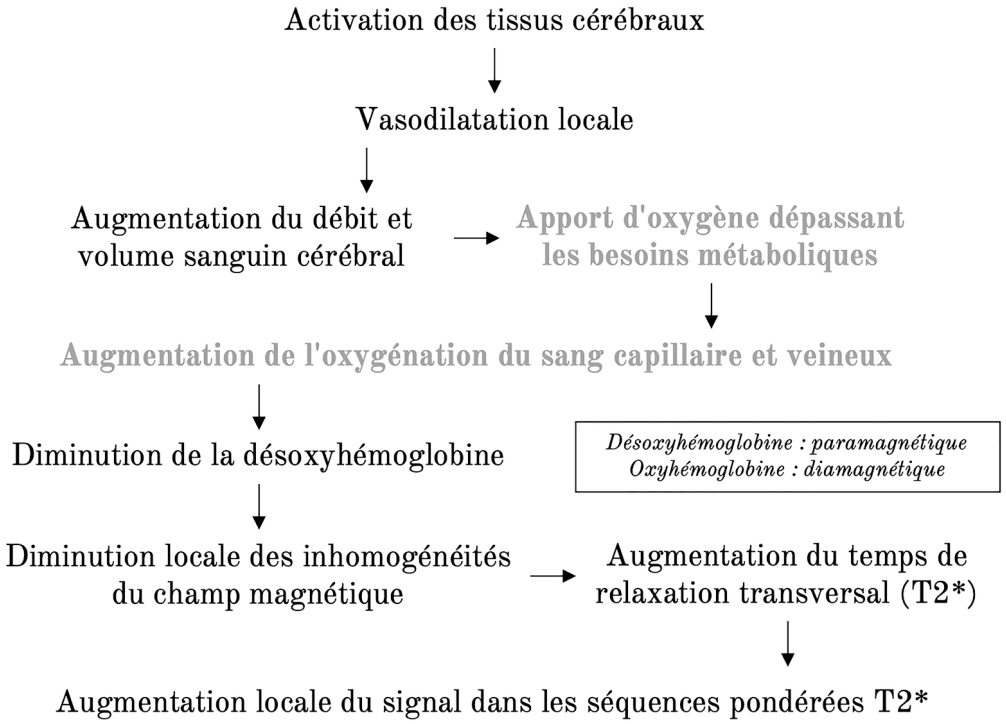

Figure 3 : Organigramme de la relation entre l'activité neuronale et le contraste BOLD. *Les deux éléments clés sont l'apport en oxygénation dépassant les besoins métaboliques (en gris clair) et le changement de susceptibilité de l'hémoglobine en fonction de son oxygénation. Figure adaptée de [BAN20].*

1.1.3. Paradigmes d'IRMf de cartographie d'activité évoquée par des tâches cognitives

Une caractéristique importante du signal BOLD est que la relation qu'il entretient avec la réponse neuronale déclenchée par un événement cognitif est linéaire. Cela signifie que le modèle linéaire est optimal pour l'analyse du signal BOLD [BOY96]. Comme illustré sur la Figure 4, la linéarité de la réponse hémodynamique par rapport à la réponse neuronale conduit à une augmentation d'un facteur a du signal BOLD si la réponse neuronale augmente d'un facteur a. La linéarité implique également le principe d'additivité ; si deux événements se produisent à proximité dans le temps l'un de l'autre, alors le signal BOLD résultant sera la somme des signaux BOLD indépendants de ces deux événements.

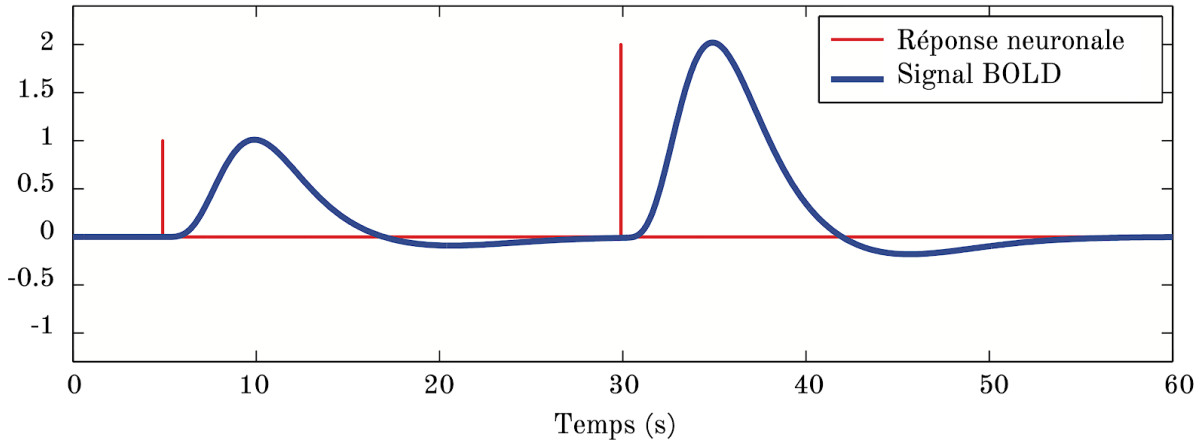

Figure 4 : Exemples de dépendance linéaire entre la réponse neuronale et le signal BOLD. *Illustration de l'augmentation d'un facteur a du signal BOLD (en bleu) lorsque le signal neuronal est augmenté d'un facteur a. Figure adaptée de [POL11].*

A la différence de la technique de différence de cartes moyennes obtenues dans une condition A et B en TEP, l'étude des bases anatomo-fonctionnelles d'un processus cognitif en IRMf est réalisée via la corrélation du décours temporel du signal BOLD avec le paradigme : c'est l'analyse par régresseur. Les paradigmes d'IRMf sont caractérisés par des périodes qui alternent entre la réalisation de la tâche A et de la tâche B par le sujet. Afin d'isoler les régions impliquées dans le ou les processus cognitifs ciblés, une ou des tâches de référence sont incluses dans le protocole afin d'être prises en compte dans l'analyse par régresseur. La ou les tâches de référence ont des composantes cognitives ne faisant pas l'objet de l'étude. Elles sont alors considérées comme des régresseurs dans l'analyse et permettent d'isoler les régions impliquées dans le ou les processus cognitifs ciblés. La carte d'activation, obtenue via l'analyse par régresseurs, peut elle-même faire l'objet d'une analyse par contraste. De la même manière qu'en TEP, et à l'image de l'analyse par régresseur, soustraire les activations d'une tâche de référence à une tâche d'intérêt permet d'isoler les composantes cognitives ciblées par l'analyse. Par exemple, pour étudier les régions de la production de la phrase (Figure 5), nous avons réalisé le contraste suivant au sein de la base de données BIL&GIN [MAZ16] : soustraire l'activité cérébrale lorsqu'un individu réalise une tâche de production d'une liste de mots sur-appris à l'activité cérébrale induite par la production d'une phrase. Ce contraste permet d'éliminer les composantes de la tâche telles que le suivi, la sélection et le maintien en mémoire des instructions, ainsi que le traitement paralinguistique : c'est-à-dire le traitement

contextuel, émotionnel et prosodique. Le contraste à une tâche de référence permet ainsi de discriminer les aires du langage parmi celles impliquées dans la réalisation de la tâche [BIN11]. Il faut noter qu'une tâche de référence consistant à fixer une croix puis cliquer sur un bouton quand celle-ci se transforme en carré, a été utilisée comme régresseur dans l'analyse des tâches de production de phrase et de liste de mots.

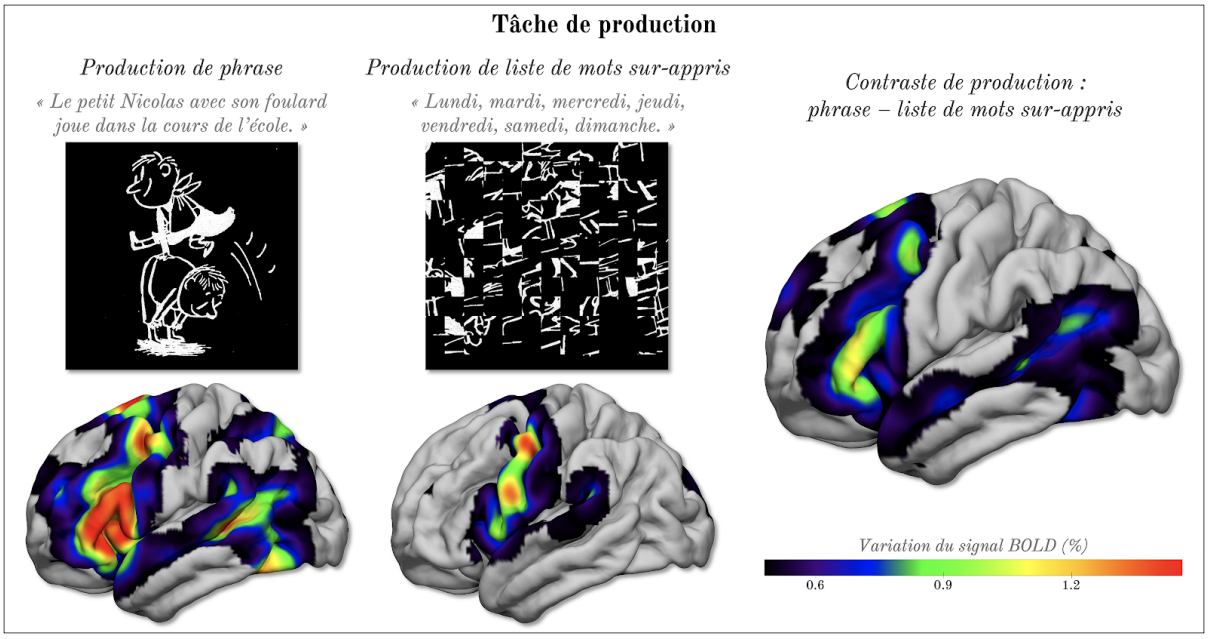

Figure 5 : Exemple, en IRMf, de l'obtention de l'activité cérébrale des bases anatomo-fonctionnelles de la production de phrase chez des individus droitiers (données et protocole de la BIL&GIN [MAZ16]). **A gauche** ; *variation moyenne du signal BOLD (%) lors de la tâche de production de phrase. Le participant voit le stimulus apparaître (image du Petit Nicolas) et doit mentalement produire une phrase commençant par un sujet et un complément, suivi par un verbe décrivant l'action se déroulant et finissant par un complément de lieu.* **Au centre :** *variation moyenne du signal BOLD (%) lors de la tâche de production de liste de mot sur-appris. Lors de l'apparition du stimulus (image brouillée), le participant doit mentalement réciter la liste des jours de la semaine.* **A droite :** *variation moyenne du signal BOLD (%) lors du contraste phrase moins liste. Vue latérale de l'hémisphère gauche ; rendu 3D de la surface de la matière grise du gabarit de la BIL&GIN dans l'espace MNI, réalisé à l'aide du logiciel Surf Ice*[17].

Le Groupe d'Imagerie Neurofonctionnelle[18] (GIN) a mis au point une tâche de référence non spécifique à la modalité de la tâche dans le cadre de l'étude du langage [MAZ93], des saccades visuelles [PET96], de l'attention auditive [TZO97] et de l'imagerie mentale [MEL98]. Cette tâche de référence, appelée "état de repos", consiste à cartographier un volontaire auquel la consigne suivante a été donnée :

[17] Surf Ice : https://www.nitrc.org/projects/surfice/

[18] Le GIN a été fondé en 1989 au CEA au sein du Service hospitalier Frédéric Joliot à Orsay, à l'initiative du Dr. Nathalie Tzourio-Mazoyer, du Pr. Bernard Mazoyer et du Dr. Marc Joliot (https://www.gin.cnrs.fr/fr/le-gin/histoire/).

“gardez les yeux fermés, détendez-vous, évitez de bouger, tout en restant éveillé et laissez aller et venir vos pensées librement, sans entrer dans une activité structurée comme réciter un poème ou réviser vos cours”. Cette tâche a été mise au point car elle permet de servir de référence à des tâches très différentes sur le plan de la modalité et donc de procéder ensuite à des comparaisons ou des méta-analyses.

L’analyse par régresseurs[19] (Figure 6) des cartes BOLD tridimensionnelles obtenues toutes les 1 ou 2 secondes pendant que le volontaire effectue une tâche cognitive permet de mesurer les régions dont le décours BOLD est significativement corrélé à la tâche. Les voxels dont l’activité augmente spécifiquement (ou “activation”) pendant la tâche cible sont ainsi mis en évidence lorsque le régresseur est construit à partir de deux états différents (le résultat est proche d’un contraste de différence tel qu’il était calculé en TEP).

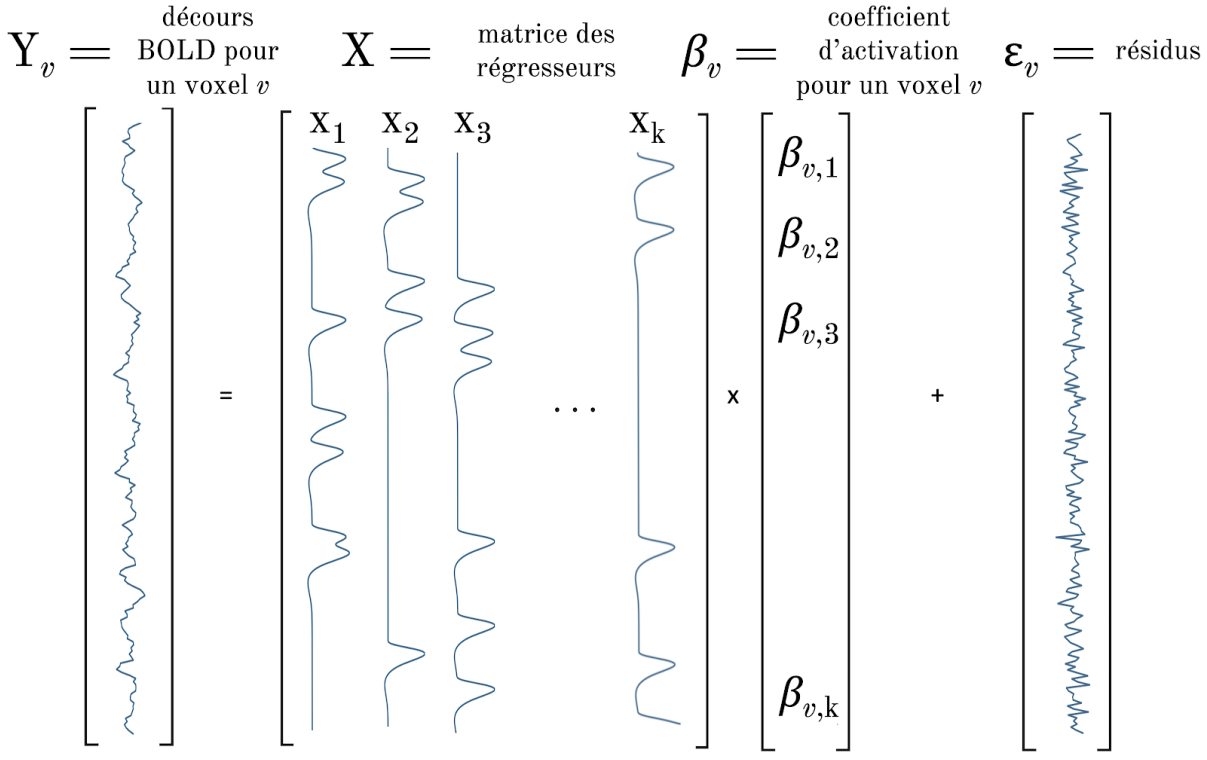

Figure 6 : Illustration de l’analyse par régresseur du signal BOLD. *Le modèle linéaire généralisé exprime le signal BOLD observé (Y) sous la forme d'une combinaison linéaire de régresseurs (x) plus un terme d'erreur (ε). Chaque régresseur de la matrice d’expérience (X) est la convolution de la réponse hémodynamique de référence et de la fonction du stimulus, qui est de 1 lorsque le stimulus est présent et de 0 sinon. L’amplification relative d’une condition donnée, ou activation, est alors l’espérance des coefficients d’activation (β).*

[19] Un régresseur est une fonction qui représente la façon dont le signal BOLD varie au cours du temps suivant les différentes conditions expérimentales. Cette fonction est obtenue par la convolution des périodes de stimulation avec une réponse hémodynamique canonique.

Il est à noter que d'autres approches ont été mises au point afin d'analyser le signal BOLD, notamment des approches stochastiques permettant d'étudier la dynamique causale (*Dynamic Causal Modelling* : DCM, [FRI03]) présente dans les décours temporels du signal. Ce modèle se base sur l'approximation de l'activité neuronale par développement limité, ou plus récemment, par une méthode utilisant les équations différentielles pour modéliser l'ensemble de l'activité neuronale conduisant à la réponse hémodynamique : *i.e.* en prenant en compte les connexions neuronales afférentes et efférentes d'une région cérébrale, tout comme les différents types de signaux (inhibiteurs ou excitateurs) des neurones qui la compose [FRI19]. L'analyse DCM est plus appropriée pour les paradigmes expérimentaux visant à étudier la réponse neuronale résultante d'un stimulus au cours de l'expérience et peu pertinent pour les études exploratoires [STE10]. Une troisième approche existe pour analyser les fluctuations du signal BOLD : l'analyse des patterns pluri-voxels (*MultiVoxel Pattern Analysis* : MVPA), originellement développée par le Pr. James Haxby en 2001 dans un article étudiant la représentation des visages et des objets dans le cortex temporal ventral [HAX01]. Les MVPA diffèrent de l'approche univariée dans le sens où il n'est plus question de regarder si la moyenne du décours temporel d'une région donnée présente une activité plus élevée lors d'un stimulus que lors d'une condition de référence, mais si deux (ou plus) conditions expérimentales peuvent être distinguées l'une de l'autre sur la base de leur pattern d'activité observée (Figure 7, [TON12]). Sur le plan mathématique, la MVPA utilise des méthodes de classification supervisée tel que les séparateurs à vaste marge (SVM : [BOS92]) ou encore l'analyse discriminante linéaire (LDA : [COH83]). Il est important de noter que la MVPA peut permettre de distinguer des patterns d'activité différents pour deux conditions et ce même si le niveau moyen d'activité ne diffère pas entre les conditions [HAX12]. Les techniques de MVPA permettent également de reconstruire le stimulus perçu par le sujet à partir du décodage de son activité cérébrale locale [NAS09].

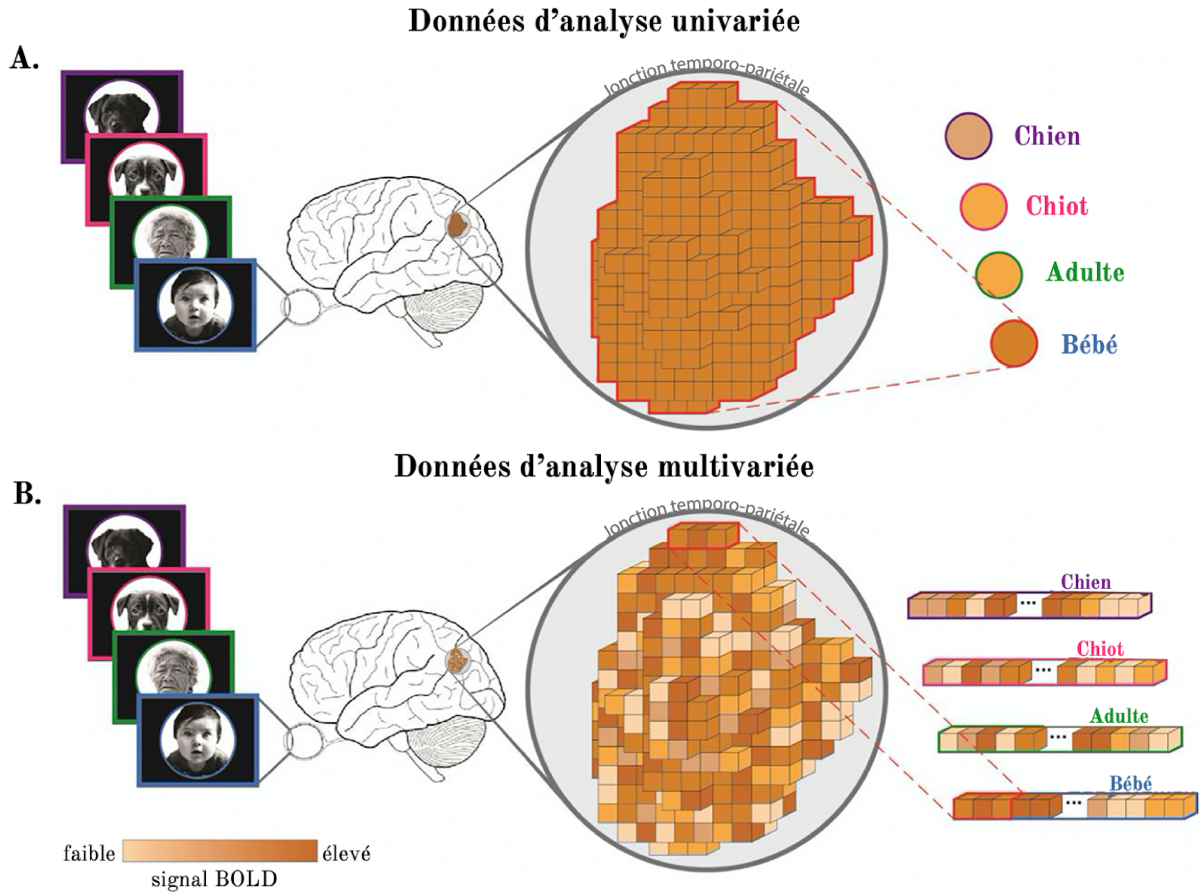

Figure 7 : Comparaison des données lors d'une analyse uni- ou multivariée (*MultiVoxel Pattern Analysis* : MVPA). Cette figure illustre les différences entre la manière dont les données obtenues par quatre stimuli (ici, l'observation de visages humains ou canins, jeunes et vieux) sont utilisées dans l'analyse univariée (A.) et la MVPA (C). **A.** *L'analyse univariée dans la région définie a priori (ici, la jonction temporo-pariétale) utilise une statistique de résumé (par exemple, la valeur moyenne de la région) pour décrire l'amplitude de la réponse BOLD dans toute la région.* **B.** *L'analyse par MVPA dans la région définie a priori utilise le pattern de la réponse neuronale, résumé dans un vecteur contenant l'ensemble des moyennes d'activations des voxels composant la région. Ce vecteur est par la suite utilisé par la méthode de classification supervisée afin d'identifier la signature neuronale de tel ou tel stimulus. Figure adaptée de [WAE20].*

1.2. L'IRMf de repos ou l'étude de l'activité intrinsèque

1.2.1. La découverte des régions du mode par défaut par inversion du paradigme de différence

Plusieurs études à la fin des années 90 mettent en évidence qu'un ensemble de régions présente une activité plus importante pendant une tâche de bas niveau (telle qu'une tâche de fixation) par rapport à la tâche étudiée. Shulman & al. produisent ainsi, en 1997, une première méta-analyse regroupant un ensemble de 9 expérimentations réalisées en PET. Ces expérimentations contrastent des tâches visuelles passives à des

tâches visuelles actives. Ils mettent en évidence un ensemble de régions frontales et pariétales médianes ainsi que des aires pariétales latérales plus activées durant les tâches passives que durant les tâches visuelles actives [SHU97]. La question se pose alors de savoir si ces régions désactivées durant les tâches actives sont dues à l'implication des processus cognitifs réalisés au cours du repos qui ne le seraient pas durant la tâche, ou bien si ces désactivations sont induites lors de l'exécution de la tâche étudiée. Une seconde question fondamentale est de comprendre à quel processus physiologique correspondrait l'activité cérébrale au cours de l'état de repos conscient chez l'Homme.

En 2001 et dans la lignée de l'étude de ces régions désactivées, Mazoyer & al. publient[20] et démontrent à l'aide d'une méta-analyse de 9 tâches cognitives différentes (mémoire de travail, langage, calcul, imagerie mentale, raisonnement logique et tâche motrice) que l'état de repos conscient chez l'humain est soutenu par un large réseau cérébral d'aires corticales distribuées à travers le cortex hétéromodal associatif[21] pariétal et frontal qui sont activées lors de l'inversion du paradigme de différence. Mazoyer & al. font l'hypothèse [MAZ01b] que cet ensemble de régions pourrait refléter les processus de rappel et de maintien de pensée plurimodales libres qui caractérisent l'état mental durant l'état de repos tel que la Pr. Nancy Andreasen l'avait défini en 1995. En effet, elle avait proposé alors, pour la première fois, qu'il existait un réseau de régions support de l'activité de la pensée aléatoire, incluant la mémoire épisodique et prospective (*Random Episodic Silent Thinking* pour REST ; [AND95]) permettant de faire l'expérience de l'identité personnelle[22], de la conscience[23] et de la conscience de soi [24].

Cet ensemble de régions sera nommé, la même année, Réseau du Mode par Défaut par le Pr. Marcus Raichle (*Default Mode Network* ; DMN, [RAI01], Figure 8).

---

[20] Après une présentation de leurs travaux en 1999 lors de la 5ème conférence d'OHBM à Düsseldorf en Allemagne.

[21] *cf.* Partie II - *1.2.2.3.* pour une définition du cortex hétéromodal associatif.

[22] le fait pour un individu d'être distinct des autres et de demeurer unique à travers le temps [OLS19].

[23] relation entre un système cognitif et un objet de réflexion en tant que représentation mentale. Cet objet est sélectionné pour un traitement ultérieur, verbal ou non. L'information consciente est alors disponible pour l'organisme ; nous pouvons la rappeler, en parler et agir dessus. Ces informations constituent le contenu de la conscience [DEH17].

[24] relation autoréférentielle dans laquelle le système cognitif est capable de surveiller son propre fonctionnement et d'obtenir des informations sur lui-même [DEH17].

Le DMN est ainsi supporté par un large ensemble de régions distribuées à travers le cortex associatif hétéromodal ; le cortex préfrontal ventro- et dorso-médian, le cortex cingulaire postérieur, le précuneus, le gyrus temporal moyen et le cortex pariétal latéral, et est caractérisé par une moindre activité lors d'une tâche demandant un engagement de l'attention comparée à une tâche passive.

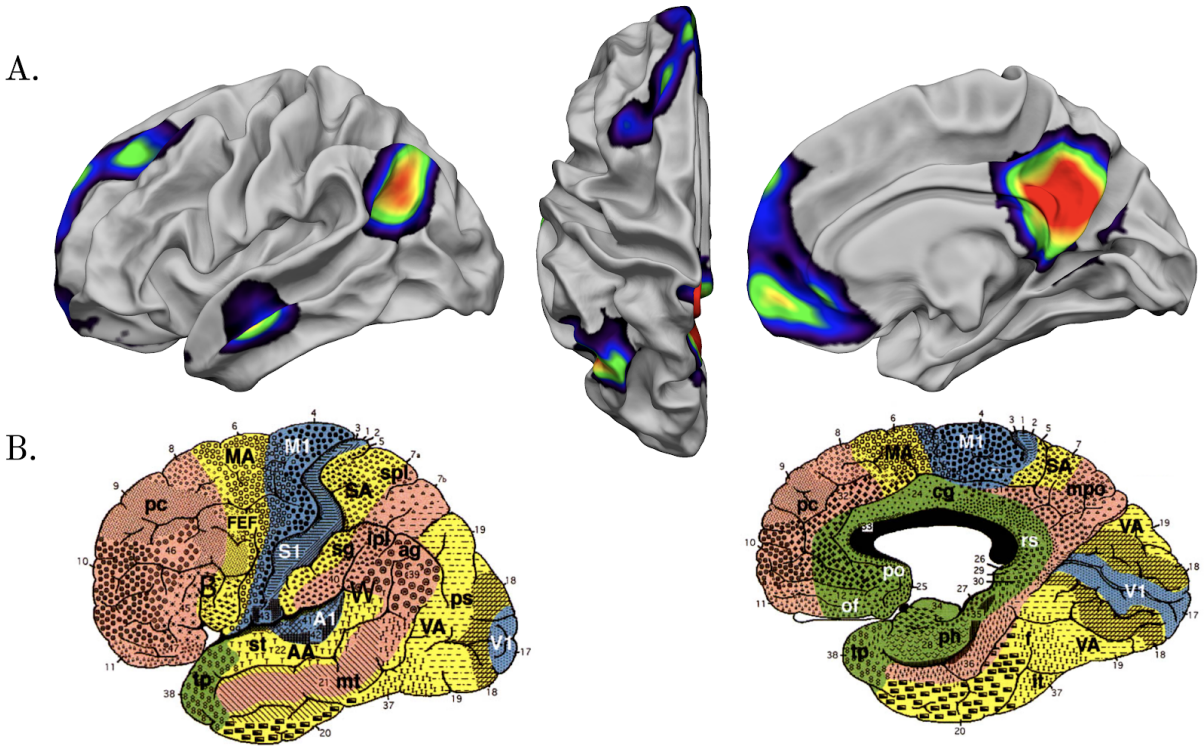

Figure 8 : Illustration du réseau du mode par défaut chez l'humain et de sa correspondance avec les régions cérébrales fonctionnelles. **A.** *Réseaux du repos détecté par analyse en composantes indépendantes à partir de la connectivité intrinsèque de 435 sujets de la BILG&GIN*[25]*. Vue latérale, supérieure et médiale de l'hémisphère gauche ; rendu 3D de la surface de la matière blanche du gabarit de la BIL&GIN dans l'espace MNI, réalisé à l'aide du logiciel Surf Ice.* **B.** *Distribution des aires fonctionnelles en relation aux aires de Brodmann. En vert, les aires paralimbiques ; en saumon, les aires associatives hétéromodales ; en jaune, les aires associatives unimodales ; en bleu, les aires primaires. Figure adaptée de [MES00].*

Grâce à une série d'étude physiologiques *in vivo* en TEP, l'équipe du Pr. Marcus Raichle caractérise les changements métaboliques en termes de consommation de glucose, de débit sanguin, de volume et d'extraction d'oxygène lors de l'exécution d'un processus cognitif lors de l'état de repos [GUS01]. Cette équipe démontre ainsi que 99,9% de l'énergie cérébrale, produite par la phosphorylation oxydative, est dédiée à l'activité de repos ou activité intrinsèque. Pour avoir un ordre d'idée de ce que représente la consommation d'énergie au repos, le débit sanguin cérébral total est de

[25] La BIL&GIN est décrite dans l'article de Mazoyer & al. de 2016 [MAZ16].

750 mL/min (soit 45 L/h), la consommation de glucose de 90 mg/min (soit 5,4 g/h) et la consommation d'oxygène de 50 ml/min (soit 3 L/h). Par opposition les changements observés pendant une tâche cognitive ne représentent, *in fine*, qu'une fluctuation de l'ordre d'un pour cent [RAI06a]. En particulier en 2004, le Pr. Robert Shulman (membre de l'équipe du Pr. Marcus Raichle) publie un article montrant que 80% de l'énergie cérébrale consommée au repos est dédiée à l'activité synaptique [SHU04].

La caractérisation du DMN s'est poursuivie avec la mise en évidence de connexions anatomiques directes entre les régions qui le constituent[26] ([BIN09] & [ALV19]), la description de sa composition myélo- et cyto-architectonique[27] qui n'est pas homogène [BUC08] et la mise évidence de l'implication de circuits thalamo-corticaux dans le contrôle de son activité [PIN04].

Le DMN est présent chez les nouveau-nés [FRA07], et il évolue au cours de l'enfance [FAI08] et de l'apprentissage [POW10]. C'est également un réseau que l'on a mis en évidence chez des espèces très éloignées phylogénétiquement de l'Homme. Il a en effet été montré qu'il existe par exemple chez le macaque [VIN07], le chat [POP09], le rat [LU12], le ver *caenorhabditis elegans*[28] [SCH13], la souris [STA14] ou encore le ouistiti [BUC19a]. L'activité intrinsèque du cerveau est donc une caractéristique fondamentale du fonctionnement cérébral.

1.2.2. Connectivité intrinsèque et réseaux cérébraux

1.2.2.1. La connectivité fonctionnelle intrinsèque comme marqueur des réseaux cérébraux

Avant même la découverte du DMN, le Pr. Bharat Biswal a montré en 1995 que les fluctuations du signal BOLD de basse fréquence (< 0.1 Hz) des régions du cortex sensori-moteur primaire associées aux mouvements de la main étaient fortement corrélées entre elles et entre les hémisphères ([BIS95], Figure 9) alors même que le

[26] connexions par tractographie [ALV19] : le précunéus, le cortex cingulaire postérieur et le cortex préfrontal ventromédian par le cingulum antérieur ; le cortex préfrontal dorsomédian et le cortex pariétal latéral par le faisceau longitudinal supérieur ; le gyrus temporal moyen et le cortex pariétal latéral par le faisceau arqué postérieur.

[27] La cytoarchitectonie désigne la répartition et la distribution spatiale des différents types de cellules dans le cortex cérébral. La myéloarchitectonie concerne l'arrangement des connexions des axones qui connectent les neurones entre eux.

[28] Le *caenorhabditis elegans* est un nématode marin de 1 mm de long, possédant 20 000 gènes, 959 cellules et ayant le plus petit cerveau du monde avec un total de 302 neurones pour 5 000 synapses.

participant de l'étude ne bouge pas les mains. Quelques années auparavant, en 1993, le Pr. Karl Friston avait défini la connectivité fonctionnelle en TEP comme étant la corrélation temporelle d'un indice neurophysiologique mesuré dans différentes régions cérébrales [FRI93]. Or, les fluctuations du flux sanguin et de l'oxygénation utilisée par Friston & al. comme indice neurophysiologique sont analogues aux fluctuations à basse fréquence du signal BOLD au repos obtenu en IRMf comme mis en évidence par le Dr. Bharat Biswal [BIS95]. L'IRMf acquise au repos permet donc de mesurer, grâce à une analyse par corrélation de Pearson du signal BOLD entre les différentes régions cérébrales, la connectivité fonctionnelle entre des ensembles de régions, plus ou moins éloignées les unes des autres, alors que les participants ne sont impliqués dans aucune tâche cognitive structurée. Notons qu'un ensemble de régions partageant des corrélations temporelles positives élevées (respectivement négatives) définit un réseau fonctionnellement connecté (resp. antagoniste) au repos (Figure 9).

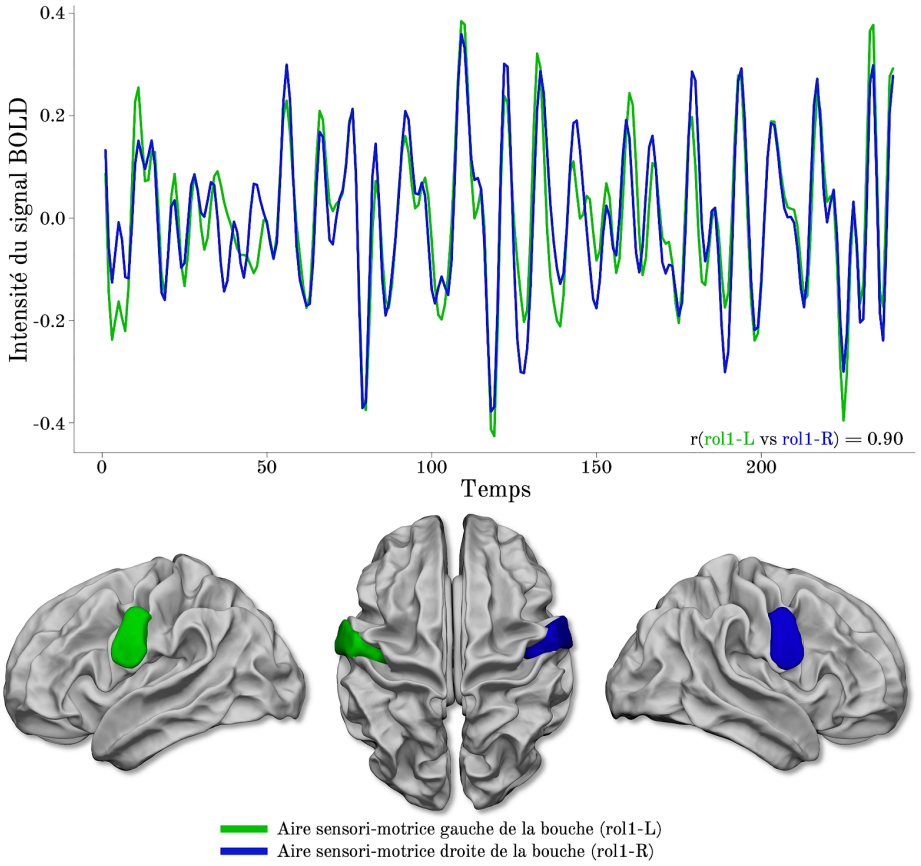

Figure 9 : Illustration de la connectivité intrinsèque entre deux régions. **En haut :** *décours temporels moyen des signaux BOLD de 435 participants de la BIL&GIN des aires homotopes sensori-motrice de la bouche.* **En bas :** *Vue latérale gauche, vue supérieure et vue latérale droite de l'aire sensorimotrice de la bouche. Rendu 3D de la surface de la matière blanche du gabarit de la BIL&GIN dans l'espace MNI, réalisé à l'aide du logiciel Surf Ice.*

En 2003, Greicius & al. étudient les données de connectivité intrinsèque de 14 individus et démontrent que les fluctuations de l'activité spontanée des aires cérébrales composant le DMN sont très fortement corrélées les unes avec les autres [GRE03].

Au total, deux méthodes complémentaires, l'inversion du contraste du paradigme de différence des études d'activation et la connectivité intrinsèque, ont permis l'identification d'un ensemble de régions formant le DMN. De récentes études soulignent malgré tout une différence entre le DMN identifié à l'aide de l'inversion du paradigme de différence et celui identifié à l'aide de la connectivité intrinsèque. Bien que se superposant spatialement en partie, Parker & Razlighi identifient une différence entre les processus neurophysiologiques sous-jacents des deux DMN. Les activations des régions composant le DMN identifié via l'inversion du contraste de paradigme sont significativement associées avec les performances individuelles durant une tâche cognitive, alors qu'aucune relation significative n'est identifiée entre les performances cognitives et les corrélations du signal au repos dans les régions du DMN identifiées à l'aide de la connectivité intrinsèque [PAR19]. Les résultats de Sjøgård & al., à l'aide de la magnétoencéphalographie (MEG), vont également dans ce sens en identifiant deux propriétés neurophysiologique du DMN : l'une extrinsèque, associée aux corrélations de phase du signal MEG, qui montre un découplage entre ces régions lors d'une tâche dirigée, similairement au DMN dont la définition est obtenue par l'inversion du contraste dans le paradigme de différence, et l'autre intrinsèque, associée aux corrélations d'amplitude du signal MEG, qui serait associée à l'organisation générale en réseau du cerveau à l'état de repos [SJØ20]. De plus, Dohmato & al. ont récemment proposé un cadre mathématique théorique concernant le rôle fonctionnel du DMN dans l'organisation cognitive [DOH20] basé sur l'hypothèse que l'activité cérébrale est dédiée au développement et à la maintenance d'un modèle probabiliste de simulation interne permettant de maximiser les résultats d'une action [RAI05]. Dohmato & al. modélisent le rôle du DMN à l'aide d'un processus décisionnel de Markov. Ce modèle théorique voit le DMN comme un agent étant chargé de faire la part des choses entre les connaissances provenant du milieu intérieur et les informations perceptives en provenance du monde extérieur dans le but d'optimiser les choix comportementaux et d'obtenir le meilleur résultat en termes de récompense à court ou long terme en relation à la prise de décision.

1.2.2.2. Mise en évidence de l'organisation cérébrale au repos en réseaux multiples

Les avancées mathématiques, et en particulier les analyses par composantes indépendantes ([HER85] et [COM94]) du signal BOLD à l'état de repos au niveau du voxel[29], ont permis par la suite de découvrir l'existence de nombreux réseaux fonctionnels au cours de l'état de repos, dont chacun présente une activité spontanée spécifique ([BEC05][30], [SMI09], [YEO11], [NAV12] et [GOR16] par exemple). Damoiseaux & al. montrent en 2006, que ces réseaux fonctionnels du repos sont constants quels que soient les sujets [DAM06]. Yeo & al. reproduisent ce résultat en 2013 et ajoutent que les réseaux du repos sont également constants d'une base de données à l'autre, et ce, quelle que soit la méthode d'estimation des réseaux, c'est-à-dire qu'elle provienne d'une analyse en composantes indépendantes ou d'une analyse discriminante linéaire [YEO13]. Kliemann & al. montrent également en 2019 que l'organisation en réseau à l'état de repos est préservée dans l'hémisphère intact de 6 individus ayant subi une hémisphérectomie infantile[31] (2 individus ayant l'hémisphère gauche réséqué, 4 l'hémisphère droit), avec cependant une corrélation entre les réseaux d'une intensité supérieure à celle d'un groupe contrôle [KLI19]. Cependant, il faut noter que l'absence de méthode faisant consensus pour définir les réseaux du repos, conduit à l'identification de réseaux différents en nombre et en arrangement spatial comme on peut le constater dans la littérature ([FRA13] et [DOU19], Figure 10).

[29] Première application de l'analyse par composantes indépendantes à des données d'IRMf dans [MCK98]. McKeown & al. démontrent que cette méthode permet à la fois ; de détecter les décours temporels et les régions activées par la tâche, et les autres composantes du signal liées aux mouvements et aux autres artefacts.

[30] Première étude sur des données d'IRMf de repos.

[31] Procédure chirurgicale visant à enlever tout ou partie d'un des deux hémisphères cérébraux.

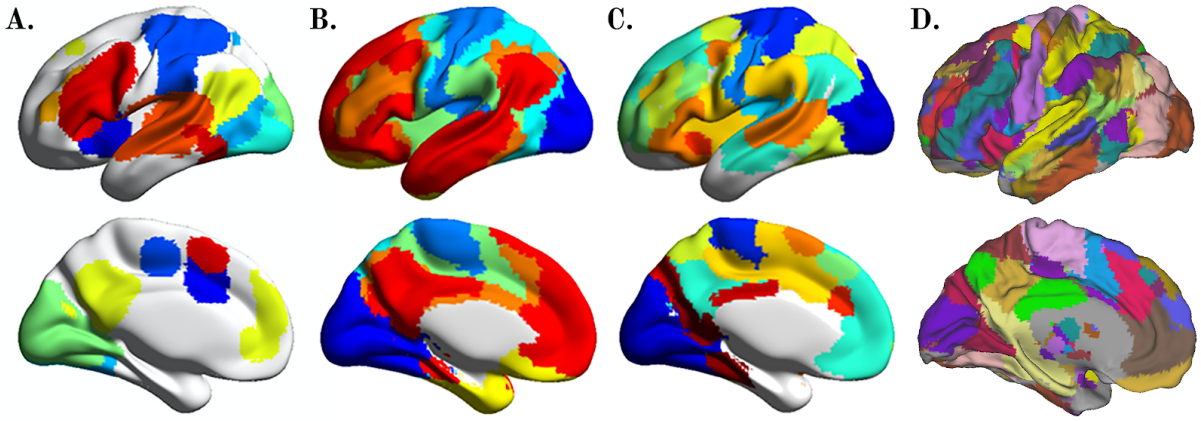

Figure 10 : Exemple de 4 ensembles de réseaux intrinsèques fonctionnels. Chaque couleur représente un réseau. **A.** Dix *réseaux fonctionnels de l'état de repos de [SMI09]. Réseaux définis à partir de 36 individus (de 20 à 35 ans) par analyse en composantes indépendantes.* **B.** Sept *réseaux fonctionnels de l'état de repos de [YEO11]. Réseaux définis à partir de 1000 individus (de 18 à 35 ans) par classification des profils de connectivité intrinsèque des voxels [LAS10].* **C.** Douze *réseaux fonctionnels de l'état de repos de [GOR16]. Réseaux définis à partir de 108 individus (de 18 à 33 ans) par détections des frontières dans le gradient de connectivité intrinsèque [COH08].* **D.** *Vingt-huit réseaux fonctionnels [NAV12]. Réseaux définis à partir de 282 individus (de 18 à 57 ans) par analyse en composantes indépendantes individuelle. Figures A., B. et C. adaptées de [DOU19].*

En 2005, Fox & al. démontrent que le réseau extrinsèque, dédié à l'attention et aux stimuli externes, et le réseau intrinsèque, dédié aux stimuli internes c'est-à-dire aux pensées et à la manipulation de l'information, sont ségrégés l'un par rapport à l'autre [FOX05]. Cette ségrégation se traduit au repos par une corrélation négative entre les deux réseaux, reflétant l'organisation dynamique, continue et fonctionnelle du cerveau. Ces résultats suggèrent une interaction dynamique au sein et entre des systèmes cérébraux à large échelle représentant différentes composantes de notre vie mentale. Ils ouvrent également la voie à une étude du fonctionnement cérébral comme étant un système possédant une organisation intrinsèque modulée par les informations sensorielles de l'environnement externe[32].

A partir d'une nouvelle méthode d'analyse en composantes indépendantes prenant en compte la variabilité interindividuelle de 180 individus et résultant en

[32] Ce principe de modulation a précédemment été suggéré par [ARI96], [KEN03] et [FIS04a] qui démontrent que l'activité neuronale spontanée du cortex visuel prédit et conditionne l'activité évoquée lors d'une tâche visuelle chez le chat (pour les 2 premières études) et le furet (pour la dernière). Dans ces études, l'enregistrement de l'activité électrique au niveau du neurone a été réalisé par électrode et imagerie optique.

l'identification de 28 réseaux du repos[33] (Figure 10 - D, [NAV12]), Doucet & al. proposent un modèle d'organisation hiérarchique des réseaux du repos ainsi identifiés [DOU11]. Leur modèle repose sur l'identification, à l'aide d'un algorithme de classification ascendante hiérarchique, de 2 systèmes cérébraux. S'appuyant sur la littérature en neuroimagerie cognitive, ils identifient le premier système comme étant le réseau cérébral supportant l'activité intrinsèque. Ce premier système est composé de trois modules : le DMN, un module de manipulation et de maintenance de l'information, et un dernier module de contrôle entre le milieu externe et interne. Le second système correspond au réseau cérébral de l'activité extrinsèque. Ce dernier est composé de deux modules : l'un correspond au réseau attentionnel, sensori-moteur et auditif, l'autre au réseau visuel. Doucet & al. montrent une forte intégration de l'information au sein de chacun des deux systèmes, se traduisant par des corrélations positives entre les modules qui les composent respectivement. Malgré la très forte ségrégation entre les deux systèmes, tel que [FOX05] l'a montré, Doucet & al. mettent en évidence l'existence d'un cinquième module de contrôle positivement corrélé entre les systèmes intrinsèque et extrinsèque, et qui jouerait le rôle de médiateur du transfert de l'information entre les intentions externes et internes du sujet.

1.2.2.3. Etat de repos et organisation cérébrale

La description de l'organisation cérébrale suivant le flux de l'intégration sensorielle, tel que proposée par le Pr. Marsel Mesulam, est un modèle d'organisation topographique du cortex cérébral à l'échelle macroscopique [MES98]. Ce modèle est une référence en neuroimagerie cognitive.

Dans ce modèle "de la perception vers l'action", l'information est tout d'abord perçue à partir de l'environnement extérieur par les récepteurs périphériques (vue, toucher, audition...), puis les nerfs sensoriels conduisent l'information vers les aires sensorielles du cortex primaire (Figure 11 - A.). Les régions du cortex associatif unimodal et hétéromodal (Figure 11 - A.) servent alors de médiatrices entre le milieu externe et interne, afin que les réponses de ce dernier soient en accord avec les contraintes et possibilités du monde extérieur. Le cortex associatif unimodal est

[33] L'algorithme proposé dans [NAV12], nommé MICCA (*Multi-scale Independent Component Clustering Algorithm*), réalise, pour chaque sujet, une ICA sur les données d'IRMf à l'état de repos, puis regroupe, à travers les sujets, les composantes spatialement similaires.

subdivisé en une voie ascendante et une voie descendante. Les aires de la voie ascendante sont séparées de leur aire primaire correspondante par seulement une synapse. Celles de la voie descendante sont séparées par deux synapses ou plus de leur aire primaire apparentée. Le cortex associatif unimodal est caractérisé par des neurones répondant préférentiellement (et presque uniquement) à des stimuli d'une seule modalité sensorielle, et des informations sensorielles provenant principalement des aires sensorielles du cortex sensoriel primaire et des autres régions associatives unimodales de la même modalité [MES00]. Les lésions des aires unimodales conduisent principalement à des déficits dans l'exécution de tâche impliquant la modalité de l'aire lésée. Le cortex associatif hétéromodal est caractérisé par une réponse neuronale répondant à tout type de modalité sensorielle. Les informations qu'il reçoit proviennent essentiellement des aires associatives unimodales et des aires hétéromodales, et sa lésion résulte en des pathologies multimodales ne se limitant pas à des tâches sous la supervision d'une seule modalité [MES00]. Le cortex associatif est le dernier à se développer chez l'être humain [HIL10] et le dernier à être apparu en termes d'évolution [BUC13a].

La diffusion de l'information à travers les régions du cortex associatif unimodal, hétéromodal puis paralimbique permet l'association, aux informations sensorielles, des stratégies de réponses motrices adéquates à partir de l'intégration de l'expérience aux émotions et à la motivation fournies par le cortex paralimbique. Une fois la réponse comportementale appropriée sélectionnée par le milieu interne, l'information est renvoyée aux aires motrices du cortex primaire afin d'agir et de se mouvoir dans l'environnement.

Le modèle global hiérarchique d'intégration de l'information sensorielle s'applique également au réseau du langage. Le Pr. Marsel Mesulam suggère en effet dans [MES98] que l'ensemble des processus cognitifs résultent de l'intégration de l'information sensorielle ; les propriétées anatomiques et physiologiques des aires hétéromodales traversées par l'information déterminant la fonction cognitive opérée. Il définit ainsi ces régions comme des épicentres pour un réseau cognitif à large échelle donné [MES90]. Les épicentres montrent une spécialisation relative pour une composante comportementale spécifique à la principale fonction cognitive qu'il supporte. Les aires de Broca et Wernicke sont ainsi définies par M. Mesulam comme

des épicentres pour le réseau du langage. Broca et Wernicke sont en effet les aires hétéromodales liées à la coordination de l'intégration entre la forme sensorielle du mot et ses significations sémantique et émotionnelle arbitraires [MES90].

Ce modèle d'organisation cérébrale à large échelle – qui correspond à une échelle spatiale macroscopique (≃ 6 mm^3) compatible avec l'échelle de la neuroimagerie a été repris par le Dr. Daniel Margulies pour proposer une nouvelle modélisation mathématique de l'organisation cérébrale à l'état de repos (Figure 11 - B).

Les travaux du Dr. Daniel Margulies sont un autre exemple de la fructueuse interaction entre mathématiques appliquées et neurosciences cognitives. Il démontre en effet qu'en utilisant une technique de réduction de dimension non linéaire [COI05] basée sur la matrice de similarité cosinus de la matrice de connectivité intrinsèque, il retrouve le modèle d'intégration sensorielle proposé par le Pr. Marsel Mesulam [MES98]. Cette technique permet d'extraire deux composantes principales (qu'il appelle gradients) qui conservent l'organisation topographique du cortex. En effet, le Dr. Daniel Margulies montre qu'une grande partie de la variance des fluctuations du signal BOLD à l'état de repos est capturée par ces gradients, qui s'étendent du cortex primaire sensori-moteur au cortex associatif hétéromodal ([MAR16], Figure 11 - B.), tel que proposé par le modèle de Mesulam. Au vu de cette modalisation en gradients, l'intégration hiérarchique de l'information est conservée dans le fonctionnement du cerveau à l'état de repos [HUN18].

Un autre point à souligner de l'organisation cérébrale à l'état de repos est l'existence de différences de connectivité intrinsèque, en termes de force des corrélations, entre les différentes régions cérébrales. Les corrélations entre les régions homotopes[34] sont plus élevées comparées aux autres relations inter- ou intra-hémisphériques [STA08]. Plus précisément, parmi les corrélations homotopes, celles des régions du cortex primaire sont les plus élevées (Figure 11 - C.). Ces

[34] Une paire de région homotope correspond à deux régions symétriques l'une de l'autre par la scissure inter-hémisphérique ; *i.e.* une région dans chaque hémisphère cérébral.

corrélations inter-hémisphériques sont le support de la symétrie[35] spatiale inter-hémisphérique des réseaux fonctionnels de l'état de repos ([BEC05] et [HEU10a]).

Un point important concerne les relations entre la connectivité intrinsèque et la connectivité anatomique. Récemment, Mollink & al. ont démontré qu'une partie de la variabilité interindividuelle de la connectivité intrinsèque de régions homotopiques peut être expliquée par les propriétés micro-structurelles du tractus callosal les reliant et que cette relation anatomo-fonctionnelle semble être supportée génétiquement [MOL19]. Le support neurophysiologique des corrélations inter-hémisphériques au repos a été validé par l'étude à l'état de repos du cerveau d'un jeune enfant de 6 ans souffrant d'épilepsie réfractaire[36]. Un des traitements de cette pathologie est une section complète du corps calleux[37] afin d'éviter la généralisation des crises et leur transfert inter-hémisphérique. Le corps calleux est un ensemble de faisceaux de fibres nerveuses reliant les deux hémisphères et permettant leur interaction. Pour comprendre les bases anatomiques de la connectivité intrinsèque, l'étude a donc combiné des acquisitions cérébrales à l'état de repos avant et après la chirurgie chez ce jeune patient. La comparaison de la connectivité intrinsèque pré-opératoire avec la connectivité intrinsèque post-opératoire a montré une perte considérable des corrélations inter-hémisphériques intrinsèques, alors que les corrélations intra-hémisphériques étaient conservées [JOH08].

La connectivité intrinsèque a donc bien une réalité physiologique et s'appuie, pour ce qui est de la connectivité inter-hémisphérique, sur les fibres blanches composant le corps calleux. Plus généralement, l'hypothèse selon laquelle la connectivité structurelle établie à l'aide de la substance blanche, contraint et supporte, tout du moins en partie, la dynamique de la connectivité intrinsèque a récemment été vérifiée dans une étude de Cornblath & al. qui montrent que la dynamique de l'activité neuronale à l'état de repos (*i.e.* la connectivité intrinsèque) est fortement restreinte par

[35] malgré une asymétrie bien connu de l'anatomie cérébrale [AMU10] : notons par exemple la déviation Yakovlevienne [TOG03], et des fonctions cognitives [TZO16a] sur laquelle nous reviendrons plus tard dans ce manuscrit.

[36] L'épilepsie réfractaire est une forme d'épilepsie résistante aux médicaments.

[37] Le corps calleux est la plus large commissure inter-hémisphérique (10 cm de long environ), composé de plus de 200 millions de fibres blanches (axones), reliant les deux hémisphères cérébraux [LUD10].

la propagation du signal neuronal le long des fibres de la substance blanche (*i.e.* la connectivité structurelle) [COR20].

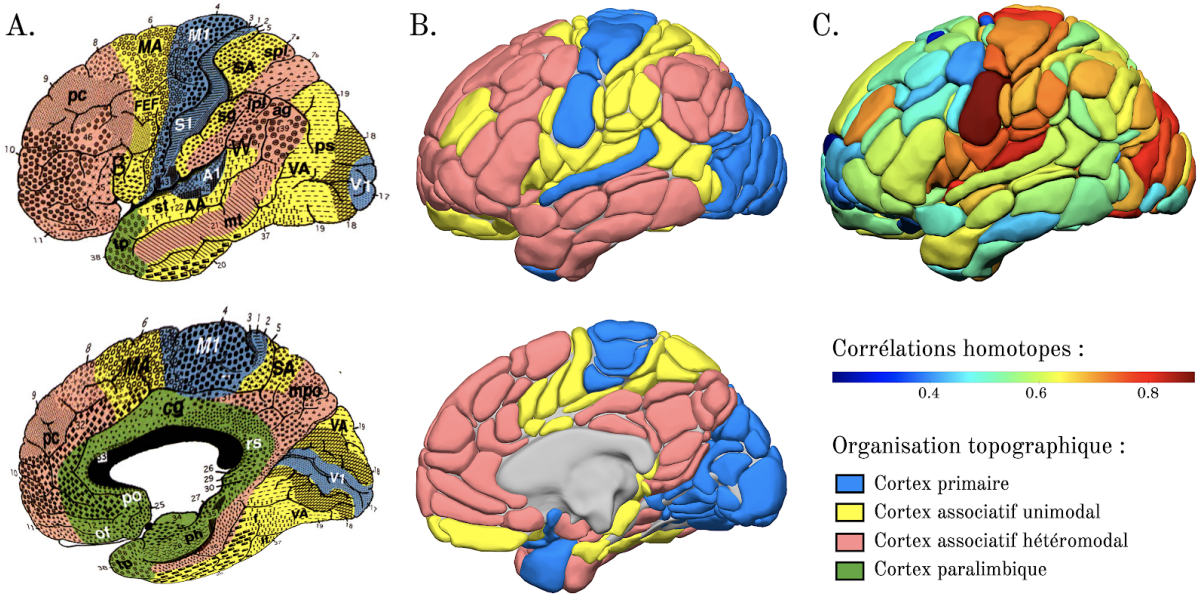

Figure 11 : Illustration de l'organisation topographique cérébrale à l'état de repos. **A.** *Modèle de l'organisation topographique à large échelle de l'intégration de l'information du Pr. Marsel Mesulam. Figure adaptée de [MES00].* **B.** *Organisation topographique à large échelle de la connectivité intrinsèque basée sur la parcellisation cérébrale de l'atlas AICHA [JOL15] en utilisant la méthode présentée dans [MAR16] afin d'obtenir les 2 premières composantes de la matrice de similarité cosinus de la matrice de connectivité intrinsèque. L'illustration a été réalisée à partir de la matrice moyenne de connectivité intrinsèque de 67 sujets fortement typiques pour le langage (les sujets proviennent de la BIL&GIN [MAZ16], la typicité est définie dans [LAB20]). Les régions ont par la suite été regroupées en 3 groupes en utilisant un algorithme de classification des k-moyennes sur les 2 premières composantes. Les composantes ont été obtenues grâce à la fonction "diffuse" et la classification via la fonction "diffusionKmeans" de la librairie R diffusionMap [JOS19]. Les couleurs sont établies en accord avec le modèle de Mesulam.* **C.** *Corrélations inter-hémisphériques homotopes des régions de l'atlas AICHA. Les données proviennent de la matrice moyenne de connectivité intrinsèque des 67 individus précédemment cités.* **B** et **C.** *Vue latérale (et médiane pour* **B***) de l'hémisphère gauche ; rendu 3D des régions de l'atlas AICHA sur la surface blanche du gabarit de la BIL&GIN dans l'espace MNI, réalisé à l'aide du logiciel Surf Ice.*

La Figure 11 présente un comparatif entre : 1) le modèle d'intégration sensorielle proposé par le Pr. Marsel Mesulam à partir de l'intégration des différentes connaissances sur le plan cytoarchitectonique et fonctionnel disponibles à la fin des années 90 (Figure 11 - A., [MES98]), 2) le modèle mathématique de l'organisation topographique cérébrale (Figure 11 - B.) proposé par le Dr. Daniel Margulies [MAR16], appliqué aux données de connectivité intrinsèque à partir de la parcellisation cérébrale de l'atlas AICHA [JOL15] de 67 individus de la BIL&GIN [MAZ16], identifiés comme fortement typiques (latéralisés à gauche) pour le langage [LAB20], et 3) les corrélations inter-hémisphériques homotopes (Figure 11 - C.) des régions de

l'atlas AICHA de la matrice moyenne de connectivité intrinsèque des 67 individus susmentionnés.

Tout d'abord, il convient de noter qu'il existe une superposition remarquable entre les différents types de cortex définis par le modèle de Mesulam et notre modèle mathématique défini à partir de la connectivité intrinsèque de la BIL&GIN. Il existe néanmoins quelques différences, le cortex limbique par exemple n'est pas identifié via la connectivité intrinsèque, ou encore la délimitation du cortex unimodal qui n'est pas totalement identique : par exemple le sillon précentral est identifié comme appartenant au cortex hétéromodal à l'aide de la connectivité intrinsèque alors que le Pr. M. Mesulam l'identifie comme une aire associative unimodale. Ces différences peuvent notamment s'expliquer par les méthodes différentes utilisées pour déterminer les différents types de cortex : sur la Figure 11 - A. la méthode est multimodale, en B. unimodale. En effet, en A. la délimitation des cortex s'appuie sur le rôle d'intégration sensorielle fonctionnelle des régions, mais prend également en compte leur cytoarchitectonie. Le cortex limbique (en vert en A.), étant essentiellement défini à partir de données cytoarchitectoniques, il n'est pas étonnant de ne pas le retrouver en B. qui prend uniquement en compte la connectivité fonctionnelle intrinsèque des régions. Il en est de même pour les délimitations du cortex associatif unimodal (en jaune en A. et B.) : en prenant pour exemple le sillon précentral, il est considéré comme appartenant au cortex unimodal en A. alors qu'il appartient au cortex associatif hétéromodal en B. Avec les connaissances actuelles en termes d'activité cérébrale fonctionnelle, la requalification du sillon précentral en tant qu'aire hétéromodale est légitime. Il a notamment été montré que cette aire est impliquée dans la compréhension de l'action que la modalité soit visuelle ou verbale [JOU15], mais également qu'elle est impliquée dans le processus de traitement de la phrase de haut niveau que la modalité soit visuelle, auditive ou verbale [LAB19]. De même, la partie inférieure du gyrus frontal moyen (en jaune en B.) supposément hétéromodal est ici catégorisée comme une aire unimodale (même observation dans [MAR16]) : cette catégorisation reste une question en suspens.

De plus, en comparant la Figure 11 - B. et C., il est remarquable de constater que le gradient de la force des corrélations inter-hémisphériques suit également l'organisation topographique de l'intégration sensorielle. Les corrélations les plus

fortes (en rouge foncé en C.) sont retrouvées dans les aires du cortex primaire (en bleu en B.), puis suivent les corrélations d'une force intermédiaire (de l'orange clair au rouge clair en C.) dans le cortex associatif unimodal (en jaune en B.), et enfin les faibles corrélations inter-hémisphériques (du bleu foncé au vert en C.) des aires associatives hétéromodales (en rose en B.).

1.2.2.4. Réseaux de repos et réseaux cognitifs évoqués

Les résultats concernant l'organisation fonctionnelle cérébrale à l'état de repos, conduisent à l'hypothèse selon laquelle les réseaux de connectivité intrinsèque peuvent être vus comme le support des fonctions cognitives. Dans ce sens, Smith & al. concluent de leur étude sur la correspondance entre les réseaux du repos calculés chez 30 témoins volontaires et l'organisation spatiale des réseaux cognitifs à partir de données de méta-analyse d'activations[38] que le répertoire complet des réseaux fonctionnels utilisés par le cerveau en "action" est continuellement et dynamiquement actif, même lorsqu'il est au "repos" ([SMI09] et [LAI13]). Cole & al. viennent nuancer ces propos en montrant que bien que les matrices de connectivité intrinsèque expliquent une grande part de la variance des matrices de connectivités fonctionnelles induites par des tâches cognitives (également montré dans [TAV16] & [NIU20]), il existe des différences majeures de similarité sur certaines connexions entre activité de repos et activité évoquée [COL14]. Mennes & al. suggèrent également dans une étude de 2012, que les patterns d'activations évoqués par les tâches cognitives de haut-niveau ne coïncident pas avec les réseaux détectés à l'état de repos [MEN12]. Ces auteurs concluent alors que l'architecture cérébrale de la connectivité intrinsèque est un état cérébral de base qui est dynamiquement modifié dans le temps, autant que nécessaire, afin de répondre aux besoins fonctionnels de la tâche réalisée [FOR12a]. Cette hypothèse va d'ailleurs dans le même sens que les conclusions de l'étude de Fox & al. qui suggèrent que les régions cérébrales similairement modulées par une tâche ou un stimuli externe, montrent des corrélations significatives des fluctuations spontanées de leurs signaux BOLD et ce même en l'absence de tâche ou de stimulus externe [FOX05].

[38] Les réseaux fonctionnels d'activations sont ici basés sur les données d'une méta-analyse d'articles en neuroimagerie cognitive.

De nombreux auteurs ont labellisé les réseaux de l'état de repos conscient en fonction de ce qui était connu grâce aux paradigmes d'activation de neuroimagerie cognitive, alors même que la question reste ouverte et qu'aucune donnée définitive, à ma connaissance, ne porte sur une étude de la superposition spatiale exacte de ces différents réseaux. Yeo & al. par exemple, nomment leur réseau du repos en fonction des données obtenues par neuroimagerie cognitive [YEO11], mais ils précisent dans leur article que cette heuristique de nommage des réseaux du repos a des limites. En effet, le réseau qu'ils ont nommé DMN par exemple, a été décomposé en plusieurs sous réseaux par d'autres auteurs ([AND10a] et [BUC19b]). De plus, Greene & al. montrent dans une étude récente que les patterns de connectivité fonctionnelle provenant des fluctuations du signal BOLD induites par des tâches cognitives prédisent mieux les performances comportementales que les patterns de connectivité intrinsèque [GRE18]. Bijsterbosch & al. quant à eux ont récemment mis en avant que la superposition spatiale entre les réseaux du repos explique significativement une certaine part de la variance interindividuelle des performances comportementales [BIJ19]. Finalement, des études ont également montré que les performances lors de l'exécution d'une tâche cognitive modulent directement la connectivité intrinsèque entre les réseaux du repos ([MEN11] et [GOR12]). Il est à noter que la superposition entre les patterns d'activations induits par des tâches et les réseaux du repos ne montre qu'un chevauchement partiel ([MEN13] et [GOR17]).

En résumé, bien que les organisations cérébrales au repos[39] et pendant les tâches cognitives soient en partie superposables, il n'existe aujourd'hui que peu d'éléments qui rendent compte des règles qui permettent de passer de l'un à l'autre. Certains auteurs ont proposé que l'activité au repos, organisée en réseau, sert de phase de consolidation des réseaux d'activation fonctionnels, de planification du futur, ou encore de renforcement des apprentissages [BUC07]. Néanmoins une meilleure connaissance des relations quantitatives, et pas seulement spatiales, entre ces deux

[39] Le repos est ici entendu au sens large du terme, puisqu'il a également été montré que l'activité à l'état de repos conscient se poursuit lors du sommeil ([FUK06] et [LAR09]) et même sous anesthésie [VIN07]. Bien que l'organisation fonctionnelle en réseau de l'activité cérébrale sous anesthésie (induisant une perte de conscience) est plus proche de l'organisation en réseau structurelle (modelé par les connexions anatomiques des fibres blanches) que de l'organisation en réseau fonctionnelle induite par "l'action" [UHR18].

états physiologiques reste à acquérir, et cela a été un des objectifs originaux de mon travail.

Pour entreprendre une telle étude, un élément essentiel est de s'appuyer sur une parcellisation du cerveau qui puisse permettre une telle comparaison. Comme nous allons le voir de nombreux atlas cérébraux ont été développés, répondant à des objectifs qui ont varié au cours du temps et cette approche est un autre des éléments fondamentaux de mon travail de thèse.

2. Les atlas *in vivo* du cerveau Humain

Mon travail de thèse se situe dans le cadre de la définition d'atlas avec un objectif original : celui de définir des atlas en relation avec des fonctions cognitives spécifiques et en intégrant une dimension oubliée dans les travaux précédents, celle de l'organisation fonctionnelle du cerveau suivant les règles de la spécialisation hémisphérique[40]. La conception d'atlas de fonctions cognitives se situe dans la lignée de la création d'atlas et de leurs innovations instrumentales et mathématiques présentées dans cette partie.

Les atlas cérébraux, *i.e.* la parcellisation de cerveau en régions d'intérêt (ROI : *Region of Interest*), permettent de fournir un cadre de travail systémique aux neurosciences [YEO16]. Comme l'a montré en 2012 le Dr. Cameron Craddock, les atlas offrant une parcellisation en ROIs ont l'avantage, comparé aux analyses en voxels, d'avoir une meilleure sensibilité et interprétabilité (lorsque le signal regardé et celui utilisé pour élaborer la parcellisation est le même) en augmentant le rapport signal sur bruit des données [CRA12] : c'est l'homogénéité mathématique. De plus, l'utilisation d'atlas permet de réduire la dimensionnalité des données d'IRMf de l'ordre de 10^6 voxels à seulement quelques centaines de régions, et ce, sans perdre d'informations concernant les processus cognitifs cérébraux latents. Cette réduction de dimension permet de contrôler le problème des comparaisons statistiques en réduisant drastiquement le nombre de tests requis lors de l'analyse des données [ZAL12].

Deux exemples illustrent à quel point les atlas ont été des instruments essentiels au développement de la neuroimagerie. Le premier est celui de l'atlas de Talairach qui a

[40] *cf.* Introduction à la Partie II pour une définition de la spécialisation hémisphérique.

permis l'essor de la neuroimagerie fonctionnelle par mesure de l'activité évoquée au cours de tâches cognitives avec la TEP puis en IRMf. L'espace stéréotaxique de Talairach a fourni un espace de normalisation des cerveaux à partir d'images obtenues *in vivo* et, couplé à son atlas, a permis de localiser les activations TEP dans les années 1980-1990 [FOX85]. Il est important de souligner que le concept d'espace stéréotaxique apporté par Talairach a été conservé et constamment amélioré. Le deuxième exemple est celui de l'atlas AAL [TZO02] qui a accompagné l'essor de la connectivité fonctionnelle étudiée au repos. Pour illustrer ce deuxième exemple, j'ai procédé à une brève étude de la bibliographie des 4 grands sous-domaines de la neuroimagerie concernant directement le sujet de cette thèse que sont l'IRMf, la connectivité intrinsèque, la parcellisation cérébrale et la théorie des réseaux.

D'après Web of Science[41], il existe un corpus de 419 articles référencés comme étant les plus cités dans les 4 sous-domaines précédemment mentionnés. Ce corpus de textes couvre une période de 19 ans (de 2001 à 2020), inclus 152 sources différentes[42] (journaux, livres *etc*...), et mentionne un total de 33 289 références. Une analyse de la carte historiographique[43] de ces 419 références (Figure 12) à l'aide de la librairie R "*bibliometrix*" [ARI17] permet de mettre en avant que l'atlas AAL [TZO02] et la mise en évidence du DMN via les publications concomitantes de [MAZ01b] et de [RAI01] sont à l'origine de ce corpus de travaux scientifiques, et que les études issues des atlas, de la connectivité intrinsèque et de la théorie des réseaux ont conduit à la mise au point de l'atlas multimodal du Dr. Matthew Glasser [GLA16]. L'atlas AAL a été un outil fondateur du sous-domaine de la neuroimagerie concernant la théorie des réseaux appliquée aux neurosciences ([BUL11] et [SPO11], *cf.* Figure 12). C'est donc un exemple qui montre que la mise au point d'un atlas est un des éléments de l'application de théories mathématiques (ici la théorie des réseaux) à l'étude de l'organisation fonctionnelle cérébrale.

[41] Résultat en juin 2020 des requêtes suivantes sur Web of Sciences, en ne sélectionnant que les articles "*Highly Cited in Field OR Hot Papers in Field*" ; TOPIC: (Functional magnetic resonance imaging) AND TOPIC: (MRI) AND TOPIC: (functional MRI), TOPIC: (network neuroscience), TOPIC: (brain parcellation) et TOPIC: (intrinsic connectivity).

[42] *Neuroimage* étant le journal arrivant en tête avec 52 articles y étant publié, le second étant *Trends in Cognitive Sciences* avec un total de 23 publications.

[43] Une carte historiographique est une visualisation permettant de représenter le réseau chronologique des citations directes les plus pertinentes résultant du recueil bibliographique analysé [GAR04].

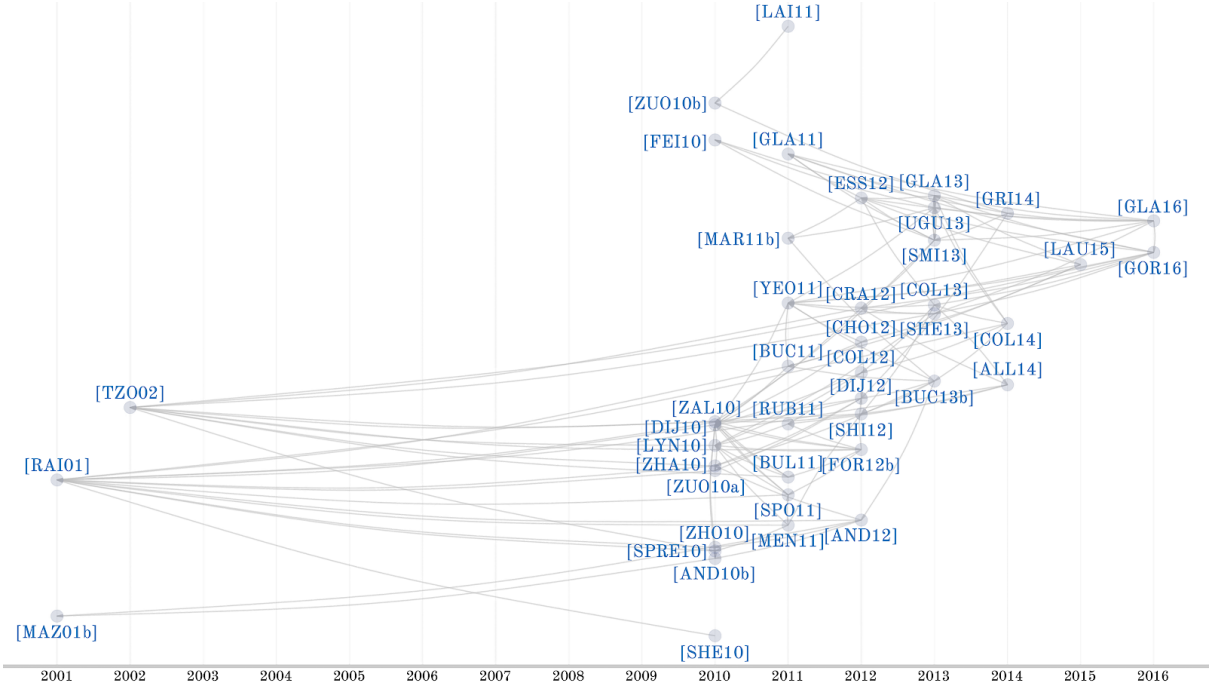

Figure 12 : Carte historiographique du recueil bibliographique des 419 articles les plus cités délimitant les grands thèmes abordés dans cette thèse (IRMf, neuroscience des réseaux, parcellisation cérébrale et connectivité intrinsèque). *Le graphe est orienté d'après les citations directes d'un article à l'autre : une flèche d'un article B vers A signifie que l'article B cite A. Les articles sont ordonnés par année de publication. Chaque cercle représente un article, dont la référence est disponible dans la Bibliographie.*

2.1. Revue descriptive et chronologique des atlas de neuroimagerie dans l'espace stéréotaxique

Le chapitre qui suit présente une bibliographie descriptive d'un ensemble de 21 atlas cérébraux dans l'espace stéréotaxique commun publiés à ce jour. Ces derniers sont présentés dans l'ordre chronologique de publication et sont classés en fonction de la ou des modalité(s) utilisée(s) pour les construire : marqueurs anatomiques, connectivité structurelle (anatomie des fibres blanches), connectivité intrinsèque et multimodalité. En effet, la parcellisation en ROIs, peut être réalisée de plusieurs façons en fonction des objectifs des auteurs : suivant les données provenant d'IRM anatomique (repères anatomiques, connectivité structurelle, myélinisation intracorticale...), ou bien suivant les données d'IRMf (variations d'activité obtenues au cours de tâches cognitives, connectivité intrinsèque) ou encore une combinaison des deux. Une ROI regroupe alors soit un ensemble de voxels qui sont homogènes entre eux pour une, ou dans les cas d'atlas multimodaux, pour plusieurs de ces caractéristiques [GEN18], soit

un ensemble de voxels qui sont dissimilaires de leur voisin pour une ou plusieurs modalités [EIC18a]. Le Pr. Per Roland souligne que pour qu'une parcellisation ait un sens en termes de rôle fonctionnel, elle se doit de respecter les champs fonctionnels[44] en prenant en compte des mesures quantitatives dans la définition des ROIs [ROL98].

2.1.1. Les atlas anatomiques

Tableau 1 : Caractéristiques des atlas anatomiques obtenus à partir de la gyrification. *La colonne correspondant à l'atlas de Talairach [TAL67] est grisée car ce dernier n'est pas un atlas de neuroimagerie à proprement parler.*

	[TAL67][45]	**[TZO02]**	**[DES06]**	**[DES10]**	**[AUZ16]**
$N_{Individus}$	1	1	40	24	137
Données	individuelles	individuelles	individuelles et moyennes	individuelles et moyennes	individuelles et moyennes
Âge (années)	60	"jeune"	19 - 86	18 - 25	-
IRM	-	1.5 T Philips	1.5 T Siemens	1.5 T Siemens	1.5 T Siemens
Type de morphométrie	volume	volume	surface	surface	surface et volume
Méthode de construction de l'atlas	Annexes : 1	gyrification manuelle	modèle de Markov caché [FIS04b]	modèle de Markov caché [FIS04b]	HIP-HOP[46] [AUZ13]
Régions par hémisphère	47, 34, 19, 13[47]	48	34	74	48
Critère de sélection du nombre de régions	anatomique et histologique	anatomique	anatomique	anatomique	critère d'arrêt de la méthode HIP-HOP
But	localisation	localisation	anatomie individuelle	anatomie individuelle	cartographie fonctionnelle + intégration multimodale

[44] L'hypothèse des champs fonctionnels suppose que l'organisation fonctionnelle du cortex cérébral humain repose sur des champs fonctionnels qui occupent chacun une partie plus ou moins grande du territoire cortical. Ces champs fonctionnels, d'une surface d'au moins 3 cm^2, sont les entités fonctionnelles cérébrales les plus grandes. Ces champs fonctionnels sont alors les manifestations physiologiques de l'activité cérébrale [ROL85].

[45] L'atlas de Talairach n'est pas basé sur des données d'IRM d'un individu sain, mais sur une étude histologique de l'hémisphère gauche d'un cerveau conservé dans le formol d'une femme de 60 ans. Le Pr. Jean Talairach fournit ainsi la labellisation de l'ensemble du cerveau d'après les aires Brodmann [BRO12], la gyrification cérébrale et les ganglions de la base.

[46] HIP-HOP : *Harmonic Intrinsic Parameterization - Harmonic Orthogonal Parameterization*

[47] 47 aires corticales, 34 gyri et sulci, 19 faisceaux et ventricules et 13 ganglions de la base

L'atlas de Talairach est le premier atlas anatomique du cerveau humain qui ait été appliqué à l'imagerie fonctionnelle [FOX85] et bien qu'il ne soit pas à proprement parler un atlas de neuroimagerie il est inclus dans cette synthèse (Figure 13 - A, [TAL67]). Ces atlas anatomiques (Figure 13), élaborés à partir d'imagerie IRM, se basent sur des marqueurs anatomiques et en particulier sur la gyrification corticale afin de définir les limites des ROIs et comportent en moyenne 50 régions (± 15). Les différentes caractéristiques de ces atlas peuvent être trouvées dans le Tableau 1.

Les avancées qui ont suivi l'utilisation de l'atlas de Talairach ont consisté en une amélioration du gabarit ou template. Le gabarit de l'atlas de Talairach, constitué de l'hémisphère gauche d'une femme de 60 ans conservé dans le formol, a été progressivement remplacé par des images de CT-scan comme dans l'atlas de Matsui [MAT78], puis par des images anatomiques d'IRM avec une amélioration de la résolution anatomique et du nombre de sujets inclus dans leur construction au cours du temps (MNI[48], *cf.* [EVA12] pour une revue concernant les gabarits dans l'espace stéréotaxique[49]). Il est courant aujourd'hui de définir un gabarit par étude, ou par population, afin de prendre en compte les caractéristiques de la population étudiée et celle de l'appareil d'Imagerie par Résonance Magnétique (IRM) utilisé. La procédure de création de gabarit utilisée dans cette thèse, a consisté en l'alignement des IRMs anatomiques de chacun des sujets de la base de données BIL&GIN [MAZ16] normalisées vers un des gabarits de l'espace MNI.

Il est important de noter que ces avancées ont également été marquées par l'évolution de la normalisation : originellement proportionnelle à 8 paramètres, elle est maintenant opérée avec des algorithmes non-linéaires et tridimensionnels [ASH99].

[48] Le premier gabarit de l'espace MNI ne se base pas sur un, mais sur un ensemble de 305 IRM cérébraux d'individus sains. Cet espace a été construit en deux étapes ; tout d'abord, les 305 sujets ont été normalisés dans le référentiel de Talairach, puis moyennés entre eux afin de créer un premier gabarit. Par la suite, chacune des 305 IRM a individuellement été alignée sur le premier gabarit à l'aide d'un modèle d'alignement linéaire. Ces 305 cerveaux ainsi ré-alignés ont finalement été moyennés pour produire le template de l'espace MNI final. Aujourd'hui la normalisation vers l'espace stéréotaxique se fait par le biais du template MNI. Les gabarits de l'espace MNI (Montreal Neurological Institute ; [EVA93]) sont communément utilisés, notamment par les logiciels SPM [PEN11] et FSL [SMI04] ; deux logiciels de référence en neuroimagerie cérébrale.

[49] Il existe 5 gabarits se situant dans l'espace MNI : le MNI305, le Colin27, le ICBM152, le MNI152 et l'ICBM452. Ces gabarits diffèrent par le type de méthode d'alignement utilisée pour les construire, le nombre de sujets utilisés ou encore la puissance de la machine IRM utilisée.

Le premier atlas anatomique provenant de données d'IRM, et le plus cité[50] dans le domaine de la neuroimagerie, est l'atlas AAL (*Automated Anatomical Labelling*) [TZO02]. L'atlas AAL (Figure 13 - B) a été construit dans l'espace commun stéréotaxique à partir de marqueurs anatomiques tels que le positionnement des sillons via la délinéation manuelle des images axiales du gabarit[51] du cerveau de référence de l'espace stéréotaxique de l'époque. L'objectif initial d'AAL était de permettre une détection automatique de la localisation anatomique des coordonnées stéréotaxiques des pics d'activation des tâches évoquées en PET. L'usage d'AAL a ensuite été détourné par les chercheurs qui l'ont utilisé pour obtenir des données quantitatives régionales, puis pour réaliser des mesures de connectivité cérébrale intrinsèque et structurelle.

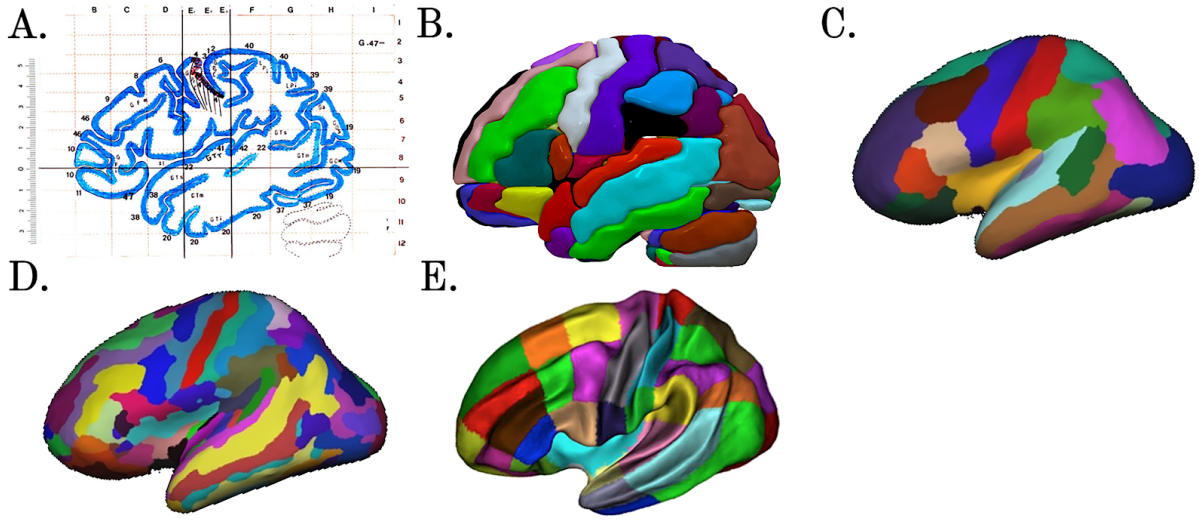

Figure 13 : Rendu de la face latérale de l'hémisphère gauche des atlas anatomiques obtenus à partir de la gyrification. **A.** *29ème coupe sagittale de l'hémisphère gauche de l'atlas de Talairach [TAL67].* **B.** *Rendu en volume de l'hémisphère gauche de l'atlas AAL [TZO02].* **C.** *Rendu en surface de l'hémisphère gauche de l'atlas Desikan [DES06].* **D.** *Rendu en surface de l'hémisphère gauche de l'atlas Destrieux [DES10].* **E.** *Rendu en surface de l'hémisphère gauche du MarsAtlas [AUZ16].*

La mise au point d'une méthode de déploiement du cortex [ESS98] a représenté un tournant dans l'analyse des données anatomiques qui s'est accompagné de la mise au point d'atlas surfaciques ([DES06], [DES10] et [AUZ16]). Sur le plan anatomique, les méthodes surfaciques permettent de calculer l'épaisseur corticale et la surface corticale de manière indépendante. Sur le plan fonctionnel, le passage d'une analyse en

[50] Avec plus de 5 000 citations, l'atlas AAL publié en 2002 est le plus cité de la revue NeuroImage. C'est le second article le plus cité du CEA depuis 1975 parmi 115 000 publications référencées sur Web of Science [LER16].

[51] Ce gabarit cérébral a été obtenu à partir de l'acquisition IRM d'un "jeune" homme dont le cerveau a été scanné 27 fois.

volume à une analyse en surface permet une meilleure définition et quantification du signal des régions se situant au fond des sillons cérébraux [BRO20], ce qui est particulièrement utile lors de l'étude de l'organisation rétinotopique du cortex visuel par exemple ([ABD14] et [GLA16]). Les atlas de Desikan [DES06] (Figure 13 - C) et de Destrieux [DES10] (Figure 13 - D) permettent d'identifier automatiquement et individuellement les ROIs anatomiques à partir de la surface corticale après un apprentissage à l'aide d'un modèle probabiliste de Markov caché de la labélisation relative de chaque voxel par rapport aux autres [FIS04b]. Finalement, le MarsAtlas [AUZ16] (Figure 13 - E) construit sa parcellisation à partir d'un système de coordonnées polaires de l'organisation corticale des sillons cérébraux dans l'optique d'étudier l'intégration des données fonctionnelles multimodales. Contrairement à ses semblables, le MarsAtlas fournit une nouvelle vision de la cartographie cérébrale en se basant sur l'emplacement des sillons corticaux.

Tableau 2 : Caractéristiques des atlas anatomiques obtenus à partir de la substance blanche.

	[ZHU13]	**[FAN16]**
$N_{Individus}$	$11 + 23 + 20 + 89 = 143$	80
Données	individuelles	individuelles et moyennes
Âge (années)	11 - 89	17 - 35
Appareil IRM	3 T General Electrics (multiples appareils)	3 T Siemens
Type de morphométrie	volume	volume
Méthode de construction de l'atlas	à partir d'un ensemble de connectome individuel ; maximisation de cohérence des connectomes [ZHU12]	partitionnement spectral
Régions par hémisphère	189	123
Critère de sélection du nombre de régions	inspection visuelle des tracts obtenus à partir des repères corticaux (régions)	test V de Cramer
But	Repères corticaux de connectivité anatomique et fonctionnelle	relation structure - fonction

Un second type d'atlas anatomique se base sur l'imagerie de diffusion. L'imagerie de diffusion donne un indice de l'orientation des fibres de la substance blanche à partir du mouvement des molécules d'eau qui les entourent (*cf.* Tableau 2).

Deux atlas peuvent être cités : l'atlas DICCOL (Dense Individualized and Common Connectivity-Based Cortical Landmarks : [ZHU13], Figure 14 - A) et l'atlas Brainnetome ([FAN16], Figure 14 - B). Le premier parcellise le cerveau en repères corticaux en regroupant les voxels en fonction de l'homogénéité de leur pattern probabiliste de connectivité anatomique. Le second combine les cartes de probabilité de connectivité à partir de l'imagerie de diffusion avec des données de connectivité fonctionnelle obtenues au repos pour parcelliser le cortex en 123 ROIs par hémisphère.

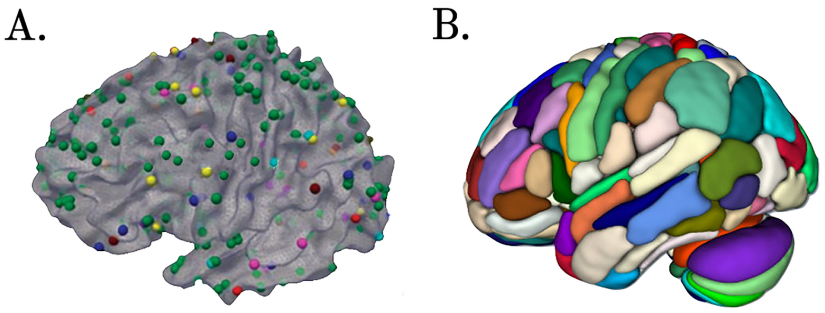

Figure 14 : Rendu de la face latérale de l'hémisphère gauche des atlas anatomiques obtenus à partir de la substance blanche. **A.** *Localisation dans l'espace MNI des centres de masse des 189 régions de l'atlas DICCCOL [ZHU13].* **B.** *Rendu en volume de l'hémisphère gauche du Brainnetome Atlas [FAN16].*

Il faut noter l'existence d'un atlas récent, extrêmement novateur, et construit avec les technologies anatomiques et informatiques de pointe qui devrait accompagner le développement de l'imagerie à très haute résolution (Figure 15). Cet atlas est basé sur un seul cerveau humain cartographié à très haute résolution (20 micromètres). Conçu dans le cadre du projet BigBrain [AMU13], il vise à fournir à la communauté neuroscientifique la reconstruction 3D de 7 404 coupes histologiques numérisées du cerveau d'un homme de 65 ans, placé dans l'espace commun.

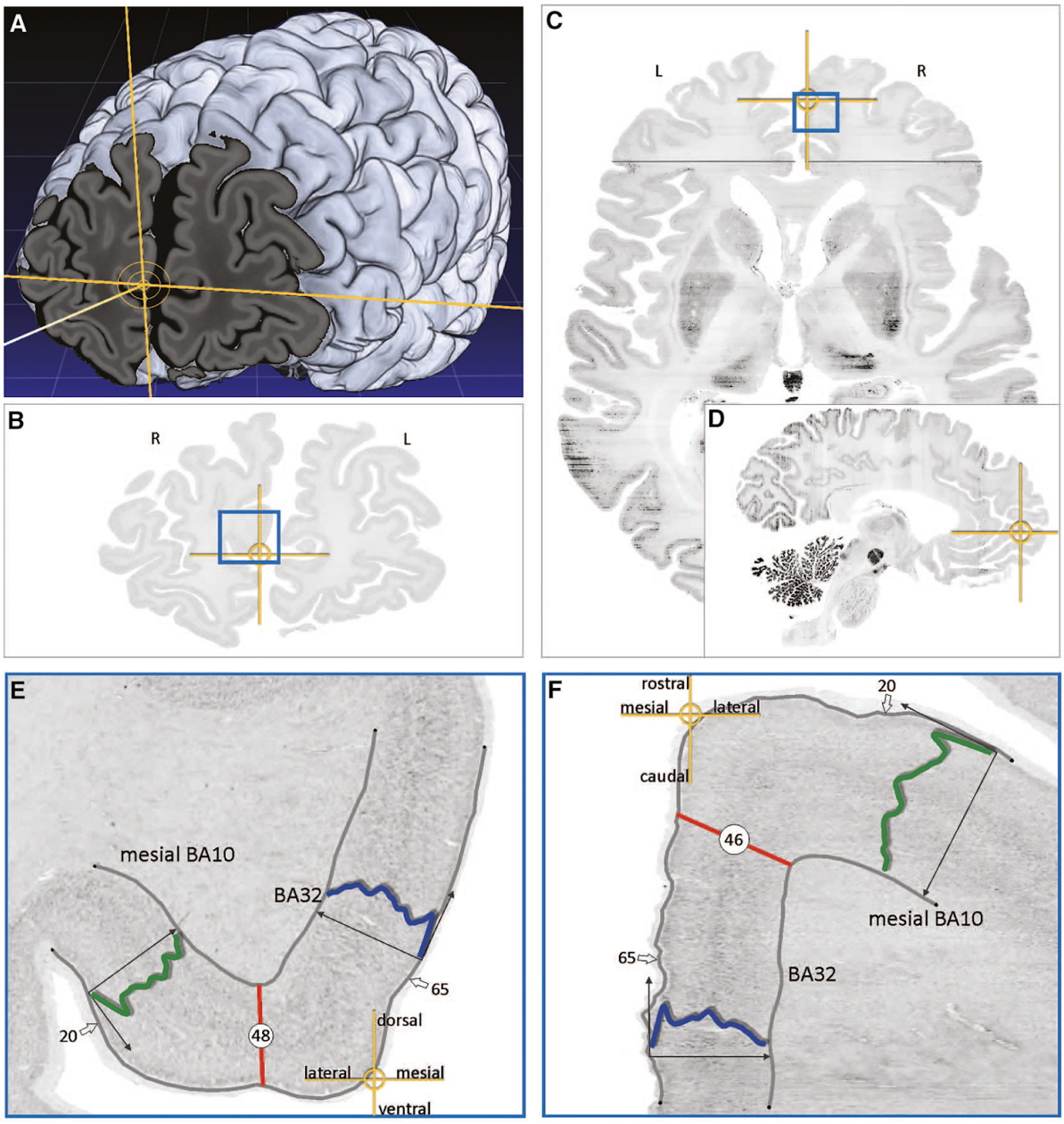

Figure 15 : Illustration de l'atlas BigBrain : élaboration des contours d'une ROI dans le cortex frontal. **A.** *Rendu surfacique de la reconstruction 3D du cerveau du projet BigBrain. La croix jaune correspond à la région cible pour l'élaboration de la ROI.* **B.** *Section coronale de la 6 704ème coupe histologique.* **C.** *Reconstruction 3D axiale de la 2 740ème section histologique et reconstruction sagittale de la 3 588ème section (***D.***).* **E - F.** *Définition des bordures des ROIs correspondant à l'encadré bleu en* **B.** *et* **C.** *En bleu, courbe du profil histologique moyen de l'aire de Brodmann 32, en vert, celle de l'aire 10. Figure adaptée de [AMU13].*

2.1.2. Les atlas de connectivité intrinsèque

Tableau 3 : Caractéristiques des atlas en réseaux de la connectivité intrinsèque.

	[POW11]	[YEO11]	[WAN15]	[KON19]
$N_{Individus}$	340	1000	229	$60 + 30 + 900 = 999$
Données	moyennes	individuelles et moyennes	individuelles et moyennes	individuelles et moyennes
Âge (années)	"jeune"	18 - 35	18 - 59	18 - 35
IRM	1.5 et 3T Siemens	3 T Siemens	3 T Siemens	3 T Siemens et GE
Morphométrie	volume	surface	surface	surface
Méthode de construction de l'atlas	Infomap community detection [ROS08]	modèle de mélange de von Mises-Fisher [LAS10]	méthode de [LAS10]	méthode de [YEO11]
Nombre de réseaux	14	7 - 17	18	17
Critère de sélection du nombre de régions	minimisation de la *map equation* [ROS09]	analyse de la stabilité : *model explorer algorithm* [BEN01]	arrêt lorsque 98% des voxels ne changent plus de réseau	méthode de [YEO11]
But	topographie de l'organisation cérébrale fonctionnelle	topographie de l'organisation cérébrale fonctionnelle	topographie de l'organisation cérébrale au niveau individuel	topographie de l'organisation cérébrale au niveau individuel

Un certain nombre d'atlas définissent des réseaux intrinsèques en fonction de leur homogénéité en termes de connectivité intrinsèque[52] ([POW11], [YEO11], [WAN15] et [KON19], Figure 16, Tableau 3). Les ROIs de ces atlas correspondent à des réseaux fonctionnels à large échelle. L'objectif de l'élaboration de ces atlas est de répondre à la question de la topographie de l'organisation cérébrale, que ce soit au niveau individuel ou moyen, en étudiant notamment la transmission de l'information entre les différents réseaux que ce soit chez l'individu sain, via par exemple l'étude de la variabilité interindividuelle de la connectivité [MUE13], ou chez l'individu pathologique, comme par exemple la caractérisation de la connectivité des réseaux intrinsèques des troubles dépressifs [KAI15].

[52] *i.e.* quels sont les regroupements de voxels partageant le même profil de connectivité intrinsèque avec le reste des voxels du cerveau.

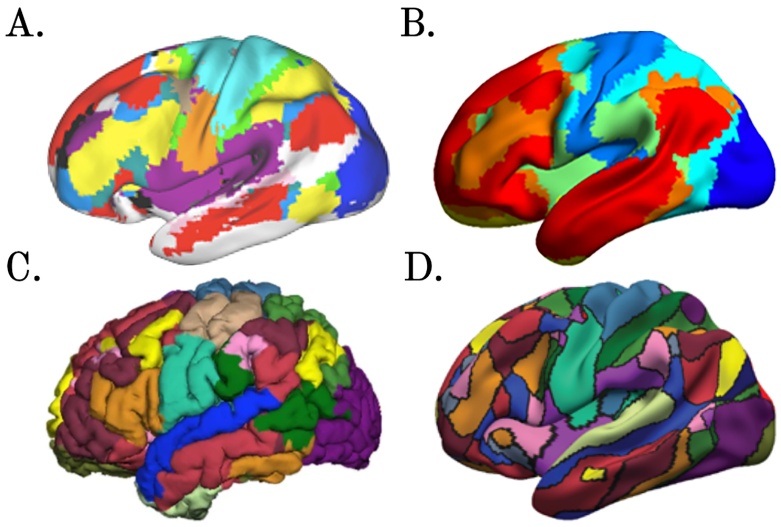

Figure 16 : Rendu des atlas en réseaux de la connectivité intrinsèque. **A.** *Rendu en surface des 14 réseaux de l'hémisphère gauche de [POW11].* **B.** *Rendu en surface des 7 réseaux de l'hémisphère gauche de [YEO11].* **C.** *Rendu en surface des 18 réseaux de l'hémisphère gauche de [WAN15].* **D.** *Rendu en surface des 17 réseaux de l'hémisphère gauche de [KON19].*

Tableau 4 : Caractéristiques des atlas en régions de la connectivité intrinsèque.

	[CRA12]	[SHE13]	[JOL15]	[GOR16]	[SCH18]	[URC19]
$N_{Individus}$	41	79	281	120	1489	198
Données	individuelles et moyennes	individuelles et moyennes	individuelles et moyennes	moyennes	individuelles et moyennes	individuelles et moyennes
Âge (années)	18 - 55	-	18 - 57	19 - 32	18 - 35	18 - 30
IRM	3 T Siemens	3 T Siemens	3 T Philips	3 T Siemens	3 T Siemens	3 T Siemens
Morphométrie	volume	volume	volume	surface et volume	surface et volume	volume
Méthode de construction de l'atlas	*spatially constrained n-cut parcellisation*	*K-way spectral clustering*	réseaux : ICA, ROI : k-moyenne	*gradient based parcellisation*	*Markov model* pondéré par gradient	*bootstrap analysis of stable clusters*
Régions par hémisphère	200 - 600 - 1000	47 - 94 - 140	192	178	100 - 200 - 400 - 600 - 800 - 1000	7 - 12 - 20 - 36 - 64 - 122 - 197 - 210 - 325 - 444
Critère de sélection du nombre de régions	minimisation de la fonction de coût de l'algorithme[53]	jointly optimizes the group and the individual parcellisation	index de Rand	inspection visuelle	*graph cut optimization* [DEL10]	maximisation de la mesure de stabilité
But	connectivité fonctionnelle (CF)	CF + application théorie des graphes	étude de la SH + homotopie	homogénéité des régions + recouvrement CT[54]	homogénéité des régions et recouvrement CT	CF

[53] poids des arêtes reliant deux clusters minimum
[54] CT : aires CyToarchitectoniques.

Dans la perspective d'obtenir des atlas plus fins en termes de résolution, des atlas des régions fonctionnelles ont été développés ([CRA12], [SHE13], [JOL15], [GOR16], [SCH18] et [URC19], Figure 17, Tableau 4) dont les ROIs sont définies comme des ensembles de voxels partageant la même connectivité intrinsèque, *i.e.* appartenant aux mêmes réseaux du repos, subdivisés en régions fonctionnellement homogènes. Ces atlas ont pour but l'étude de la connectivité fonctionnelle via notamment l'application de la théorie des réseaux.

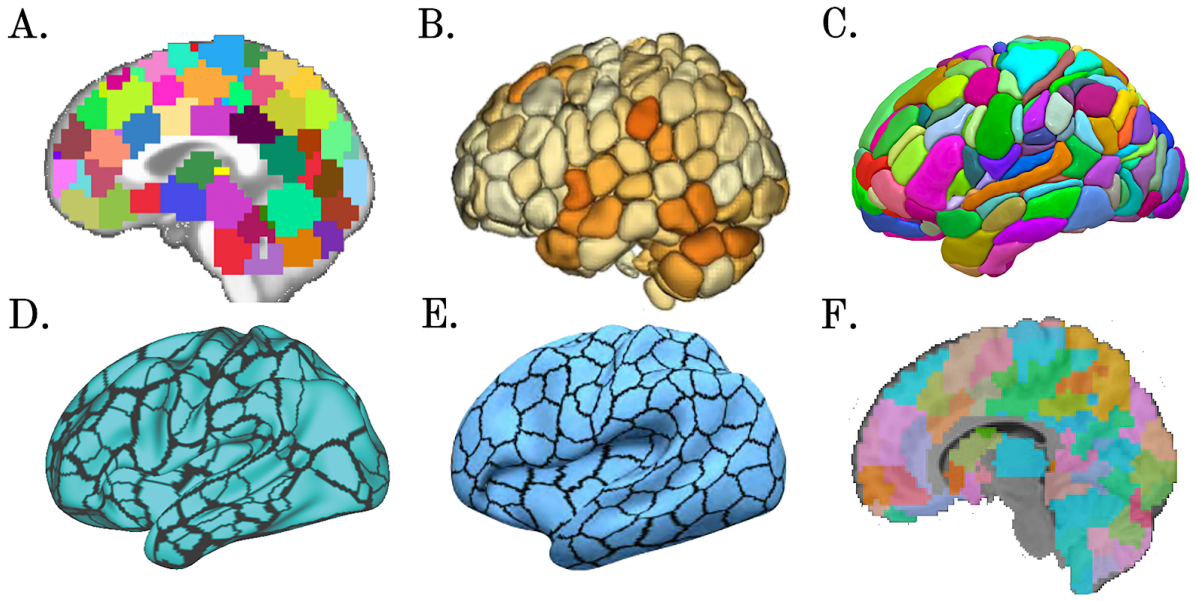

Figure 17 : Rendu des atlas en régions de la connectivité intrinsèque. **A.** *Coupe sagittale (z_{MNI} = 0 mm) de l'hémisphère gauche de l'atlas de [CRA12].* **B.** *Rendu en volume de l'hémisphère gauche de l'atlas de [SHE13].* **C.** *Rendu en volume de l'hémisphère gauche de l'atlas AICHA [JOL15].* **D.** *Rendu en surface de l'hémisphère gauche de l'atlas de [GOR16].* **E.** *Rendu en surface de l'hémisphère gauche de l'atlas de [SCH18].* **F.** *Coupe sagittale (z_{MNI} = -10 mm) de l'hémisphère gauche de l'atlas MIST [URC19].*

L'atlas AICHA ([JOL15], Figure 17 - C) est un atlas unique en son genre qui parcellise les régions corticales et sous-corticales en régions d'intérêt fonctionnellement homotopes : hROIs (*cf.* 1.2.2.3 Etat de repos et organisation cérébrale, pour une définition de l'homotopie). La parcellisation d'AICHA est basée sur les données de connectivité intrinsèque individuelle de 281 sujets de la base de données BIL&GIN [MAZ16]. Les paragraphes suivants présentent les étapes de la construction de la parcellisation d'AICHA (Figure 18).

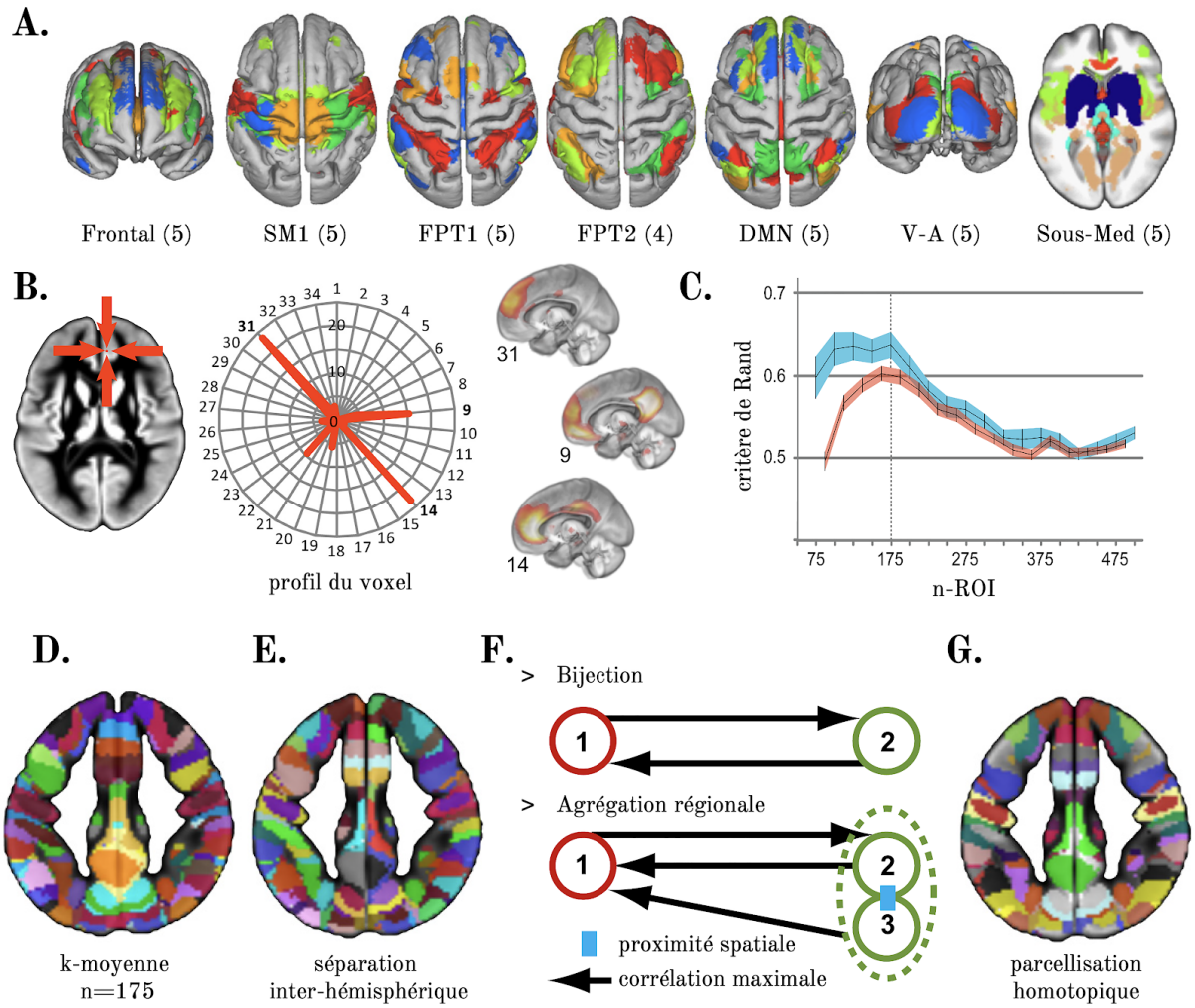

Figure 18 : Principales étapes de la construction de l'atlas AICHA. **A.** *Un rendu 3D ou axial des 34 réseaux d'état de repos identifiés par MICCA ([NAV12], SM : Sensori-moteur, FPT : Fronto-pariéto-temporal, V-A : Visuel-Auditif, Sub-Med : Sous-cortical et médial).* **B.** *Illustration du profil de connectivité d'un voxel.* **C.** *Sélection de la parcellisation optimale à l'aide de l'indice de Rand. La ligne verticale en pointillés indique la valeur optimale du nombre n de ROI.* **D.** *Parcellisation optimale.* **E.** *Parcellisation optimale après la séparation hémisphérique.* **F.** *Règles pour la détermination et le regroupement en paire de régions homotopiques.* **G.** *Parcellisation homotopique (la même couleur est utilisée pour les régions homotopiques). Figure adaptée de [JOL15].*

La parcellisation se base sur la définition, chez chaque individu, de 34 réseaux du repos (Figure 18 - A) avec l'algorithme MICCA (*cf.* Note de bas de page n°33, [NAV12]). Chacun des voxels appartenant à la substance grise possède alors une empreinte faisant état de son profil vectoriel à travers les 34 réseaux du repos (Figure 18 - B). L'algorithme des *k-means* permet ensuite de regrouper entre eux les voxels ayant un profil similaire à travers les 34 réseaux : l'index de Rand (Figure 18 - C) conduit à une parcellisation des 144 216 voxels en 175 ROIs (Figure 18 - D). Les deux hémisphères sont ensuite déconnectés en éliminant les voxels chevauchant la scissure inter-hémisphérique. L'algorithme des *k-means* n'ayant pas de contrainte

spatiale, les voxels isolés ont été groupés avec les voxels de la ROI la plus proche avec laquelle il partageait le maximum de voisins. Ces étapes ont conduit à l'identification de 221 ROIs dans l'hémisphère gauche et 239 dans le droit (Figure 18 - E).

La dernière étape de la construction de l'atlas[55] s'appuie sur le fait que la connectivité inter-hémisphérique homotope est la plus forte ([STA08], Figure 11 - C). Le décours temporel du signal BOLD de l'état de repos est alors calculé dans chacune des 460 ROIs chez les 281 sujets. Pour chaque région identifiée, sa région homotope est identifiée comme étant la région controlatérale (*i.e.* dans l'hémisphère opposé) qui a le coefficient de corrélation de Pearson inter-hémisphérique moyen maximal entre les sujets. La relation d'homotopie a ainsi été définie en deux étapes (Figure 18 - F). La première étape, établissant l'homotopie régionale, définit deux ROIs homotopes si la corrélation temporelle entre A et B est bijectivement maximale et qu'aucune autre région n'a de corrélation maximale avec A ou B. Cette première étape conduit en l'identification de 137 paires de ROIs homotopes : 84 ROIs dans l'hémisphère gauche et 102 dans le droit n'ayant alors pas de contrepartie homologue. La deuxième étape concerne le cas où 2 ROIs : B et C, ont une corrélation inter-hémisphérique maximale avec A. Si B et C sont adjacentes et que la corrélation inter-hémisphérique de A est maximale avec B ou C, alors B et C sont regroupées et la paire (A ; B ∪ C) est définie comme paire homotope si elle remplit les conditions de bijection de la première étape.

La parcellisation résultante : *Atlas of Inter-Connected Homotopic Area* (AICHA), est présentée Figure 19 et conduit à la création de 192 paires de ROIs homotopes (hROIs) par hémisphère. AICHA est un atlas qui a été spécialement construit pour l'étude de la spécialisation hémisphérique puisqu'il permet de calculer des asymétries dans des régions fonctionnellement homogènes et homotopes d'un hémisphère à l'autre.

[55] L'étape consistant à rendre fonctionnellement homotope les deux hémisphères peut être appliquée aux ROIs de n'importe quel atlas.

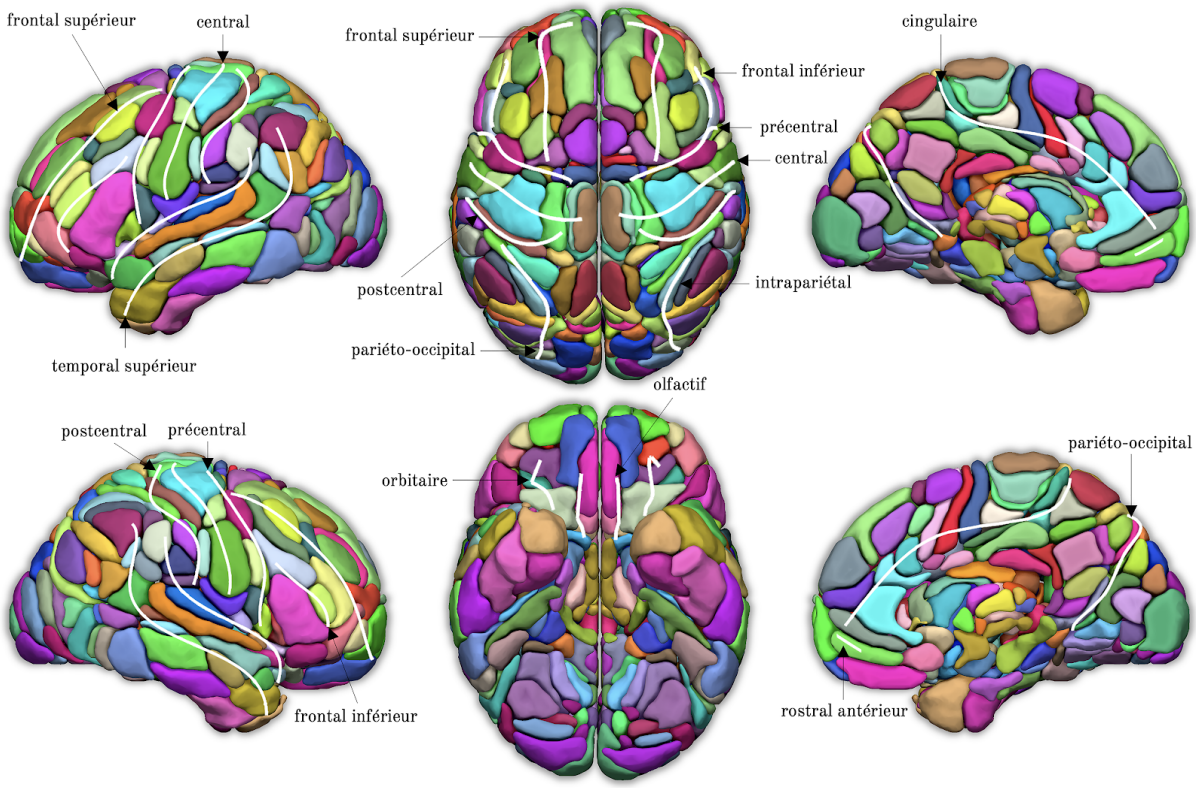

Figure 19 : Rendu 3D des régions de l'atlas AICHA dans l'espace MNI, réalisé à l'aide du logiciel Surf Ice. *Les lignes blanches correspondent aux principaux sillons cérébraux utilisées afin de nommer les hROIs. Figure adaptée de [JOL15].*

2.1.3. Atlas fonctionnel relatif à l'imagerie fonctionnelle évoquée par des tâches cognitives

Un atlas fonctionnel, unique en son genre, est basé sur les tâches évoquées ([DAD20], Figure 20, Tableau 5). Les ROIs de l'atlas sont construites en fonction de l'homogénéité des voxels qui la compose en termes d'activation au cours de différentes tâches cognitives. Il est à noter que les données d'activations proviennent de méta-analyses à partir de la base de données OpenNeuro[56] et donc issues de groupes d'individus différents. Chacune des ROIs de l'atlas se voit attribuer un vecteur contenant les fonctions cognitives les plus probables qui lui sont attribuées (langage, attention, calcul etc...). Une spécificité de cet atlas est que ses ROIs se superposent partiellement ce qui permet de respecter le fait qu'une région cérébrale peut être impliquée dans de multiples tâches cognitives.

[56] OpenNeuro : https://openneuro.org.

Tableau 5 : Caractéristiques de l'atlas fonctionnel d'activation.

	[DAD20]
$N_{Individus}$	522
Données	méta-analyses
Âge (années)	-
IRM	3 T Siemens, 1.5 T Siemens, 3 T General Electrics, 1.5 T General Electrics, 3 T Philips
Morphométrie	volume
Méthode de construction de l'atlas	*sparse dictionary learning*
Régions par hémisphère	32 - 64 - 128 - 256 - 512
Critère de sélection du nombre de régions	optimisation de la fonction d'apprentissage
But	standardiser l'analyse d'images fonctionnelles pour les méta-analyses

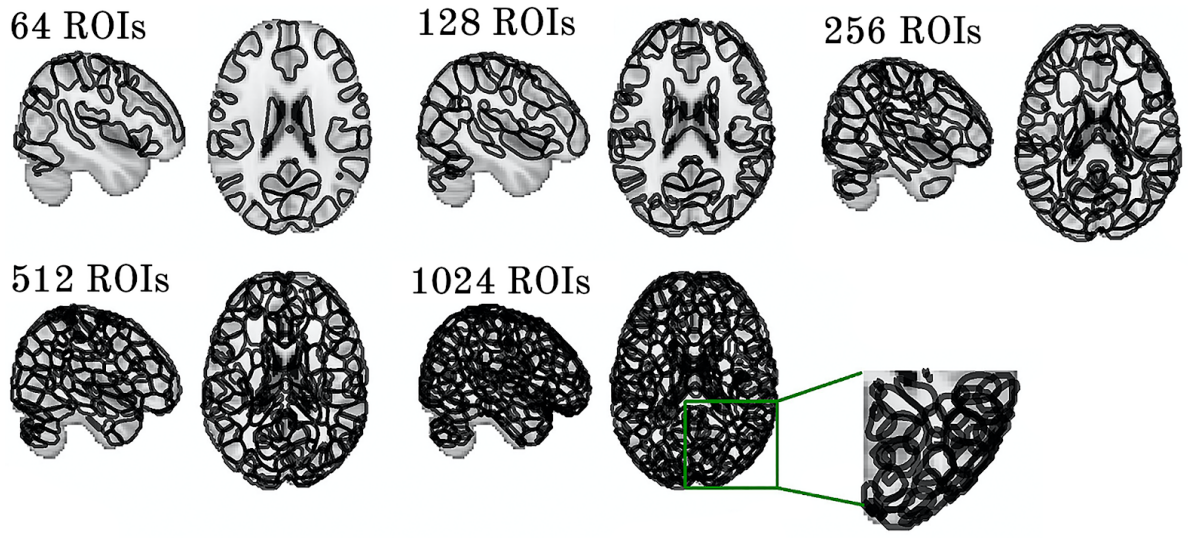

Figure 20 : Rendu de l'atlas fonctionnel d'activation. *Présentation de 5 niveaux de résolution différents : 64, 128, 256 512 et 1024 régions d'intérêts. En bas à droite : zoom sur la résolution à 1024 ROIs permettant de visualiser le recouvrement partiel des régions de l'atlas. Coupes sagittales et axiales de l'hémisphère gauche de l'atlas de [DAD20]. Figure adaptée de [DAD20].*

2.1.4. Les atlas multimodaux

Tableau 6 : Caractéristiques des atlas multi-modaux.

	[DIE15]	[JAM16]	[GLA16]
$N_{Individus}$	12	29	449
Données	moyennes	individuelles et moyennes	individuelles et moyennes
Âge (années)	24 - 46	20 - 50	22 - 35
IRM	1.5 Philips	3 T Philips	3 T Siemens
Morphométrie	volume	volume	surface
Méthode de construction de l'atlas	*spatially constrained n-cut parcellation* pour identification des régions, puis classification ascendante hiérarchique[57] pour identification des réseaux	*spatially constrained n-cut parcellation*	gradient avec *a priori* anatomique, perceptron multicouche[58]
Régions par hémisphère	20	110	180
Critère de sélection du nombre de régions	optimisation de la modularité entre réseaux [GIR02]	minimisation de la fonction de coût de l'algorithme (poids des arêtes reliant deux clusters minimum)	inspection visuelle des gradients
But	relation connectivité structurelle et fonctionnelle	définitions de régions fonctionnellement homogènes au cours de différentes tâches	organisation cérébrale fonctionnelle + étude variabilité interindividuelle

Les atlas multimodaux définissent une ROI en intégrant les informations de différentes modalités d'imagerie ([DIE15], [JAM16] et [GLA16], Figure 21, Tableau 6).

L'atlas de Diez & al., combine l'imagerie de repos et l'imagerie de diffusion ([DIE15], Figure 21 - A). Cet atlas définit des réseaux en regroupant des ROIs dont les limites sont calculées en regroupant les voxels fonctionnellement homogènes (d'après leur matrice de connectivité intrinsèque de l'état de repos) à l'aide de l'algorithme *n-cut* spatialement contraint par leur matrice probabiliste de connectivité structurelle de la substance blanche. L'atlas de James & al. combine la connectivité

[57] Dissimilarité cosinus utilisée pour la classification ascendante hiérarchique.

[58] Le perceptron multicouche est utilisé pour optimiser la position du contour des régions en fonction de leur probabilité de présence à travers les sujets.

intrinsèque avec les résultats des activations obtenues au cours d'un ensemble de 9 tâches cognitives ([JAM16][59], Figure 21 - B).

Le dernier atlas est celui de Glasser & al. qui est le seul à combiner un large ensemble de modalités disponibles en IRM. Il effectue sa parcellisation à partir de variables anatomiques incluant l'épaisseur corticale, la surface corticale, les cartes de myélinisation corticale[60] et un index de gyrification cérébrale, ainsi que des variables fonctionnelles avec la connectivité intrinsèque et les cartes d'activations obtenues au cours de 7 tâches cognitives[61] ([GLA16], Figure 21 - C).

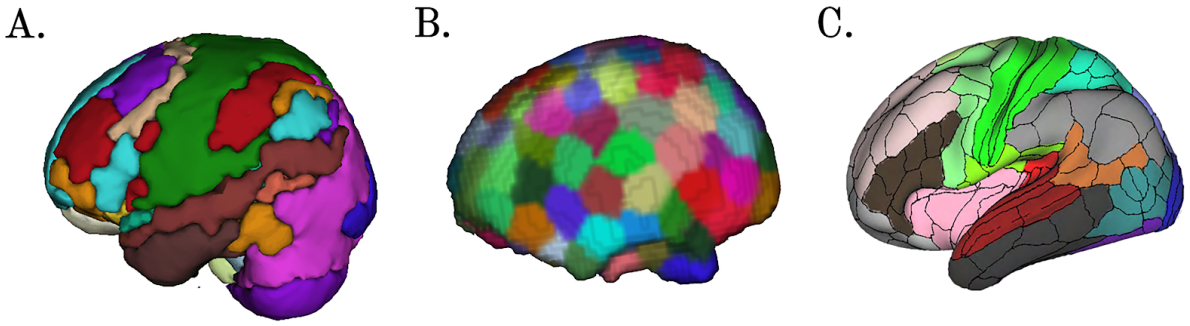

Figure 21 : Rendu des atlas multi-modaux. **A.** *Rendu en volume de l'hémisphère gauche de l'atlas de [DIE15] combinant connectivité intrinsèque et structurelle.* **B.** *Rendu en surface de l'hémisphère gauche de l'atlas de [JAM16] combinant connectivité intrinsèque et activation au cours de 9 tâches cognitives.* **C.** *Rendu en surface de l'hémisphère gauche de l'atlas de [GLA16] combinant connectivité intrinsèque, activations au cours de 7 tâches cognitives, myélinisation et épaisseur corticale.*

2.2. Points méthodologiques sur la création des atlas

2.2.1. Définition manuelle *versus* automatique des limites des ROIs

Méthodologiquement, les premiers atlas anatomiques de Talairach [TAL67] et de Tzourio [TZO02] sont basés sur un sujet particulier.

[59] Basé sur de la connectivité intrinsèque et des activations au cours de 9 tâches cognitives (*Controlled Oral Word Association Task*, *Rating and Recognizing affective images*, *Judgment of Line Orientation task*, *N-back*, *Iowa Gambling Task*, *finger tapping*, *Multi-source Interference Task*, *Verbal Paired Associates*, *Tower of London* and *flashing visual checkerboard*).

[60] La myéline est une gaine de lipide entourant l'axone des neurones afin d'augmenter la vitesse à laquelle les potentiels d'actions sont conduits [KAN13]. L'axone myélinisé peut être comparé à un fil électrique (l'axone) entouré d'un matériau isolant (la myéline).

[61] Basé sur de la connectivité intrinsèque, des activations au cours de 7 tâches cognitives (*N-back*, *gambling task*, mouvement moteur : des mains, des pieds et de la langue, *Auditory sentence presentation with detection of: semantic, syntactic and pragmatic violations*, *Frith–Happe animations of social and random interactions* (théorie de l'esprit), *valence judgments and Hariri Hammer Task, alternating blocks of judgments about relations among features versus feature matching*), des cartes de myélinisation et des cartes d'épaisseurs corticales.

Les méthodes utilisées pour définir les atlas anatomiques les plus récents comme celui de Glasser ou de Destrieux et Desikan combinent des méthodes supervisées ou d'apprentissage avec une approche manuelle basée sur l'expertise, à l'inverse des autres atlas qui se basent sur des méthodes mathématiques automatisées et non supervisées. Citons par exemple, parmi les plus utilisées, la méthode des *k-means* [STE56], la classification ascendante hiérarchique [SNE73], et l'algorithme *n-cut* [SHI00] qui regroupent les voxels en fonction de leur homogénéité. Ces algorithmes se basent soit sur les composantes principales d'une analyse en composantes indépendantes des matrices de connectivité intrinsèque, soit sur une analyse spectrale de ces mêmes matrices.

Le seul atlas mélangeant les deux techniques, à la fois supervisée et non supervisée, est l'atlas de Glasser [GLA16] qui intègre en effet un *a priori* anatomique avant de définir ces régions. Les experts sélectionnent, au cours de la procédure, les contours des régions étant les plus en accord avec des dizaines d'années de connaissances sur l'anatomie cérébrale. Ces connaissances peuvent *a priori* contraindre la parcellisation régionale finale obtenue [EIC18b].

2.2.2. Construction de ROIs à partir d'un seul individu ou d'une moyenne d'individus

67% des atlas se basent sur une combinaison de l'analyse des données individuelles et moyennes, 19% sur la moyenne de l'ensemble des données et 14% exclusivement sur l'analyse des données individuelles. Pour la plupart des atlas présentés, la variabilité interindividuelle et l'éloignement des individus à la moyenne sont donc pris en compte lors de l'élaboration de la parcellisation du cortex cérébral en régions d'intérêts.

2.2.3. Nombre de régions d'intérêts

Les atlas récents proposent plusieurs niveaux de parcellisation, *i.e.* pour un même atlas un nombre différent de régions sera proposé en fonction de la granularité souhaitée lors des analyses. Dans cette revue, le nombre de régions d'intérêts par hémisphère s'étend de 7 à 1000 pour un total de 43 parcellisations différentes disponibles, avec une moyenne de 206 ROIs ($\pm$ 255). Concernant le nombre optimal de

ROIs, ce dernier n'existe pas, puisqu'il dépend de la résolution envisagée pour une étude donnée et de la puissance de l'appareil à IRM. Les études s'accordent malgré tout pour un nombre adéquat entre 150 et 200 ROIs par hémisphère ([ESS12], [MES20] et [DAD20]) étant donné la résolution des appareils aujourd'hui disponibles (≃ 3T).

2.3. Conclusion concernant les atlas cérébraux

En conclusion, cette revue des atlas existants montre une parcellisation du cerveau complète et la possibilité d'intégrer plusieurs modalités, selon l'objectif fixé. Une lecture attentive montre que la méthodologie utilisée pour chaque atlas dépend de l'usage envisagé, par exemple : localisation anatomique pour l'atlas de Talairach [TAL67] ou AAL [TZO02], identification de régions fonctionnelles incluant la profondeur des sillons pour l'atlas de Glasser [GLA16], mise à disposition de l'organisation en termes de connectivité anatomique et/ou fonctionnelle ([ZHU13] et [YEO11]).

L'objectif de cette thèse était de créer une parcellisation cérébrale des régions et des réseaux sous-tendant les grandes fonctions cognitives latéralisées : langage, attention, motricité, calcul... Cet objectif nous a donc conduit à développer une méthodologie originale qui nous permet de définir ces atlas de régions et de réseaux, en débutant avec le langage. Voici les particularités de la construction des atlas présentés dans cette thèse :

- Nous avons travaillé à partir d'une seule base de données où ces fonctions sont documentées chez chaque sujet (BIL&GIN, [MAZ16]) acquis sur la même machine de manière à optimiser l'homogénéité et la sensibilité.
- Contrairement aux atlas précédents qui n'ont pas procédé à une sélection *a priori* des individus constituant les templates, notre objectif nous a conduit à sélectionner les sujets droitiers présentant peu de variabilité en termes d'asymétries fonctionnelles.
- Pour identifier les régions spécifiques constituantes d'un atlas donné, comme pour les autres atlas, nous avons défini les variables pertinentes : les asymétries et conjonctions à travers plusieurs tâches. Une fois ces régions, support de l'activité cognitive, identifiées avec une approche

multi-tâches, nous avons utilisé l'état de repos, pour poser la question de l'organisation en réseaux au sein de ces régions.

- Pour préciser le type d'organisation des réseaux des fonctions cognitives et mettre en évidence les hubs, permettant de cibler les aires dites "essentielles" ou épicentres : c'est-à-dire celles dont la lésion provoque un déficit [MES90], nous avons utilisé les mesures fournies par la théorie des réseaux (centralité de degré, sunexité et coefficient de participation).
- Comme dans [DIE15], nous avons utilisé un algorithme de classification ascendante hiérarchique afin de regrouper en réseau les ROIs ayant un pattern de connectivité intrinsèque similaire.
- Nous avons utilisé l'atlas AICHA [JOL15] comme parcellisation initiale, car il définit un nombre de ROI optimal et permet de réaliser des mesures d'asymétries.

3. Application de l'analyse par conjonction, des outils de classification hiérarchique et de la théorie des réseaux à la construction et la caractérisation d'atlas

3.1. Identification du support anatomique des fonctions cognitives latéralisées

Comme nous l'avons vu, les atlas issus de la littérature sont des atlas parcellisant le cerveau dans sa globalité. Les atlas développés au cours de cette thèse ont la particularité d'être des atlas des fonctions cognitives latéralisées. Une étape importante de la mise au point de ces atlas concerne alors la sélection des régions cérébrales (ou ROIs) dédiées à la fonction et ciblant le niveau hiérarchique d'intérêt.

Pour identifier des ROIs communes à différentes tâches d'un même processus cognitif, il est courant en neuroimagerie d'utiliser une approche par conjonction. Elle consiste simplement à identifier les ROIs significativement activées et/ou asymétriques dans plusieurs tâches et cette approche statistique est disponible dans SPM [PEN11] en fixant un seuil statistique donné. La méthode par conjonction offre une approche

robuste pour la cartographie et l'identification d'unités fonctionnelles (au sens des champs fonctionnels) [EIC18a].

Les méthodes d'identification des ROIs engagées dans une fonction cognitive spécifique dépendent du type de tâche et du type de processus impliqué dans celle-ci. Par exemple, pour SENSAAS (*SENtence Supramodal Areas AtlaS*, [LAB19]) les *a priori* sont multiples : 1- les processus de bas niveau (dont : engagement attentionnel, maintenance de la consigne, articulation...) liés au langage ont été supprimés par l'utilisation de tâches de référence (production, écoute et lecture de liste de mots sur-appris, Figure 5) permettant de calculer un contraste "phrase - liste" (production, écoute et lecture de phrase) ; 2- les ROIs dont le profil est supramodal[62]ont été sélectionnées comme impliquées dans les 3 tâches de langage (production, écoute et lecture) ; 3- enfin de manière à sélectionner les régions langagières un critère d'activation et d'asymétrie gauche a également été appliqué.

Le même type d'*a priori* a été appliqué à la construction de WMCA (*Word-list Multimodal Cortical Atlas*, [HES19]), mais la sélection a été réalisée sur les tâches de langage de bas niveau et nous avons sélectionné pour cet atlas les ROIs activées et asymétriques dans l'un ou l'autre des deux hémisphères cérébraux (Figure 22).

[62] Les régions cérébrales supramodales font fi de la modalité du stimulus.

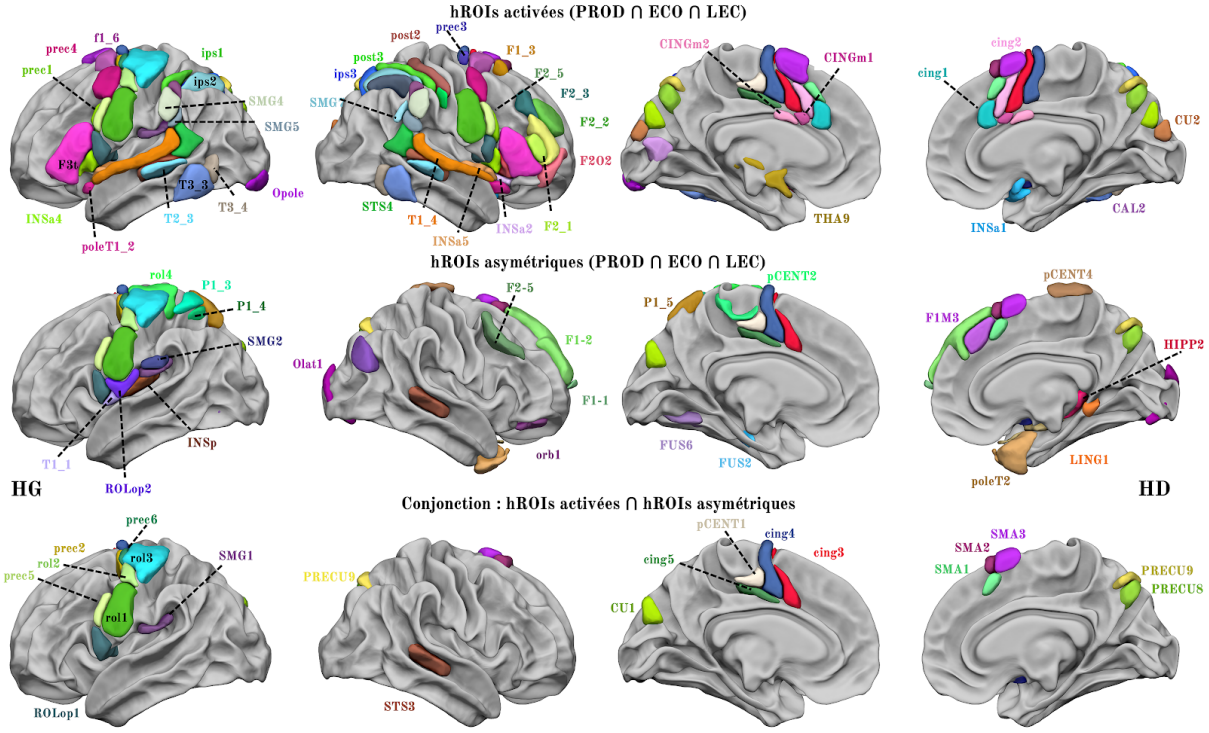

Figure 22 : Régions de WMCA. **Ligne du haut :** *Régions de l'atlas AICHA significativement activées dans les 3 tâches (PROD : production, ECO : écoute, LEC : lecture de liste de mots sur-appris).* **Ligne du milieu :** *hROIs asymétriques dans les 3 tâches.* **Ligne du bas :** *hROIs significativement co-activées et co-asymétriques dans les 3 tâches. HG : hémisphère gauche, HD : hémisphère droit. Les hROIs sont projetées sur la surface de la substance blanche du gabarit de la BIL&GIN dans l'espace MNI, réalisée à l'aide du logiciel Surf Ice. Les noms complets des hROIs correspondant aux abréviations peuvent être trouvés dans [HES19]. Figure adaptée de [HES19].*

Concernant l'identification des 12 ROIs supportant le contrôle sensorimoteur de la main (*Hand Atlas of MOTor Areas* : HAMOTA, [TZO20]), les *a priori* étaient l'activation et l'asymétrie des régions controlatérales à la main utilisée pour réaliser la tâche (FTT : *Finger-Tapping Test*[63]), et donc changeant d'hémisphère avec la main utilisée. Cette procédure de sélection des hROIs a été réalisée séparément dans une population de droitiers et dans une population de gauchers. Les hROIs finalement sélectionnées sont les hROIs communes aux droitiers et aux gauchers (Figure 23).

[63] La tâche de FTT permet de mesurer l'habileté manuelle d'un individu [PET78]. L'individu doit taper avec son index sur le bloc-réponse à une fréquence de 2 Hz, aussi régulièrement que possible.

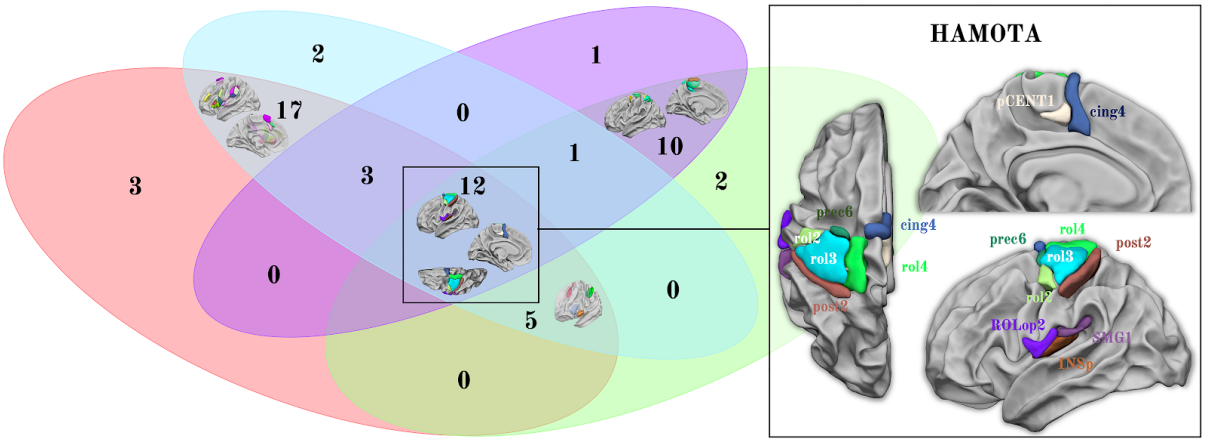

Figure 23 : Diagramme de Venn et régions de HAMOTA. *Diagramme de Venn de l'analyse par conjonction conduisant en l'identification du support anatomique de la préférence manuelle [TZO20]. Le cercle rouge correspond aux hROIs significativement activées controlatéralement durant la tâche de FTT chez les droitiers. En bleu : les hROIs significativement activées controlatéralement chez les gauchers. En violet : les hROIs significativement asymétriques controlatéralement chez les gauchers. En vert : les hROIs significativement asymétriques controlatéralement chez les droitiers. Le nombre en noir correspond au nombre de régions identifiées pour la conjonction regardée. L'encadré correspond aux hROIs de l'intersection des 4 cercles : i.e. le support anatomique de la préférence manuelle. Les noms complets des hROIs correspondant aux abréviations peuvent être trouvés dans [TZO20]. Vues de l'hémisphère gauche ; rendu 3D de la surface de la substance blanche du gabarit de la BIL&GIN dans l'espace MNI, réalisé à l'aide du logiciel Surf Ice.*

Un dernier atlas a été développé au cours de cette thèse concernant les bases anatomo-fonctionnelles de l'attention [ZAG20] : *Atlas of Lateralized Attention Networks* (ALANs, Figure 24). La question des réseaux cérébraux sous-tendant la dominance des fonctions attentionnelles spatiales chez l'Homme est une question ouverte [HER13]. Nous proposons d'identifier les réseaux latéralisés de l'attention en utilisant un critère d'asymétrie et d'activation en faveur de l'hémisphère droit au cours d'une tâche attentionnelle de haut niveau : une tâche de Jugement de Bissection de Ligne[64] (JBL). L'attention est en effet une fonction latéralisée dans l'hémisphère droit chez les droitiers [ZAG16]. Le premier *a priori* que nous avons posé pour la sélection des aires attentionnelles était une activation et une asymétrie droite. Pour choisir les hROIs de haut niveau, nous avons utilisé une tâche de Saccades Guidées Visuellement[65] (SGV) comme référence. Cela nous a permis de distinguer : 1- Les hROIs à la fois activées et asymétriques droites durant les tâches de SGV et de JBL ; 2- Les hROIs

[64] La tâche de Jugement de Bissection de Ligne (JBL) permet d'évaluer les processus attentionnels en jugeant si la barre verticale présentée à l'écran est au centre, déviée à droite ou à gauche du segment horizontal coupé en deux par une petite barre verticale [MAZ16].

[65] La tâche de Saccades Guidées Visuellement (SGV) permet d'évaluer les processus attentionnels en suivant un repère visuel qui apparaît de manière alternative à gauche ou à droite de l'écran [MAZ16].

activées à droite dans les deux tâches et asymétriques droites uniquement pendant JBL ; 3- Les hROIS activées et asymétriques droites uniquement au cours de JBL. Ceci a permis de distinguer les hROIs impliquées par le déplacement de l'attention et l'activité oculomotrice lors de la tâche de SGV des hROIs sous-tendant les mécanismes attentionnels intégrés spécifiques de la tâche de JBL (Figure 24).

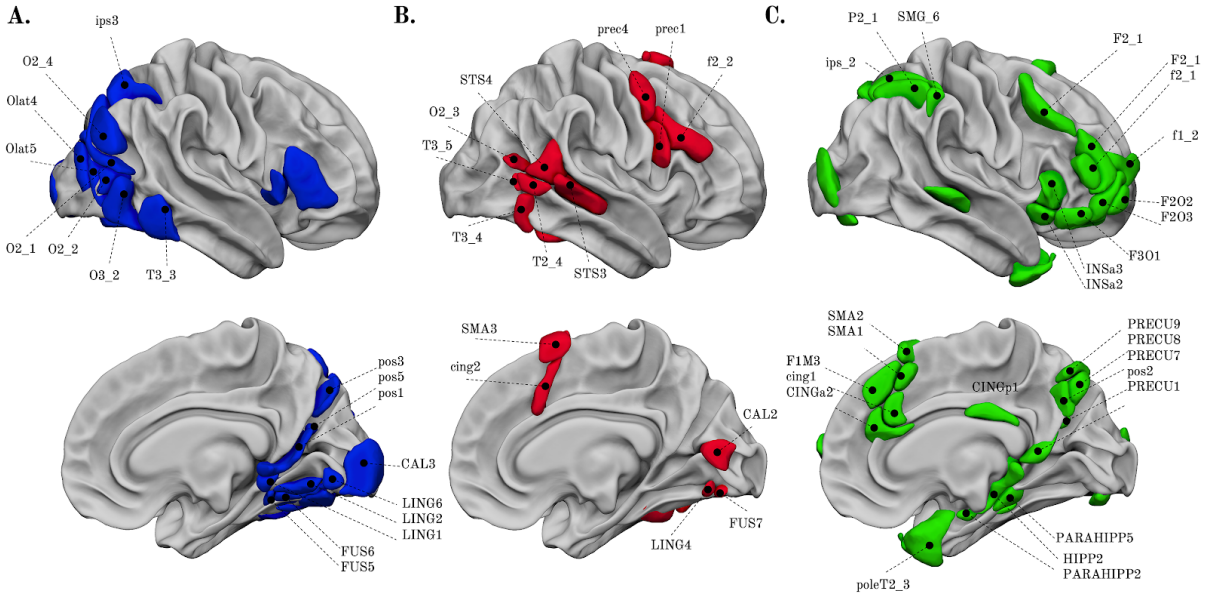

Figure 24 : Régions de ALANS. *Les trois panels correspondent aux régions de l'atlas AICHA significativement activées et asymétriques dans l'hémisphère droit durant la tâche de Jugement de Bissection de Ligne (JBL).* **A.** *En bleu : les hROIs également activées à droite dans la tâche de Saccades Guidées Visuellement (SGV).* **B.** *En rouge : les hROIs également activées et asymétriques à droite dans SGV.* **C.** *En vert : les hROIs spécifiques à JBL. Les hROIs sont projetées sur la surface de la substance blanche du gabarit de la BIL&GIN dans l'espace MNI, réalisé à l'aide du logiciel Surf Ice. Les noms complets des hROIs correspondant aux abréviations peuvent être trouvés dans[ZAG20]. Figure adaptée de [ZAG20].*

Afin de permettre une représentation des données applicables à des définitions variables en fonction du besoin, j'ai développé un outil, qui a été mis à la disposition de l'équipe, permettant, pour un seuil statistique fixé, de visualiser à l'aide d'un diagramme de Venn [VEN80] l'ensemble des conjonctions possibles pour différentes combinaisons d'*a priori* préalablement définis. Par exemple, concernant HAMOTA, cette approche permet de mettre en évidence, pour des groupes de sujets différents : *i.e.* droitiers ou gauchers, les ROIs asymétriques controlatérales dans les 2 tâches de FTT (réalisée avec la main gauche ou droite), l'absence de ROIs uniquement controlatéralement activées et asymétriques chez les droitiers ou les gauchers, et finalement de visualiser les 12 régions respectant l'ensemble des contraintes, au centre du diagramme (Figure 23).

La visualisation via le diagramme de Venn garantit une vision d'ensemble concernant les profils d'implication des régions cérébrales dans les différents processus cognitifs.

L'outil que j'ai développé permet dans un premier temps de réaliser l'analyse par conjonction, puis d'appliquer une classification hiérarchique suivant les critères voulus (que nous présenterons dans le sous-chapitre suivant), et finalement de procéder à une analyse topographique des hROIs constituantes des partitions identifiées (également présentée par la suite).

Je présente ci-dessous les possibilités offertes par l'outil développé afin de réaliser l'analyse par conjonction.

Pour l'identification des réseaux du langage du traitement de la phrase [LAB19] les *a priori* concernant la sélection des hROIs sont multiples. Une hROI, pour se voir sélectionnée, doit en effet dans un premier temps respecter un critère d'activation et d'asymétrie en faveur de l'hémisphère gauche : *i.e.* significativement activée en moyenne ($\overline{BOLD_{HG}} > 0$ et $p\text{-}value < 0.05$, test de Student bilatéral) et asymétrique gauche ($\overline{Asymétrie} > 0$ et $p\text{-}value < 0.05$, test de Student bilatéral). La deuxième contrainte, permettant de sélectionner les hROIs supramodales, consiste en la conjonction des hROIs sélectionnées par la première contrainte à travers les 3 tâches cognitives disponibles dans la BIL&GIN : l'écoute, la lecture et la production du langage. Concernant le traitement de la phrase, l'analyse est restreinte à l'hémisphère gauche. L'outil permet également de réaliser des analyses sur les 2 hémisphères à la fois comme illustré dans [HES19] qui identifie le support anatomique du traitement du mot.

L'outil d'analyse par conjonction permet également d'ajuster le seuil de significativité de sélection d'une hROI comme par exemple dans le cas de l'étude des réseaux supportant les processus attentionnels [ZAG20]. Dans le cadre de cette étude une correction de Bonferroni [BON36] a été appliquée puisqu'aucune conjonction entre tâches cognitives n'a été réalisée. La correction de Bonferroni permet de contrôler le taux d'erreur de première espèce du test de Student employé, en corrigeant le seuil de

significativité par le nombre de tests réalisés. L'erreur de première espèce correspond à la probabilité de rejeter l'hypothèse nulle alors que celle-ci est vraie. L'utilisation de la correction de Bonferroni dans le cadre de la construction de nos atlas permet donc de s'assurer de la réelle implication d'une hROI dans le processus cognitif regardé en étant conservatif, bien que cette correction augmente le risque de seconde espèce qui correspond au rejet de l'hypothèse alternative alors qu'elle est vraie [NAK04].

3.2. La classification hiérarchique : un outil multifonction pour la création des atlas cérébraux et leurs études

J'ai utilisé la classification ascendante hiérarchique (CAH) pour répondre à trois questions différentes : celle des différences des profils de hROIs communément activées et asymétriques dans une ou plusieurs tâches (cas *1*), l'identification des réseaux fonctionnels au sein d'ensembles de hROIs à partir des mesures de connectivité intrinsèque (cas *2*), et l'identification de groupes d'individus en fonction de leurs caractéristiques régionales en termes d'activations, d'asymétries et de connectivité intrinsèque dans le cadre de l'étude de la variabilité interindividuelle (cas *3*).

La classification ascendante hiérarchique ([SNE73]) est une méthode ayant pour objectif d'établir une hiérarchie de classes en répartissant les n variables de son ensemble de construction Ω en un certain nombre de partitions. La méthode se base sur le calcul d'une matrice symétrique de dissimilarité D ($dim(D) = n * n$) représentant la distance entre les $n(n-1)/2$ paires d'objets possibles. Dans les cas *(1)* et *(3)*, la distance utilisée correspond à la distance Euclidienne usuelle calculée à partir des variables dont les valeurs ont été centrées et réduites. Dans le cas *(2)*, la matrice des distances $D_{i,j}$ utilisée est construite à partir de la matrice des corrélations ($M_{i,j}$) telle que $D_{i,j} = (1 - M_{i,j})/2$ [LAN79], pour $(i, j) = 1, 2 \ldots n$. La hiérarchie entre les n objets est établie par itération en regroupant successivement les objets dont la dissimilarité est la plus faible. Lorsqu'un objet doit être agrégé avec une classe contenant plusieurs objets, la dissimilarité est calculée en utilisant le critère de Ward [WAR63] qui permet de maximiser l'inertie inter-classe et donc d'obtenir *in fine* des partitions dont la variance interne est minimale.

Le nombre “optimal” de classes a été déterminé à l'aide de la librairie R "*NbClust*" [CHA14]. Cette librairie fournit 30 indices statistiques permettant de déterminer le nombre “optimal” de classe d’une CAH et propose le meilleur regroupement à partir des différents résultats obtenus en faisant varier toutes les combinaisons du nombre de classes pour la méthode choisie, en l'occurrence une classification ascendante hiérarchique utilisant le critère de Ward.

3.2.1. La classification ascendante hiérarchique comme outil de caractérisation de l’implication des hROIs dans un processus cognitif d’intérêt

Dans le *1er* cas, en prenant pour exemple le travail sur WMCA [HES19], bien que l’analyse par conjonction nous permette de conclure quant à la nature hétéromodale des hROIs identifiées, elle ne nous apporte aucune information concernant la variabilité de l’implication et de latéralisation de chaque hROI dans les processus mis en jeu. Dans ce cadre, la CAH est un outil *ad hoc* permettant de caractériser l’ensemble de hROIs identifiées en regroupant les hROIs ayant un profil similaire d’activations et d’asymétries. Dans le cadre de cette étude, la CAH a notamment mis en avant une partition en 3 classes dans l’hémisphère gauche : une classe contenant les hROIs correspondant au gyrus supramarginal, une classe motrice et une autre prémotrice, supportant l’hypothèse selon laquelle le circuit perception-action [PUL16] est impliqué dans les processus phonologiques et ce, quelle que soit la modalité de la tâche. Ces résultats sont disponibles dans la première version de l’article déposé sur la plateforme *bioRxiv*, résultats qui n’ont pas été publiés dans la version finale de ce travail.

3.2.2. La classification ascendante hiérarchique comme outil d’identification des réseaux du repos

La seconde manière d’utiliser la CAH au cours de cette thèse portait sur l’identification des réseaux de connectivité intrinsèque présents au sein des ensembles de hROIs identifiées à l’aide de l’analyse par conjonction (cas *2*). Dans cette perspective, la CAH a été réalisée en utilisant l’algorithme de Ward qui est particulièrement adapté puisqu’il permet d’estimer la représentation multi-échelles de l’activité cérébrale à l’état de repos ([MIC12] et [ORB15]). Plus particulièrement,

l'organisation hiérarchique des partitions obtenues à partir du signal BOLD à l'état de repos est plus stable via une analyse sur la moyenne de la population [ORB15], comme c'est ici le cas.

Dans l'exemple de [HES19], la CAH a été réalisée sur la matrice moyenne de connectivité intrinsèque représentant la connectivité fonctionnelle de 21 hROIs situées sur l'hémisphère gauche pour 14 d'entre elles et droit pour le reste. La classification a alors permis d'établir un modèle cérébral anatomo-fonctionnel de l'organisation des processus phonologiques. Ce modèle repose notamment sur un réseau intrinsèque impliquant de manière concomitante le sillon temporal de l'hémisphère droit (*i.e.* l'aire postérieure de la voie humaine : [PER15]) et le gyrus supramarginal de l'hémisphère gauche reflétant, pour la première fois, l'imbrication hétéromodale entre l'information prosodique[66] et phonémique[67]. Ces résultats ont récemment été appuyés par l'étude de Floegel & al. [FLO20].

3.2.3. La classification ascendante hiérarchique comme outil de l'étude de la variabilité interindividuelle

Bien que 90 % de la population soit considérée comme typique pour la production du langage [MAZ14], les 10% restants présentent une forte variabilité allant d'une dominance bi-hémisphérique ou une dominance inverse alors supportée par l'hémisphère droit [ZAG17]. Cette dominance traduit la spécialisation hémisphérique d'une fonction cognitive : spécialisation définie comme la relation d'interdépendance hémisphérique entre une fonction et son support anatomique [TZO16b]. La caractérisation des patterns régionaux, des structures anatomiques et de leur relation avec la préférence manuelle chez les individus atypiques est alors une question fondamentale afin d'étudier si cette atypicité est valable pour d'autres phénotypes fonctionnels cognitifs et si ces phénotypes sont associés à des variations de comportement et de capacités cognitives.

L'examen de l'organisation fonctionnelle du réseau du langage dans l'hémisphère dominant ainsi que sa coordination interhémisphérique avec son contraposé dans

[66] La prosodie correspond à l'ensemble des traits vocaux au cours de l'expression verbale : inflexion, ton, tonalité, intonation, accent et modulation de la voix, entre d'autres termes la prosodie est la musique de la parole.

[67] Un phonème est la plus petite unité sonore de l'expression verbale. Le français par exemple comprend 36 phonèmes : 16 voyelles et 20 consonnes.

l'hémisphère opposé est donc nécessaire. J'ai ainsi questionné la variabilité inter-individuelle (cas *3*) de la spécialisation hémisphérique pour le langage en utilisant l'atlas SENSAAS [LAB19] dans un échantillon de 287 individus [LAB20]. Pour ce faire, j'ai utilisé la CAH sur plusieurs modalités et plusieurs échelles. En effet, chacune des partitions obtenues se caractérise non seulement par des valeurs d'asymétries lors de trois tâches langagières (production, écoute et lecture), mais également par le degré de centralité et de corrélation inter-hémisphérique, tant au niveau régional que du réseau du langage de haut niveau identifié dans SENSAAS. Ce travail identifie trois classes d'individus caractérisés par des organisations inter- et intra-hémisphériques du réseau du langage différentes : deux groupes d'individus typiques et un groupe d'individus atypiques. Il nous a également permis de caractériser dans ces 3 groupes la variabilité de l'intégration de l'information au repos dans les régions de SENSAAS, d'analyser l'occurrence des dissociations de latéralisation du langage au cours de différentes modalités et de mettre en avant des différences d'organisation anatomique et de compétences cognitives.

J'ai d'autre part développé au cours de cette thèse une méthode de CAH permettant de prendre en compte la variabilité inter-individuelle (cas *3*) lors de la classification et de questionner l'existence de sous-populations au sein d'une population de départ (*cf.* Partie III), notamment dans le cadre des données de connectivité intrinsèque qui sont de véritables empreintes digitales et permettent d'identifier un individu [FIN15]. Actuellement, il n'existe pas de méthode adaptée afin de répondre à cette question avec le type de données dont nous disposons : des données d'IRMf tridimensionnelles, *i.e.* une matrice de connectivité intrinsèque par individu. En 2006, Suzuki & Shimodaira ont développé une méthode, nommée *pvclust* [SUZ06], permettant d'évaluer la stabilité d'une partition d'un dendrogramme à l'aide du calcul d'une *p-value* non biaisée obtenue par ré-échantillonnage [EFR96]. Cette méthode convient à des données classiques en 2 dimensions, mais lorsqu'elle est adaptée à des données tridimensionnelles, la *p-value* obtenue ne reflète pas la stabilité des partitions à travers la population, mais la proportion d'individus nécessaire afin d'obtenir une matrice de connectivité moyenne stable à un seuil fixé.

3.3. La théorie des graphes comme outil pour la caractérisation topographique du support anatomo-fonctionnel des réseaux cérébraux

Le dernier outil utilisé au cours de cette thèse a été la théorie des graphes (ou réseaux) dans le but de caractériser l'organisation topographique des réseaux cérébraux supportant la latéralisation des fonctions cognitives au repos.

Le concept de *connectome* est au coeur de la réflexion actuelle sur les réseaux cérébraux [FOR15]. Ce terme a été introduit pour la première fois en 2005 dans la publication du Pr. Olaf Sporns : *the human connectome* [SPO05], afin de définir une matrice représentant toutes les paires possibles de connexions anatomiques entre les différents éléments cérébraux (du neurone à la région). Initialement, ce terme représente donc l'état canonique des connaissances sur les connexions structurelles de la substance blanche. Cependant, au cours des 15 dernières années, l'étude du *connectome* cérébral humain a connu un développement important. Le concept s'est généralisé et il inclut à la fois les matrices de connexions structurelles entre des régions cérébrales obtenues à l'aide de la tractographie [GU15], les matrices d'interactions fonctionnelles obtenues via la connectivité intrinsèque (en IRMf : [ZUO12], ou en iEEG[68] : [HE08b]) et les matrices quantifiant les oscillations d'activité neuronale à plus hautes fréquences détectables par les techniques d'électro- [ENG13] et magnéto-physiologie [KIT15].

Au total, le cadre du *connectome* offre une approche conceptuelle visant à quantifier, visualiser et comprendre l'organisation en réseaux de l'activité neuronale à de multiples échelles variant dans le temps et l'espace ([BAS17], Figure 25). Le domaine de la théorie des graphes appliquée aux neurosciences permet également, grâce à l'étude des propriétés topologiques des réseaux à différentes échelles (spatiales et temporelles), d'étudier la manière dont l'information est analysée et transmise d'une échelle à l'autre, mais aussi de quelle façon la structure des réseaux contraint cette transmission de l'information ([BET17], Figure 26).

[68] iEEG : ElectroEncéphaloGraphie intracrânienne. L'iEEG permet l'enregistrement des potentiels de champs locaux directement sur la surface corticale au moyen d'électrodes.

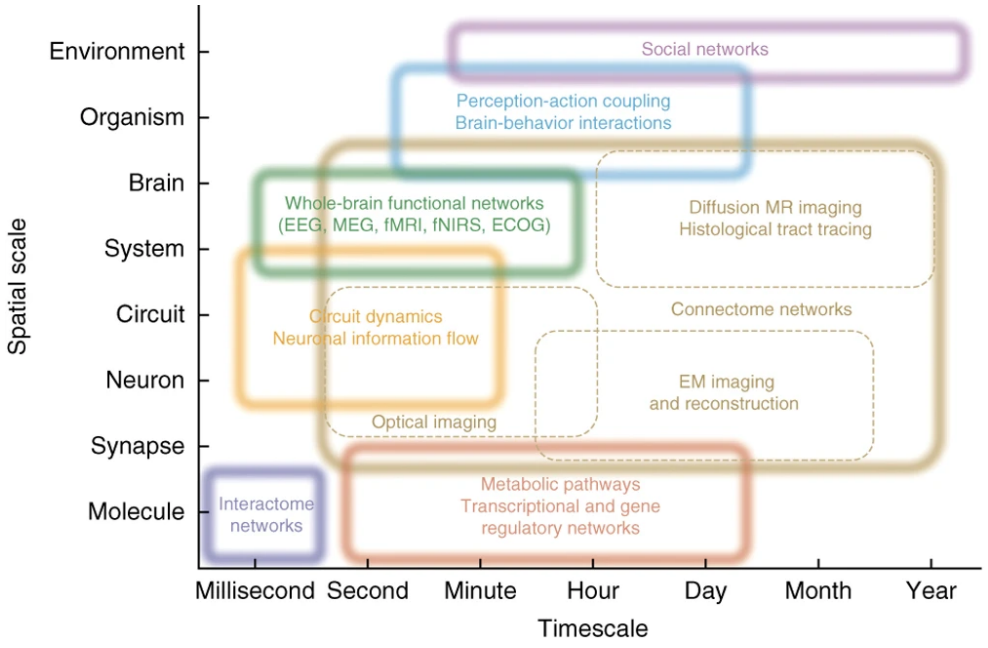

Figure 25 : Illustration des différentes échelles temporelles et spatiales couvertes par le concept de connectome dans le cadre de l'étude de l'organisation cérébrale et du comportement humain. *Chaque cadre représente les différents éléments étudiés à l'aide de la théorie des graphes pour une échelle temporelle et spatiale donnée. Cette figure peut être mise en parallèle à la Figure 2. Figure adaptée de [BAS17].*

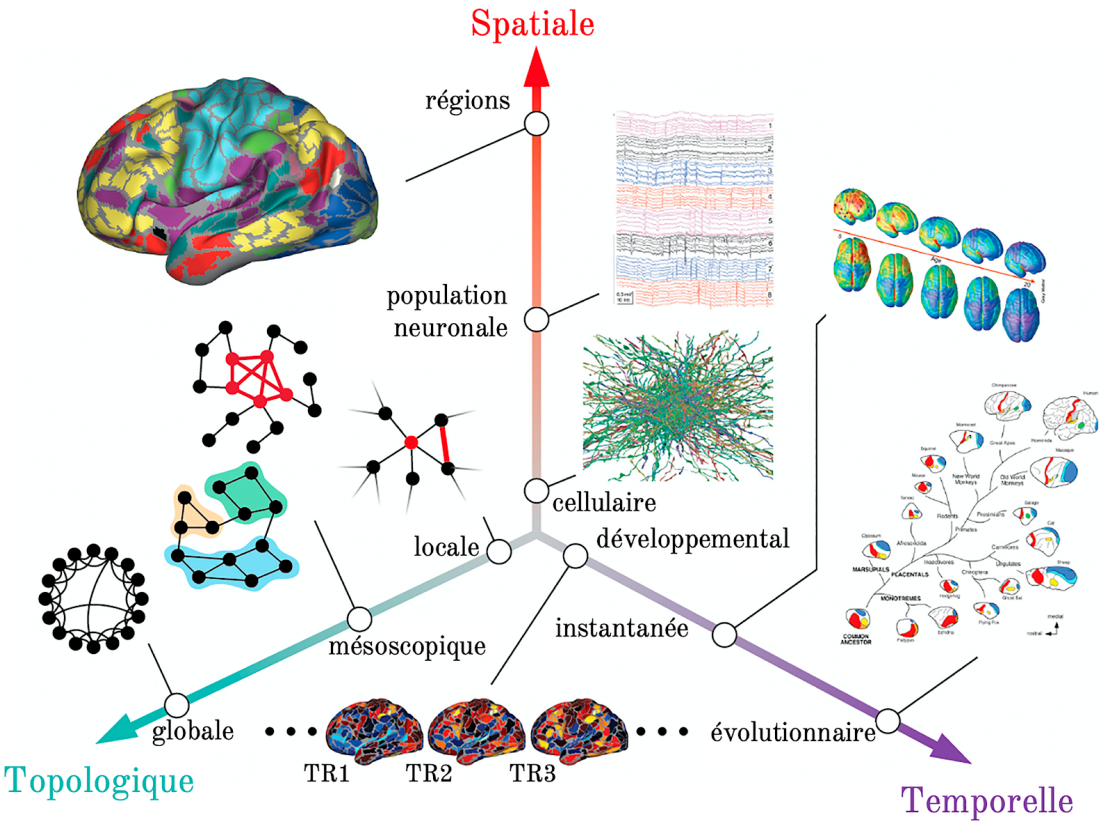

Figure 26 : Illustration du cerveau à différentes échelles et de ses mesures topologiques. *Les réseaux cérébraux sont organisés à plusieurs échelles spatio-temporelles et peuvent être analysés à des échelles topologiques (réseaux) allant des propriétés des sommets individuellement, au réseau dans son ensemble. Figure adaptée de [BET17].*

Dans le cadre de ma thèse, j'ai travaillé sur le *connectome* fonctionnel : *i.e.* l'étude topologique des sommets des graphes constitués à partir des matrices de connectivité intrinsèque. Dans ce cadre, chaque ligne ou colonne de la matrice $M_{i,j}$ représente une région cérébrale différente correspondant aux n sommets du graphe, tandis que les valeurs de chaque élément $M_{i,j}$ ($(i, j) = 1, 2 \ldots n$) de la matrice représente le poids de l'arête reliant les deux sommets i et j considérés (Figure 27). Afin de quantifier l'organisation topologique d'un tel graphe [BUL09], il est possible de calculer plusieurs mesures issues de la théorie des graphes telles que la centralité de degré et la sunnexité (ou centralité d'intermédiarité).

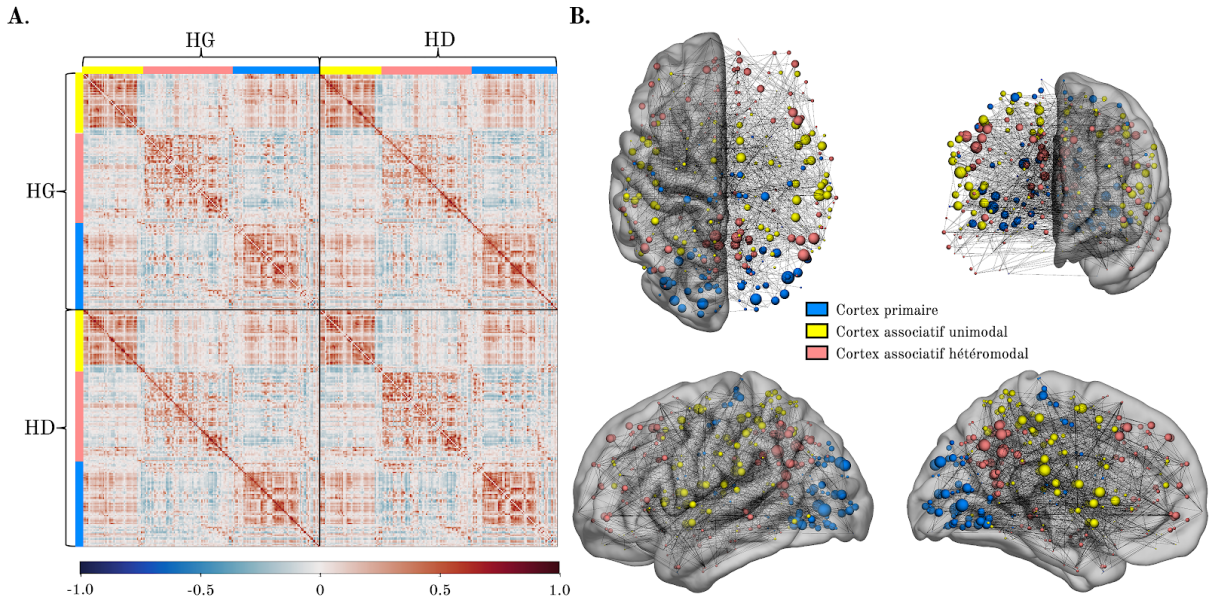

Figure 27 : Représentation en réseau de la connectivité intrinsèque cérébrale globale. **A.** *Matrice de connectivité intrinsèque moyenne de 67 individus droitiers typiques (d'après [LAB20]). Chaque ligne/colonne correspond à une des 384 hROIs d'AICHA. Les rectangles jaune, saumon et bleu correspondent aux hROIs du cortex associatif unimodal, hétéromodal et primaire respectivement (d'après les résultats illustrés en Figure 11). Les valeurs de la matrice correspondent aux corrélations entre 2 signaux BOLD à l'état de repos : plus la case est bleue, plus la corrélation est négative, plus elle est rouge, plus elle est positive. HG : hémisphère gauche, HD : hémisphère droit.* **B.** *Visualisation sous forme de graphe, projeté dans l'espace MNI, de la matrice de connectivité intrinsèque présentée en* **A**. *Les sommets (ou hROIs) du graphe sont représentés par des sphères dont les coordonnées correspondent au centre de masse des hROIs d'AICHA. La taille des sphères est proportionnelle à leur valeur de centralité de degré pondérée. Seuls les 5% des corrélations positives les plus élevées sont affichées. Les segments noirs correspondent aux arêtes reliant deux sommets.*

Le calcul des différentes mesures caractérisant les sommets du graphe est uniquement réalisé sur les coefficients de corrélation de Pearson positifs de la matrice de connectivité intrinsèque, en conservant les coefficients de corrélation faibles. En effet, les méthodes actuelles de théorie des réseaux ne permettent pas de quantifier le

rôle des corrélations fonctionnelles négatives dans l'organisation globale d'un réseau ([RUB10] et [POW10]). Les faibles corrélations positives (≃0) sont conservées depuis que leur importance a été démontrée, notamment dans la caractérisation de la topologie des individus atteints de schizophrénie [BAS12], et dans l'explication de la variabilité interindividuelle des performances cognitives ([COL12] et [SAN14]).

La centralité de degré pondérée (DC : *degree centrality*, [RUB10]) est la mesure la plus simple qu'il est possible de calculer dans un graphe. La DC correspond à la somme des corrélations de chaque sommet j :

$$DC_i = \sum_{j}^{n} M_{i,j}$$

La DC est interprétée comme étant la quantité d'informations qu'une région va recevoir de la part des autres régions du réseau auquel elle est directement connectée. Elle mesure alors l'importance d'une région donnée au sein de son réseau en fonction du nombre et de la force des interactions qu'elle entretient avec les autres régions. Sur le plan physiologique, la DC a été mise en relation avec l'agrégation de β-amyloïdes[69] dans la maladie d'Alzheimer : *i.e.* plus une région cérébrale intègre de l'information à l'état de repos, plus celle-ci est ciblée par le dépôt de β-amyloïdes [BUC09]. La DC est également associée aux profils d'expression des gènes ([FRE11] et [WOL11]). Au cours de cette thèse j'ai démontré qu'une forte valeur de DC est corrélée à l'amplitude d'activation au cours de la réalisation de tâches langagières, confirmant de fait son support physiologique [LAB19].

J'ai calculé la sunnexité (BC : *betweenness centrality*, [RUB10]) au sens de [OPS10] à l'aide de la librairie R "*igraph*" [CSA06]. La BC d'une région est définie comme le taux de participation de cette région parmi l'ensemble des plus courts chemins entre une paire de sommets du graphe. La BC mesure la dépendance du réseau à une région spécifique pour sa communication globale.

Finalement, à partir des valeurs de DC et de BC, il est possible d'identifier des régions dites *hubs*. J'ai utilisé la définition du *hub* multi-critères de Sporn [SPO07] et de van den Heuvel [HEU10b]. Une région est un *hub* si ses valeurs de DC et de BC

[69] La β-amyloïde est une protéine se déposant sur les neurones, conduisant à la formation de plaque qui vont bloquer la communication synaptique. Cette protéine a été mise en relation avec la maladie d'Alzheimer [FIN07], bien que son rôle exact dans l'apparition et le développement de la maladie ne soit pas connu.

sont plus grandes que la moyenne plus une fois l'écart-type des valeurs de DC et de BC de l'ensemble du graphe (Figure 28). Il a été montré qu'il existe un lien étroit entre le débit sanguin cérébral mesuré en TEP et la topologie des réseaux cérébraux à l'état de repos [LIA13], offrant un support physiologique aux *hubs*. De même, les *hubs* ont été localisés dans des régions cérébrales ayant un taux élevé de métabolisme du glucose via des mesures réalisées en TEP [TOM13]. Finalement, la caractéristique topologique faisant d'une région cérébrale un *hub* semble être associée à son expression génique [FUL16].

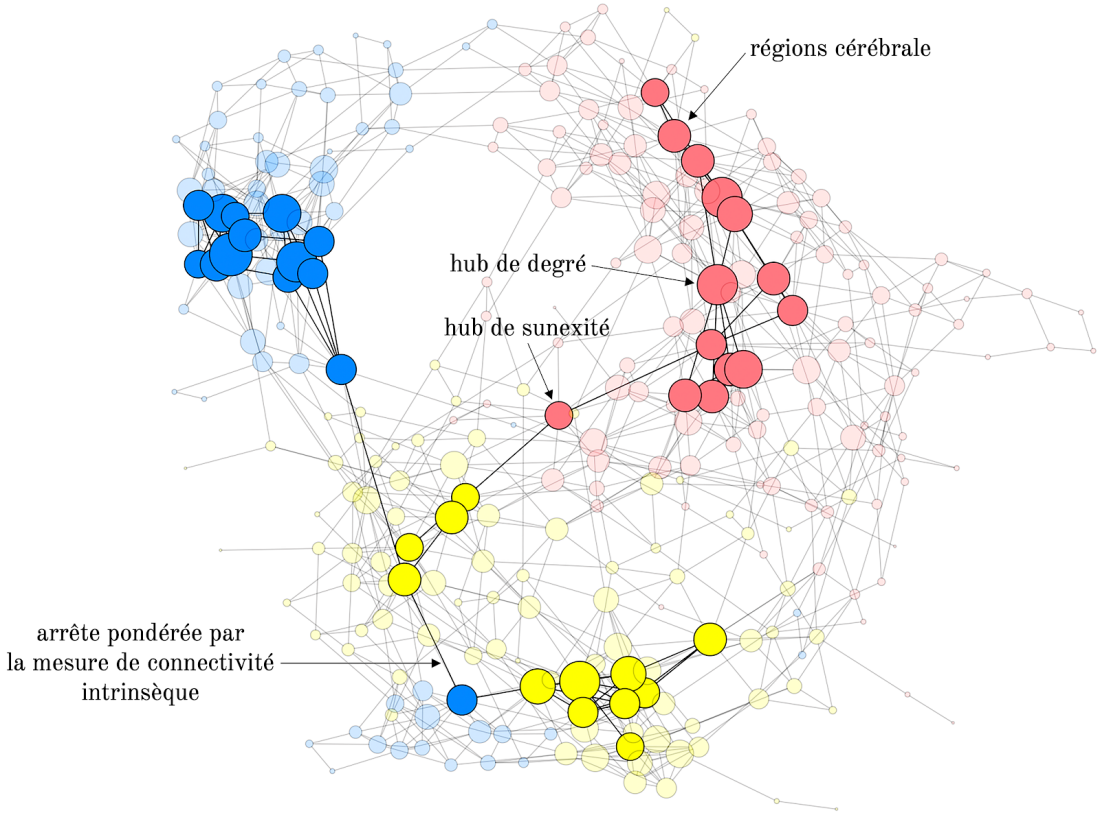

Figure 28 : Représentation du réseau de connectivité intrinsèque cérébrale globale dans l'espace topologique. *Graphe obtenu à partir de la matrice de la Figure 27 - A., seuillée pour ne conserver que les 5% des corrélations positives les plus élevées. Le réseau de sommets les plus connectés entre eux (ou rich-club) est ici mis en avant, les autres sommets ayant un niveau de transparence plus élevé. En jaune, saumon et bleu les hROIs du cortex associatif unimodal, hétéromodal et primaire respectivement (d'après les résultats illustrés en Figure 11).*

La théorie des graphes appliquée aux neurosciences offre également la possibilité d'étudier les pathologies psychiatriques ou neurologiques comme la schizophrénie ([BAS08] et [HE08a]) ou la maladie d'Alzheimer ([SUP08] et [BUC09]). Les conséquences de ces pathologies, telles que des déficits fonctionnels,

peuvent alors être associées à des perturbations de la topologie du réseau cérébral, topologie mise en évidence par les mesures de théorie des graphes.

La théorie des graphes a également permis de mettre en avant l'agencement complexe du cerveau via la mise en évidence de son organisation en réseau "petit monde" (*small-world*, [BAS17b]) : *i.e.* un réseau ni totalement désordonné, ni totalement régulier. Ce type de réseau est caractérisé par une tendance à contenir un ensemble de sous-réseaux dont les connexions entre les régions qui les composent sont presque complètes : c'est-à-dire qu'une région d'un sous-réseau est connectée à l'ensemble des autres régions de son sous-réseau. Un tel type d'organisation implique que les sous-réseaux sont alors connectés entre eux par les régions *hubs* qui forment donc entre elles un réseau dit *rich-club*[70] ([HAG08], Figure 28).

Une revue complète des possibilités offertes par la théorie des graphes appliquée aux neurosciences est disponible dans [RUB10] et [BAS17]. Bertolero & Basset proposent quant à eux une revue exhaustive concernant le caractère mécanistique[71] des explications offertes par la théorie des graphes en neuroscience et de quelle manière elles s'interjectent et contribuent aux explications classiques des neurosciences [BER20].

[70] Un réseau dit *rich-club* est formé par des régions *hubs* densément inter-connectées qui ont un rôle central dans la diffusion efficace du flux d'information dans le réseau global.

[71] La mécanistique est une théorie philosophique qui considère que tout phénomène est le produit des propriétés mécaniques de la matière.

Partie II

Atlas supramodal des réseaux du traitement de la phrase et atlas hétéromodal des réseaux du traitement de listes de mots

L'objectif original de cette thèse est de construire des atlas de régions d'intérêts des réseaux cognitifs latéralisés. Je présenterai plus particulièrement les deux atlas du langage que nous avons développés et qui ont été publiés.

Mon travail s'est basé sur une procédure "inverse" qui est fondée sur l'identification des régions à partir de leur implication au cours de tâches et de contrastes spécifiques d'un domaine donné de la cognition. Nous avons donc favorisé une homogénéité fonctionnelle, obtenue à partir de l'activité évoquée par les tâches, en partant d'un *a priori* sur leur implication dans un domaine de la cognition, plutôt que sur une homogénéité du signal des ROIs. Définir les rôles fonctionnels de ROIs à partir d'activations évoquées obtenues chez les mêmes sujets, tous cartographiés sur le même appareil d'IRM, offre une homogénéité et une sensibilité similaire à travers les sujets et les différentes tâches cognitives explorées.

Pour faire ce travail nous avons exploité la BIL&GIN [MAZ16], une base de données qui offre la possibilité d'identifier les réseaux évoqués dans plusieurs domaines de la cognition. Elle inclut en effet 300 témoins volontaires sains ayant été cartographiés en IRMf pendant la complétion de 11 tâches cognitives et pendant une acquisition de repos. Parmi l'ensemble des participants de la BIL&GIN, nous avons sélectionné les individus droitiers pour la construction des atlas, l'équipe ayant démontré leur homogénéité en termes de dominance de l'hémisphère gauche pour le langage ([MAZ14][72] et [ZAG16]).

L'autre aspect méthodologique original de ce travail de thèse est la prise en compte d'un élément essentiel de l'organisation cérébrale dans la construction des atlas des réseaux du langage : la spécialisation hémisphérique. La spécialisation hémisphérique se traduit par des asymétries d'activation qui sont le marqueur direct de la spécialisation d'un hémisphère pour une fonction donnée. La spécialisation hémisphérique est donc une relation d'interdépendance hémisphérique entre une fonction motrice, sensorielle ou cognitive et un ensemble de structures cérébrales. Cette interdépendance comprend à la fois la localisation dans un hémisphère donné des réseaux qui ont des propriétés fonctionnelles uniques et les mécanismes qui permettent la coordination inter-hémisphérique nécessaire pour un traitement efficace [TZO16b].

[72] 98% des droitiers ont leur hémisphère gauche dominant pour la production du langage [MAZ14].

Le cas le plus étudié est celui du langage : les asymétries gauches mesurées en IRMf pendant les tâches de langage sont en effet concordantes avec la mise en évidence de l'hémisphère dit dominant pour le langage, c'est-à-dire l'hémisphère qui, lorsqu'il est inactivé par son anesthésie au cours du test de Wada [WAD60], entraîne une aphasie[73] ([DYM01], [DRO04] et [MES14]). La contrainte d'identification de ROIs latéralisées pour le langage sous-entend le calcul de leurs asymétries au cours des différentes tâches linguistiques regardées. Pour ce faire, nous avons utilisé les hROIs de l'atlas AICHA qui permettent le calcul d'asymétries d'activations basées sur une organisation homotope, c'est-à-dire de hROIs fonctionnellement équivalentes dans les deux hémisphères [JOL15].

La connectivité intrinsèque de l'état de repos permettant d'identifier et caractériser l'organisation en réseaux sous-tendant les fonctions cognitives ([BIS95] et [YEO11]), nous avons appliqué aux hROIs sélectionnées par les tâches évoquées une analyse de leur connectivité intrinsèque. En effet cette méthode est efficace pour caractériser l'organisation en réseaux des fonctions cognitives ([BIS95] et [YEO11]). Cette approche nous a permis de distinguer, au sein des régions co-activées et co-asymétriques, celles qui sont fonctionnellement connectées en un ou plusieurs réseaux. Turken et Dronkers fournissent un exemple de ce concept appliqué au domaine du langage en réalisant une analyse par *seed* des corrélations à l'état de repos du gyrus temporal moyen (région dont les lésions sont associées à des troubles aphasiques) et par ce biais mettent en avant un réseau d'aires connectées au repos sous-tendant la compréhension du langage [TUR11]. De plus, et comme le souligne le Pr. Bharat Biswal, l'étude de l'organisation des ROIs en sous-réseaux cérébraux (ici les sous-réseaux du langage) contient des propriétés supplémentaires de celles obtenues à partir des réseaux cérébraux identifiés à l'aide de la connectivité intrinsèque de l'ensemble du cerveau [BIS12]. Par ailleurs, les mesures de connectivité peuvent fournir des informations essentielles sur la manière dont les hROIs sont connectées entre elles et sur leur organisation en réseau. Les méthodes d'analyse de graphe[74]

[73] Le terme "aphasie" désigne une perturbation du traitement du langage causée par une dysfonction dans certaines régions du cerveau. Les troubles aphasiques incluent des difficultés ou une impossibilité totale de la compréhension du langage et/ou de sa production, causée par des lésions respectivement des régions du langage postérieures ou antérieures. [MES00]

[74] *cf.* Partie I - 3.3. La théorie des graphes comme outil pour la caractérisation topographique du support anatomo-fonctionnel des réseaux cérébraux.

appliquées à la connectivité intrinsèque offrent ainsi la possibilité de caractériser une région à travers son rôle topologique dans le réseau à laquelle elle appartient. Cette caractérisation peut être effectuée par l'identification de régions essentielles à un réseau donné et donc essentielles à la ou les fonctions cognitives qu'elles soutiennent : ce sont les *hubs* du réseau [SPO07].

Cette approche originale, et multimodale, nous a permis à la fois de produire des atlas mais également de caractériser les régions cérébrales sous-tendant les bases anatomo-fonctionnelles de la latéralisation du langage et les relations entre activation et connectivité.

1. SENSAAS : un atlas des aires supra-modales de la phrase

Labache, L., Joliot, M., Saracco, J., Jobard, G., Hesling, I., Zago, L., ... & Tzourio-Mazoyer, N. (2019). A SENtence Supramodal Areas AtlaS (SENSAAS) based on multiple task-induced activation mapping and graph analysis of intrinsic connectivity in 144 healthy right-handers. *Brain Structure and Function, 224*(2), 859-882.

Brain Structure and Function (2019) 224:859–882
https://doi.org/10.1007/s00429-018-1810-2

ORIGINAL ARTICLE

A SENtence Supramodal Areas AtlaS (SENSAAS) based on multiple task-induced activation mapping and graph analysis of intrinsic connectivity in 144 healthy right-handers

L. Labache[1,2,3,4,5] · M. Joliot[1,2,3] · J. Saracco[5,6] · G. Jobard[1,2,3] · I. Hesling[1,2,3] · L. Zago[1,2,3] · E. Mellet[1,2,3] · L. Petit[1,2,3] · F. Crivello[1,2,3] · B. Mazoyer[1,2,3] · Nathalie Tzourio-Mazoyer[1,2,3]

Received: 5 March 2018 / Accepted: 1 December 2018 / Published online: 7 December 2018

Abstract

We herein propose an atlas of 32 sentence-related areas based on a 3-step method combining the analysis of activation and asymmetry during multiple language tasks with hierarchical clustering of resting-state connectivity and graph analyses. 144 healthy right-handers performed fMRI runs based on language production, reading and listening, both with sentences and lists of over-learned words. Sentence minus word-list BOLD contrast and left-minus-right BOLD asymmetry for each task were computed in pairs of homotopic regions of interest (hROIs) from the AICHA atlas. Thirty-two hROIs were identified that were conjointly activated and leftward asymmetrical in each of the three language contrasts. Analysis of resting-state temporal correlations of BOLD variations between these 32 hROIs allowed the segregation of a core network, SENT_CORE including 18 hROIs. Resting-state graph analysis applied to SENT_CORE hROIs revealed that the pars triangularis of the inferior frontal gyrus and the superior temporal sulcus were hubs based on their degree centrality (DC), betweenness, and participation values corresponding to epicentres of sentence processing. Positive correlations between DC and BOLD activation values for SENT_CORE hROIs were observed across individuals and across regions regardless of the task: the more a SENT_CORE area is connected at rest the stronger it is activated during sentence processing. DC measurements in SENT_CORE may thus be a valuable index for the evaluation of inter-individual variations in language areas functional activity in relation to anatomical or clinical patterns in large populations. SENSAAS (SENtence Supramodal Areas AtlaS), comprising the 32 supramodal sentence areas, including SENT_CORE network, can be downloaded at http://www.gin.cnrs.fr/en/tools/.

Keywords fMRI · Left hemisphere · Sentence · Language production · Reading · Speech comprehension · Intrinsic connectivity · Graph analysis · Right-handers · Resting-state

Abbreviations

aHCA	Agglomerative hierarchical cluster analysis
AICHA	Atlas of intrinsic connectivity of homotopic areas
AU	Approximately unbiased p value
BC	Betweenness centrality
DC	Degree centrality
DMN	Default mode network
FIR	Finite impulse response
fMRI	Functional magnetic resonance imaging
FWHM	Full width at half maximum
hROIS	Homotopical regions of interest
$LISN_{SENT-WORD}$	Sentence minus word-list contrast for listening task

Electronic supplementary material The online version of this article (https://doi.org/10.1007/s00429-018-1810-2) contains supplementary material, which is available to authorized users.

✉ Nathalie Tzourio-Mazoyer
nathalie.tzourio-mazoyer@u-bordeaux.fr

1 Univ. Bordeaux, IMN, UMR 5293, 33000 Bordeaux, France

2 CNRS, IMN, UMR 5293, 33000 Bordeaux, France

3 CEA, GIN, IMN, UMR 5293, 33000 Bordeaux, France

4 Univ. Bordeaux, IMB, UMR 5251, 33405 Talence, France

5 INRIA Bordeaux Sud-Ouest, CQFD, UMR 5251, 33405 Talence, France

6 Bordeaux INP, IMB, UMR 5251, 33405 Talence, France

MNI	Montreal Neurological Institute
pIndex	Participation index
$PROD_{SENT\text{-}WORD}$	Sentence minus word-list contrast for production task
$READ_{SENT\text{-}WORD}$	Sentence minus word-list contrast for reading task
rs-fMRI	Resting-state fMRI
SD	Standard deviation
SPM	Statistical parametric mapping

Introduction

Defining language areas is a complex enterprise because of the numerous possible approaches currently available to identify language-related regions. The gold standard is to consider that language areas correspond to regions wherein lesions lead to aphasia. Even when limiting the definition of language areas to that of essential language areas, different identification methods exist that provide various kinds of information. Wada testing allows identification of the hemisphere controlling language but does not provide regional information (Wada and Rasmussen 1960). By contrast, surgical cortical stimulation studies have documented left hemisphere language areas in large samples of patients (Ojemann et al. 1989; Tate et al. 2014), but such mapping of eloquent areas is still limited to the cortical regions available to the neurosurgeon and is conducted in patients having potentially modified language organization. The probabilistic mapping of lesions combined with fine-grained aphasic patient evaluations of language performance have provided the community with very accurate descriptions of essential language areas (Dronkers and Ogar 2004; Dronkers et al. 2004) although this very important approach does not reveal how these cortical areas are organized in networks. Because each multiple cortical area altered by a given pathology is not involved in the language deficit, the comprehensive identification of language areas from lesions is a complex issue [see (Genon et al. 2018a, b) for a review].

Functional neuroimaging provides a way to map multiple areas activated during the completion of various language tasks in a large number of individuals. Furthermore, neuroimaging methodology is very efficient at compiling results obtained in multiple laboratories across the world, thereby allowing meta-analyses across laboratories that provide the location of areas activated at an acceptable spatial resolution within a common normalization space for a variety of language tasks. Similar to the results obtained with cortical stimulation (Ojemann et al. 1989), meta-analyses of neuroimaging data have provided the landscape of the left hemisphere cortical areas involved in language tasks in healthy individuals, which covers nearly the entire hemisphere surface (Price 2000, 2010, 2012; Vigneau et al. 2006).

Despite the vast amount of information obtained from the methods cited above, an atlas of left hemisphere language areas in healthy individuals having a typical left-hemisphere dominance for language is still lacking, and with respect to language areas, the absence of a consensus is clear. The posterior part of the superior temporal gyrus and the supramarginal gyrus (Tomasi and Volkow 2012; Klingbeil et al. 2017) are phonological regions that can be found under the label "Wernicke's area", while lesion-based studies (Dronkers and Ogar 2004; Yourganov et al. 2015) as well as lesion studies in association with activation studies (Saur et al. 2006) have shown deep aphasia associated with lesions of the posterior region of the middle temporal gyrus and superior temporal sulcus (Binder 2015, 2017). There is greater consistency concerning the location of frontal language areas under the label of Broca's area because its original definition was anatomical. Most people define Broca's area as the pars triangularis of the inferior frontal gyrus (Clos et al. 2013; Friederici and Gierhan 2013; Yourganov et al. 2015). However, the extent of Broca's area in the left frontal lobe varies, and the anterior insula (Baldo et al. 2011) is sometimes added, as reviewed in Amunts (Amunts and Zilles 2012). Moreover, posterior lesions can also lead to Broca's aphasia (Richardson et al. 2012), demonstrating that these anterior and posterior language poles work tightly together. This relation enhances the importance of networks in cognitive processing, as defined by Fuster (Fuster and Bressler 2012). An atlas of language areas and networks in healthy individuals would thus be a useful tool, especially when individual task-induced mapping is not available. This atlas would be especially helpful for patients having difficulties completing language tasks and for the exploration of genetic language bases in large cohorts of individuals, in cohorts targeting normal or pathological brains, including those with developmental pathologies, and/or in individuals mapped for their anatomy and/or resting state while not performing a language task (Thompson et al. 2017).

To elaborate such an atlas, increasing the specificity for language areas is important because as uncovered by lesion studies, not all areas revealed by task-induced activation studies are essential language areas. Components of the task, such as monitoring, selecting, and holding the instructions, as well as paralinguistic processing, such as context, emotional and prosodic processing, are responsible for activations that exceed the essential language areas of the left hemisphere. The strong right-hemisphere activations observed with functional imaging during various language tasks have even led some authors to claim that neuroimaging methods are not adequate to map language regions (Sidtis 2007). One way to overcome this issue is using appropriate reference tasks. To discriminate language areas among those involved in the completion of a given task, Binder has suggested using well-designed reference tasks. The idea is

to remove the non-specific or non-lateralized activations of primary areas and/or executive regions by applying the difference paradigm (Binder 2011). Compared to a non-verbal reference, the use of a verbal reference tasks allows left hemisphere language areas to be specifically highlighted, as shown by Ferstl's meta-analysis (Ferstl et al. 2008). The use of verbal reference tasks with functional magnetic resonance imaging (fMRI) has proven to successfully measure activation asymmetry, a proxy of language dominance strongly concordant with Wada testing. Note that this is true whether hemispheric or regional asymmetry of activations is used for the evaluation of language hemispheric dominance [review in Dym et al. (2011)].

Thus, asymmetry represents an additional method for increasing the specificity of identifying left hemisphere language areas. Typical language organization, seen in 90% of the healthy population (Mazoyer et al. 2014) and 97% of healthy right-handers (Zago et al. 2017), is characterized by a strong left hemisphere dominance, giving rise to regional leftward asymmetries in fMRI. Adding to the detection of activated areas (by comparison to a high-level verbal reference task), a criterion based on leftward asymmetry would certainly increase the specificity of identifying left hemisphere language areas.

Another difficulty in identifying essential language areas with functional imaging is the fact that different tasks lead to different patterns of activation. One way to overcome this difficulty is to combine several language tasks in the same participant and apply conjunction analyses to unravel the activated and asymmetrical regions independent of the type of task or modality involved (Papathanassiou et al. 2000; Jobard et al. 2007; Dodoo-Schittko et al. 2012).

Finally, the task-induced approach does not provide any information on how the different activated areas are organized. The co-activation of a group of regions does not indicate that they are all strongly functionally connected and thus constitute a network. Resting-state intrinsic connectivity has proven to be capable of identifying the organization of brain networks underpinning cognitive functions. A good illustration of this concept is provided by Turken and Dronkers, who conducted correlation analysis in resting-state images of healthy participants using the posterior middle temporal gyrus region as the seed (Turken and Dronkers 2011). In this work, this seed region was selected because its lesion was associated with strong comprehension deficits in aphasics, and its location was previously identified by probabilistic lesion mapping (Dronkers et al. 2004). Using this approach, Turken et al. revealed a network of areas connected at rest that support speech comprehension in healthy individuals. Investigating intrinsic connectivity would thus be an interesting means to investigate the networks existing at rest among the areas activated during language tasks. Connectivity measures can provide essential information on how regions are connected and how they are organized in networks. Graph analysis methodology applied on resting-state connectivity also permits the measurement of the connectivity strength of each region with all other regions of a given network to which it belongs, thereby characterizing its role in the network. In particular, identifying the topological roles of the regions is possible, i.e., identifying hubs, regions essential to a given network and therefore essential to the cognitive function(s) they support (Sporns et al. 2007).

To propose an atlas of left hemisphere high-order language areas, we first combined multiple-language fMRI task-induced activation mapping and conjunction analysis to select a set of both activated and leftward asymmetrical areas during sentence processing. Second, we clustered the regions identified in the first step into networks based on their intrinsic connectivities at rest. Third, we applied graph analysis to characterize the roles of the regions in communication within and across networks. To this end, we utilized BIL&GIN, a database dedicated to the study of hemispheric specialization (Mazoyer et al. 2015), and selected 144 right-handers who were mapped during sentence production, reading and listening tasks compared to the production, reading and listening of lists of words, respectively. All but six participants were also mapped during the resting state. Most investigations of the resting-state and task-induced activation networks have relied on whole-brain comparisons between the functional connectivities measured in these two conditions [review in Wig (2017)], although they correspond to very different physiological states (Raichle and Mintun 2006; Raichle 2015). Here, we aimed to find resting-state markers of left hemisphere activation in discrete language areas to provide a comprehensive tool for further research on the inter-individual variability of language areas. Such markers of language activation are likely to be of interest for studies in which no task-induced activations are documented but instead include a resting-state acquisition. Consequently, we used homotopical regions of interest (hROIs) from the AICHA atlas, a functional atlas obtained from intrinsic connectivity analysis (Joliot et al. 2015). We used AICHA hROIs because (1) we needed an atlas suitable for functional imaging and, in that respect, AICHA, which was elaborated from resting-state connectivity, is optimal for analysing functional data; (2) AICHA has been specifically designed to identify functionally homotopic regions of interest, enabling the accurate computation of functional asymmetries since it avoids the potential bias that anatomical and functional areas do not strictly overlap. The different sets of hROIs corresponding to the supramodal sentence processing areas of the proposed atlas (SENSAAS) are available in the Montreal Neurological Institute (MNI) space at http://www.gin.cnrs.fr/en/tools/.

Materials and methods

Participants

From the BIL&GIN database, we selected 144 healthy right-handers (72 women) who completed the fMRI battery, including several language tasks (Mazoyer et al. 2015). The sample mean age was 27 years (SD = 6 years), and the women were two years younger than the men (women 26 ± 5; men: 28 ± 7, $p = 0.053$). The mean educational level of the participants was 16 years (SD = 6 years), with no significant difference between the men and women ($p > 0.05$). All participants reported themselves as right-handed; their mean normalized finger tapping test asymmetry ([(right number of taps − left number of taps)/(left + right number of taps)] × 100) was 6.25 (SD = 4.3), and their mean Edinburgh score was 93.5 (SD = 11), confirming their right-handedness. There was no difference between gender for the Edinburgh score ($p = 0.47$), although there was a slightly stronger rightward manual laterality in women (finger tapping test asymmetry in women: 6.9 ± 3.8; men: 5.7 ± 4.7, $p = 0.08$, controlling for age).

Of these participants, 138 (mean age 27 years (SD = 6 years), 68 women) also completed a resting-state fMRI (rs-fMRI) acquisition lasting 8 min. Note that this resting-state acquisition was performed on average 9 months (SD = 9.6 months) before the language task acquisition in all but five cases. In these five cases the resting-state acquisition occurred approximately 1 year after the language session [range (11.2–13.8) months].

Image acquisition and processing

Structural imaging

Structural images were acquired using the same 3T Philips Intera Achieva scanner including high-resolution T1-weighted volumes (sequence parameters: TR, 20 ms; TE, 4.6 ms; flip angle, 10°; inversion time, 800 ms; turbo field echo factor, 65; sense factor, 2; field of view, $256 \times 256 \times 180$ mm^3; isotropic voxel size $1 \times 1 \times 1$ mm^3). For each participant, the line between the anterior and posterior commissures was identified on a mid-sagittal section, and the T1-MRI volume was acquired after orienting the brain in the bi-commissural coordinate system. T2*-weighted multi-slice images were also acquired [T2*-weighted fast field echo (T2*-FFE), sequence parameters: TR = 3,500 ms; TE = 35 ms; flip angle = 90°; sense factor = 2; 70 axial slices; $2 \times 2 \times 2$ mm^3 isotropic voxel size].

Task-induced functional imaging

Training To ensure proper task execution, the participants were trained outside the scanner in the hour preceding the fMRI session. The training used stimuli that were of the same nature but different from those used during the fMRI session.

Language tasks Three runs were administered to the participants. They included a sentence task involving phonological, semantic, prosodic and syntactic processing and a word-list reference task, a less complex, albeit high-level, verbal task. To achieve homogeneity in the sentence task material, 51 line drawings illustrating the stories of 'Le petit Nicolas' (Little Nicholas), a classic French children's series, were used. The three tasks consisted of a randomized alternation of event-related trials devoted to sentence processing, with event-related trials devoted to the verbal reference task, i.e., lists of words. The drawings used for the reference task were scrambled versions of the line drawings, and the stimuli presented either orally or visually were lists of months, days and/or seasons. Within each trial, the subject was shown either a line drawing or a scrambled drawing for 1 s, immediately followed by a central fixation crosshair. While fixating the cross, the subject performed either the sentence task or the word reference task. Once the task was completed, a low-level reference task, detecting the transformation of a centrally displayed cross into a square, was presented. When the subjects detected this change, they were asked to press a button with their index finger of the assigned hand. The square was then displayed until the end of the trial. This second part of the trial, which lasted at least half of the total trial duration, aimed at refocusing the subject's attention to a non-verbal stimulus and controlling for manual motor response activation, which was also present in the first part of the trial. A 12-s presentation of a fixation crosshair preceded and followed the first and last trial. Note that except during the drawings display, the subjects were asked to keep fixating the cross, and the star and square were then presented on the centre of the screen.

Sentence and list of word production tasks During the production run, after seeing a Little Nicholas line drawing, the subject was instructed to covertly generate a sentence beginning with a subject (The little Nicholas…, The gentleman…) and a complement (with his satchel…, in shorts…, with glasses…), followed by a verb describing the action taking place and ending with an additional complement of a place (in the street…, in the playground…, on the beach…) or a manner (with happiness…, nastily…). When a scrambled drawing was displayed, the subject was asked to covertly generate the list of the months of the year. The production paradigm randomly alternated ten 18-s trials of sentence generation with ten 18-s trials of generating the list of months. The response time limit, indicated by the transformation of the cross in a star, was 9 s, including the 1-s drawing display. The entire experimental run lasted 6 min and 24 s. The mean sentence production time was 5617 ms

(SD = 935 ms), while the mean duration of word-list production was 5249 ms (SD = 1131 ms).

Sentence and list of word-listening tasks When a Little Nicholas line drawing was displayed, the subject was instructed to carefully listen to a sentence dealing with the line drawing and click at the end of the sentence. For the LISN, when a scrambled drawing was displayed, he/she was instructed to listen to the list of the months, days of the week and/or seasons and click at the end of the list.

The paradigm consisted of a randomized alternation of thirteen 14-s sentence-listening trials with thirteen 14-s list-listening trials. The mean durations of auditory presentation were 4371 ± 468 ms for the sentences and 4386 ± 484 ms for the lists. The entire experimental run lasted 6 min and 28 s. The reaction times after sentence and list listening were 387 ms (SD = 125 ms) and 478 ms (SD = 97 ms), respectively.

Sentence and list of word-reading tasks Like in the other two tasks, when a line drawing was displayed, the subject was instructed to read a sentence based on the line drawing. When a scrambled drawing was displayed, he/she was instructed to read the list of months, days of the week and/or seasons.

The paradigm consisted of a randomized alternation of thirteen 14-s sentence-reading trials with thirteen 14-s list-reading trials. The entire experimental run lasted 6 min and 28 s. The average time for reading sentences was 3729 ms (SD = 567 ms), while reading the lists of words required 4412 ms (SD = 602 ms).

Debriefing the fMRI tasks Right after the fMRI sessions, the participants were asked to rate the difficulty of the task on a five-point scale (1-easy to 5-very difficult) and answer some debriefing questions about how they accomplished the task.

The production task had the highest task difficulty score reported by the participants (2.73), while the reading and listening tasks had low scores (1.14 and 1.20, respectively). All participants were able to recollect the sentence they produced when presented with the corresponding drawing for at least 5 of 10 images (mean = 9.43 images, SD = 0.96), with the mean number of words per sentence being 12.4 (SD = 2).

Functional image acquisition

The functional volumes were acquired as T2*-weighted echo-planar EPI images (TR = 2 s; TE = 35 ms; flip angle = 80°; 31 axial slices with a 240×240 mm^2 field of view and $3.75 \times 3.75 \times 3.75$ mm^3 isotropic voxel size). In the three runs, 192, 194 and 194 T2*-weighted volumes were acquired for the sentence production, listening and reading tasks, respectively.

Resting-state functional imaging (rs-fMRI)

Spontaneous brain activity was monitored for 8 min (240 volumes) using the same imaging sequence (T2*-weighted echo-planar images) as that used for the language tasks. Immediately prior to rs-fMRI scanning, the participants were instructed to "keep their eyes closed, to relax, to refrain from moving, to stay awake and to let their thoughts come and go".

Image analysis

Functional imaging analysis common to task-induced and resting-state acquisitions For each participant, (1) the T2*-FFE volume was rigidly registered to the T1-MRI; (2) the T1-MRI was segmented into three brain tissue classes: grey matter, white matter and cerebrospinal fluid; and (3) the T1-MRI scans were normalized to the BIL&GIN template including 301 volunteers from the BIL&GIN database (aligned to the MNI space) using the SPM12 "normalise" procedure with otherwise default parameters.

For each of the three fMRI runs, data were corrected for slice timing differences. To correct for subject motion during the runs, all the T2*-weighted volumes were realigned using a six-parameter rigid-body registration. The EPI-BOLD scans were then registered rigidly to the structural T2*-FFE image. The combination of all registration matrices allowed for warping the EPI-BOLD functional scans to the standard space with a single trilinear interpolation.

Specific task-induced functional imaging analysis First, a 6-mm full width at half maximum (Gaussian filter) was applied to each run. Global linear modelling (statistical parametric mapping (SPM), http://www.fil.ion.ucl.ac.uk/spm/) was used for processing the task-related fMRI data. For each participant, BOLD variations corresponding to each sentence versus the list belonging to the same run were computed [sentence minus word-list production ($PROD_{SENT\text{-}WORD}$), sentence minus word-list reading ($READ_{SENT\text{-}WORD}$), and sentence minus word-list listening ($LISN_{SENT\text{-}WORD}$)]. Finally, contrast maps (defined at the voxel level) were subjected to hROI analysis. BOLD signal variations were measured in 192 pairs of functionally defined hROIs of the AICHA atlas (Joliot et al. 2015) adapted to SPM12, excluding 7 hROIs pairs belonging to the orbital and inferior temporal parts of the brain in which signals were reduced due to susceptibility artefacts. For each participant, we computed contrast maps of the three language conditions. We then calculated the right and left hROI BOLD signal variations for each of the 185 remaining pairs by averaging the contrast BOLD values of all voxels located within the hROI volume.

Specific analysis of resting-state functional images Time series white matter and cerebrospinal fluid (individual average time series of voxels that belonged to each tissue class) and temporal linear trends were removed from the rs-fMRI data series using regression analysis. Additionally, rs-fMRI data were temporally filtered using a least squares linear-phase finite impulse response filter design bandpass (0.01–0.1 Hz).

For each participant and hROI (the same 185 homotopic ROIs as those used in the task-induced analysis), an individual BOLD rs-fMRI time series was computed by averaging the BOLD fMRI time series of all voxels located within the hROI volume.

Part 1: Identification and characterization of hROIs exhibiting both leftward activation and leftward asymmetrical activation in all three tasks

To complete the identification of high-order language areas, we first searched for hROIs that were both significantly co-activated and significantly leftward asymmetrical on average among the 144 participants during the $PROD_{SENT\text{-}WORD}$, $READ_{SENT\text{-}WORD,}$ and $LISN_{SENT\text{-}WORD}$ tasks.

Statistical analysis

hROI selection

Using JMP14 (http://www.jmp.com, SAS Institute Inc., 2018), conjunction analysis was conducted to select the left-hemisphere hROIs exhibiting BOLD signal variations that were both significantly positive and significantly larger than that in their right counterparts in all three tasks. An hROI was selected whenever it was significantly activated in each of the three task contrasts using a significance threshold set to $p < 0.05$ per contrast. The significance threshold for the conjunction of activation in the three tasks was thus $0.05 \times 0.05 \times 0.05 = 1.25 \times 10^{-4}$. The second criterion for hROI selection was the existence of a significant leftward asymmetry in each of the three task contrasts, the threshold of significance of this second conjunction being again 1.25×10^{-4}. Finally, since to be selected, a given hROI had to fulfil both criteria, the overall significance threshold for the conjunction of conjunction analyses was $1.5 \times 10^{-8} = (1.25 \times 10^{-4})^2$.

Results

hROI selection

Among the 80 hROIs jointly activated in the 3 contrasts (Table 1), 46 also showed joint asymmetries. In total, 32 hROIs showed both joint activation on the left and joint asymmetry (Fig. 1; Table 2).

On the lateral surface of the left frontal lobe, the regions having both joint activation and leftward asymmetry during the three language tasks covered the left inferior frontal gyrus (pars triangularis: F3t and pars opercularis: F3O1), the adjacent inferior frontal sulcus (f2_2), the junction of the middle frontal gyrus with the precentral sulcus (prec4), and the upper part of the precentral sulcus (prec3) located dorsally to prec4. The medial part of the superior frontal gyrus (F1_2), the upper paracentral gyrus (pCENT4), and the pre-superior motor areas (SMA2 and SMA3) were also part of these areas in the medial frontal lobe. Two hROIs were located within the anterior insula (INSa2 and INSa3), while the INSa1 hROI was located medially and ventrally close to the amygdala. On the lateral surface of the temporal lobe, the hROIs overlapped the entire length of the superior temporal sulcus (STS2, STS3 and STS4), extending to the temporal pole anteriorly (STS1), to the superior temporal gyrus dorsally (T1_4), to the supramarginal (SMG7) and angular gyri (AG2) posteriorly, crossing the middle temporal gyrus (T2_3 and T2_4) and joining the inferior temporal gyrus (T3_4), the inferior occipital gyrus (O3_1), and ventrally the fusiform gyrus (FUS4). Regions located within the hippocampus (HIPP2), parahippocampal gyrus (pHIPP1) and amygdala (AMYG) were also part of the selected areas. In the posterior medial wall, the dorsal part of the precuneus (PRECU6) together with the posterior cingulum (CINGp3) were selected using this approach. Sub-cortical areas jointly activated and leftward asymmetrical during the three tasks

Table 1 Results of conjunction analyses across each sentence minus word-list contrasts for production ($PROD_{SENT\text{-}WORD}$), listening ($LISN_{SENT\text{-}WORD}$) and reading ($READ_{SENT\text{-}WORD}$) tasks in terms of the number of hROIs

	L activation	L asymmetry	Conjunction of activation and asymmetry
$PROD_{SENT\text{-}WORD}$	133	93	75
$LISN_{SENT\text{-}WORD}$	116	73	64
$READ_{SENT\text{-}WORD}$	97	60	43
Conjunctions of 3 contrasts	80	46	32

Numbers of hROIs with significant left activation, leftward asymmetry or conjunction of activation and asymmetry for the three "sentence minus word" contrasts

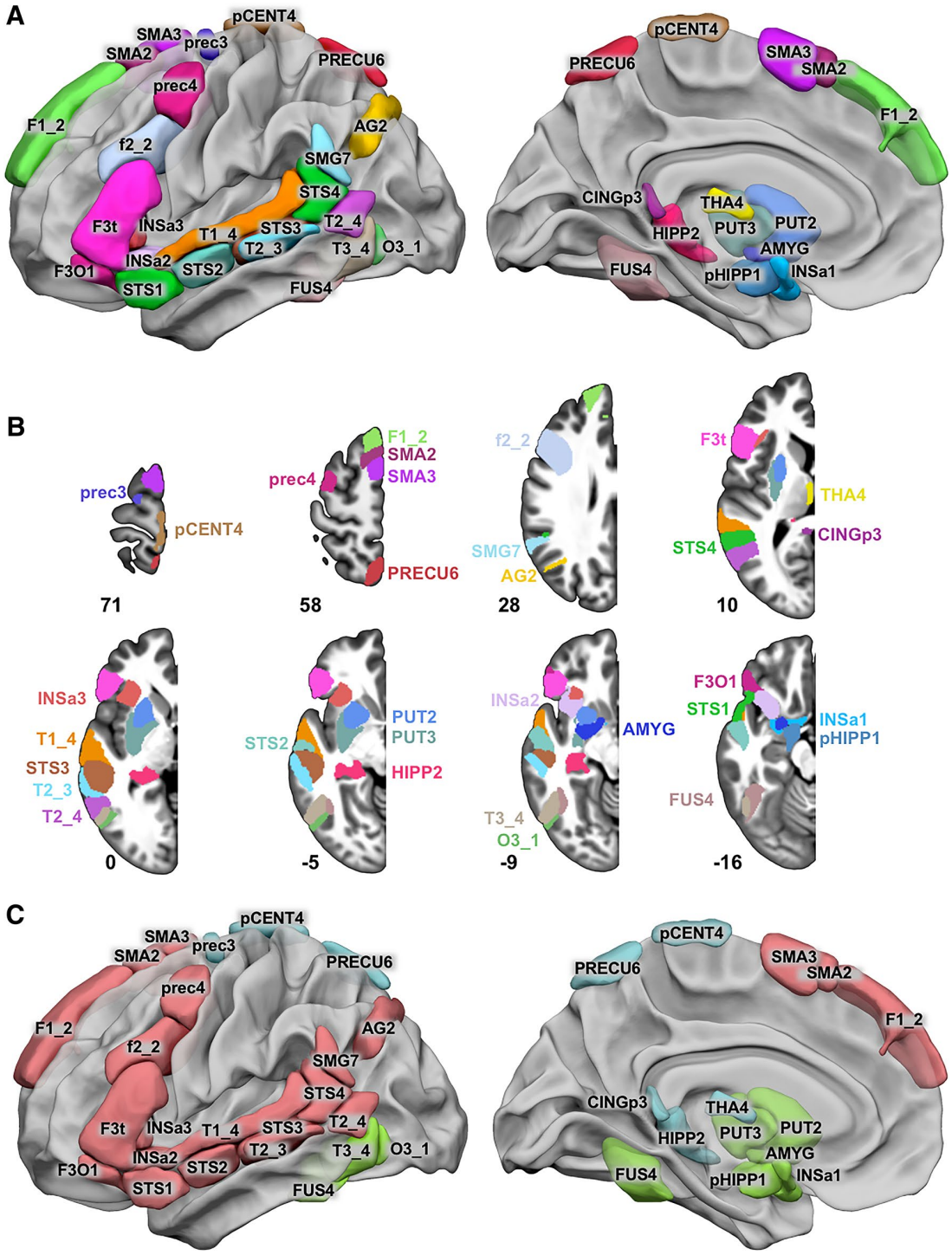

Fig. 1 Locations of the 32 hROIs co-leftward activated and co-leftward asymmetrical during the completion of 3 sentence minus word-list tasks by 144 healthy right-handers and corresponding networks after hROI clustering based on resting-state connectivity. **a** Left lateral view of 3D surfaces rendering the 32 hROIs on the BIL&GIN display template in the MNI space with Surf Ice software (https://www.nitrc.org/projects/surfice/). **b** Representation of hROIs on left hemisphere axial slices from the BIL&GIN display template; the hROI numbers correspond to the *z*-axis in the MNI space. **c** Lateral and medial views of the three identified networks. SENT_CORE network: red, SENT_MEM: light blue and SENT_VISU: green. Correspondences between the abbreviations and the full names of the AICHA atlas can be found in Table 2

Table 2 Names and abbreviations of the 32 hROIs showing joint left activation and left asymmetry during the three sentences minus word-list contrasts for production ($PROD_{SENT\text{-}WORD}$), listening ($LISN_{SENT\text{-}WORD}$) and reading ($READ_{SENT\text{-}WORD}$) tasks; the network label to which they were clustered; and their coordinates in MNI space after SPM12 normalization of the AICHA atlas

	AICHA hROI name	Abbreviation	Cluster	*X* (mm)	*Y* (mm)	*Z* (mm)
Frontal and insula	S_Precentral-3	prec3	SENT_MEM	−18.2	−8.7	69.3
	S_Precentral-4	prec4	SENT_CORE	−42.2	0.7	49.9
	G_Frontal_Sup-2	F1_2	SENT_CORE	−11.9	46.5	41.4
	S_Inf_Frontal-2	f2_2	SENT_CORE	−43.1	14.8	29.4
	G_Frontal_Inf_Tri-1	F3t	SENT_CORE	−49.4	25.6	4.7
	G_Frontal_Inf_Orb-1	F3O1	SENT_CORE	−42.2	30.5	−16.9
	G_Insula-anterior-1	INSa1	SENT_VISU	−20.3	5.0	−19.3
	G_Insula-anterior-2	INSa2	SENT_CORE	−33.8	16.8	−12.7
	G_Insula-anterior-3	INSa3	SENT_CORE	−33.7	23.7	0.6
Temporal and parietal	G_Temporal_Sup-4	T1_4	SENT_CORE	−58.7	−23.3	3.7
	G_Temporal_Mid-3	T2_3	SENT_CORE	−61.0	−35.0	-4.8
	G_Temporal_Mid-4	T2_4	SENT_CORE	−53.1	−59.4	7.0
	G_Temporal_Inf-4	T3_4	SENT_VISU	−50.0	−60.6	−7.6
	S_Sup_Temporal-1	STS1	SENT_CORE	−49.7	14.0	−21.5
	S_Sup_Temporal-2	STS2	SENT_CORE	−54.9	−7.2	−12.8
	S_Sup_Temporal-3	STS3	SENT_CORE	−54.7	−33.0	−1.7
	S_Sup_Temporal-4	STS4	SENT_CORE	−56.5	−48.4	13.4
	G_SupraMarginal-7	SMG7	SENT_CORE	−55.2	−51.7	25.5
	G_Angular-2	AG2	SENT_CORE	−37.5	−70.4	39.5
	G_Occipital_Inf-1	O3_1	SENT_VISU	−48.4	−69.0	−4.3
	G_Fusiform-4	FUS4	SENT_VISU	−43.1	−49.8	−17.4
	G_ParaHippocampal-1	pHIPP1	SENT_VISU	−15.7	−4.0	−18.4
	G_Hippocampus-2	HIPP2	SENT_MEM	−24.9	−32.5	−2.7
Internal surface	G_Supp_Motor_Area-2	SMA2	SENT_CORE	−10.6	18.2	63.1
	G_Supp_Motor_Area-3	SMA3	SENT_CORE	−7.2	7.6	65.6
	G_Paracentral_Lobule-4	pCENT4	SENT_MEM	−6.4	−29.2	75.9
	G_Cingulum_Post-3	CINGp3	SENT_MEM	−5.1	−42.9	10.0
	G_Precuneus-6	PRECU6	SENT_MEM	−7.4	−61.3	64.1
Sub-cortical	N_Amygdala-1	AMYG	SENT_VISU	−21.9	−0.4	−11.5
	N_Thalamus-4	THA4	SENT_MEM	−3.2	−14.4	8.4
	N_Putamen-2	PUT2	SENT_VISU	−23.3	6.3	0.8
	N_Putamen-3	PUT3	SENT_VISU	−28.0	−6.3	1.8

covered almost the entire putamen (PUT2 and PUT3) and a thalamic hROI located medially (THA4).

Part 2: Identification of networks based on the resting-state connectivity matrix of the 32 hROIs co-activated and co-leftward asymmetrical during the 3 sentence minus word-list tasks

In a second step, we investigated the intrinsic functional organization of the 32 hROIs selected in the first step. We computed the intrinsic connectivity matrix between these 32 hROIs for the subsample of 138 right-handed participants who completed a resting-state acquisition. We completed a hierarchical clustering analysis of this intrinsic connectivity matrix to identify temporally coherent networks within this set of hROIs.

Methods

Calculation of the intrinsic connectivity matrix

An intrinsic connectivity matrix was calculated for each of the 138 individuals and for each of the 496 possible pairs of hROIs $(N \times (N-1))/2$, with $N=32$). The intrinsic connectivity matrix off-diagonal elements were the Pearson correlation coefficients between the rs-fMRI time series of

the hROI pairs. The intrinsic connectivity matrix diagonal elements were set to zero because no information on the correlation for a specific hROI with itself exists (Rubinov and Sporns 2010). The individual intrinsic connectivity matrix was then Fisher z-transformed before being averaged over the subsample of 138 individuals, thereby producing a mean intrinsic connectivity matrix.

Identification and characterization of networks

The agglomerative hierarchical cluster analysis (aHCA) method was applied to extract brain networks from this mean intrinsic connectivity matrix. We first transformed the Pearson correlation ($r_{i,j}$) between hROI i and hROI j into a distance ($d_{i,j}$) using the equation $d_{i,j}=(1-r_{i,j})/2$, as in Doucet et al. (2011), resulting in a 32×32 dissimilarity matrix. According to Lance and Williams (1979), the previous equation is "unequivocally the best" to transform a correlation into a distance on real data sets. Finally, we used an agglomerative hierarchical clustering algorithm [aHCA, (Sneath and Sokal 1973)] for clustering and the Ward distance (Ward 1963) for aggregating the different hROIs into clusters. The number of clusters (networks) was determined using the R library NbClust (Charrad et al. 2014). This package provides 30 statistical indices for determining the optimal number of clusters and proposes the best clustering scheme from the different results obtained by varying all combinations of number of clusters for the chosen method, in this case, aHCA with Ward's distance. We chose the number of clusters that fulfilled a maximum of indices.

To characterize each network, we calculated its mean volume activation for each task contrast as the sum of the activations of all hROIs composing the network weighted by their individual volume and then divided by the sum of their volumes. The same computation was performed for the right hemisphere equivalent of each network, which was then used for computing the left-minus-right asymmetry of each network activation. We then compared activation amplitude and asymmetry values across networks and across tasks using a mixed-model ANOVA.

Reliability of the network identification across individuals

We used multiscale bootstrap resampling (Efron et al. 1996) to assess the reliability of the identification of each cluster. In total, 10,000 multiscale bootstrap resampling datasets, including 50–140% of sample data from the 138 participants, were processed. Applying the R package "pvclust" (Suzuki and Shimodaira 2006) function to the multiscale bootstrap resampling outputs, we measured the approximately unbiased (AU) p value for each cluster. The AU p value for a network, the probability of this network occurring among the 138 participants, indicates the network's reliability.

Robustness of the networks identification with respect to the clustering method

We also assessed the robustness of the clustering method by comparing its output to those of three other clustering methods: aHCA with the average distance method (instead of Ward's), Gaussian mixture model, and k-means (see supplementary material). Gaussian mixture modelling was conducted with the "Rmixmod" package with Normalized Entropy Criterion to find well-separated clusters and with a Gaussian model with diagonal variance matrices (Lebret et al. 2015).

We then compared the four different partitions through the adjusted Rand index (Hubert and Arabie 1985) allowing to get a similarity measure between two different classifications, an adjusted Rand index of 1 indicating similar partitions.

Temporal correlation across networks and significance

To compute the mean intrinsic functional correlations between two networks, we used the same methodology as that used to compute the mean intrinsic connectivity matrix (see above).

First, for each individual and for each network, we computed the corresponding rs-fMRI time series by averaging the individual resting time series of all voxels of all hROIs belonging to this network.

Then, for each individual, we computed the Pearson correlation coefficients between all pairs of networks that we further Fisher z-transformed. Finally, each of these z-transformed coefficients was averaged across the sample of 138 individuals, providing a mean intrinsic functional correlation (r) for each pair of networks. We assessed the significance of each of these mean intrinsic functional correlations compared to 0 using a non-parametric sign test at the 0.05 significance level (Bonferroni correction for the number of network pairs).

Results

Identification and characterization of networks

Hierarchical clustering analysis revealed three networks from the selected set of 32 hROIs (Fig. 2).

SENT_CORE network The first network (Fig. 1c, red), termed SENT_CORE, was composed of 18 hROIs and was the most distant from the 2 others in terms of inertia. SENT_CORE included all lateral and medial hROIs of the frontal lobe, apart prec3, pCENT4 and anterior insula INSa2 and INSa3. SENT_CORE also included all temporal and parietal hROIs

of the lateral surface, except T3_4, which was aggregated with the network gathering visual hROIs.

We named this network SENT_CORE because it included essential sentence processing regions, as further described below. SENT_CORE was the largest network in terms of volume, as it was 9.2 times larger than SENT_MEM and 3.4 times larger than SENT_VISU (Table 3).

SENT_VISU network This group of clusterized areas included the inferior temporal and occipital gyri laterally (T3_4, O3_1); the mid-fusiform (FUS4) ventrally; the parahippocampal region; the amygdala (AMYG) and INSa1, close to the amygdala medially (Fig. 1c, green); and the two hROIs of the putamen (PUT2 and PUT3). We labelled it SENT_VISU because it aggregated four hROIs acknowledged as involved in visual processing.

SENT_MEM network This network (Fig. 1c, light blue) included three regions of the medial wall—the paracentral gyrus (pCENT4), the precuneus (PRECU6) and the posterior cingulate (CINGp3)—and the posterior part of the hippocampus (HIPP2) as well as one frontal area at the upper end of the precentral sulcus (prec3) and the THA4 hROI located medially in the thalamus. We named it SENT_MEM because these posterior areas belong to both the posterior regions of the DMN involved in the posterior hippocampus in episodic memory, as further discussed below.

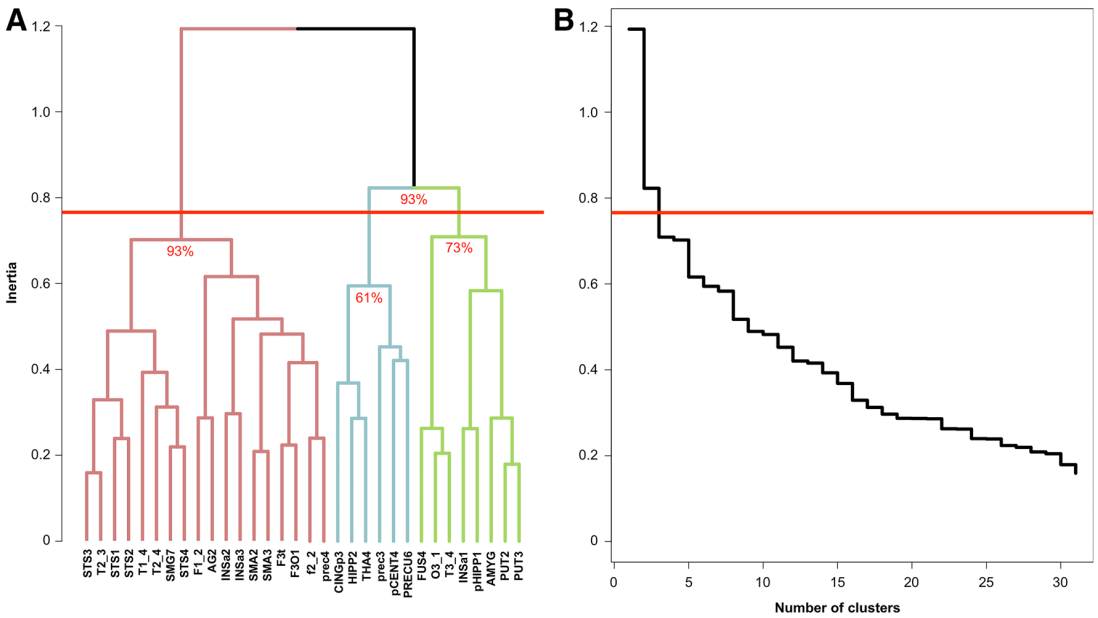

Fig. 2 Results of the agglomerative hierarchical cluster analysis method. **a** Dendrogram of aHCA of the mean intrinsic connectivity matrix (SENT_CORE network: red, SENT_MEM: light blue, SENT_VISU: green). Approximately unbiased *p* values are indicated for each identified network. **b** Scree plot of aHCA of the mean intrinsic connectivity matrix. For both graphs, the red horizontal line corresponds to the threshold applied to select the number of networks

Table 3 Mean volumetric activation (and standard deviation) of the four language networks in each sentence minus word-list contrast for production ($PROD_{SENT\text{-}WORD}$), listening ($LISN_{SENT\text{-}WORD}$) and reading ($READ_{SENT\text{-}WORD}$) tasks in 144 healthy right-handers

	Volume (mm^3)	Left activation			Leftward asymmetry		
		$PROD_{SENT\text{-}WORD}$	$LISN_{SENT\text{-}WORD}$	$READ_{SENT\text{-}WORD}$	$PROD_{SENT\text{-}WORD}$	$LISN_{SENT\text{-}WORD}$	$READ_{SENT\text{-}WORD}$
SENT_CORE	83,232	0.73 ± 0.31	0.43 ± 0.20	0.55 ± 0.26	0.41 ± 0.22	0.25 ± 0.14	0.28 ± 0.19
SENT_MEM	9024	0.40 ± 0.36	0.28 ± 0.23	0.21 ± 0.26	0.11 ± 0.17	0.08 ± 0.12	0.07 ± 0.14
SENT_VISU	24,368	0.37 ± 0.27	0.30 ± 0.17	0.25 ± 0.21	0.16 ± 0.13	0.11 ± 0.08	0.12 ± 0.10

The mean volumetric activation for a network was calculated from the sum of the activations of the hROIs comprising the network weighted by their individual volumes and then divided by the volume of the network

Profile comparisons between networks

In terms of mean voluminal activity (Table 3), ANOVA revealed a significant network effect, a task effect and a network × task interaction (all post hoc Tukey's HSD: $p < 10^{-4}$).

The interaction occurred because while in SENT_CORE, there was greater activation in PROD, followed by READ and then by LISN (all $p < 10^{-4}$), SENT_MEM and SENT_VISU had different profiles. Although the greatest activation values were also observed during PROD (all $p < 0.003$), activation values were significantly higher during LISN than during READ in both networks (SENT_VISU: $p = 0.01$; SENT_MEM: $p = 0.0067$).

ANOVA on asymmetries also revealed a significant network effect, a task effect and a network × task interaction (all post hoc Tukey's HSD: $p < 10^{-4}$). The interaction was due to different profiles of asymmetry in SENT_CORE than in the two other networks. In SENT_CORE, the profile of asymmetries was the same as that of activation: larger in PROD, followed by READ and then by LISN (all post hoc Tukey's HSD: $p < 10^{-4}$). In SENT_VISU, the asymmetry during PROD was slightly larger than that during READ (SENT_VISU: $p = 0.0005$; SENT_MEM: $p = 0.01$) and larger than that during LISN ($p = 0.0001$). In addition, there was no difference in asymmetry between PROD and LISN in SENT_MEM ($p = 0.075$) and no difference in asymmetry between READ and LISN in SENT_VISU ($p = 0.52$) or SENT_MEM ($p = 0.25$). The task main effect was related to larger asymmetries in PROD and the network main effect to larger asymmetries in SENT_CORE (all $p < 0.0001$).

Assessing the reliability of the identification of 3 networks across individuals in the 138 participants

The AU p values provided by the multiscale bootstrap resampling method showed that each network of the first partition was reliable at levels of 93%, corresponding to SENT_CORE on one side and to the SENT_VISU and SENT_MEM on the other side (Fig. 2). However, for the second partition, SENT_VISU and SENT_MEM were reliable at 73% and 61%, respectively, indicating a lower reliability.

Robustness of the identified networks with respect to the clustering method

The SENT_CORE network was identified by all 4 clustering methods, including at least 13 of the 18 hROIs initially found with the aHCA method using Ward's distance (see supplementary Table 1). The aHCA method using the average distance metric led to an adjusted Rand index of 1, indicating a clustering similar to that achieved using the aHCA method with Ward's distance. Comparing the Gaussian Mixture Model and aHCA methods led to an adjusted Rand index of 0.76, indicating two highly similar partitions. Comparing the aHCA and k-means methods led to the lowest adjusted Rand index of 0.43.

Only one hROI of SENT_CORE (AG2) was segregated in SENT_MEM by Gaussian mixture modelling and by k-means, while all 17 other hROIs were classified together by all clustering methods but k-means (supplementary Table 1), although PUT3 joined SENT_CORE according to Gaussian mixture modelling. k-means classified INSa3, T2-4, T1-4 and f2-2 in SENT_VISU rather than in SENT_CORE.

Only prec3 was classified in SENT_VISU rather than SENT_MEM with both Gaussian mixture modelling and k-means, while pHIPP1 shifted from SENT_VISU to SENT_MEM only with k-means.

Temporal correlation across networks and significance

The chord diagram shown in Fig. 3 describes the average correlations between each pair of hROIs in the three networks. Strong and highly significant negative mean intrinsic correlations were found between SENT_CORE and SENT_MEM ($R = -0.27$; 92.03% of the participants showed a negative correlation, $p < 10^{-4}$), and a positive correlation was present between SENT_MEM and SENT_VISU ($R = 0.058$, 62.32% of the participants showed a positive correlation, $p = 0.0024$), while there was no significant correlation between SENT_CORE and SENT_VISU ($R = -0.037$; 56.52% of the participants showed a positive correlation, $p = 0.074$).

Part 3: Graph theory analysis of the SENT_CORE network

We applied graph theory analysis to the SENT_CORE hROI pairwise correlation matrix, including only positive correlations since the inclusion of negative correlations in graph theory analysis remains controversial (Rubinov and Sporns 2010). Note that the graph theory analysis of intra-network communication was completed for only SENT_CORE, as the other two networks had too few nodes.

Statistical analysis

Identification of hubs using graph analysis metrics of the networks

Measurements of weighted centrality We measured the degree centrality (DC) of the hROIs composing the SENT_

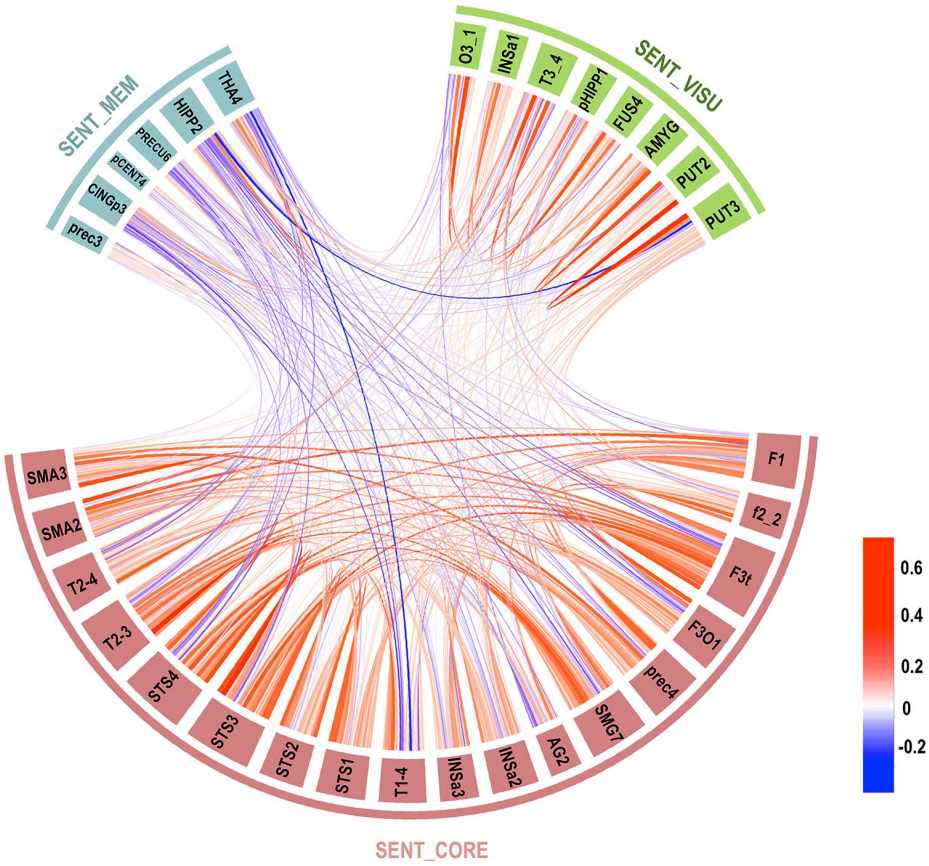

Fig. 3 Chord diagram of the temporal correlation across each hROI composing the three networks averaged in the whole group. Abbreviations for hROIs of the AICHA atlas can be found in Table 2 (colour scale goes from red for positive correlation to blue for negative correlations, and the line width indicates the strength of the correlation)

CORE network, corresponding to the sum of the strength of the positive correlation of each node (hROI). DC can thus be interpreted as the amount of information that a given hROI receives from the hROIs to which it is directly connected, i.e., the DC measures the importance of a given hROI within its network according to the number and strength of interactions it undergoes with the other hROIs.

The betweenness centrality (BC) was also measured for SENT_CORE as defined by Opsahl et al. (2010). The BC of an hROI can be interpreted as the participation rate of that hROI in the set of shortest paths between any pair of nodes within the network; i.e., BC measures the dependence of the network on a specific hROI for its communication.

Hub definition and clustering To discriminate hubs among SENT_CORE, we applied a combination of Sporns et al. (2007) and van den Heuvel et al. (2010) definitions. We considered that an hROI had the properties of a hub when its DC and BC values were larger than the means plus one standard deviation of the DC and BC values of the hROI set in the network.

To assess whether the hubs identified in SENT_CORE participated in communication with the other two networks or whether its communication was only intra-SENT_CORE, we calculated the participation index (pIndex) criteria as defined by Guimera (Guimera and Amaral 2005). hROIs having the 15% highest pIndex values were considered connector hubs (i.e., between networks) (van den Heuvel and Sporns 2011), while the other hROIs corresponded to provincial hubs, i.e., an hROI communicating with only its own network.

Investigation of the relationship between intrinsic connectivity and activation measured during the language tasks

Relationships between DC and BOLD variation at the hROI level We investigated whether an hROI exhibiting high intrinsic connectivity with other areas of the SENT_CORE was more activated during language tasks. For this, we performed a MANCOVA with repeated measures with a TASK main effect, a DC main effect and a DC by TASK interaction. Correlations values and corresponding p values between the DC and activation were computed for each hROI and each task.

To test the specificity of this relationship, we completed similar MANCOVA with DC measurements obtained for the 185 hROIs of the AICHA atlas covering the entire

left hemisphere. Therefore, the DC values were computed considering the connections of hROIs belonging to SENT_CORE with all other hROIs of the left hemisphere. This analysis made it possible to more deeply characterize whether the relationship between the DC and activation during the language tasks was specific to the essential language network intrinsic connectivity or whether this relationship was held at the hemispheric level.

Relationships between the DC measured in the SENT_CORE network and BOLD variation upon pooling all hROIs and participants To test whether the relationship previously identified between DC and BOLD signal variation for each hROI of SENT_CORE was a general property that could be extrapolated to any hROI of any participant, we applied the method proposed by Buckner for evaluating the relationship between DC and beta-amyloid accumulation in Alzheimer's disease (Buckner et al. 2009). Correlation coefficients obtained for the three tasks between DC values and BOLD variations were compared using the R package "cocor" (Diedenhofen and Musch 2015) to determine whether there was any difference across language tasks.

Results

Graph analysis of SENT_CORE

Sample distributions of DC and BC values DC variation across the hROIs spanned from 2.24 to 6.48 (Table 4), and the DC standard deviation was very consistent across hROIs ranging from 1.17 to 1.79.

By contrast, BC variation across the hROIs spanned from 0.72 to 18.98 (Table 4). Notably, only 3 hROIs had low numbers of BC null values across the sample of 138 participants: F3t, STS3 and STS4 (1%, 6% and 2% null values, respectively, Table 4).

Hub identification and characterization Three hROIs corresponded to the hub definition, i.e., BC and DC values above the chosen significance thresholds (mean + SD) of 10.26 and 5.55, respectively (Table 4). The first hROI (F3t) was located in the frontal lobe, and the other two were located in the posterior third of the STS (STS3 and STS4). The BC values of these 3 hubs were over 11, and their DC values were over 5.5, with F3t having the strongest values (Fig. 4; Table 4). Note that no other hROI exhibited a supra-threshold value for any of the centrality indices.

Table 4 Betweenness and degree centrality of SENT_CORE hROIs

	AICHA hROI	Betweenness centrality			Degree centrality				
		Mean	SD	% Null values	Mean	SD	Skewness	Kurtosis	*p* norm
Frontal and insula	prec4	6.88	7.00	11	4.94	1.50	−0.07	−0.24	0.87
	F1_2	6.30	5.42	17	4.64	1.40	0.28	−0.32	0.27
	f2_2	3.33	4.45	37	3.35	1.53	0.60	−0.42	0.0002
	F3t	**18.98**	**9.77**	**1**	**6.48**	**1.26**	**−0.06**	**−0.29**	**0.78**
	F3O1	2.18	4.04	54	4.31	1.50	0.50	−0.02	0.018
	INSa2	2.49	3.66	43	3.84	1.46	0.27	−0.23	0.14
	INSa3	2.54	3.98	40	3.01	1.29	0.76	0.63	0.0005
Temporal and parietal	T1_4	0.75	2.19	77	3.12	1.47	0.56	−0.20	0.0012
	T2_3	5.28	5.96	29	5.44	1.43	0.05	−0.17	0.71
	T2_4	2.21	4.28	58	3.46	1.79	0.24	−0.60	0.074
	STS1	2.46	3.57	41	4.55	1.52	−0.10	−0.18	0.44
	STS2	3.07	4.85	41	4.30	1.44	0.14	−0.58	0.11
	STS3	**13.04**	**9.66**	**6**	**6.32**	**1.36**	**−0.36**	**0.23**	**0.088**
	STS4	**13.33**	**8.25**	**2**	**5.58**	**1.51**	**0.09**	**−0.22**	**0.95**
	SMG7	6.23	6.86	22	5.28	1.60	−0.21	−0.64	0.037
	AG2	0.72	1.65	71	2.24	1.17	0.88	1.11	0.0002
Internal surface	SMA2	2.21	3.58	46	4.35	1.33	0.33	−0.09	0.32
	SMA3	2.24	3.60	49	4.22	1.28	0.05	−0.36	0.45

The means and standard deviations (SD) of the betweenness centrality (BC) and degree centrality (DC) were computed by averaging the BC and DC values of each participant for each SENT_CORE hROI. For BC, the percentage of null values is based on the number of BC values at zero among the 138 subjects for one hROI. For DC, the skewness, kurtosis and Shapiro–Wilk normality test (*p* norm) correspond to information regarding the normality of the DC distribution for each hROI. A value above 0.05 for the Shapiro–Wilk normality test indicates that the DC was normally distributed. hROIs in bold are those we found to be hubs

Concerning the pIndex, hubs were defined as the top 15% of the highest index (pIndex ranging from 0.587 to 0.989). Five hROIs were thus defined as connector hubs: T2_3 (pIndex = 0.989), F3t (pIndex = 0.987), F1_2 (pIndex = 0.984), STS3 (pIndex = 0.983) and SMA2 (pIndex = 0.983).

Note that the centrality hubs F3t and STS3 were also connector hubs, meaning that they are important for both communication among the three different networks and for communication within the SENT_CORE network.

Note that T2_3 was a connector hub characterized by high DC and BC values (Table 4), although it did not meet the criteria to be labelled as a centrality hub (Fig. 4).

Relationship between the DC at rest and activations during the language tasks in the SENT_CORE network

Relationship at the individual hROI level Using DC values computed from only SENT_CORE hROIs, we observed significant positive correlations between activations during the 3 language tasks and these DC values in 12 hROIs among the 18 constituting SENT_CORE together with a trend for PREC4 and f2_2 (Table 5). Among these hROIs, DC values were positively correlated with activations during the language tasks and the *R* value varied between 0.17 and 0.33. Moreover, in 8 of these 12 hROIs, there was no DC by Task interaction, meaning that the correlation between the DC and activation did not differ between the tasks. In the f2_2, INSa2, INSa3, T1_4 and SMG7 hROIs, a significant DC by Task interaction was observed. In f2_2, the interaction was due to non-significant correlation for the production task contrast, while the correlation was strong and significant for the reading and listening task contrasts. In INSa2, INSa3 and T1_4, the interaction was due to non-significant correlation for the listening task, while there were strong and significant correlations for production and reading. In SMG7, the interactions were due to a lower correlation during listening (Table 5).

The results obtained using DC values computed from the entire set of 185 left hemisphere hROIs were strikingly different. There was a significant main effect of the DC in only 2 hROIs (F3t and SMG7, see supplementary Table 2), meaning that, except for these two regions, the strength of the correlation when the DC was calculated across the hROIs of the entire hemisphere did not explain the activation variations in SENT_CORE hROIs.

Relationship at the global level using all participants and hROIs There was a significant correlation between the DC values and BOLD variations measured in each of the 3 tasks when considering the 18 SENT_CORE hROIs and the 138 participants in a single analysis (Fig. 5) for each task. The coefficient correlation values were 0.158, 0.216 and 0.294 for sentence production, sentence listening and sentence reading, respectively. The correlation for reading was significantly larger than that for both listening ($p = 0.0025$) and production ($p = 0.0075$), and the latter two were not significantly different ($p = 0.80$).

Summary of results

Conjunction analysis of left-activated and leftward asymmetrical hROIs in 144 right-handed participants performing three language tasks ($PROD_{SENT\text{-}WORD}$, $READ_{SENT\text{-}WORD}$ and $LISN_{SENT\text{-}WORD}$) uncovered a set of 32 supramodal regions involved in lexico-syntactic processing. The hierarchical bottom-up clustering of the intrinsic connectivity between these 32 hROIs led to the identification of 3 networks, including a network of essential language areas (SENT_CORE) with strong positive correlations at rest across its 18 hROIs in more than 90% of the participants. The two other identified

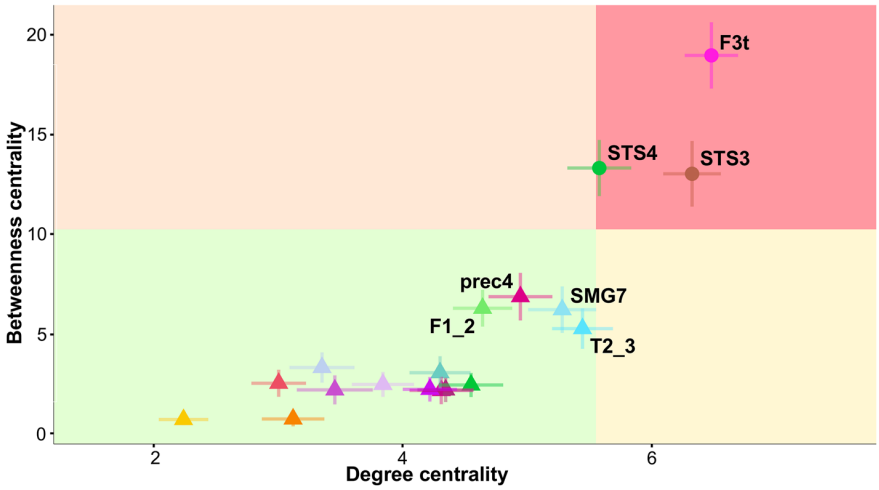

Fig. 4 Plot of degree centrality (DC) versus betweenness centrality (BC) in SENT_CORE. The mean plus standard deviation values of DC and BC define the quadrants. hROIs located in the superior right quadrant are hubs. Abbreviations for the hROIs of the AICHA atlas can be found in Table 2

Table 5 Correlation analysis between the degree centrality measured in the SENT_CORE network and the mean activation in each of the three language tasks

	AICHA hROI	MANCOVA		$PROD_{SENT-WORD}$		$LISN_{SENT-WORD}$		$READ_{SENT-WORD}$	
		DC	DC*Task	*R*	*p*	*R*	*p*	*R*	*p*
Frontal and insula	prec4	0.072	0.84	0.066	0.44	0.163	0.056	0.146	0.088
	F1_2*	0.0065	0.24	0.181	0.033	0.116	0.18	0.206	0.016
	f2_2	0.092	0.0008	−0.115	0.18	0.229	0.0068	0.248	0.0034
	F3t*	< 0.0001	0.35	0.264	0.0018	0.255	0.0025	0.245	0.0037
	F3O1*	0.02	0.75	0.161	0.060	0.196	0.022	0.113	0.19
	INSa2*	0.0025	0.032	0.200	0.019	0.072	0.40	0.267	0.0015
	INSa3*	0.0006	0.017	0.231	0.0063	0.037	0.67	0.289	0.0006
Temporal and parietal	T1_4*	0.0006	0.0008	0.316	0.0002	0.026	0.77	0.260	0.0021
	T2_3*	0.009	0.06	0.266	0.0016	0.173	0.043	0.210	0.013
	T2_4*	0.0008	0.21	0.124	0.15	0.183	0.032	0.261	0.0020
	STS1*	0.0002	0.27	0.289	0.00060	0.228	0.0073	0.231	0.0064
	STS2	0.67	0.33	0.084	0.33	−0.028	0.75	0.033	0.70
	STS3*	0.021	0.36	0.198	0.020	0.153	0.073	0.140	0.10
	STS4*	0.0010	0.08	0.250	0.0032	0.187	0.028	0.283	0.0008
	SMG7*	< 0.0001	0.007	0.329	0.0001	0.204	0.016	0.303	0.0003
	AG2	0.41	0.78	0.009	0.92	0.091	0.29	0.065	0.45
Internal surface	SMA2	0.28	0.058	0.095	0.27	−0.061	0.48	0.149	0.082
	SMA3	0.16	0.66	0.111	0.20	0.074	0.39	0.076	0.37

Correlations (*R*) were calculated within each hROI of the left hemisphere constituting the SENT_CORE network, and the DC values were calculated in the SENT_CORE network. hROIs with a * are those with significant correlations between activation and DC values ($p < 0.05$)

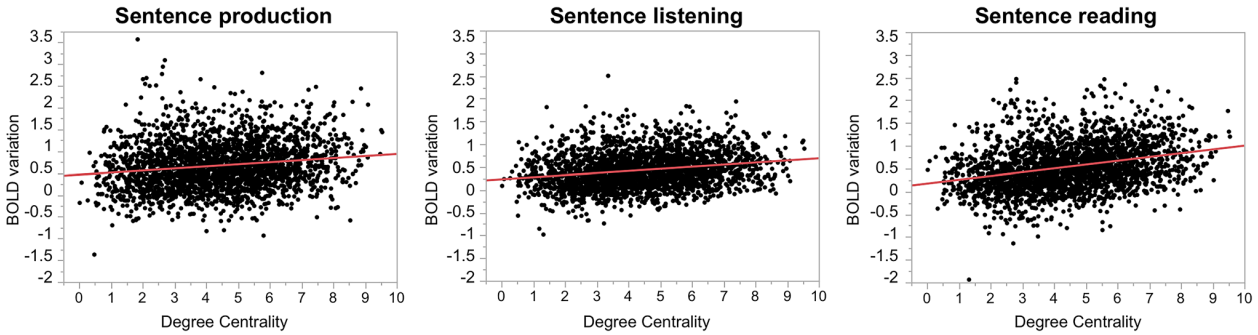

Fig. 5 Correlation between DC values and activations in SENT_CORE across participants and across the 18 hROIs during each of the 3 language tasks. Plots of DC values and BOLD variations of the sentence minus word contrasts calculated for sentence production (left), sentence listening (middle), sentence reading (right) and degree centrality. The positive correlation coefficients ($N = 138 \times 18 = 2484$) are 0.158 for sentence production, 0.216 for sentence listening, and 0.295 for sentence reading

networks had lower inter-individual consistency, one including visual language areas at the interface between visual and syntactic processing (SENT_VISU) and the other including posterior DMN areas including posterior hippocampus (SENT_MEM). Intrinsic connectivity analysis showed that SENT_CORE was negatively correlated with SENT_MEM but was not correlated with SENT_VISU. Graph analysis metrics obtained for the SENT_CORE network revealed that F3t, STS3, and STS4 were hubs of both degree and betweenness centrality, and F3t and ST3 were also hubs of participation, meaning that these are key areas for both intra-network communication and inter-network communication between SENT_CORE and the other 2 networks. Importantly, a positive correlation across individuals was observed between the DC measured at rest and the strength of activation in most SENT_CORE regions, meaning that participants with higher DC values in a given region had higher activations than participants with lower DC values.

Moreover, such a positive correlation between the DC and activation was still significant when all regions of all participants in the three tasks were pooled, meaning that this was true regardless of the cortical area considered.

Discussion

Methodological issues

In this study, we selected right-handers from the BIL&GIN database because we previously demonstrated that these participants have a left hemisphere dominance for language at both the group level (Tzourio-Mazoyer et al. 2016) and the individual level (Zago et al. 2017), with only 5 (3%) of the 144 participants having a co-dominant right hemisphere. This sample group is optimal for selecting areas specific for sentence processing based on a conjunction of activations and leftward asymmetries. In addition, the inclusion of a fairly considerable number of participants ($N = 144$) provided us a high sensitivity for detecting supramodal sentence areas while minimizing the risk of overlooking some.

However, we must underline that the present atlas is not all-inclusive. First, we selected map regions involved in only high-order language processing and lexico-syntactic processing. Using the list of familiar words as the reference condition, we removed the dorsal route of language, including the phonological loop, responsible for articulation and sound-to-articulation mapping (Saur et al. 2008; Rauschecker and Scott 2009) In addition, the regions selected herein focused on the left hemisphere and did not account for right hemisphere-specialized aspects of sentence processing, such as emotional prosody (Beaucousin et al. 2007; Hurschler et al. 2012) and context processing (Grindrod and Baum 2003; Ferstl et al. 2005).

Second, the presence of susceptibility artefacts combined with averaging the large number of participants led to incomplete mapping of the inferior part of the temporal lobe, prohibiting us from documenting some areas, such as the basal language area in the anterior part of the fusiform gyrus. This essential language area, first identified using deep electrical recordings (Nobre et al. 1994), has been shown with positron emission tomography (PET) to be activated during both the production and auditory comprehension of language (Papathanassiou et al. 2000).

Third, small size regions may also be lacking in this atlas since we provided data at the hROI scale rather than at the voxel scale.

Concerning the clustering methods of correlation values at rest, a perfect match was observed between the Ward and average clustering methods (see supplementary material Table 1), and a good score was obtained with the Gaussian mixture model for global clustering at the 32 hROI levels. The weakest score was that of the *k*-means method, and such a difference in clustering observed with *k*-means compared to that in the other 3 methods is consistent with the fact that, as reported by Thirion et al., *k*-means forms clusters spatially close and connected but with poor reproducibility using the sample studied. By contrast, hierarchical clustering using Ward's method, which we selected to segregate the networks, was reported to create connected clusters that are highly reproducible using the studied samples (Thirion et al. 2014).

A large set of supramodal language areas is involved in sentence processing tasks

We carefully designed each of the language tasks such that joint analyses were possible; the design was identical in the three tasks, and we chose to make them close enough to allow comparisons and conjunctions in terms of the number of words or the complexity of sentences. As mentioned above, the use of a high-level verbal reference task for controlling the involvement of primary areas (auditory, visual and motor) and removing phonological and automatic word processing kept the lexico-syntactic aspects common to all three tasks.

The first set of 32 hROIs provides left hemispheric regions that are dedicated to the monitoring and completion of tasks based on sentence processing. Although not all regions can be considered essential language areas, all were determined to be modulated by the verbal material with which they are associated (left activation and leftward asymmetry) and are thus part of an extended language network functioning during language tasks.

Unsupervised hierarchical clustering based on the resting-state connectivity between hROIs successfully segregated three different networks, including networks hosting core language, visual areas, and posterior areas of the DMN and posterior hippocampus. Within the systems to which they belonged, these networks hosted areas dedicated to the interaction/interface with language systems. For example, the current analysis extracted from among the visual areas involved in picture processing those areas specifically dealing with picture–sentence meaning integration.

Sentence comprehension essential network (SENT_CORE)

Clustering the resting-state correlation between these 32 hROIs allowed the discrimination of SENT_CORE, a network of 18 strongly and positively correlated hROIs, including frontal and temporo-parietal hROIs located on the lateral surface of the left hemisphere and anterior insula areas. In particular, SENT_CORE included areas of the antero-posterior language networks, named in reference to the

Broca–Wernicke model in aphasia literature and reported with consistency in meta-analyses of healthy individuals mapped during language tasks see Fig. 6 (Vigneau et al. 2006; Price 2010, 2012). Note that SENT_CORE was the largest network in terms of volume (in mm^3), as it included more than half of the hROIs (18/32), all of which were strongly activated and leftward asymmetrical.

In the following, we discuss the potential roles of the identified areas in relation to the literature. However, it is now acknowledged that, apart from very specific regions where a lesion can be closely associated with a specific defect, the role of a given area documented with functional imaging must be understood as the combination of its functional properties with those of the regions with which it constitutes a network to complete a given cognitive task. For example, prec4 is not part of the regions commonly labelled as "language areas". The present work shows that prec4, located at the junction between the precentral and middle frontal gyrus, is both strongly activated and leftward asymmetrical in the three sentence tasks. Language meta-analyses have reported prec4 as part of the language areas involved in lexico-syntactic processing (named F2p in Vigneau et al. 2006, Fig. 6), and in word selection and hierarchical sequencing (named dPrec in Price 2010, Fig. 6). Applying Neurosynth to prec4 coordinates ($x = -42.2$, $y = 0.7$, $z = 50$, Table 3) with an association test reveals the greatest number of studies with the terms "sentence", "comprehension", "language", and "sentences", followed by "eye" and "premotor". Jouen et al. (2018) propose that prec4 is "involved in the understanding of actions during verbal and non-verbal tasks". In the present protocol, the sentences involved human actions, closely consistent with that role proposed by Jouen et al. (2018). Using a network approach, Saur et al. (2008) found that prec4 belongs to the sentence comprehension functional network. In Glasser's atlas, prec4 corresponds to "language area 55b" (Glasser et al. 2016) and overlaps the posterior part of the "rostro-ventral module" described by Genon et al. (2018a, b). In this last work based on peaks meta-analysis, this module is connected with the inferior frontal gyrus, orbital frontal and inferior parietal as prec4 in the present work. The present study further demonstrates that prec4 is involved in a supramodal manner during

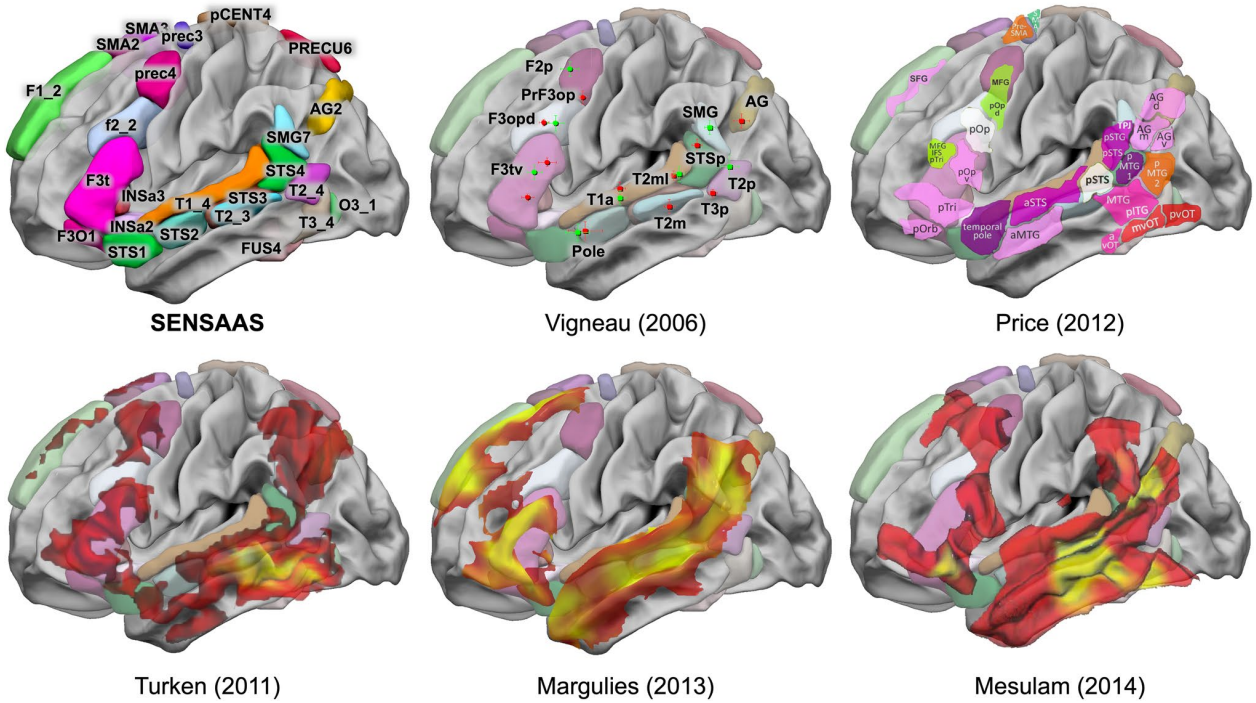

Fig. 6 Schematic comparison of SENSAAS with the literature. This figure shows the results of neuroimaging meta-analyses and clinical studies superimposed on the hROI of SENSAAS of the lateral surface of the left hemisphere of the BIL&GIN display template. In the first row: left SENSAAs hROIs of the left hemisphere lateral surface; middle: clusters of the meta-analysis of semantics (red) and sentence processing (green) adapted from Vigneau et al. (2006) with their labels: right: schematic representation of the meta-analysis of language-related activation studies (adapted from Price (2012); sentence: purple; semantics: light and dark pink; visual: red; word retrieval: green; integration: white). In the second row, left: functional connectivity of the left middle temporal gyrus centred on the site where lesion results in deep aphasia (orange, adapted from Turken 2011); middle: functional connectivity from a seed centred on the left inferior frontal gyrus (BA 45, red, adapted from Margulies and Petrides 2013); right: zones of atrophy observed when pooling all types of PPA (orange, adapted from Mesulam et al. 2014)

sentence processing, is strongly leftward asymmetrical, and is strongly and positively connected at rest with the network of areas we named SENT_CORE that hosts essential language areas. These findings are consistent with the fact that prec4 is part of the areas that are conjointly atrophied in patients suffering from nonfluent primary progressive aphasia (PPA) (Mesulam et al. 2014) (Fig. 6).

Indeed, in the frontal lobe, SENT_CORE includes the whole inferior frontal gyrus (F3t and F3O) corresponding to Broca's area according to most authors, whose lesion is responsible for conversational deficits, as is also the case for the anterior insula (INSa2, INSa3) (Borovsky et al. 2007). The posterior part of the inferior frontal sulcus (f2_2), also part of SENT_CORE, has been underlined as an area involved in lexico-syntactic processing (named F3opd in Vigneau et al. 2006, Fig. 6). Price also targeted f2_2 as being involved in word selection and hierarchical sequencing (named mFG in Price 2010, Fig. 6). Another indication of the important role of f2_2 in language is that together with F3t and prec4, it is the location of atrophy in nonfluent PPA [(Mesulam et al. 2014) see Fig. 6].

In the medial part of the frontal lobe, SENT_CORE includes both preSMA and the superior frontal gyrus (here, SMA2, SMA3 and F1_2), which have been reported in tasks involving sentences dealing with characters (Hervé et al. 2012), as in the present paradigm. The activation of these areas has been attributed to processing the social aspects of verbal material (Ferstl and von Cramon 2002). As discussed below, these medial frontal areas are strongly connected with the posterior part of the middle temporal gyrus (Turken and Dronkers 2011). Notably, these medial frontal areas are also the sites of atrophy in PPA (Wilson et al. 2010a, b; Tetzloff et al. 2018).

In the temporal lobe, SENT_CORE included the STS together with the posterior part of the middle and superior temporal gyri, extending to the angular and supramarginal gyri. This characterization is consistent with the proposal by Price that these areas are involved in amodal semantic combinations, a process common to the three sentence tasks (Price 2010). A recent work on the time course of sentence processing areas has also shown that the posterior temporal lobe, here corresponding to STS3 and T2_3, is involved in lexico-syntactic processing, with the processing of individual words in relation to the syntactic structure (Matchin et al. 2018). These posterior temporal areas have been documented to be essential language areas since the lesion of each results in specific deficits in sentence comprehension (Dronkers et al. 2004). In particular, lesion of the posterior parts of the middle temporal gyrus results in deep aphasia due to a loss of word meaning (Dronkers et al. 2004), consistent with the specific atrophy observed in logopenic PPA (Wilson et al. 2010a, b). STS4, located dorsally to STS3 and T2_3, is involved in sentence-level high-order processing, and Matchin, in his work on the time course of sentence processing investigated with MEG, proposed that "increased activation at the end of the sentence suggests a response associated with the interpretation of the sentence" (Matchin et al. 2018). The integration gradient of sentence meaning from lexical to conceptual progresses posteriorly with SMG7, which corresponds to the area labelled STSp in Vigneau et al.'s meta-analysis (Fig. 6). Vigneau et al. reported the following: "STSp role seems to process the semantic integration of complex linguistic material. This statement comes from the observation that it is recruited when subjects listen to coherent rather than syntactically or pragmatically incoherent sentences (Kuperberg et al. 2000; Luke et al. 2002), and it is involved in context processing and syntactic generation—more activated when subjects have to choose between two words to end a sentence or have to generate the final word of a sentence (Kircher et al. 2001). STSp activity is very likely related to the linkage of linguistic structure to meaning: it is more activated when sentences are linked as dialogue (Homae et al. 2002) or syllogisms (Goel et al. 1998) than when they are unlinked. It is also more activated during text comprehension, either presented auditory [compared to reverse speech (Kansaku et al. 2000; Crinion et al. 2003) or words (Jobard et al. 2007)] or visually [compared to words (Jobard et al. 2007) or pseudo-word reading (Vingerhoets et al. 2003)]". Price made an alternative proposal in her meta-analysis in 2000 stating that the equivalent of SMG7 (vSMG and pPT) is activated by sentence processing, particularly when the sentences increase in difficulty, and she therefore suggested that SMG7 is involved in subvocal articulation. The present results demonstrating that SMG7 is involved and leftward asymmetrical not only during production and reading but also during sentence listening, which was cited as a easy task by the participants, suggests its involvement in meaning elaboration. The angular gyrus is the final location where this integration towards conceptual knowledge operates dorsally. Known to be involved in lexico-semantic processing, as identified by language task-induced activation studies [(Vigneau et al. 2006; Price 2010), see Fig. 6], the angular gyrus is specifically involved in conceptual knowledge as shown by neuropsychological studies. Lesion of this area leads to the inability to associate a sound or image related to the same concept (Saygin et al. 2004), and inactivation of the angular gyrus in the left hemisphere induces a deficit in semantic integration (Price et al. 2016). The angular hROI identified herein corresponds to Wang's C5 and C6 parcels, involved in both language and theory-of-mind tasks (Wang et al. 2017). This last observation confirms that the role of the angular gyrus includes the interfacing between sentence processing and the understanding of human actions, a process that is part of the present sentence tasks.

The similitude between the areas composing the SENT_CORE network and the regions showing atrophy in all types of PPA [(Mesulam et al. 2014), see Fig. 6] is striking and a key element evidencing that SENT_CORE contains essential language areas, although the anterior part of the inferior temporal gyrus hosting the basal temporal language area (Nobre et al. 1994; Papathanassiou et al. 2000) is lacking for the methodological reasons discussed above. Finally, the language functional network, which shares a common molecular basis of interaction highlighted by Zilles et al. using neurotransmitter receptor fingerprints (Zilles et al. 2015), overlaps the hROIs of SENT_CORE, apart from AG2. Based on Zilles et al. report, we can hypothesize that the two other sentence-related networks we have identified are likely to have different fingerprints from those of SENT_CORE. However, because the hROIs of these networks were selected as both activated and leftward asymmetrical in the three sentence tasks, it would be of interest to investigate what subset of fingerprints the hROIs of SENT_VISU and SENT_MEM may share in common with SENT_CORE to deepen our understanding of network interactions.

Hubs of SENT_CORE

The computation of betweenness and degree centralities allowed us to identify three hubs within SENT_CORE: one in the inferior frontal gyrus (F3t) and two others along the posterior part of the temporal cortex (STS3 and STS4). These high centrality figures demonstrate that these hROIs play a central role in communications with other parts of SENT_CORE, and the participation indices of F3t and STS3 further indicate their key role in communication with the other networks identified. Such properties are consistent with the definition of epicentres proposed by Mesulam et al. (2014), and these regions can be considered essential for sentence/test comprehension independent of the modality. According to Mesulam, the network epicentre specializes in a specific behavioural component, which is language in this study, and the destruction of transmodal epicentres causes global impairments. In fact, as noted above, these hROIs overlap the middle temporal gyrus targeted in the aphasics investigation by Dronkers et al. (2004) as well as the regions showing the highest atrophy in all types of PPA (Mesulam et al. 2014), confirming that they do correspond to epicentres. In addition, these hubs are distributed in the anterior and posterior cortices, constituting an antero-posterior loop across areas belonging to the same hierarchical level in terms of cortical organization, consistent with Fuster's model for cognition (Fuster and Bressler 2012).

Other studies involving functional connectivity at rest have shown the strong connection of the left inferior frontal gyrus at rest with all SENT_CORE areas [(Margulies and Petrides 2013), Fig. 6]. The similarity between the regions found by these authors when seeding the posterior part of the middle temporal gyrus (here, STS3 and STS4) and the areas constituting SENT_CORE is also clear [(Turken and Dronkers 2011), Fig. 6]. These two observations are consistent with the present observation that these regions are hubs for sentence processing and, more generally, the language comprehension network. Such a framework is also thought to correspond to the Broca–Wernicke language model, with F3t serving as Broca's area and STS3 and STS4 serving as regions involved in the supramodal integration of meaning, consistent with the location of posterior areas leading to comprehension deficits (Pillay et al. 2017). These posterior STS areas are also considered by Binder as areas supporting meaning integration during sentence comprehension (Binder 2017). Considering that a left deficit in this area leads to deficits in language comprehension, we propose to label it Wernicke's area, although as reviewed by Binder, such a definition is different from the location currently proposed for Wernicke's area in the superior temporal gyrus. In the present work, closely adhering to an anatomo-functional definition in reference to deficits in comprehension associated with Wernicke's aphasia (Dronkers et al. 2004; Binder 2015, 2017), we propose that F3t, STS3 and STS4, regions strongly activated and asymmetrical during sentence processing in different modalities and hubs of the SENT_CORE network, are the epicentres of sentence comprehension.

Other areas contributing to sentence tasks

Because there was a low inter-individual consistency in the segregation of the networks labelled SENT_VISU and SENT_MEM, we will discuss the potential role of the 14 hROIs that were not part of SENT_CORE together.

Since each event of the sentence tasks included task monitoring, such as shifting between the word list and sentence tasks when a picture was presented or providing a motor response at the end of sentence processing, the involvement of executive areas was expected. Conjunction analyses indeed revealed that, in addition to the anterior insula at play in the three tasks (see above), putamen hROIs were involved and are a key neural support of executive functions and task monitoring (Monchi et al. 2006; Sefcsik et al. 2009). Moreover, a recent meta-analysis involving connectivity modelling showed that the left and right putamen areas are different in terms of their respective co-activations, which are specifically co-involved in language areas (Viñas-Guasch and Wu 2017).

The posterior cingulate, precuneus, and paracentral lobule together with the posterior hippocampus are part of the DMN, which has been shown to be involved in both episodic thinking and processing of "self". At rest, these areas constituted a network that had a very strong and negative correlation with SENT_CORE, confirming that, although

they belong to different networks, they are related at rest. Task-induced activation studies have demonstrated that posterior DMN regions are part of mind-reading areas together with the angular gyrus (Spreng et al. 2009). Activated and leftward lateralized during language tasks, this set of areas likely interacts with SENT_CORE during language tasks to process the sentence content dealing with social interactions (Hervé et al. 2012). The angular gyrus is a likely candidate for such an interaction since it segregated with SENT_MEM areas in two clustering methods and is involved in both language and theory-of-mind tasks (Wang et al. 2017).

The fact that these posterior areas were segregated with the posterior hippocampus, involved in both the actual perception and the encoding of scenes (Zeidman and Maguire 2016), suggests that the SENT_MEM network is also involved in the image processing of the drawings, a component common to the three sentence tasks. In fact, all participants performed well in the recall of these sentences (more than nine out of ten images recalled).

Finally, three hROIs were located along the occipito–temporal junction. The posterior part of the inferior temporal lobe (T3_4), the inferior occipital gyrus (O3_1) and the mid-fusiform gyrus (FUS4), with activity and leftward asymmetry, are likely related to the processing of the sentence content in relation to the one-second drawing presentation (minus the scramble version of the word-list reference tasks) common to all tasks. In her meta-analysis, Price considered these areas to be involved in direct visual combinations (Price 2010), consistent with the design of the present paradigm wherein the participants dealt with images related to sentence content regardless of the sentence task modality and the fact that the mean value and asymmetry of this network did not vary with the language tasks. Furthermore, in her 2012 review, Price considered these areas to be involved in sentence processing depending on the task demand (Price 2012). FUS4 is a region of the ventral route that corresponds to the visual word form area (Mellet et al. 2018). It is notable that this region was activated and leftward asymmetrical during the three tasks and segregated with the other visual regions at rest. Such a behaviour is in accordance with Price and Devlin's proposal that the mid-fusiform area is involved not only in word and visual processing but is a multimodal area whose function is determined by the set of interacting areas (Price and Devlin 2003). FUS4 involvement in the present study is likely to be in the association between the meaning conveyed by the pictures and the sentences and appears to be at play whatever the sentences' modality. The fact that FUS4 did segregate with visual areas rather than sentence areas at rest supports this hypothesis (Fig. 2). In fact, visual hROIs were not correlated with SENT_CORE networks, meaning that they do not exchange information at rest. However, these areas involved in visual processing, as well as the other hROIs that did not constitute a network at rest with sentence core areas, showed a strong leftward activation during the language tasks, suggesting that their involvement during sentence is, at least in part, related to top-down influences from language networks.

The degree of centrality measured in SENT_CORE explains the activation variability during the three language tasks

To our knowledge, this study is the first to report a positive correlation between DC and task-induced activation values. Considering that the correlations between DC values and activation were positive for all hROIs, we suggest that the mechanism underlying this result may be that regions more highly connected within the SENT_CORE network are more highly recruited during language tasks. Such a hypothesis is supported by a very recent work conducted with electrocortical stimulation that demonstrated that critical language sites have significantly higher connectivity (Rolston and Chang 2018). It is also important to note that for 8 of the 13 hROIs, no significant effect of the nature of the task on the correlation strength was observed: the positive correlation did not differ regardless of whether the participants produced, read or listened to sentences compared to listing words. Such a relationship was also observed when plotting all SENT_CORE regions of all subjects, as reported by others in a different context (Buckner et al. 2009), meaning that the relationship between resting-state intrinsic connectivity and activation strength remains regardless of the participant and cortical area being considered. In Buckner's study, the authors hypothesized that beta amyloid accumulates in high DC regions because their high metabolism makes them more vulnerable to the disease, consistent with the report that the DC calculated at the voxel level in the entire hemisphere is correlated with cerebral blood flow values (Liang et al. 2013). Similarly, DC values computed at the hROI level in the SENT_CORE network may also indicate the metabolism of language areas in a given individual, which may be of interest in the evaluation of pathological states. Mesulam et al. reported the selective atrophy of right hemisphere areas in a PPA patient with right hemisphere dominance for language, an observation suggesting that language networks are specifically targeted by this illness (Mesulam et al. 2005). DC measurements in SENT_CORE may thus be a valuable index with which to evaluate inter-individual variations in language area activities in relation to anatomical and clinical patterns in such pathologies.

Previous investigations dealing with the relationships between tasks and the resting state have compared the functional connectivity during cognitive tasks with that measured during the resting state (Cole et al. 2014; Gerchen and Kirsch 2017), as reviewed by Wig (2017). Reports more closely related to the approach used herein have compared resting-state

connectivity and hemispheric activation asymmetries obtained during language production in healthy individuals (Joliot et al. 2016) and epileptic patients (Doucet et al. 2014), or during story listening (Raemaekers et al. 2018). Other investigations have found correlations between the task-induced and intrinsic connectivity asymmetries measured in selected sets of hROIs (Liu et al. 2009), such as the set of regions involved in a semantic decision task (Wang et al. 2014). Seeding specific language areas, a previous study involving epileptic patients demonstrated that the functional connectivity measured at rest was correlated with lateralization indices measured during language tasks. In this last work, the intrinsic connectivity most strongly correlated with asymmetry of task-induced fMRI was between the inferior frontal and temporo-parietal language areas, all regions constituting SENT_CORE (Teghipco et al. 2016). The set of consistent findings across the latter studies show that asymmetries of intrinsic connectivity partially explain the variability in activation asymmetries measured during language tasks. However, to our knowledge, there are no previous reports of a relationship between intrinsic DC and activation strength, probably because such a relationship is lacking when comparing whole-brain intrinsic connectivity to variations in activity triggered by cognitive tasks that are underpinned by specific networks. In fact, in the present study, this relationship was observed when the DC computation considered only the 18 hROIs of the SENT_CORE network and disappeared when the DC computation included all of the left hemisphere hROIs. This is an important observation because it underlines the necessity of exploring the properties of intrinsic connectivity within specific networks rather than at the whole-brain level.

Considering that the rs-fMRI acquisition was completed on average 11 months before the language fMRI session herein, it was surprising that the rs-fMRI-derived DC values explained up to 11% of the variance in the language fMRI-derived activation amplitudes in 12 of the 18 SENT_CORE network regions. Thus, DC values at rest in regions constituting SENT_CORE can be considered as proxies of their potential involvement during sentence processing. However, to generalize this observation, we need to both investigate how the SENT_CORE DC is modified in individuals atypical for language and to confirm that such a relationship between the DC value during the resting state and activation strength also exists for networks supporting other cognitive domains, specifically the attentional system, in the same participant.

Conclusion

Based on the fMRI analysis of 3 language tasks performed by 144 healthy adult right-handers combined with the analysis of intrinsic resting-state connectivity in 138 of the participants, we propose a SENSAAS atlas of high-order sentence processing areas. This atlas includes 32 regions decomposed into 3 networks, including one (SENT_CORE) specifically composed of essential areas for sentence reading, listening and production. This atlas also contains the features of these three networks, a graph analysis of the intrinsic connectivity of regions that compose SENT_CORE (their degree centrality values that correlate with their strength of activation during the language tasks) as well as the relationships across the different language networks at rest. Such a positive correlation between the DC at rest and the language task-induced activation amplitude in the left hemisphere language network opens the way for investigating participants with language pathologies or population neuroimaging studies searching for the genetic basis of language by analysing only resting-state acquisition. Finally, the methodology we applied, identifying regions from activation studies for selecting the networks at play, advanced the specificity of resting-state graphical analysis and shed light on the relationships between resting-state and task-related networks.

Acknowledgements The authors thank Daniel Margulies for having provided images from his work to complete the Fig. 6 and enrich the discussion.

Funding This work was supported by a grant from the FLAG-ERA Human Brain Project 2015 (ANR-15-HBPR-0001-03-MULTI-LATERAL) awarded to FC, BM, NTM, and MJ and the Ginesis-Lab project (ANR 16 LCV2 0006 01), a grant awarded to MJ, BM, NTM, EM, CF, and LP.

Compliance with ethical standards

Conflict of interest The authors declare that they have no conflict of interest.

Ethical approval The study has been approved by the Basse-Normandie research ethics committee and was performed in accordance with the ethical standards as laid out in the 1964 Declaration of Helsinki and its later amendments or comparable ethical standards.

Informed consent Informed written consent was obtained from all individual participants included in the study.

References

Amunts K, Zilles K (2012) Architecture and organizational principles of Broca's region. Trends Cogn Sci 16:418–426

Baldo JV, Wilkins DP, Ogar J, Willock S, Dronkers NF (2011) Role of the precentral gyrus of the insula in complex articulation. Cortex 47:800–807
Beaucousin V, Lacheret A, Turbelin MR, Morel M, Mazoyer B, Tzourio-Mazoyer N (2007) FMRI study of emotional speech comprehension. Cereb Cortex 17:339–352
Binder JR (2011) Functional MRI is a valid noninvasive alternative to Wada testing. Epilepsy Behav 20:214–222
Binder JR (2015) The Wernicke area: modern evidence and a reinterpretation. Neurology 85:2170–2175
Binder J R O M (2017) Current controversies on Wernicke's area and its role in language. Curr Neurol Neurosci Rep 17: 58
Borovsky A, Saygin AP, Bates E, Dronkers N (2007) Lesion correlates of conversational speech production deficits. Neuropsychologia 45:2525–2533
Buckner RL, Sepulcre J, Talukdar T, Krienen FM, Liu H, Hedden T, Andrews-Hanna JR, Sperling RA, Johnson KA (2009) Cortical hubs revealed by intrinsic functional connectivity: mapping, assessment of stability, and relation to Alzheimer's disease. J Neurosci 29:1860–1873
Charrad M, Ghazzali N, Boiteau V, Niknafs A (2014) NbClust: an R package for determining the relevant number of clusters in data set. J Stat Soft 61:1–36
Clos M, Amunts K, Laird AR, Fox PT, Eickhoff SB (2013) Tackling the multifunctional nature of Broca's region meta-analytically: co-activation-based parcellation of area 44. Neuroimage 83:174–188
Cole MW, Bassett DS, Power JD, Braver TS, Petersen SE (2014) Intrinsic and task-evoked network architectures of the human brain. Neuron 83:238–251
Crinion JT, Lambon-Ralph MA, Warburton EA, Howard D, Wise RJ (2003) Temporal lobe regions engaged during normal speech comprehension. Brain 126:1193–1201
Diedenhofen B, Musch J (2015) cocor: a comprehensive solution for the statistical comparison of correlations. PLoS One 10:e0121945
Dodoo-Schittko F, Rosengarth K, Doenitz C, Greenlee MW (2012) Assessing language dominance with functional MRI: the role of control tasks and statistical analysis. Neuropsychologia 50:2684–2691
Doucet G, Naveau M, Petit L, Delcroix N, Zago L, Crivello F, Jobard G, Tzourio-Mazoyer N, Mazoyer B, Mellet E, Joliot M (2011) Brain activity at rest: a multiscale hierarchical functional organization. J Neurophysiol 105:2753–2763
Doucet GE, Pustina D, Skidmore C, Sharan A, Sperling MR, Tracy JI (2014) Resting-state functional connectivity predicts the strength of hemispheric lateralization for language processing in temporal lobe epilepsy and normals. Hum Brain Mapp 36:288–303
Dronkers N, Ogar J (2004) Brain areas involved in speech production. Brain 127:1461–1462
Dronkers NF, Wilkins DP, Van Valin RD, Redfern BB, Jaeger JJ (2004) Lesion analysis of the brain areas involved in language comprehension. Cognition 92:145–177
Dym RJ, Burns J, Freeman K, Lipton ML (2011) Is functional MR imaging assessment of hemispheric language dominance as good as the Wada test?: a meta-analysis. Radiology 261:446–455
Efron B, Halloran E, Holmes S (1996) Bootstrap confidence levels for phylogenetic trees. Proc Natl Acad Sci 92:13429
Ferstl EC, von Cramon DY (2002) What does the frontomedian cortex contribute to language processing: coherence or theory of mind? Neuroimage 17:1599–1612
Ferstl EC, Rinck M, von Cramon DY (2005) Emotional and temporal aspects of situation model processing during text comprehension: an event-related fMRI study. J Cogn Neurosci 17:724–739
Ferstl EC, Neumann J, Bogler C, Yves von CD (2008) The extended language network: a meta-analysis of neuroimaging studies on text comprehension. Hum Brain Mapp 29:581–593
Friederici AD, Gierhan SM (2013) The language network. Curr Opin Neurobiol 23:250–254
Fuster JM, Bressler SL (2012) Cognit activation: a mechanism enabling temporal integration in working memory. Trends Cogn Sci 16:207–218
Genon S, Reid A, Li H, Fan L, Müller VI, Cieslik EC, Hoffstaedter F, Langner R, Grefkes C, Laird AR (2018a) The heterogeneity of the left dorsal premotor cortex evidenced by multimodal connectivity-based parcellation and functional characterization. Neuroimage 170:400–411
Genon S, Reid A, Langner R, Amunts K, Eickhoff SB (2018b) How to characterize the function of a brain region. Trends Cogn Sci 22:350–364
Gerchen MF, Kirsch P (2017) Combining task-related activation and connectivity analysis of fMRI data reveals complex modulation of brain networks. Hum Brain Mapp 38:5726–5739
Glasser MF, Coalson TS, Robinson EC, Hacker CD, Harwell J, Yacoub E, Ugurbil K, Andersson J, Beckmann CF, Jenkinson M, Smith SM, Van Essen DC (2016) A multi-modal parcellation of human cerebral cortex. Nature 536:171–178
Goel V, Gold B, Kapur S, Houle S (1998) Neuroanatomical correlates of human reasoning. J Cogn Neurosci 10:293–302
Grindrod CM, Baum SR (2003) Sensitivity to local sentence context information in lexical ambiguity resolution: evidence from left- and right-hemisphere-damaged individuals. Brain Lang 85:503–523
Guimera R, Amaral LAN (2005) Functional cartography of complex metabolic networks. Nature 433:895–900
Hervé P-Y, Razafimandimby A, Vigneau M, Mazoyer B, Tzourio-Mazoyer N (2012) Disentangling the brain networks supporting affective speech comprehension. Neuroimage 61:1255–1267
Homae F, Hashimoto R, Nakajima K, Miyashita Y, Sakai KL (2002) From perception to sentence comprehension: the convergence of auditory and visual information of language in the left inferior frontal cortex. Neuroimage 16:883–900
Hubert L, Arabie P (1985) Comparing partitions. J Classif 2:193–218
Hurschler MA, Liem F, Jäncke L, Meyer M (2012) Right and left perisylvian cortex and left inferior frontal cortex mediate sentence-level rhyme detection in spoken language as revealed by sparse fMRI. Hum Brain Mapp 34:30182–33192
Jobard G, Vigneau M, Mazoyer B, Tzourio-Mazoyer N (2007) Impact of modality and linguistic complexity during reading and listening tasks. Neuroimage 34:784–800
Joliot M, Jobard G, Naveau M, Delcroix N, Petit L, Zago L, Crivello F, Mellet E, Mazoyer B, Tzourio-Mazoyer N (2015) AICHA: an atlas of intrinsic connectivity of homotopic areas. J Neurosci Methods 254:46–59
Joliot M, Tzourio-Mazoyer N, Mazoyer B (2016) Intra-hemispheric intrinsic connectivity asymmetry and its relationships with handedness and language lateralization. Neuropsychologia 93:437–447
Jouen AL, Ellmore TM, Madden-Lombardi CJ, Pallier C, Dominey PF, Ventre-Dominey J (2018) Beyond the word and image: II—structural and functional connectivity of a common semantic system. Neuroimage 166:185–197
Kansaku K, Yamaura A, Kitazawa S (2000) Sex differences in lateralization revealed in the posterior language areas. Cereb Cortex 10:866–872
Kircher TT, Brammer M, Tous Andreu N, Williams SC, McGuire PK (2001) Engagement of right temporal cortex during processing of linguistic context. Neuropsychologia 39:798–809
Klingbeil J, Wawrzyniak M, Stockert A, Saur D (2017) Resting-state functional connectivity: an emerging method for the study of language networks in post-stroke aphasia. Brain Cogn. https://doi.org/10.1016/j.bandc.2017.08.005

Kuperberg GR, McGuire PK, David AS (2000) Sensitivity to linguistic anomalies in spoken sentences: a case study approach to understanding thought disorder in schizophrenia. Psychol Med 30:345–357

Lance GN, Williams WT (1979) INVER: a program for the computation of distance-measures between attributes of mixed types. Aust Comput J 11:27–28

Lebret R, Iovleff S, Langrognet F, Biernacki C, Celeux G, Govaert G (2015) Rmixmod: the R package of the model-based unsupervised, supervised and semi-supervised classification mixmod library. J Stat Softw 67:1–29

Liang X, Zou Q, He Y, Yang Y (2013) Coupling of functional connectivity and regional cerebral blood flow reveals a physiological basis for network hubs of the human brain. Proc Natl Acad Sci USA 110:1929–1934

Liu H, Stufflebeam SM, Sepulcre J, Hedden T, Buckner RL (2009) Evidence from intrinsic activity that asymmetry of the human brain is controlled by multiple factors. Proc Natl Acad Sci USA 106:20499–20503

Luke KK, Liu HL, Wai YY, Wan YL, Tan LH (2002) Functional anatomy of syntactic and semantic processing in language comprehension. Hum Brain Mapp 16:133–145

Margulies DS, Petrides M (2013) Distinct parietal and temporal connectivity profiles of ventrolateral frontal areas involved in language production. J Neurosci 33:16846–16852

Matchin W, Brodbeck C, Hammerly C, Lau E (2018) The temporal dynamics of structure and content in sentence comprehension: Evidence from fMRI-constrained MEG. Hum Brain Mapp. https://doi.org/10.1002/hbm.24403

Mazoyer B, Zago L, Jobard G, Crivello F, Joliot M, Perchey G, Mellet E, Petit L, Tzourio-Mazoyer N (2014) Gaussian mixture modeling of hemispheric lateralization for language in a large sample of healthy individuals balanced for handedness. PLoS One 9:e101165

Mazoyer B, Mellet E, Perchey G, Zago L, Crivello F, Jobard G, Delcroix N, Vigneau M, Leroux G, Petit L, Joliot M, Tzourio-Mazoyer N (2015) BIL&GIN: a neuroimaging, cognitive, behavioral, and genetic database for the study of human brain lateralization. Neuroimage 124:1225–1231

Mellet E, Salagnon M, Majkic AC, Joliot S, Jobard M, Tzourio Mazoyer GB, d'Errico N F (2018) Neuroimaging supports the representational nature of the earliest human engravings. BioRxiv. https://doi.org/10.1101/464784

Mesulam M, Weintraub S, Parrish T, Gitelman D (2005) Primary progressive aphasia: reversed asymmetry of atrophy and right hemisphere language dominance. Neurology 64:556–557

Mesulam M-M, Rogalski EJ, Wieneke C, Hurley RS, Geula C, Bigio EH, Thompson CK, Weintraub S (2014) Primary progressive aphasia and the evolving neurology of the language network. Nat Rev Neurol 10:554–569

Monchi O, Petrides M, Strafella AP, Worsley KJ, Doyon J (2006) Functional role of the basal ganglia in the planning and execution of actions. Ann Neurol 59:257–264

Nobre AC, Allison T, McCarthy G (1994) Word recognition in the human inferior temporal lobe. Nature 372:260–263

Ojemann G, Ojemann J, Lettich E, Berger M (1989) Cortical language localization in left, dominant hemisphere. An electrical stimulation mapping investigation in 117 patients. J Neurosurg 71:316–326

Opsahl T, Agneessens F, Networks JS-S (2010) Node centrality in weighted networks: generalizing degree and shortest paths. Soc Netw 32:245–251

Papathanassiou D, Etard O, Mellet E, Zago L, Mazoyer B, Tzourio-Mazoyer N (2000) A common language network for comprehension and production: a contribution to the definition of language epicenters with PET. Neuroimage 11:347–357

Pillay SB, Binder JR, Humphries C, Gross WL, Book DS (2017) Lesion localization of speech comprehension deficits in chronic aphasia. Neurology 88:970–975

Price CJ (2000) The anatomy of language: contributions from functional neuroimaging. J Anat 197:335–359

Price CJ (2010) The anatomy of language: a review of 100 fMRI studies published in 2009. Ann N Y Acad Sci 1191:62–88

Price CJ (2012) A review and synthesis of the first 20 years of PET and fMRI studies of heard speech, spoken language and reading. Neuroimage 62:816–847

Price CJ, Devlin JT (2003) The myth of the visual word form area. Neuroimage 19:473–481

Price AR, Peelle JE, Bonner MF, Grossman M, Hamilton RH (2016) Causal evidence for a mechanism of semantic integration in the angular gyrus as revealed by high-definition transcranial direct current stimulation. J Neurosci 36:3829–3838

Raemaekers M, Schellekens W, Petridou N, Ramsey NF (2018) Knowing left from right: asymmetric functional connectivity during resting state. Brain Struct Funct 223:1909–1922

Raichle ME (2015) The brain's default mode network. Annu Rev Neurosci 38:433–447

Raichle ME, Mintun MA (2006) Brain work and brain imaging. Annu Rev Neurosci 29:449–476

Rauschecker JP, Scott SK (2009) Maps and streams in the auditory cortex: nonhuman primates illuminate human speech processing. Nat Neurosci 12:718–724

Richardson JD, Fillmore P, Rorden C, Lapointe LL, Fridriksson J (2012) Re-establishing Broca's initial findings. Brain Lang 123:125–130

Rolston JD, Chang EF (2018) Critical language areas show increased functional connectivity in human cortex. Cereb Cortex 28:4161–4168

Rubinov M, Sporns O (2010) Complex network measures of brain connectivity: uses and interpretations. Neuroimage 52:1059–1069

Saur D, Lange R, Baumgaertner A, Schraknepper V, Willmes K, Rijntjes M, Weiller C (2006) Dynamics of language reorganization after stroke. Brain 129:1371–1384

Saur D, Kreher BW, Schnell S, Kümmerer D, Kellmeyer P, Vry MS, Umarova R, Musso M, Glauche V, Abel S (2008) Ventral and dorsal pathways for language. Proc Natl Acad Sci 105:18035

Saygin AP, Wilson SM, Dronkers NF, Bates E (2004) Action comprehension in aphasia: linguistic and non-linguistic deficits and their lesion correlates. Neuropsychologia 42:1788–1804

Sefcsik T, Nemeth D, Janacsek K, Hoffmann I, Scialabba J, Klivenyi P, Ambrus GG, Haden G, Vecsei L (2009) The role of the putamen in cognitive functions—a case study. Learn Percept 1:215–227

Sidtis JJ (2007) Some problems for representations of brain organization based on activation in functional imaging. Brain Lang 102:130–140

Sneath PH, Sokal RR (1973) Numerical taxonomy. The principles and practice of numerical classification (a series of books in biology), vol 573. WF Freeman and Co., San Francisco

Sporns O, Honey CJ, Kötter R (2007) Identification and classification of hubs in brain networks. PLoS One 2:e1049

Spreng RN, Mar RA, Kim AS (2009) The common neural basis of autobiographical memory, prospection, navigation, theory of mind, and the default mode: a quantitative meta-analysis. J Cogn Neurosci 21:489–510

Suzuki R, Shimodaira H (2006) Pvclust: an R package for assessing the uncertainty in hierarchical clustering. Bioinformatics 22:1540–1542

Tate MC, Herbet G, Moritz-Gasser S, Tate JE, Duffau H (2014) Probabilistic map of critical functional regions of the human cerebral cortex: Broca's area revisited. Brain 137:2773–2782

Teghipco A, Hussain A, Tivarus ME (2016) Disrupted functional connectivity affects resting state based language lateralization. Neuroimage Clin 12:910–927

Tetzloff KA, Duffy JR, Clark HM, Strand EA, Machulda MM, Schwarz CG, Senjem ML, Reid RI, Spychalla AJ, Tosakulwong N, Lowe VJ, Jack CR, Josephs KA, Whitwell JL (2018) Longitudinal structural and molecular neuroimaging in agrammatic primary progressive aphasia. Brain 141:302–317

Thirion B, Varoquaux G, Dohmatob E, Poline JB (2014) Which fMRI clustering gives good brain parcellations. Front Neurosci 8:167

Thompson PM, Andreassen OA, Arias-Vasquez A, Bearden CE, Boedhoe PS, Brouwer RM, Buckner RL, Buitelaar JK, Bulayeva KB, Cannon DM, Cohen RA, Conrod PJ, Dale AM, Deary IJ, Dennis EL, de Reus MA, Desrivieres S, Dima D, Donohoe G, Fisher SE, Fouche JP, Francks C, Frangou S, Franke B, Ganjgahi H, Garavan H, Glahn DC, Grabe HJ, Guadalupe T, Gutman BA, Hashimoto R, Hibar DP, Holland D, Hoogman M, Pol HEH, Hosten N, Jahanshad N, Kelly S, Kochunov P, Kremen WS, Lee PH, Mackey S, Martin NG, Mazoyer B, McDonald C, Medland SE, Morey RA, Nichols TE, Paus T, Pausova Z, Schmaal L, Schumann G, Shen L, Sisodiya SM, Smit DJA, Smoller JW, Stein DJ, Stein JL, Toro R, Turner JA, van den Heuvel MP, van den Heuvel OL, van Erp TGM, van Rooij D, Veltman DJ, Walter H, Wang Y, Wardlaw JM, Whelan CD, Wright MJ, Ye J, ENIGMA C (2017) ENIGMA and the individual: predicting factors that affect the brain in 35 countries worldwide. Neuroimage 145:389–408

Tomasi D, Volkow ND (2012) Resting functional connectivity of language networks: characterization and reproducibility. Mol Psychiatry 17:841–854

Turken AU, Dronkers NF (2011) The neural architecture of the language comprehension network: converging evidence from lesion and connectivity analyses. Front Syst Neurosci 5:1

Tzourio-Mazoyer N, Joliot M, Marie D, Mazoyer B (2016) Variation in homotopic areas' activity and inter-hemispheric intrinsic connectivity with type of language lateralization: an FMRI study of covert sentence generation in 297 healthy volunteers. Brain Struct Funct 221:2735–2753

van den Heuvel MP, Sporns O (2011) Rich-club organization of the human connectome. J Neurosci 31:15775–15786

van den Heuvel MP, Mandl RC, Stam CJ, Kahn RS, Hulshoff Pol HE (2010) Aberrant frontal and temporal complex network structure in schizophrenia: a graph theoretical analysis. J Neurosci 30:15915–15926

Vigneau M, Beaucousin V, Hervé PY, Duffau H, Crivello F, Houdé O, Mazoyer B, Tzourio-Mazoyer N (2006) Meta-analyzing left hemisphere language areas: phonology, semantics, and sentence processing. Neuroimage 30:1414–1432

Viñas-Guasch N, Wu YJ (2017) The role of the putamen in language: a meta-analytic connectivity modeling study. Brain Struct Funct 22:3991–4004

Vingerhoets G, Van Borsel J, Tesink C, van den Noort M, Deblaere K, Seurinck R, Vandemaele P, Achten E (2003) Multilingualism: an fMRI study. Neuroimage 20:2181–2196

Wada J, Rasmussen T (1960) Intracarotid injection of sodium amytal for the lateralization of cerebral speech dominance: experimental and clinical observations. J Neurosurg 17:266–282

Wang D, Buckner RL, Liu H (2014) Functional specialization in the human brain estimated by intrinsic hemispheric interaction. J Neurosci 34:12341–12352

Wang J, Xie S, Guo X, Becker B, Fox PT, Eickhoff SB, Jiang T (2017) Correspondent functional topography of the human left inferior parietal lobule at rest and under task revealed using resting-state fMRI and coactivation based parcellation. Hum Brain Mapp

Ward JH Jr (1963) Hierarchical grouping to optimize an objective function. J Am Stat Assoc 58:236–244

Wig GS (2017) Segregated systems of human brain networks. Trends Cogn Sci 21:981–996

Wilson SM, Dronkers NF, Ogar JM, Jang J, Growdon ME, Agosta F, Henry ML, Miller BL, Gorno-Tempini ML (2010a) Neural correlates of syntactic processing in the nonfluent variant of primary progressive aphasia. J Neurosci 30:16845–16854

Wilson SM, Henry ML, Besbris M, Ogar JM, Dronkers NF, Jarrold W, Miller BL, Gorno-Tempini ML (2010b) Connected speech production in three variants of primary progressive aphasia. Brain 133:2069–2088

Yourganov G, Smith KG, Fridriksson J, Rorden C (2015) Predicting aphasia type from brain damage measured with structural MRI. Cortex 73:203–215

Zago L, Hervé P-Y, Genuer R, Laurent A, Mazoyer B, Tzourio-Mazoyer N, Joliot M (2017) Predicting hemispheric dominance for language production in healthy individuals using support vector machine. Hum Brain Mapp 38:5871–5889

Zeidman P, Maguire EA (2016) Anterior hippocampus: the anatomy of perception, imagination and episodic memory. Nat Rev Neurosci 17:173–182

Zilles K, Bacha-Trams M, Palomero-Gallagher N, Amunts K, Friederici AD (2015) Common molecular basis of the sentence comprehension network revealed by neurotransmitter receptor fingerprints. Cortex 63:79–89

2. WMCA : un atlas des aires hétéro-modales du mot

Hesling, I., **Labache, L.**, Joliot, M., & Tzourio-Mazoyer, N. (2019). Large-scale plurimodal networks common to listening to, producing and reading word lists: an fMRI study combining task-induced activation and intrinsic connectivity in 144 right-handers. *Brain Structure and Function*, *224*(9), 3075-3094.

Brain Structure and Function (2019) 224:3075–3094
https://doi.org/10.1007/s00429-019-01951-4

ORIGINAL ARTICLE

Large-scale plurimodal networks common to listening to, producing and reading word lists: an fMRI study combining task-induced activation and intrinsic connectivity in 144 right-handers

Isabelle Hesling[1,2,3,6] · L. Labache[1,2,3,4,5] · M. Joliot[1,2,3] · N. Tzourio-Mazoyer[1,2,3]

Received: 24 May 2019 / Accepted: 29 August 2019 / Published online: 7 September 2019

Abstract

We aimed at identifying plurimodal large-scale networks for producing, listening to and reading word lists based on the combined analyses of task-induced activation and resting-state intrinsic connectivity in 144 healthy right-handers. In the first step, we identified the regions in each hemisphere showing joint activation and joint asymmetry during the three tasks. In the left hemisphere, 14 homotopic regions of interest (hROIs) located in the left Rolandic sulcus, precentral gyrus, cingulate gyrus, cuneus and inferior supramarginal gyrus (SMG) met this criterion, and 7 hROIs located in the right hemisphere were located in the preSMA, medial superior frontal gyrus, precuneus and superior temporal sulcus (STS). In a second step, we calculated the BOLD temporal correlations across these 21 hROIs at rest and conducted a hierarchical clustering analysis to unravel their network organization. Two networks were identified, including the WORD-LIST_CORE network that aggregated 14 motor, premotor and phonemic areas in the left hemisphere plus the right STS that corresponded to the posterior human voice area (pHVA). The present results revealed that word-list processing is based on left articulatory and storage areas supporting the action–perception cycle common not only to production and listening but also to reading. The inclusion of the right pHVA acting as a prosodic integrative area highlights the importance of prosody in the three modalities and reveals an intertwining across hemispheres between prosodic (pHVA) and phonemic (left SMG) processing. These results are consistent with the motor theory of speech postulating that articulatory gestures are the central motor units on which word perception, production, and reading develop and act together.

Keywords Word production · Word perception · Word reading · Hemispheric specialization · Resting state

Introduction

Language is one of the most important and specific cognitive abilities of human beings. According to De Saussure (1975), language is a universal structure encompassing the abstract, systematic rules and conventions of a unifying system, which is independent of individual users, while speech is the personal use of language, thus presenting many different variations such as style, grammar, syntax, intonation, rhythm, and pronunciation. Though neuroimaging studies of language at the word/phonological level have demonstrated bilateral activation during language tasks, calculation of asymmetries provides results that are consistent with the neuropsychological evidence that language is implemented in large areas located along the left sylvian fissure (Vigneau et al. 2006, 2011). More specifically, word processing is underpinned by cortical areas involved in the auditory, visual, and motor areas spreading over the left hemisphere depending on the

✉ Isabelle Hesling
isabelle.hesling@u-bordeaux.fr

1 University of Bordeaux, IMN, UMR 5293, 33000 Bordeaux, France

2 CNRS, IMN, UMR 5293, 33000 Bordeaux, France

3 CEA, GIN, IMN, UMR 5293, 33000 Bordeaux, France

4 University of Bordeaux, IMB, UMR 5251, 33405 Talence, France

5 INRIA Bordeaux Sud-Ouest, CQFD, INRIA, UMR 5251, 33405 Talence, France

6 IMN Institut des Maladies Neurodégénératives UMR 5293, Team 5: GIN Groupe d'imagerie Neurofonctionnelle, CEA-CNRS, Université de Bordeaux, Centre Broca Nouvelle-Aquitaine-3ème étage, 146 rue Léo-Saignat-CS 61292-Case 28, 33076 Bordeaux Cedex, France

type of language modality (Price 2010, 2012). However, the question of the existence of core areas independent of the modality of the language task is still open. Regarding the left hemisphere arrangement of language areas, two divergent theories explain the relations of speech perception and speech production to language. The former, called the horizontal view, proposes that the elements of speech are sounds that rely on two separate processes (one for speech perception, the other for speech production) that are not specialized for language until a cognitive process connects them to each other and then to language (Fodor 1983). The latter, called the vertical view (or motor theory of speech perception), posits that speech elements are articulatory gestures serving both speech perception and production processes that are immediately linguistic, thus requiring no cognitive process (Liberman and Whalen 2000). More generally, the existence of a bilateral dorsal–ventral model of speech processing with preferential leftward involvement has been widely accepted (Binder et al. 1996; Hickok and Poeppel 2004; Rauschecker and Tian 2000). This model posits the coexistence of (1) a dorsal pathway, i.e. the "where stream," in which an acoustic–phonetic–articulatory transformation linking auditory representations to motor representations is reported to occur in superior temporal/parietal areas and ultimately in frontal areas (Buchsbaum et al. 2001); and (2) a ventral pathway, i.e. the "what stream", in which speech-derived representations interface with lexical semantic representations, reported to involve the superior, middle, and inferior temporal gyri (Binder et al. 2000; Hickok and Poeppel 2000). Interestingly, concerning the dorsal pathway, the postulated existence of an auditory–motor system (Hickok and Poeppel 2000) has been supported by studies that aimed at examining the role of motor areas in speech perception. Hence, an fMRI study revealed that listening to syllables and producing the same syllables led to a common bilateral network encompassing a superior part of the ventral premotor cortex, suggesting the existence of a common phonetic code between speech perception and production (Wilson et al. 2004). Furthermore, another study has not only suggested that the cortical motor system is organized in a somatotopic way along the precentral cortex with the lip area being superior to the tongue area, but also revealed that these precentral regions are consistently activated by syllable articulation and syllable perception, hence demonstrating a shared speech-sound-specific neural substrate of these sensory and motor processes (Pulvermüller et al. 2006). These findings were supported by a meta-analysis revealing that in right-handers, activations of the posterior part of the frontal lobe distributed along the precentral gyrus were strongly left lateralized during both production and auditory tasks at the word or syllable level, together with the involvement of the supramarginal gyrus (SMG) (Vigneau et al. 2006). Moreover, a recent MEG study reported a synchronization between the anterior motor regions involved in syllable articulation and the posterior regions involved in their auditory perception during perception of these syllables (Assaneo and Poeppel 2018). In addition, studies on split-brain patients have demonstrated a strict leftward lateralization concerning phonological processing, with split-brain patients' right hemisphere lacking categorical perception of phonemes (Gazzaniga 2000; Sidtis et al. 1981). Such a leftward lateralization was confirmed by studies using the Wada test procedure (Dym et al. 2011), and the leftward asymmetry of the audio–motor loop measured with functional imaging actually supports the left hemisphere specialization for the phonological processing of speech (Vigneau et al. 2006, Zago et al. 2008).

Though mastered afterwards, human beings have developed other ways of using language through other sensory modalities, such as the visual system in the case of reading. Accurate perception and production of speech sounds are essential for learning the relationship between sounds and letters. Phonological awareness, i.e. the ability to detect and manipulate speech sounds, or phonemes, is the best predictor of reading ability. Reading is based on both the ability to hear and segment words into phonemes and then to associate these phonemes with graphemes, with the mapping of orthographic to phonological representations during reading being intrinsically cross-modal (McNorgan et al. 2014). Research has revealed that a phonological processing deficit underlies reading difficulties in dyslexic children, establishing a link between perception and reading abilities (Gillon 2004). In the case of disorders of oral language development, specific language impairment (SLI) is the most frequently studied developmental disorder. Children with specific language impairment have been reported to present impairments in phonological processing, whether in phonological awareness or in phonological memory, which is evidence of a link between production and reading abilities; the neural support of this link still needs to be clarified (Catts et al. 2005). Different studies examining the word processing cerebral networks common to the auditory and visual modalities have revealed the supramodal involvement of anterior regions [supplementary motor area (SMA) and prefrontal, premotor and inferior frontal gyri], whereas variations have been observed in the temporal lobe depending on the language task (Booth et al. 2002a, b; Buckner et al. 2000; Chee et al. 1999), making it difficult to conclude the existence of a common antero-posterior network for plurimodal word processing. Regarding semantic processing, it should be noted that one study addressing production and reading in four languages revealed a common bilateral network involved in these two tasks (Rueckl et al. 2015). Moreover, since the complete development of speech in literate individuals leads to the mastering of the written language, we expected that the core word areas developing conjointly in

the three modalities would include some visual areas, which would be part of a large-scale plurimodal network underpinning word processing. It is worth emphasizing that, even if less investigated, the first phase of speech acquisition in newborn babies is perceptual, as the infant hears others' vocalizations, highlighting the importance of prosody in speech processing. Speech prosody, i.e. the musical aspects of speech, is an early-developing component of speech, which could be compared to a musical stave upon which phonemes would be placed (Locke and Pearson 1990). This perceptual phase is crucial considering the inability to learn spoken language or even normally babble when infants are born deaf (Oller and MacNeilage 1983) or in the case of wild children (Curtiss 1977). In other words, children have to listen to the prosody of their mother tongue to be able to reproduce it. Lesional studies have revealed that the tonal prosodic brain areas are located in the right hemisphere along the STS, which includes the posterior human voice area (pHVA), highlighting the potential role of these right hemispheric regions during development. The second phase of speech acquisition is production. In fact, children master the prosodic dimension before producing their first words (Bever et al. 1971). Production develops through the process of imitation, highlighting that prosodic processing is one element of the construction of a strong dependency between perception and production throughout development. This is illustrated, for example, by persisting difficulties in speech production encountered by infants who were tracheotomized at a time when they should have normally babbled (Locke and Pearson 1990). Interestingly, metre in speech, whose acoustic correlate is stress, has been revealed to be important for both speech perception (Jusczyk et al. 1993) and production (Gerken et al. 1990). Once the metrical rules (which provide important cues for speech segmentation within the continuous speech stream) have been acquired, a speech metre contributes to phonological (Pitt and Samuel 1990), semantic (Schwartze et al. 2011) and syntactic (Roncaglia-Denissen et al. 2013) processing. Musical rhythmic priming, using metres, has been revealed to enhance phonological production in hearing-impaired children due to an enhanced perception of sentences (Cason et al. 2015). Furthermore, in the context of speech rehabilitation therapies, musical rhythm has been revealed to be a fluency-enhancing tool (Thaut 2013). More generally, the prosodic dimension of speech has been used to restore the speech of Broca's aphasic patients, and the term Melodic Intonation Therapy was coined to refer to this technique based on the use of melody and singing, which would be core musical elements predominantly engaging the right hemisphere (Thaut and McIntosh 2014). The right STS specialization for tonal processing was evidenced by a neuroimaging study as a rightward asymmetry of activation (Zatorre and Belin 2001). Other studies have highlighted the role of the right hemisphere, particularly the right STS, in the prosodic dimension of speech (Beaucousin et al. 2007; Belin et al. 2004; Sammler et al. 2015). Given the importance of prosody in language development, we hypothesized that in addition to left hemisphere participation, right hemispheric regions hosting the tonal dimension of speech prosody may be involved in all three tasks, i.e. production, perception and reading tasks.

In summary, previous studies on phonological/word processing have, at best, dealt with two different language modalities (either production and listening or production and reading) focusing on discrete cortical areas a priori selected (articulatory motor areas and SMG). In the present work, we assessed the three main language modalities: listening, production and reading. Furthermore, considering the importance of lateralization reported above, we took into consideration the right and left hemisphere contribution to task completion at the word or syllable levels in the present work. Finally, we integrated the connectivity data provided by a resting-state acquisition to propose a comprehensive view of the plurimodal large-scale networks for phonological/word processing and their potential roles.

To achieve the identification of plurimodal large-scale networks for word-list processing, a large population of 144 right-handers who completed word-list processing in the three modalities, production, reading and listening, during task-induced fMRI acquisition, was selected from the BIL&GIN database (Mazoyer et al. 2016). In this sample of healthy right-handers, we (1) identified left brain regions showing both leftward joint activation and leftward joint asymmetry and right brain regions showing both rightward joint activation and rightward joint asymmetry during the three word-list tasks; (2) identified the network organization at play within the areas previously identified based on the hierarchical clustering of the BOLD temporal correlation measured during a resting-state acquisition completed in the same individuals; and finally, (3) conducted a comprehensive investigation of how these areas were modulated according to the task and integrate the present results into the literature to elucidate the identified supramodal word-list network's function/role.

Materials and methods

Participants

The present study included a sample of 144 right-handers balanced for sex (72 women) and picked from the BIL&GIN database, which is a multimodal imaging/psychometric/genetic database specifically designed for studying the structural and functional neural correlates of brain lateralization (Mazoyer et al. 2016). The selected participants had French as a mother tongue and were

free from developmental disorders and neurological and psychiatric histories. A local ethics committee (CCPRB Basse-Normandie, France) approved the experimental protocol. The participants gave their informed, written consent and received an allowance for their participation. All subjects were free of brain abnormalities as assessed by an inspection of their structural T1-MRI scans by a trained radiologist.

The mean (± standard deviation) age of the sample was 27 ± 6 years (range 19–53), and the mean level of education (corresponding to the number of schooling years since the first grade of primary school) was 16 ± 2 years (range 11–20), corresponding to 4 years at the university level.

Handedness was self-reported by the subjects, and their manual lateralization strength was assessed using the Edinburgh inventory (Oldfield 1971) with values ranging from − 100 to + 100. The average MLS value of the subjects was 93.48 (SD = 11.49).

Functional imaging

Paradigm of the word-list tasks

Three runs were administered. The participants had to covertly generate (PROD), listen to (LISN) or covertly read (READ) lists of words (Word-List). These tasks were part of a run that alternated these word tasks with sentence tasks (see Labache et al. 2019 for the complete methodology).

The stimuli were lists of over-learnt words, such as months of the year, making it possible to decrease the weight of lexico-semantic and syntactic processing and enhancing phonetic encoding, phonology, articulation and word retrieval while inducing prosodic processing due to the specific metrics of serial automatic speech. For each task, the participants were shown a scrambled drawing for 1 s, immediately followed by a central fixation crosshair (see Fig. 1). While fixating the cross, the subjects performed either the listening or production Word-List tasks and had to click on the response pad with their right hand after the

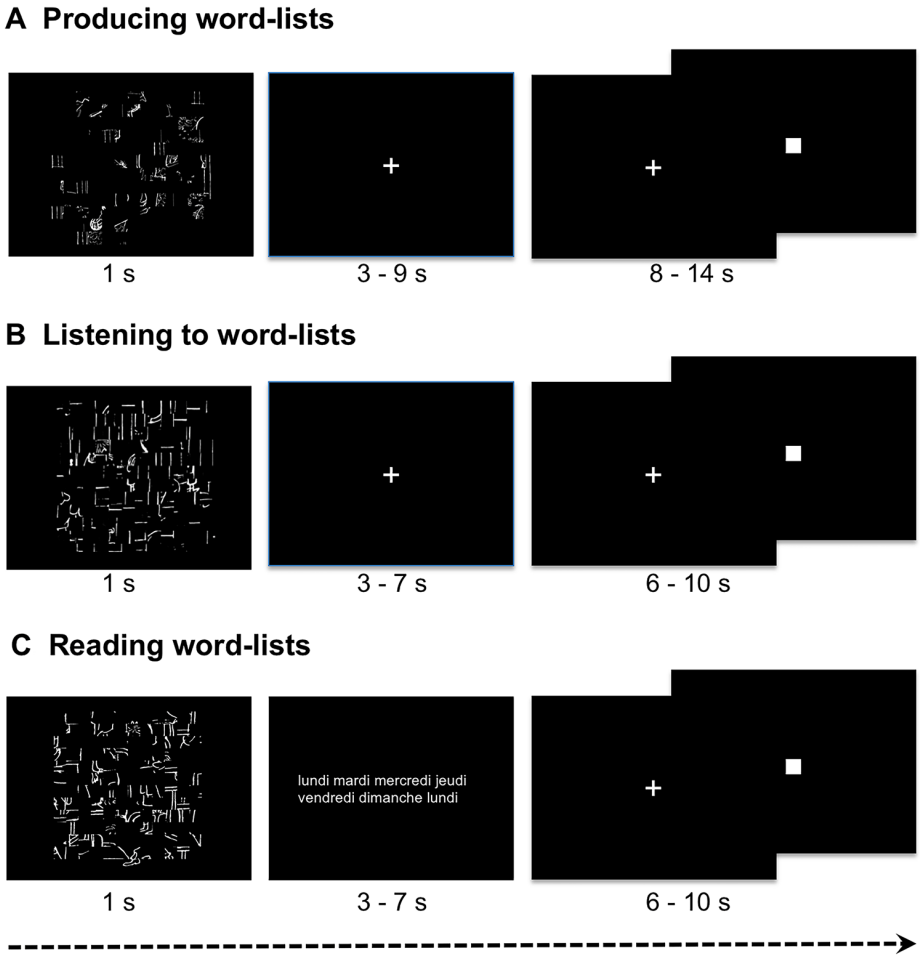

Fig. 1 Description of the paradigm for one event from each Word-List task. In the three conditions, an event was initiated by the presentation of a scrambled picture for one second, followed by a central cross that participants were instructed to look at while they were producing the list of months of the year (**a**) or listening to a list of words (**b**). During the reading run, instead of a cross fixation, lists of words (either weeks, hours, seasons, days, months) were presented. The participants had to click when they had finished producing, listening to or reading, and they subsequently had to indicate by clicking when the central cross that reappeared was changed into a square. In this figure, for reading convenience, the stimuli were zoomed in on compared to the presentation of the stimuli during the scanning session

task completion. During reading, the participants had to read lists of words that were flashed on the screen instead of fixating the cross, but still had to click on the response pad with their right hand after the task completion. Then, a low-level reference task followed each event (sentence or Word-List), consisting of sustaining visual fixation on the central cross and pressing the pad when the fixation cross was switched to a square (both stimuli covering a $0.8° \times 0.8°$ visual area). This second part of the trial, which lasted at least half the total trial duration, aimed at refocusing the participant's attention to a non-verbal stimulus and controlling for manual motor response activation, which was also present in the first part of the trial. This second part lasted from 8 to 14 s for the production task and from 6 to 10 s for the perception and reading tasks.

The design was almost identical for the three tasks. During PROD, the participants were asked to covertly generate the list of the months of the year from January to December during each of the ten Word-List trials, which lasted 18 s. During LISN, they were instructed to listen to 13 of 14-s trials of lists of the months, days of the week and/or seasons. During READ, they were asked to read lists of days of the weeks, months, and/or seasons that were flashed on the screen, and this task consisted of 13 trials lasting 14 s. Response times were recorded during the fMRI experiment for each event of each run for each participant. The mean response time corresponded to the mean response time of each of the 144 participants during a given task. Note that the participants responded with their right hand.

Image acquisition and pre-processing

Structural imaging

Structural images were acquired using a 3T Philips Intera Achieva scanner and included high-resolution T1-weighted volumes [sequence parameters: repetition time (TR), 20 ms; echo time (TE), 4.6 ms; flip angle, 10°; inversion time, 800 ms; turbo field echo factor, 65; sense factor, 2; field of view, $256 \times 256 \times 180$ mm^3; isotropic voxel size, $1 \times 1 \times 1$ mm^3]. For each participant, the line between the anterior and posterior commissures was identified on a mid-sagittal section, and the T1-MRI volume was acquired after orienting the brain in the bi-commissural coordinate system. T2*-weighted multi-slice images were also acquired [T2*-weighted fast field echo (T2*-FFE); sequence parameters: TR = 3500 ms; TE = 35 ms; flip angle = 90°; sense factor = 2; 70 axial slices; isotropic voxel size, $2 \times 2 \times 2$ mm^3].

Task-induced image acquisition and analysis

The functional volumes were acquired as T2*-weighted echo-planar images (EPI) (TR = 2 s; TE = 35 ms; flip angle = 80°; 31 axial slices; field of view, 240×240 mm^2; isotropic voxel size, $3.75 \times 3.75 \times 3.75$ mm^3). In the three runs, 192, 194 and 194 T2*-weighted volumes were acquired for the Word-List production, listening and reading tasks, respectively.

For each participant, the pre-processing of T2*-weighted echo-planar EPI images included (1) the T2*-FFE volume rigid registration to the T1-MRI; (2) the T1-MRI segmentation into three brain tissue classes: grey matter, white matter and cerebrospinal fluid; and (3) the T1-MRI scans normalization to the BIL&GIN template, which included 301 volunteers from the BIL&GIN database (aligned to the MNI space), using the SPM12 "normalize" procedure with otherwise default parameters. For each of the three fMRI runs, data were then corrected for slice timing differences and, to correct for subject motion during the runs, all the T2*-weighted volumes were realigned using a six-parameter rigid-body registration. The EPI-BOLD scans were then rigidly registered to the structural T2*-FFE image. The combination of all registration matrices allowed for warping the EPI-BOLD functional scans to the standard space with a single trilinear interpolation.

The initial analysis included the application of a 6-mm full-width at half-maximum Gaussian filter to each functional volume of each run. Global linear modelling [statistical parametric mapping (SPM), http://www.fil.ion.ucl.ac.uk/spm/] was then used to process the task-related fMRI data. For each participant, BOLD variations corresponding to each Word-List task versus the cross-change detection task belonging to the same run were computed [Word-List production (PROD), Word-List reading (READ), and Word-List listening (LISN)].

Homotopic regions of interest analysis

Since the brain presents a global torsion, the Yakovlevian torque, which prevents a perfect point-to-point correspondence between cortical areas that are functionally homotopic (Toga and Thompson 2003), the use of flipped images to calculate asymmetries appears problematic since the flipped regions do not correspond to the equivalent of the other hemisphere. A new atlas, called AICHA, based on resting-state fMRI data and composed of homotopic functional regions of interest (hROIs), has been devised to circumvent this problem and is thus suited for investigating brain hemispheric specialization and lateralization, allowing the determination of the right and left hemispheric contribution in language and for computing functional asymmetries in regions having equivalent intrinsic connectivity (Joliot et al. 2015).

BOLD signal variations were thus calculated for the right and left hROI BOLD signal variations for each of 185 pairs of functionally defined hROIs of the AICHA atlas (Joliot

et al. 2015) adapted to SPM12 in the three contrast maps (defined at the voxel level) for PROD, LISN and READ.

Part 1: identification and characterization of hROIs exhibiting both activation and asymmetry in all three tasks

To complete the identification of language areas underpinning production, listening and reading tasks at the word level, we first searched for hROIs that were both significantly co-activated and significantly co-asymmetrical on average among the 144 participants during the PROD, LISN and READ tasks for each hemisphere. The idea behind the conjunction of activations and asymmetries during the three tasks was to be selective enough to present brain areas specifically lateralized during the tasks. In a second step, we described the variation in activity and asymmetry in each hemisphere for the selected regions to obtain information on their functional nature from their modulation by the task component.

Statistical analyses

hROIs selection

Using JMP14 (http://www.jmp.com, JMP® 2018), a conjunction analysis was conducted to select the left hemispheric hROIs exhibiting BOLD signal variations that were both significantly positive and significantly larger than those of their right counterparts in all three tasks. An hROI was selected whenever it was significantly activated in each of the three task contrasts using a significance threshold set to $p < 0.05$ per contrast. The significance threshold for the conjunction of activation in the three tasks was thus $0.05 \times 0.05 \times 0.05 = 1.25 \times 10^{-4}$. The second criterion for hROI selection was the existence of a significant leftward asymmetry in each of the three task contrasts, with the threshold of significance of this second conjunction being 1.25×10^{-4}. Finally, to be selected, a given hROI had to fulfil both criteria, and the overall significance threshold for the conjunction of the conjunction analyses was $1.56 \times 10^{-8} = (1.25 \times 10^{-4})^2$. This procedure was conducted separately for the left and right hemispheres.

Characterization of hROI activations and asymmetries across tasks

Taking the right and left hROIs separately, we tested the existence of significant effects of Task (PROD, LISN, READ) on the selected hROIs, as well as the effect of Side (left or right) and their interactions, using two repeated-measures linear mixed-effects models. The analysis was conducted on the 144 individuals entering the variable Subject as a random effect.

Two-sided Tukey's range tests on the mean activation or asymmetry values were then completed for the left (14 hROIs) and right (7 hROIs) hROIs to identify the origins of the significant effects and interactions found with each linear mixed-effects model.

Results

Task performance during the scanning session

The mean response time taken for the covert generation of the months of the year was 5261 ± 1092 ms (range 2836–7360). The mean response time taken for reading the months of the year, days and seasons was 4405 ± 603 ms (range 2703–5681). The mean response time taken for listening to the months of the year, days and seasons was 486 ± 101 ms (range 282–794). As the mean response time was calculated after the delivery of the stimulus, i.e. after 4386 ± 484 ms of Word-Lists auditory presentation, the response times in the three tasks were comparable.

Regions showing both joint activation and joint asymmetry during production, listening and reading of Word-Lists

The first observation was that 14 leftward hROIs showed both joint leftward activation and joint leftward asymmetry, while 7 rightward hROIs showed both joint rightward activation and joint rightward asymmetry, demonstrating the left hemisphere dominance of brain areas dedicated to Word-List processing (Fig. 2, Table 1).

Left hemisphere

The conjunction of significant leftward activation in the three contrasts (PROD ∩ LISN ∩ READ) revealed 50 left hROIs (Fig. 2, top row). The conjunction of a significant leftward asymmetry in the three contrasts revealed 26 hROIs (Fig. 2, middle row), and 14 left hROIs showed both joint leftward activation and joint leftward asymmetry ($p < 1.56 \times 10^{-8}$; Fig. 2 bottom row, Table 1). Most of these hROIs were located in the frontal cortex, including seven hROIs straddling the Rolandic sulcus (rol1, rol2, rol3, ROLop1) and precentral sulcus (prec2, prec5, prec6) and four located on the dorsal part of the internal surface of the frontal lobe (cing3, cing4, cing5, pCENT1). One hROI was located in the parietal lobe in the supramarginal gyrus (SMG1). Finally, one hROI was located in the occipital lobe in the cuneus (CU1). Only one subcortical area, the pallidum

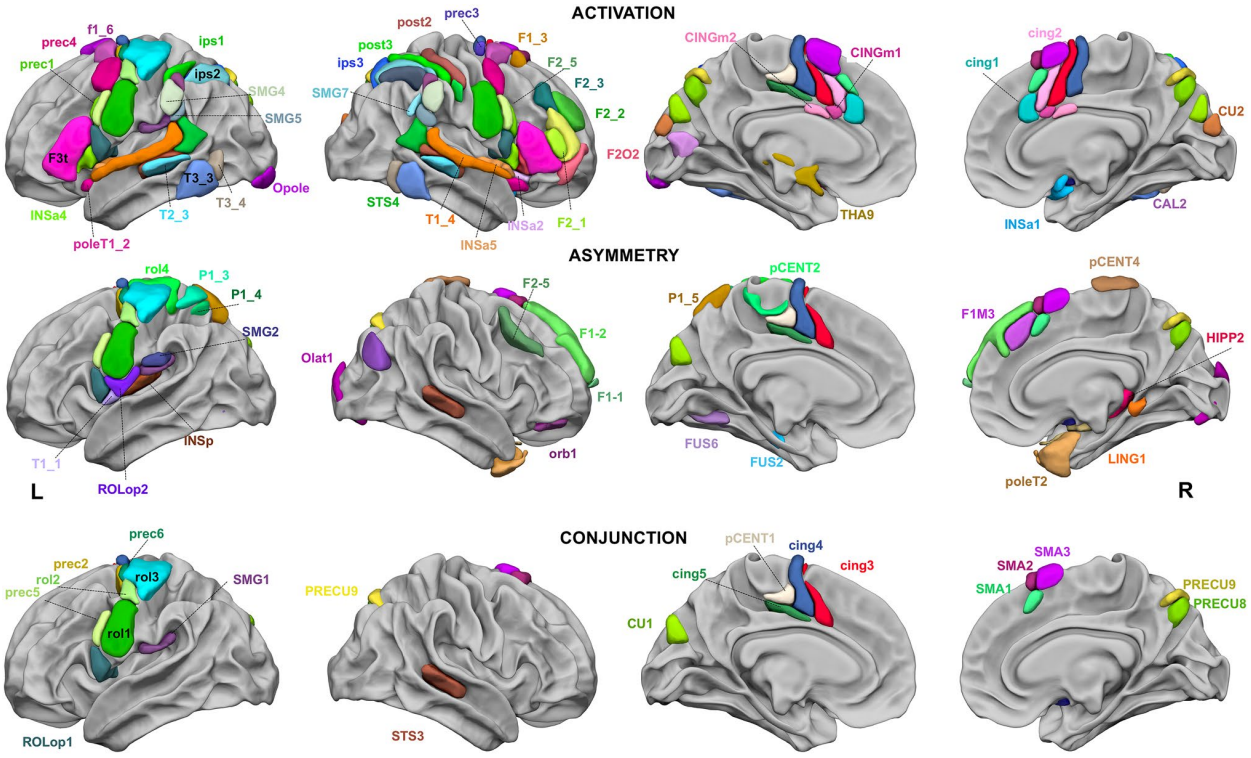

Fig. 2 Regions of the AICHA atlas significantly activated in the three tasks (top row), significantly asymmetrical in the three tasks (middle row), and significantly conjointly activated and conjointly asymmetrical in the three tasks (bottom row). The hROIs are projected on the white matter surface of the BIL&GIN template with Surf Ice (https://www.nitrc.org/projects/surfice/) software. Leftward asymmetrical hROIs, as well as conjointly leftward activated and conjointly asymmetrical hROIs, are presented on the left hemisphere, and rightward asymmetrical hROIs are presented on the right hemisphere. The hROIs considered activated or asymmetrical per hemisphere by task were selected according to a p value < 0.05; the statistical threshold applied to the conjunction of asymmetry and activation for a given task was $p < 0.0025$ for each hemisphere, and the threshold set for the three-task conjunction was $p < 6.25 \times 10^{-6}$

Table 1 Number of hROIs identified at each selection step

Contrasts	L activation	L asymmetry	L activation and asymmetry
PROD	76 (94)	22 (41)	18 (26)
LISN	75 (86)	36 (62)	20 (37)
READ	89 (101)	39 (58)	31 (39)
Conjunction 3 contrasts	63	42	14
Contrasts	R activation	R asymmetry	R activation and asymmetry
PROD	85 (106)	54 (83)	39 (58)
LISN	66 (85)	26 (52)	17 (29)
READ	93 (110)	40 (68)	25 (44)
Conjunction 3 contrasts	52	21	7

a. Number of hROIs having significant left activation, leftward asymmetry or conjunction of activation and asymmetry for the three Word-List tasks. b. Number of hROIs having significant right activation, rightward asymmetry or conjunction of activation and asymmetry for the three Word-List tasks. For a given contrast or asymmetry and for a given hemisphere, the statistical threshold was set at 0.00027 (Bonferroni correction for 184 hROIs). For the conjunction between activation and asymmetry the statistical threshold was set at 0.016 (Bonferroni correction for the conjunction of two contrasts) and for the conjunction between three tasks, the statistical threshold was set at 0.05 (Bonferroni correction the conjunction of three tasks). The number of regions at a non-corrected threshold of 0.05 is given in brackets

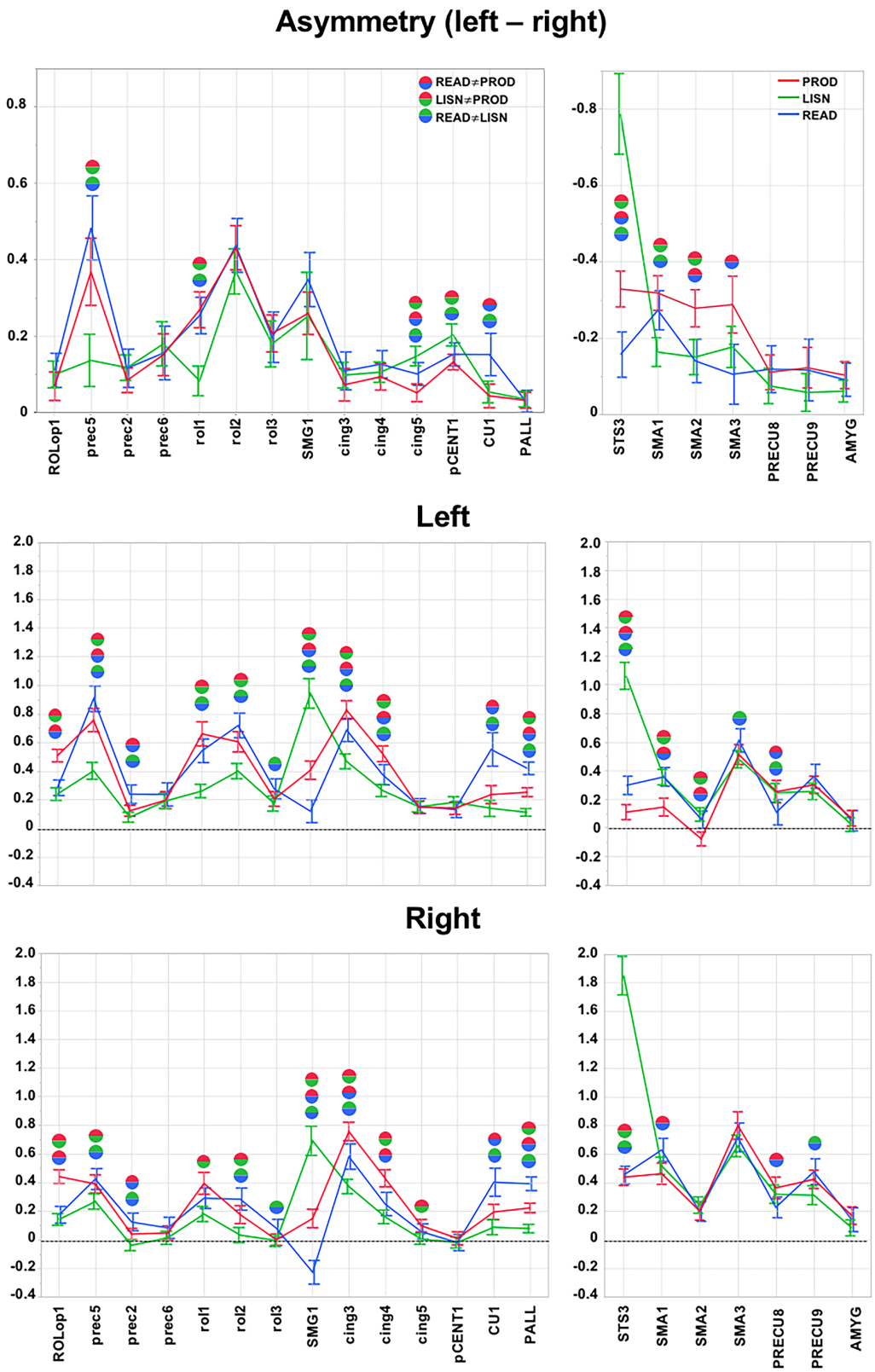
Asymmetry (left – right)
READ≠PROD
LISN≠PROD
READ≠LISN
PROD
LISN
READ
Left
Right
ROLop1
prec5
prec2
prec6
rol1
rol2
rol3
SMG1
cing3
cing4
cing5
pCENT1
CU1
PALL
STS3
SMA1
SMA2
SMA3
PRECU8
PRECU9
AMYG

◂**Fig. 3** Activity and asymmetry measured in the 21 hROIs selected at step 1. The 14 hROIs selected as leftward asymmetrical and activated are displayed on the left column, and the 7 hROIs selected as rightward and asymmetrical are displayed on the right column. The top rows are the asymmetry values in each task (red corresponds to PROD, green to LISN, and blue to READ). Note that the scale of the right hROIs has been inverted to facilitate the comparison with left regions, and significant differences (Bonferroni corrected for the number of hROIs) across tasks are indicated by spheres (the blue-red sphere corresponds to a significant difference between PROD and READ, the red-green sphere corresponds to a significant difference between PROD and LISN, and the blue-green sphere corresponds to a significant difference between LISN and READ. The middle row shows the left values of activity in the left hemisphere for the same set of regions, and the bottom row shows the activity in the right hemisphere. The abbreviations correspond to those provided in Table 1

(PALL), was selected. Abbreviations of the hROIs names are available in Table 2.

Right hemisphere

The conjunction of significant rightward activation in the three contrasts (PROD ∩ LISN ∩ READ) revealed 54 hROIs (Fig. 2, top row). The conjunction of significant rightward asymmetry revealed 19 hROIs (Fig. 2, middle row), and the conjunction of rightward activation and asymmetry revealed 7 hROIs (Fig. 2 bottom row, Table 1): 3 in the internal surface of the frontal lobe, located anteriorly to those of the left hemisphere (SMA1, SMA2, SMA3), 2 in the precuneus (PRECU8, PRECU9) and 1 in the temporal cortex (STS3) straddling the STS. Only one subcortical area, the amygdala (AMYG), was detected. Abbreviations of the hROIs names are available in Table 2.

Activation and asymmetry profiles of the selected hROIs for the three tasks

Regions of the left hemisphere

There were significant main effects of Task ($p < 0.0001$), ROI ($p < 0.0001$) and Side ($p < 0.0001$), and all interactions were significant: Task × Side ($p = 0.002$), Task × ROI ($p < 0.0001$), Side × ROI ($p < 0.0001$) and Side × Task × ROI ($p = 0.0002$).

Five left regions presented modulation in asymmetry across the different modalities of the Word-List processing (Fig. 3, Table 3). The motor and premotor areas situated in the inferior part of the central sulcus, including rol1, and prec5 (located immediately anterior to rol1) were significantly more asymmetrical and activated during the tasks involving a motor component (PROD and READ) than during LISN (Fig. 3, Table 3). Two adjacent areas located in the mid-cingulate cortex, pCENT1 and cing5, presented a larger asymmetry during LISN than during READ and PROD, due to a higher right activation during PROD and/or READ than during LISN, while left activations were comparable (Fig. 3, Table 3). Finally, the anterior and dorsal part of the cuneus (CU1) was significantly more asymmetrical and more bilaterally activated during READ than during the other two tasks (Fig. 3, Table 3).

A second set of motor regions showed little modulation of their asymmetry by the task modality. A first set corresponding to cing3 and cing4 showed no difference in asymmetry across tasks but higher activity during PROD and READ, which included a stronger motor component, than during LIST (Fig. 3, Table 3). A second region, ROLop1, situated in the Rolandic operculum area, presented no difference in asymmetry across tasks but showed more activity in PROD than the two other tasks (Fig. 3, Table 3). A third set, including prec2 and prec6 located immediately anterior to rol3, was also characterized by small inter-task differences in activation (Fig. 3, Table 3).

Finally, most of the regions selected in the left hemisphere exhibited higher bilateral activation during the tasks having a stronger motor component (PROD and READ) than during LISN (Fig. 3, Table 3). In addition, SMG1 bilateral activity was strongly increased by the auditory modality, with stronger activation during LISN than during the other two tasks.

Regions of the right hemisphere

In the right hemisphere, the main effects of Task ($p < 0.0001$), ROI ($p < 0.0001$), and Side ($p < 0.0001$) were significant, as were all interactions: Task × Side ($p = 0.0031$), Task × ROI ($p < 0.0001$), Side × ROI ($p < 0.0001$) and Side × Task × ROI ($p < 0.0001$).

Similar to the left regions, all the right hROIs showed bilateral activation except SMA2, which was deactivated on the left during PROD (Fig. 3, Table 4).

One region, STS3, located in the mid-third of the STS, presented a profile very different from all the others: STS3 presented a significantly larger rightward asymmetry during LISN than during PROD and READ (Fig. 3, Table 4). STS3 was also significantly more bilaterally activated during LISN than during the two other tasks (Fig. 3, Table 4).

Three hROIs on the internal surface of the frontal lobe, labelled SMA, located at the dorsal face and anterior part of the medial frontal gyrus, also showed a modulation of their asymmetry by the modality of the Word-List tasks. SMA1 was significantly more rightward asymmetrical during PROD and READ than during LISN, whereas SMA2

Table 2 Names and abbreviations of the 21 hROIs selected as either conjointly leftward activated and asymmetrical or conjointly rightward activated and asymmetrical during the three Word-List tasks

AICHA hROI name	Abbreviation	Network	*X* (mm)	*Y* (mm)	*Z* (mm)
Frontal and insula					
G_Rolandic_Oper-1-L	ROLop1	WORD_CORE	−46.3	3.6	9.4
S_Precentral-2-L	prec2	WORD_CORE	−25.2	−8.5	58.9
S_Precentral-5-L	prec5	WORD_CORE	−56.1	4.8	30.6
S_Precentral-6-L	prec6	WORD_CORE	−29.8	−11.2	64.7
Internal surface					
G_Cuneus-1-L	CU1	WORD_CORE	−5.2	−82.7	28.4
G_Paracentral_Lobule-1-L	pCENT1	WORD_CORE	−6.9	−16.8	50.9
G_Precuneus-8-R	PRECU8	WORD_EXE	10.5	−68.5	41.1
G_Precuneus-9-R	PRECU9	WORD_EXE	12.7	−68.4	50.3
G_Supp_Motor_Area-1-R	SMA1	WORD_EXE	5.9	20.5	49
G_Supp_Motor_Area-2-R	SMA2	WORD_EXE	10.5	18.5	62.9
G_Supp_Motor_Area-3-R	SMA3	WORD_EXE	6.4	10.1	66.5
S_Cingulate-3-L	cing3	WORD_CORE	−7.4	4.5	48.5
S_Cingulate-4-L	cing4	WORD_CORE	−7.8	−6.3	57.4
S_Cingulate-5-L	cing5	WORD_CORE	−8.5	−16.4	41.6
Parietal					
G_Supramarginal-1-L	SMG1	WORD_CORE	−54.5	−29.5	21.4
S_Rolando-1-L	rol1	WORD_CORE	−54.3	−8.4	32
S_Rolando-2-L	rol2	WORD_CORE	−43.6	−13.7	50.6
S_Rolando-3-L	rol3	WORD_CORE	−38.8	−23.1	61.4
Sub-cortical					
N_Amygdala-1-R	AMYG	WORD_EXE	21.1	1.7	−12.3
N_Pallidum-1-L	PALL	WORD_EXE	−18.6	−8.2	−0.5
Temporal					
S_Sup_Temporal-3-R	STS3	WORD_CORE	53.1	−31.9	−0.3

The network label to which they were clustered and their coordinates in MNI space after SPM12 normalization of the AICHA atlas are also provided

and SMA3 were significantly more asymmetrical during PROD than during the two other tasks (Fig. 3, Table 4).

In contrast, PRECU8, PRECU9 and AMYG did not show any variation in asymmetry according to the task modality.

Apart from STS3, the profiles of activation were comparable across tasks. However, there was less left activation in SMA1, SMA2 and SMA3 during PROD (with a deactivation for SMA3) and less left activation in PRECU8 during READ. On the right, activation was inferior during $READ_i$ in PRECU8 and PRECU9 than during PROD and LISN, respectively, and in SMA1 during PROD than during READ.

Part 2: intra- and inter-hemispheric connectivity at rest

Methods

Participants

A subset of 138 participants [mean age: 27.3 years (SD = 6.4 years); 68 women] also completed a resting-state fMRI (rs-fMRI) acquisition lasting 8 min. Note that this resting-state acquisition was performed on average 9 months (SD = 9.6 months) before the language task acquisition in all but five cases for which the resting-state acquisition occurred approximately 1 year after the language session (range 11.2–13.8 months).

Table 3 Mean activation in each Word-List contrasts of the 14 hROIs showing joint left activation and left asymmetry during the three tasks (abb corresponds to the abbreviation of the AICHA hROI name provided in Table 2)

hROIs abb	PROD			LISN			READ		
	Mean (SD)	*t*	*p*	Mean (SD)	*t*	*p*	Mean (SD)	*t*	*p*
Left activation									
CU1	0.24 (0.38)	7.45	< 0.0001	0.14 (0.35)	4.87	< 0.0001	0.55 (0.71)	9.32	< 0.0001
pCENT1	0.14 (0.27)	6.36	< 0.0001	0.18 (0.24)	9.30	< 0.0001	0.13 (0.34)	4.65	< 0.0001
ROLop1	0.51 (0.27)	22.93	< 0.0001	0.24 (0.26)	10.98	< 0.0001	0.28 (0.33)	10.28	< 0.0001
SMG1	0.41 (0.39)	12.60	< 0.0001	0.94 (0.63)	17.95	< 0.0001	0.12 (0.49)	2.98	0.0034
PALL	0.25 (0.19)	16.09	< 0.0001	0.11 (0.16)	8.23	< 0.0001	0.42 (0.27)	19.00	< 0.0001
cing3	0.83 (0.39)	25.61	< 0.0001	0.47 (0.32)	17.81	< 0.0001	0.69 (0.49)	16.74	< 0.0001
cing4	0.52 (0.34)	18.71	< 0.0001	0.27 (0.26)	12.40	< 0.0001	0.38 (0.43)	10.46	< 0.0001
cing5	0.15 (0.26)	6.88	< 0.0001	0.15 (0.22)	8.32	< 0.0001	0.16 (0.31)	6.00	< 0.0001
prec2	0.12 (0.23)	6.37	< 0.0001	0.08 (0.21)	4.48	< 0.0001	0.24 (0.39)	7.30	< 0.0001
prec5	0.76 (0.49)	18.67	< 0.0001	0.40 (0.36)	13.46	< 0.0001	0.91 (0.54)	20.09	< 0.0001
prec6	0.20 (0.36)	6.54	< 0.0001	0.19 (0.32)	7.26	< 0.0001	0.24 (0.49)	5.80	< 0.0001
rol1	0.66 (0.51)	15.45	< 0.0001	0.26 (0.29)	11.01	< 0.0001	0.54 (0.50)	13.03	< 0.0001
rol2	0.61 (0.43)	16.85	< 0.0001	0.40 (0.33)	14.78	< 0.0001	0.72 (0.52)	16.55	< 0.0001
rol3	0.21 (0.31)	7.91	< 0.0001	0.17 (0.32)	6.53	< 0.0001	0.28 (0.43)	7.70	< 0.0001
Asymmetry (left–right)									
CU1	0.04 (0.19)	2.75	0.0068	0.05 (0.17)	3.70	0.0003	0.15 (0.34)	5.40	< 0.0001
pCENT1	0.13 (0.12)	12.8	< 0.0001	0.20 (0.18)	13.88	< 0.0001	0.15 (0.18)	9.89	< 0.0001
ROLop1	0.07 (0.23)	3.62	0.0004	0.10 (0.21)	5.57	< 0.0001	0.11 (0.27)	4.86	< 0.0001
SMG1	0.26 (0.34)	9.23	< 0.0001	0.25 (0.69)	4.37	< 0.0001	0.35 (0.43)	9.69	< 0.0001
PALL	0.03 (0.13)	2.98	0.0034	0.04 (0.12)	3.36	0.0010	0.03 (0.17)	2.02	0.0451
cing3	0.07 (0.26)	3.36	0.0010	0.10 (0.20)	5.72	< 0.0001	0.11 (0.30)	4.32	< 0.0001
cing4	0.09 (0.21)	5.28	< 0.0001	0.11 (0.16)	7.77	< 0.0001	0.13 (0.22)	6.97	< 0.0001
cing5	0.05 (0.14)	4.34	< 0.0001	0.15 (0.16)	11.34	< 0.0001	0.10 (0.18)	6.70	< 0.0001
prec2	0.08 (0.20)	5.14	< 0.0001	0.12 (0.20)	6.92	< 0.0001	0.12 (0.30)	4.54	< 0.0001
prec5	0.37 (0.53)	8.26	< 0.0001	0.14 (0.42)	3.93	0.0001	0.48 (0.51)	11.42	< 0.0001
prec6	0.15 (0.33)	5.45	< 0.0001	0.18 (0.35)	6.12	< 0.0001	0.16 (0.43)	4.37	< 0.0001
rol1	0.27 (0.29)	11.29	< 0.0001	0.08 (0.24)	4.20	< 0.0001	0.25 (0.29)	10.49	< 0.0001
rol2	0.43 (0.35)	14.69	< 0.0001	0.37 (0.36)	12.32	< 0.0001	0.44 (0.43)	12.25	< 0.0001
rol3	0.21 (0.29)	8.42	< 0.0001	0.18 (5.88)	0.37	< 0.0001	0.20 (0.40)	5.88	< 0.0001

Resting-state image acquisition (rs-fMRI) and processing

Spontaneous brain activity was monitored for 8 min (240 volumes) using the same imaging sequence (T2*-weighted echo-planar images) as that used during the language task. Immediately prior to rs-fMRI scanning, the participants were instructed to "keep their eyes closed, to relax, to refrain from moving, to stay awake and to let their thoughts come and go" (Mazoyer et al. 2016). After pre-processing identical to that used for task-induced fMRI acquisition, time series of white matter and cerebrospinal fluid (individual average time series of voxels that belonged to each tissue class) and temporal linear trends were removed from the rs-fMRI data series using regression analysis. Additionally, rs-fMRI data were temporally filtered using a least squares linear-phase finite impulse response filter design bandpass (0.01–0.1 Hz).

For each of the 138 participants who completed the resting-state acquisition and for each of the same 185 homotopic ROIs, an individual BOLD rs-fMRI time series was computed by averaging the BOLD fMRI time series of all voxels located within the hROI volume.

From the BOLD fMRI time series of hROIs, we computed the Pearson correlation coefficients for each hROI pair of the 21 selected hROIs in each participant. We then averaged the Fisher *z*-transformed correlations among pairs of hROIs across the 138 individuals, resulting in a matrix of intrinsic connectivity for the whole population.

Resting-state image analysis: characterizing networks within the 21 selected hROIs

Using the same methodology as Labache et al. (2019), we applied an agglomerative hierarchical cluster analysis method on the intrinsic connectivity matrix to identify the

Table 4 Mean activation and asymmetry in each Word-List contrasts of the seven hROIs showing right activation and right asymmetry during the three tasks (abb corresponds to the abbreviation of the AICHA hROI name provided in Table 2)

hROIs abb	PROD			LISN			READ		
	Mean (SD)	*t*	*p*	Mean (SD)	*t*	*p*	Mean (SD)	*t*	*p*
Left activation									
PRECU8	0.36 (0.46)	9.48	< 0.0001	0.32 (0.39)	9.85	< 0.0001	0.23 (0.44)	6.18	< 0.0001
PRECU9	0.42 (0.39)	13.04	< 0.0001	0.31 (0.4)	9.34	< 0.0001	0.48 (0.55)	10.42	< 0.0001
SMA1	0.46 (0.45)	12.24	< 0.0001	0.52 (0.37)	16.83	< 0.0001	0.63 (0.49)	15.36	< 0.0001
SMA2	0.20 (0.38)	6.34	< 0.0001	0.24 (0.35)	8.35	< 0.0001	0.20 (0.42)	5.70	< 0.0001
SMA3	0.80 (0.58)	16.43	< 0.0001	0.66 (0.46)	17.26	< 0.0001	0.72 (0.61)	14.04	< 0.0001
AMYG	0.17 (0.37)	5.48	< 0.0001	0.08 (0.34)	2.97	0.0035	0.14 (0.51)	3.34	0.0011
STS3	0.49 (0.35)	15.05	< 0.0001	1.85 (0.82)	27.06	< 0.0001	0.45 (0.37)	14.70	< 0.0001
Asymmetry (left–right)									
PRECU8	− 0.11 (0.28)	− 4.77	< 0.0001	− 0.07 (0.28)	− 3.18	0.0018	− 0.12 (0.37)	− 3.82	0.0002
PRECU9	− 0.12 (0.32)	− 4.55	< 0.0001	− 0.06 (0.30)	− 2.30	0.0226	− 0.12 (0.49)	− 2.85	0.0051
SMA1	− 0.32 (0.28)	− 13.85	< 0.0001	− 0.16 (0.23)	− 8.56	< 0.0001	− 0.27 (0.31)	− 10.51	< 0.0001
SMA2	− 0.28 (0.30)	− 11.28	< 0.0001	− 0.15 (0.28)	− 6.43	< 0.0001	− 0.14 (0.35)	− 4.86	< 0.0001
SMA3	− 0.29 (0.45)	− 7.64	< 0.0001	− 0.18 (0.33)	− 6.48	< 0.0001	− 0.11 (0.48)	− 2.65	0.0089
AMYG	− 0.10 (0.22)	− 5.74	< 0.0001	− 0.06 (0.17)	− 4.22	< 0.0001	− 0.09 (0.26)	− 4.13	< 0.0001
STS3	− 0.33 (0.28)	− 13.85	< 0.0001	− 0.79 (0.64)	− 14.73	< 0.0001	− 0.16 (0.36)	− 5.22	< 0.0001

different networks supporting the organization across the 21 hROIs. We tested the reliability of the identified networks using a multiscale bootstrap resampling method, which provides us with an approximately unbiased (AU) *p* value representing the stability of the networks based on the average matrix of intrinsic connectivity.

Finally, we calculated the average functional intrinsic correlations between the identified networks. The significance of these correlations compared to 0 was assessed using a non-parametric sign test at a significance level of 0.05 (Bonferroni correction for the number of network pairs).

Results

Identification of networks based on the resting-state connectivity of the 21 hROIs showing both joint leftward activation and joint leftward asymmetry or both joint rightward activation and joint rightward asymmetry during the three Word-List tasks

A hierarchical clustering analysis revealed two networks from the selected set of 21 hROIs (Fig. 4); one labelled WORD-LIST_CORE was composed of 13 left hROIs and 1 right hROI, and the other we labelled WORD-LIST_CONTROL was composed of 1 left area and 6 right hROIs.

The WORD-LIST_CORE network

The WORD-LIST_CORE network (Fig. 4, green) was composed of 13 hROIs hosting motor and premotor areas of the left hemisphere gathered along the Rolandic sulcus (rol1, rol2, rol3), the precentral sulcus (prec2, prec5, prec6), the Rolandic operculum (ROLop1), motor and premotor areas of the medial surface (pCENT1, cing3, cing4, cing5), the cuneus of the occipital lobe (CU1) and SMG1 of the parietal lobe. It is important to emphasize that the WORD-LIST_CORE network is also an interhemispheric network since it comprises the right STS3 in addition to the 13 left hROIs. We named this network WORD-LIST_CORE because it included essential phonological processing regions, as further described below. WORD-LIST_CORE was the largest network in terms of volume (53136 mm^3), as it was 4.05 times larger than WORD-LIST_CONTROL (13104 mm^3).

ROLop1 appeared to be a very important hROI for communication within this network since it was among the top 5% of the strongest correlations among non-contiguous hROIs (ROLop1–SMG1: $r = 0.62$, ROLop1–cing3: $r = 0.59$, ROLop1–cing4: $r = 0.52$). It is interesting to note that the SMG1–cing4 correlation ($r = 0.53$) was also among the 5% highest correlations underlying a very strong antero-posterior tripartite connection between ROLop1, SMG1 and cing4.

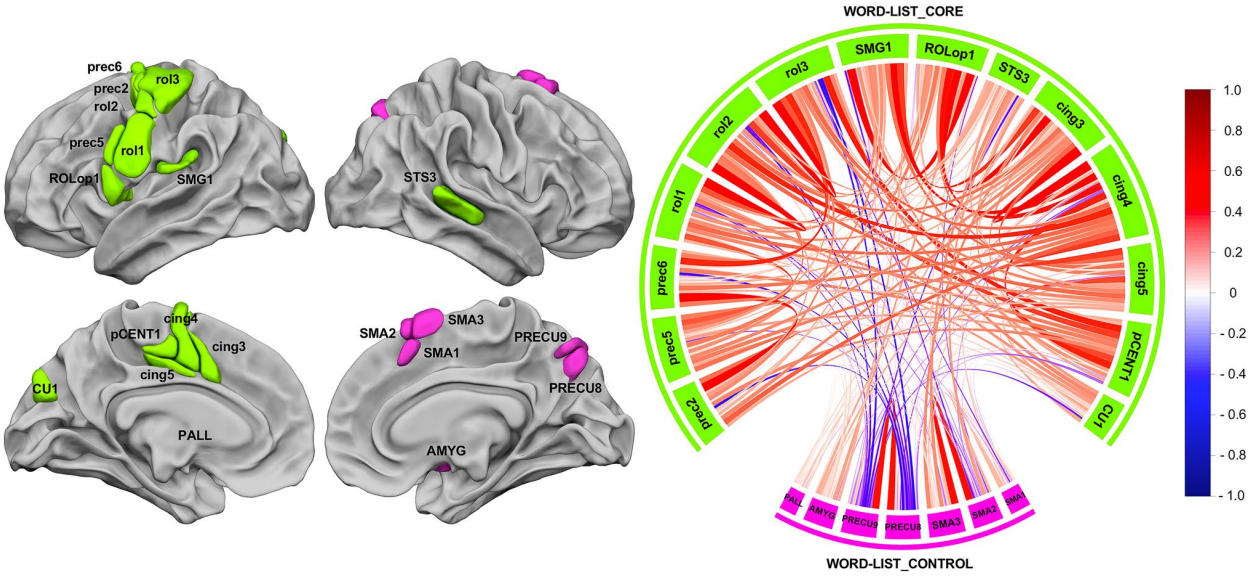

Fig. 4 Intra- and inter-hemispheric correlations at rest across the 21 hROIs selected as either conjointly leftward activated and asymmetrical or conjointly rightward activated and asymmetrical during the three language tasks. The left motor areas and the right STS are strongly and positively correlated, and they constitute the WORD-LIST_CORE network (green) that is not significantly anticorrelated with the WORD-LIST_CONTROL network, composed of the right precuneus and SMA regions and the left pallidum (pink). The chord diagram was produced by R with the "circlize" package (Gu et al. 2014)

The WORD-LIST_CONTROL network

The second network consisted of seven hROIs: six right hROIs including the three superior motor areas of the internal frontal lobe surface (SMA1, SMA2 and SMA3, which is SMA proper), the posterior part of the precuneus (PRECU8 and PRECU9) and the AMYG. In addition to these right areas, the left PALL was also part of the network. We labelled this network WORD-LIST_CONTROL because it included regions involved in the monitoring aspect of the tasks that were common to the three tasks, that is to say, maintaining the instructions, detecting the end of each word-list task and clicking on the response pad.

Note that the AU p values provided by the multiscale bootstrap resampling method showed that both networks were 81% reliable.

Temporal correlation across networks and significance

The chord diagram shown in Fig. 4 describes the average correlations between each pair of hROIs in the two networks. A non-significant negative mean intrinsic correlation was found between WORD-LIST_CORE and WORD-LIST_CONTROL ($R = -0.04$; 55.07% of the participants showed a negative correlation, $p = 0.13$).

Summary of the results of the whole study

The analysis of the connectivity at rest across the 21 hROIs common to the production, listening and reading of over-learnt lists of words made it possible to identify a set of two networks. A large WORD-LIST_CORE network made of plurimodal areas was revealed and included in the left hemisphere, premotor and motor regions that were more activated during PROD and READ than during LISN, an auditory area situated in the anterior part of the left SMG that was more activated during LISN than during PROD and READ, and a visual region, CU1 that was more activated and more asymmetrical during READ than during the two other tasks. Importantly, the strongest correlations at rest between these 21 hROIs were observed across the anterior and posterior areas (action–perception), namely, Rolop1 and cing4 with SMG1. In the right hemisphere, the WORD-LIST_CORE network included STS3, located in the mid-third of the sulcus, which was significantly more activated and asymmetrical during LISN than during PROD and READ. Note that a second network (WORD-LIST_CONTROL), composed of the right SMA1 and SMA2 (located at the preSMA), SMA3 (SMA proper) and precuneus, as well as the left PALL, was identified and was not correlated with the WORD-LIST_CORE network. The areas comprising this WORD-LIST_CONTROL network are mainly involved in extra linguistic, executive processes and attentional systems recruited to manage task completion.

Discussion

Here, we demonstrate a large-scale network of areas commonly shared by the production, listening and reading of lists of words. This network includes not only articulatory and auditory areas, but also a region of the visual cortex, the cuneus. Though more recruited during the reading task, this region, considered to be a component of accurate phonological awareness (Bolger et al. 2008), is also involved in word-list articulation and listening. During human development, speech perception and speech production, engaging auditory and motor (articulation) modalities, are initially linked together. The subsequent acquisition of reading skills, engaging the visual modality, is built upon these two components. The present results show a brain organization in adults that is a reflection of the whole developmental and learning processes of language, where action and perception circuits are interdependent and organized in networks, among which a trace of the learning modality is still present in the brain.

We will first discuss the WORD-LIST_CORE network from the left motor and premotor areas involved in action, up to the involvement of the audio–motor loop extending to the phonological loop and the right STS.

WORD-LIST_CORE network underpinning supramodal WORD-LIST processing

Left motor and premotor areas: from the speech effector areas to the hand area

On the action side, the results revealed seven areas straddling the Rolandic sulcus and precentral gyrus and four others located at the internal surface of the frontal lobe, all of which were modulated by the mere nature of the task and dependent on the modality.

The regions with the strongest motor involvement were located along the Rolandic sulcus and included primary motor areas that showed very large activations during PROD and READ. This is in accordance with Penfield's cortical stimulation studies, which provided the first functional support for the existence of somatotopy in the lower part of the Rolandic sulcus corresponding to motor control of the orofacial region (Penfield and Roberts, 1959). In fact, rol1 and adjacent rol2 match not only the area involved in speech production as described by Wilson (Wilson et al. 2004), but also the areas involved in mouth, larynx, tongue, jaw and lip movements, as reported in several studies (Brown et al. 2009, 2008; Fox et al. 2001; Grabski et al. 2012; Wilson et al. 2004) (Fig. 5). More precisely, along the dorsal-to-ventral orientation of rol1, the somatotopic representation of speech listening and mouth, lips, jaw, tongue and larynx

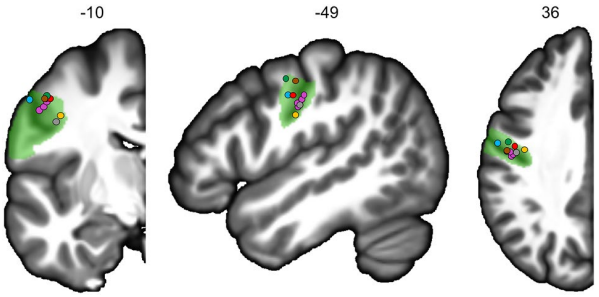

Fig. 5 Locations of the activation peaks from five studies on the left hemisphere coronal, sagittal and axial slices from the BIL&GIN display template; the hROI numbers correspond to the *x*, *y* and *z*-axes in the MNI space. In green, the representation of rol1. Larynx areas are in blue (Brown et al. 2009) and orange (Brown et al. 2008). In red, the mouth area (Fox et al. 2001). In purple, the lips, tongue, jaw and vowels areas (Grabski et al. 2012). In brown-grey, the activation peak of the motor areas for speech production (4p and 4a/6), and in green, the activation peak of the superior part of the ventral premotor cortex during listening to speech (Wilson et al. 2004)

movements clearly resembles the somatotopic organization of speech effectors proposed by Conant and collaborators (Conant et al. 2014). Moreover, the strongest asymmetry in this area during PROD and READ is consistent with the fact that these two tasks involved covert articulation or subvocalization. The premotor area prec5, tightly linked to rol1 along with cing3, was characterized by a very strong BOLD increase during READ compared to both PROD and LISN, suggesting an involvement of motor programming and articulatory coding (Dietz et al. 2005; Price 2012). Furthermore, damage to a similar region in the premotor cortex in a sample of 106 patients with diverse profiles of aphasia was shown to be strongly correlated with phonological naming errors (Schwartz et al. 2012). On the internal surface, cing3 and cing4, partly overlapping the SMA tongue area, and the anterior part of the mid-cingulate cortex situated at the tongue cingulate motor area according to Amiez et al. (2014), also presented a strong motor component, as revealed by their increased activation in PROD and READ compared to LISN. In addition, the left PALL was more activated during READ than during the two other tasks, which is in accordance with results from a meta-analysis revealing that, compared to children, adult readers recruit a larger network, including the left PALL (Paulesu et al. 2014). Importantly, the same region has been shown to be involved in the audio–motor adjustments during auditory feedback control of speech, confirming its involvement in plurimodal modulation (Tourville et al. 2008).

On the most ventral part of the Rolandic sulcus, ROLop1 presented a greater involvement in PROD than in the other tasks. This region has been reported to be activated by overt and covert articulation (Heim et al. 2002; Herbster et al. 1997; Price et al. 1996) and to be involved in phonological

rehearsal (Veroude et al. 2010) and in silent recitation of the months of the year (Wildgruber et al. 1996); moreover, lesions in this region have been associated with articulatory disorders (Tonkonogy and Goodglass 1981), which is in accordance with the motor component revealed in the present study. The lower activation of ROLop1 compared to rol1 and prec5 was because this region is a secondary motor area. It could also be suggested that ROLop1 activation could implement a simulation of phoneme production according to the model by Wilson and Iacoboni (2006), which stipulated that the prediction of the acoustic consequences of phoneme production can be compared in the superior temporal cortex with the acoustic analysis of the speech sounds heard. In the present study, we cannot disentangle an actual motor component related to subvocalization from a simulation, both being potentially engaged depending on the task: simulation during the listening task and vocalization during the production task as well as a very likely vocalization aspect during the reading task. Moreover, within the WORD-LIST_CORE network, intrinsic connectivity at rest revealed that ROLop1 was an essential hROI for communication within this network, as it was particularly correlated not only with the mid-cingulate cortex tongue areas cing3 and cing4, but also with SMG1.

On the dorsal part, a last set of areas, the prec2 and prec3 premotor areas situated along the precentral sulcus and tightly linked to rol3, which is at the location of the hand-motor area (Mellet et al. 2016), presented joint activation during the three tasks and did not show strong differences across tasks. On the internal surface, pCENT1 and cing5, located in the mid-cingulate cortex, have also been shown to be involved in hand representation (Amiez and Petrides 2014). Given their functional location, one explanation concerning the language ontogenesis observations could stipulate that the motor control of the vocal tract (speech articulators) and the motor control of the hand develop in cooperation, arguing for a hand–mouth gestural basis for language (Iverson 2010). An alternative explanation would be in relation to the motor response provided by the subjects at the end of each Word-List task; however, as the central cross-change detection is likely to cancel out most of these non-specific hand-motor activations and as there is a lack of somatosensory activation, it does not seem to support the latter hypothesis.

Involvement of the audio–motor loop and extension to the phonological loop during READ

The results of the intrinsic connectivity showed a strong correlation between SMG1 and cing4: this underlies a very strong antero-posterior tripartite connection between ROLop1, SMG1 and cing4. Therefore, there does exist a group of hROIs common to the three Word-List tasks, with a leftward involvement of brain areas specifically involved in word processing. These areas, found to be strongly and positively synchronized at rest, constitute a network including the more anterior left SMG hROI, namely, SMG1, as well as the frontal and cingulate motor and premotor areas mentioned above. These frontal and temporal regions, connected through the arcuate fasciculus tract (Catani et al. 2005), appear to consist of hROIs involved in the plurimodal representation of speech sound processing, the so-called audio–motor loop (Vigneau et al. 2006). The left areas of the audio–motor network, conjointly recruited during the three Word-List tasks, correspond at large to the neural bases of a perception–action cycle for speech sounds. Such a model, based on the link between speech perception and speech production, posits that articulatory gestures are the central motor units on which both speech perception and production develop and act according to the motor theory of speech (Liberman and Whalen 2000). More recently, neurobiological theories of speech perception have proposed a more dynamic and integrative model in which language processing relies on action–perception circuits distributed across the auditory and motor systems (Pulvermüller and Fadiga 2010, 2016). Within the WORD-LIST_CORE network, areas hosting mostly motor and premotor areas were also activated during LISN, although at a lower intensity and with a lower asymmetry. If we regard the recruitment of the SMG1 in the production task, all this taken together favours the theory supporting an involvement of action–perception circuits regardless of the Word-List task (Pulvermüller and Fadiga 2010, 2016). It is interesting to observe that READ also appears to recruit this action–perception circuit, revealing a significant activation in rol1 compared to LISN. Interestingly, this circuit, posited to subserve the mapping between sensory and motor phonological codes, is also engaged in reading (Danelli et al. 2015; Malins et al. 2016). The action–perception circuit recruited in the present study for READ also reflects the fact that the participants were instructed to engage their attention in the reading of each word and covertly articulate the lists of words at a slow speech rate. The fact that ROLop1 activation in the present study was similar for READ and LISN favours the recruitment of the action–perception circuit, and may be an indication that while reading these over-learnt words, the subjects tended to subvocalize them, which is supported by the gradient of significant activation in rol1 (production > reading > listening).

Within the large perception–action model of Fuster (2001, 2014), the literature has identified a set of areas that are considered the neural support of the phonological working memory loop postulated by Baddeley et al. (1998). In fact, experience with the Word-List automatically engages working memory processes and that component is common to the three word tasks. On the perception side, one cluster

(SMG1) was more activated and asymmetrical in LISN than in READ and PROD. Interestingly, the SMG1 is situated on the posterior part of the planum temporale, corresponding in the literature to the Sylvian–parietal–temporal area or Spt (Buchsbaum et al. 2011; Yue et al. 2018), and has been described as a sensory–motor integration area for the vocal tract. Area Spt would be part of the phonological loop described by Baddeley et al. (1998), in which the content of the phonological store can be kept active via articulatory rehearsal (Buchsbaum et al. 2011). More precisely, the Spt area has been assumed to have a storage function (Martin 2005; Smith and Jonides 1998) and to play an important role in the short-term storage of phonological representations by serving as a phonological buffer (Yue et al. 2018). The activity of area Spt is thought to be correlated with some frontal speech production areas even if their precise locations differ across studies: the pars opercularis according to Buchsbaum et al. (2001) and Poldrack et al. (Poldrack et al. 1999) and the dorsal part of the pars triangularis of the inferior frontal gyrus (F3t) according to the meta-analysis by Vigneau et al. (2006). It is noteworthy that F3t was bilaterally activated during the three tasks in the present study (Fig. 2, top row); this bilateral involvement impeded conjoint activation and asymmetry. Together with the F3t activation, on the action side, prec5 was found to show both joint leftward activation and joint leftward asymmetry during the three Word-List tasks, with a gradient of activation ranging from more activation for READ and PROD and less activation for LISN. This premotor area, prec5, has been proposed to make up a subvocal rehearsal system (Chein and Fiez 2001) and/or to support executive processes allowing the maintenance of content in verbal working memory (Smith and Jonides 1998), which is in accordance with the highest levels of activation during READ and PROD in our study. Furthermore, a single rTMS intervention targeting either the left SMG or the left posterior part of the inferior frontal gyrus, which are considered phonological nodes, was sufficient to disrupt phonological decisions, providing further support for the view that both regions contribute to efficient phonological decisions, particularly subvocal articulation (Hartwigsen et al. 2016).

Activation of the right STS3 involved in prosodic integration during PROD and READ and strong connection of the right STS3 with motor areas within the WORD-LIST_CORE network

The rightward conjoint activation of STS3 as well as its rightward asymmetry, though more activated in LISN but less activated in READ, could be accounted for by a rightward preference for non-linguistic information such as tonal prosody (Belin et al. 2002). More particularly, the right STS3, which is located in the mid-part of the STS, closely matched the activation peak showing rightward asymmetry described by Beaucousin and others (2007). This area overlaps the posterior human voice area (pHVA, Pernet et al. 2015) and corresponds to the posterior voice area described by Bodin et al. (2018). The pHVA is located on a sulcal pit corresponding to the place of the larger sulcal depth. In addition, the rightward asymmetry of this sulcal depth is specific to humans and exists regardless of the age of the subjects (infants, children or adults) (Leroy et al. 2015). The present study brings new understanding on the precise role of this region, which is not fully understood as yet. We propose that the metrics of the lists of words, resembling a reciting, are processed in this area, which is supported by its greater activation during LISN. This is in accordance with the auditory material presented to the participants, that is, the list being spoken along with the specific prosody of a list. Moreover, this region was more activated during a prosodic task than during a phonetic task (Sammler et al. 2015). During speech, words present non-verbal prosodic information that is intertwined with verbal information (Kotz and Paulmann 2007; Pell and Kotz 2011). Furthermore, prosodic and verbal cues in speech differ in their spectro-temporal properties: prosodic cues consist of slow spectral changes (over more than 200 ms) and phonemic cues consist of fast spectral changes (less than 50 ms). The right hemisphere has been suggested to be more sensitive to fine spectral details over relatively long time scales, and the left hemisphere is more sensitive to brief spectral changes (Boemio et al. 2005; Poeppel et al. 2008; Zatorre and Belin 2001).

The link between the STS3 (corresponding to pHVA), which is a prosodic integrative area, with the left SMG and rol1 instantiated in the resting-state connectivity approach reflects the intertwining between prosodic and phonemic information. The present results are supported by a recent fMRI/ERP study that revealed that activity in the left SMG together with the central sulcus area occurred earlier than in the left superior temporal cortex during phonological processing of ambiguous speech syllables, whereas attention to the spectral (prosodic) properties of the same stimuli led to activity in the right STS (Liebenthal et al. 2016). The present study demonstrated that the pHVA was part of not only the WORD-LIST_CORE network, but also showed both rightward joint activation and rightward joint asymmetry during the three Word-List tasks. These results suggest that pHVA is involved in the tonal processing of word lists that underlie speech segmentation processing for each task (PROD, LISN and READ). Moreover, the rhythmicity of the word lists processed by the right pHVA seems to be the basis of the articulatory process, which involves the left audio–motor loop, and is consistent with the recent neuroscientific literature supporting the use of musical training. Rhythmic stimulation related to the rhythm and intonation patterns of speech (prosody) has been shown to improve auditory processing,

prosodic and phonemic sensitivity in dyslexic children who perform poorly on tasks of rhythmic perception and perception of musical metres (Flaugnacco et al. 2015).

Inclusion of the right visuospatial and attentional cortical areas supporting the executive aspects of the tasks in the bilateral WORD-LIST_CONTROL network

The brain areas constituting the second network were more related to the attentional processes conjointly shared by the three tasks, which is in accordance with the anticorrelation of the WORD-LIST_CONTROL network with the WORD-LIST_CORE network (although not significant). Among these areas, SMA1, SMA2 and SMA3 overlap the location of the supplementary frontal eye fields and partially correspond to the dorsal frontal attentional network (Corbetta and Shulman 2011). The fact that these areas were more activated on the right and showed more rightward asymmetry during PROD, which was the most effortful task, is in line with a role for attentional control. The rightward asymmetry and activation of the precuneus regions, without any between-task difference, suggested that it could be related to mental imagery triggered by the scrambled version of the picture or to episodic memory encoding in reference to the list of the days and months (Cavanna and Trimble 2006).

General conclusion and perspectives

The present study, based on the fMRI analysis of three Word-List tasks performed by 144 healthy adult right-handers combined with the analysis of intrinsic resting-state connectivity in 138 of the same participants, makes it possible to propose, for the first time, a model of the neural organization of Word-List processing during production, listening and reading tasks. This model posits that (1) action and perception circuits are interdependent and organized in networks, among which a trace of the learning modality is still present in the brain; (2) the involvement of phonological action–perception circuits, such as the phonological working memory loop, in which articulatory gestures are the central motor units on which word perception, production and reading develop and act according to the motor theory of speech (Liberman and Whalen 2000), as revealed by the recruitment of leftward frontal and precentral areas together with temporo-parietal areas, and (3) the involvement of the left SMG with the right STS3 (pHVA), which is a prosodic integrative area, could reflect the intertwining between prosodic and phonemic information. The set of regions that constitutes the Word-list Multimodal Cortical Atlas (WMCA) is available for download at http://www.gin.cnrs.fr/fr/outils/wmca/.

Acknowledgements The authors would like to thank Gael Jobard, Sandrine Crémona and Bernard Mazoyer for thoughtful comments and Gaelle Leroux for dedicated technical support.

Author contributions IH, LL and NTM wrote the article. LL, NTM and MJ conducted the data analyses. NTM designed the paradigm and acquired the data, and NTM and IH analysed the fMRI language runs, which are part of the BIL&GIN. All authors have contributed to the preparation and writing of the manuscript.

Funding This work was supported by a grant from the FLAG-ERA Human Brain Project 2015 (ANR-15-HBPR-0001-03-MULTI-LATERAL) awarded to NTM and MJ.

Availability of data and material The datasets analysed in the current study to obtain the atlas are not publicly available because they were established by the laboratory. They will be available when the laboratory completes all the publications. The atlas is publicly available at http://www.gin.cnrs.fr/en/tools/.

Compliance with ethical standards

Conflict of interest The authors declare that they have no conflict of interest.

Ethics statement The study has been approved by the Basse-Normandie research ethics committee and has been performed in accordance with the ethical standards laid down in the 1964 Declaration of Helsinki and its later amendments or comparable ethical standards.

Informed consent Informed written consent was obtained from all individual participants included in the study.

References

Amiez C, Petrides M (2014) Neuroimaging evidence of the anatomo-functional organization of the human cingulate motor areas. Cereb Cortex 24:563–578

Assaneo MF, Poeppel D (2018) The coupling between auditory and motor cortices is rate-restricted: evidence for an intrinsic speech-motor rhythm. Sci Adv 4:3842

Baddeley A, Gathercole S, Papagno C (1998) The phonological loop as a language learning device. Psychol Rev 105:158–173

Beaucousin V, Lacheret A, Turbelin M-R, Morel M, Mazoyer B, Tzourio-Mazoyer N (2007) FMRI study of emotional speech comprehension. Cereb Cortex (1991) 17:339–352. https://doi.org/10.1093/cercor/bhj151

Belin P, Zatorre RJ, Ahad P (2002) Human temporal-lobe response to vocal sounds. Brain Res Cogn Brain Res 13:17–26

Belin P, Fecteau S, Bédard C (2004) Thinking the voice: neural correlates of voice perception. Trends Cogn. Sci. 8:129–135. https://doi.org/10.1016/j.tics.2004.01.008

Bever TG, Fodor JA, Weksel W (1971) Theoretical notes on the acquisition of syntax: a critique of 'contextual generalization'.

In: Bar-Adon A, Leopold WF (eds) Child language: a book of readings. Prentice-Hall, Englewood Cliffs
Binder JR, Frost JA, Hammeke TA, Rao SM, Cox RW (1996) Function of the left planum temporale in auditory and linguistic processing. Brain J Neurol 119(Pt 4):1239–1247
Binder JR, Frost JA, Hammeke TA, Bellgowan PS, Springer JA, Kaufman JN, Possing ET (2000) Human temporal lobe activation by speech and nonspeech sounds. Cereb Cortex (1991) 10:512–528
Bodin C, Takerkart S, Belin P, Coulon O (2018) Anatomo-functional correspondence in the superior temporal sulcus. Brain Struct Funct 223:221–232
Boemio A, Fromm S, Braun A, Poeppel D (2005) Hierarchical and asymmetric temporal sensitivity in human auditory cortices. Nat Neurosci 8:389–395. https://doi.org/10.1038/nn1409
Bolger DJ, Minas J, Burman DD, Booth JR (2008) Differential effects of orthographic and phonological consistency in cortex for children with and without reading impairment. Neuropsychologia 46:3210–3224
Booth JR, Burman DD, Meyer JR, Gitelman DR, Parrish TB, Mesulam MM (2002a) Functional anatomy of intra- and cross-modal lexical tasks. Neuroimage 16:7–22. https://doi.org/10.1006/nimg.2002.1081
Booth JR, Burman DD, Meyer JR, Gitelman DR, Parrish TB, Mesulam MM (2002b) Modality independence of word comprehension. Hum Brain Mapp 16:251–261. https://doi.org/10.1002/hbm.10054
Brown S, Ngan E, Liotti M (2008) A larynx area in the human motor cortex. Cereb Cortex 18:837–845. https://doi.org/10.1093/cercor/bhm131
Brown S, Laird AR, Pfordresher PQ, Thelen SM, Turkeltaub P, Liotti M (2009) The somatotopy of speech: phonation and articulation in the human motor cortex. Brain Cogn 70:31–41. https://doi.org/10.1016/j.bandc.2008.12.006
Buchsbaum BR, Hickok G, Humphries C (2001) Role of left posterior superior temporal gyrus in phonological processing for speech perception and production. Cogn Sci 25:663–678. https://doi.org/10.1016/S0364-0213(01)00048-9
Buchsbaum BR, Baldo J, Okada K, Berman KF, Dronkers N, D'Esposito M, Hickok G (2011) Conduction aphasia, sensory-motor integration, and phonological short-term memory—an aggregate analysis of lesion and fMRI data. Brain Lang 119:119–128. https://doi.org/10.1016/j.bandl.2010.12.001
Buckner RL, Koutstaal W, Schacter DL, Rosen BR (2000) Functional MRI evidence for a role of frontal and inferior temporal cortex in amodal components of priming. Brain J Neurol 123(Pt 3):620–640
Cason N, Hidalgo C, Isoard F, Roman S, Schön D (2015) Rhythmic priming enhances speech production abilities: evidence from prelingually deaf children. Neuropsychology 29:102–107
Catani M, Jones DK, Ffytche DH (2005) Perisylvian language networks of the human brain. Ann Neurol 57:8–16. https://doi.org/10.1002/ana.20319
Catts HW, Adlof SM, Hogan T, Weismer SE (2005) Are specific language impairment and dyslexia distinct disorders? J Speech Lang Hear Res 48:1378–1396
Cavanna AE, Trimble MR (2006) The precuneus: a review of its functional anatomy and behavioural correlates. Brain J Neurol 129:564–583. https://doi.org/10.1093/brain/awl004
Chee MW, O'Craven KM, Bergida R, Rosen BR, Savoy RL (1999) Auditory and visual word processing studied with fMRI. Hum Brain Mapp 7:15–28
Chein JM, Fiez JA (2001) Dissociation of verbal working memory system components using a delayed serial recall task. Cereb Cortex (1991) 11:1003–1014
Conant D, Bouchard KE, Chang EF (2014) Speech map in the human ventral sensory-motor cortex. Curr Opin Neurobiol 24:63–67. https://doi.org/10.1016/j.conb.2013.08.015
Corbetta M, Shulman GL (2011) Spatial neglect and attention networks. Annu Rev Neurosci 34:569–599. https://doi.org/10.1146/annurev-neuro-061010-113731
Curtiss S (1977) Genie: a psycholinguistic study of a modern-day "wild child". Academic Press, New York
Danelli L, Marelli M, Berlingeri M, Tettamanti M, Sberna M, Paulesu E, Luzzatti C (2015) Framing effects reveal discrete lexical-semantic and sublexical procedures in reading: an fMRI study. Front. Psychol 6:1328
De Saussure F (1975) Cours de linguistique générale. Payot, Paris
Dietz NAE, Jones KM, Gareau L, Zeffiro TA, Eden GF (2005) Phonological decoding involves left posterior fusiform gyrus. Hum Brain Mapp 26:81–93. https://doi.org/10.1002/hbm.20122
Dym RJ, Burns J, Freeman K, Lipton ML (2011) Is functional MR imaging assessment of hemispheric language dominance as good as the Wada test? A meta-analysis. Radiology 261:446–455. https://doi.org/10.1148/radiol.11101344
Flaugnacco E, Lopez L, Terribili C, Montico M, Zoia S, Schön D (2015) Music training increases phonological awareness and reading skills in developmental dyslexia: a randomized control trial. PLoS One 10:e0138715
Fodor JA (1983) The modularity of mind. MIT Press, Cambridge
Fox PT, Huang A, Parsons LM, Xiong JH, Zamarippa F, Rainey L, Lancaster JL (2001) Location-probability profiles for the mouth region of human primary motor-sensory cortex: model and validation. Neuroimage 13:196–209. https://doi.org/10.1006/nimg.2000.0659
Fuster JM (2001) The prefrontal cortex—an update: time is of the essence. Neuron 30:319–333
Fuster JM (2014) The prefrontal cortex makes the brain a preadaptive system. Proc IEEE 102:417–426
Gazzaniga MS (2000) Cerebral specialization and interhemispheric communication: does the corpus callosum enable the human condition? Brain J Neurol 123(Pt 7):1293–1326
Gerken L, Landau B, Remez RE (1990) Function morphemes in young children's speech perception and production. Dev Psychol 26(2):204
Gillon GT (2004) Phonological awareness: from research to practice. Guilford Press, New York
Grabski K, Lamalle L, Vilain C, Schwartz J-L, Vallée N, Tropres I, Baciu M, Le Bas J-F, Sato M (2012) Functional MRI assessment of orofacial articulators: neural correlates of lip, jaw, larynx, and tongue movements. Hum Brain Mapp 33:2306–2321. https://doi.org/10.1002/hbm.21363
Gu Z, Gu L, Eils R, Schlesner M, Brors B (2014) Circlize implements and enhances circular visualization in R. Bioinformatics 30:2811–2812
Hartwigsen G, Weigel A, Schuschan P, Siebner HR, Weise D, Classen J, Saur D (2016) Dissociating parieto-frontal networks for phonological and semantic word decisions: a condition-and-perturb TMS study. Cereb Cortex (1991) 26:2590–2601. https://doi.org/10.1093/cercor/bhv092
Heim S, Opitz B, Friederici AD (2002) Broca's area in the human brain is involved in the selection of grammatical gender for language production: evidence from event-related functional magnetic resonance imaging. Neurosci Lett 328:101–104
Herbster AN, Mintun MA, Nebes RD, Becker JT (1997) Regional cerebral blood flow during word and nonword reading. Hum Brain Mapp 5:84–92
Hickok G, Poeppel D (2000) Towards a functional neuroanatomy of speech perception. Trends Cogn Sci 4:131–138
Hickok G, Poeppel D (2004) Dorsal and ventral streams: a framework for understanding aspects of the functional anatomy of language. Cognition 92:67–99. https://doi.org/10.1016/j.cognition.2003.10.011

Iverson JM (2010) Developing language in a developing body: the relationship between motor development and language development. J Child Lang 37:229–261

Joliot M, Jobard G, Naveau M, Delcroix N, Petit L, Zago L, Crivello F, Mellet E, Mazoyer B, Tzourio-Mazoyer N (2015) AICHA: an atlas of intrinsic connectivity of homotopic areas. J Neurosci Methods 254:46–59. https://doi.org/10.1016/j.jneumeth.2015.07.013

JMP® (1989–2019) Version 14. SAS Institute Inc., Cary, NC

Jusczyk PW, Cutler A, Redanz NJ (1993) Infants' preference for the predominant stress patterns of English words. Child Dev 64:675–687

Kotz SA, Paulmann S (2007) When emotional prosody and semantics dance cheek to cheek: ERP evidence. Brain Res 1151:107–118. https://doi.org/10.1016/j.brainres.2007.03.015

Labache L, Joliot M, Saracco J, Jobard G, Hesling I, Zago L, Mellet E, Petit L, Crivello F, Mazoyer B, Tzourio-Mazoyer N (2019) A SENtence Supramodal Areas AtlaS (SENSAAS) based on multiple task-induced activation mapping and graph analysis of intrinsic connectivity in 144 healthy right-handers. Brain Struct Funct 224:859–882

Leroy F, Cai Q, Bogart SL, Dubois J, Coulon O, Monzalvo K, Fischer C, Glasel H, der Haegen LV, Bénézit A et al (2015) New human-specific brain landmark: the depth asymmetry of superior temporal sulcus. PNAS 112:1208–1213

Liberman A, Whalen D (2000) On the relation of speech to language. Trends Cogn Sci 4:187–196

Liebenthal E, Silbersweig DA, Stern E (2016) The language, tone and prosody of emotions: neural substrates and dynamics of spoken-word emotion perception. Front Neurosci 10:506. https://doi.org/10.3389/fnins.2016.00506

Locke JL, Pearson DM (1990) Linguistic significance of babbling: evidence from a tracheostomized infant. J Child Lang 17:1–16

Malins JG, Gumkowski N, Buis B, Molfese P, Rueckl JG, Frost SJ, Pugh KR, Morris R, Mencl WE (2016) Dough, tough, cough, rough: a "fast" fMRI localizer of component processes in reading. Neuropsychologia 91:394–406

Martin RC (2005) Components of short-term memory and their relation to language processing: evidence from neuropsychology and neuroimaging. Curr Dir Psychol Sci 14:204–208. https://doi.org/10.1111/j.0963-7214.2005.00365.x

Mazoyer B, Mellet E, Perchey G, Zago L, Crivello F, Jobard G, Delcroix N, Vigneau M, Leroux G, Petit L, Joliot M, Tzourio-Mazoyer N (2016) BIL&GIN: a neuroimaging, cognitive, behavioral, and genetic database for the study of human brain lateralization. Neuroimage 124:1225–1231. https://doi.org/10.1016/j.neuroimage.2015.02.071

McNorgan C, Awati N, Desroches AS, Booth JR (2014) Multimodal lexical processing in auditory cortex is literacy skill dependent. Cereb Cortex 24:2464–2475

Mellet E, Mazoyer B, Leroux G, Joliot M, Tzourio-Mazoyer N (2016) Cortical asymmetries during hand laterality task vary with hand laterality: a fMRI study in 295 participants. Front Hum Neurosci 10:628

Oldfield RC (1971) The assessment and analysis of handedness: the Edinburgh inventory. Neuropsychologia 9:97–113

Oller DK, MacNeilage PF (1983) Development of speech production: perspectives from natural and perturbed speech. In: MacNeilage PF (ed) The production of speech. Springer, New York, pp 91–108

Paulesu E, Danelli L, Berlingeri M (2014) Reading the dyslexic brain: multiple dysfunctional routes revealed by a new meta-analysis of PET and fMRI activation studies. Front Hum Neurosci 8:830

Pell MD, Kotz SA (2011) On the time course of vocal emotion recognition. PLoS One 6:e27256. https://doi.org/10.1371/journal.pone.0027256

Penfield W, Roberts M (1959) Speech and brain mechanisms. Princeton University Press, Princeton

Pernet CR, McAleer P, Latinus M, Gorgolewski KJ, Charest I, Bestelmeyer PE, Watson RH, Fleming D, Crabbe F, Valdes-Sosa M, Belin P (2015) The human voice areas: spatial organization and inter-individual variability in temporal and extra-temporal cortices. Neuroimage 119:164–174

Pitt MA, Samuel AG (1990) The use of rhythm in attending to speech. J Exp Psychol Hum Percept Perform 16:564–573

Poeppel D, Idsardi WJ, van Wassenhove V (2008) Speech perception at the interface of neurobiology and linguistics. Philos Trans R Soc Lond B Biol Sci 363:1071–1086. https://doi.org/10.1098/rstb.2007.2160

Poldrack RA, Wagner AD, Prull MW, Desmond JE, Glover GH, Gabrieli JD (1999) Functional specialization for semantic and phonological processing in the left inferior prefrontal cortex. Neuroimage 10:15–35. https://doi.org/10.1006/nimg.1999.0441

Price CJ (2010) The anatomy of language: a review of 100 fMRI studies published in 2009. Ann N Y Acad Sci 1191:62–88

Price CJ (2012) A review and synthesis of the first 20 years of PET and fMRI studies of heard speech, spoken language and reading. Neuroimage 62:816–847

Price CJ, Wise RJ, Warburton EA, Moore CJ, Howard D, Patterson K, Frackowiak RS, Friston KJ (1996) Hearing and saying. The functional neuro-anatomy of auditory word processing. Brain J Neurol 119(Pt 3):919–931

Pulvermüller F, Fadiga L (2010) Active perception: sensorimotor circuits as a cortical basis for language. Nat Rev Neurosci 11:351–360. https://doi.org/10.1038/nrn2811

Pulvermüller F, Fadiga L (2016) Chapter 26—brain language mechanisms built on action and perception. In: Hickok G, Small SL (eds) Neurobiology of language. Academic Press, San Diego, pp 311–324. https://doi.org/10.1016/B978-0-12-407794-2.00026-2

Pulvermüller F, Huss M, Kherif F, del Prado Moscoso, Martin F, Hauk O, Shtyrov Y (2006) Motor cortex maps articulatory features of speech sounds. Proc Natl Acad Sci USA 103:7865–7870. https://doi.org/10.1073/pnas.0509989103

Rauschecker JP, Tian B (2000) Mechanisms and streams for processing of "what" and "where" in auditory cortex. Proc Natl Acad Sci USA 97:11800–11806. https://doi.org/10.1073/pnas.97.22.11800

Roncaglia-Denissen MP, Schmidt-Kassow M, Kotz SA (2013) Speech rhythm facilitates syntactic ambiguity resolution: ERP evidence. PLoS One 8:e56000

Rueckl JG, Paz-Alonso PM, Molfese PJ, Kuo W-J, Bick A, Frost SJ, Hancock R, Wu DH, Mencl WE, Duñabeitia JA et al (2015) Universal brain signature of proficient reading: evidence from four contrasting languages. Proc Natl Acad Sci 112:15510–15515

Sammler D, Grosbras M-H, Anwander A, Bestelmeyer PEG, Belin P (2015) Dorsal and ventral pathways for prosody. Curr Biol CB 25:3079–3085. https://doi.org/10.1016/j.cub.2015.10.009

Schwartz MF, Faseyitan O, Kim J, Coslett HB (2012) The dorsal stream contribution to phonological retrieval in object naming. Brain 135(12):3799–3814

Schwartze M, Rothermich K, Schmidt-Kassow M, Kotz SA (2011) Temporal regularity effects on pre-attentive and attentive processing of deviance. Biol Psychol 87:146–151

Sidtis JJ, Volpe BT, Wilson DH, Rayport M, Gazzaniga MS (1981) Variability in right hemisphere language function after callosal section: evidence for a continuum of generative capacity. J Neurosci Off J Soc Neurosci 1:323–331

Smith EE, Jonides J (1998) Neuroimaging analyses of human working memory. Proc Natl Acad Sci USA 95:12061–12068

Thaut M (2013) Rhythm, music, and the brain: Scientific Foundations and Clinical Applications. Routledge, London

Thaut MH, McIntosh GC (2014) Neurologic music therapy in stroke rehabilitation. Curr Phys Med Rehabil Rep 2:106–113

Toga AW, Thompson PM (2003) Mapping brain asymmetry. Nat Rev Neurosci 4:37–48. https://doi.org/10.1038/nrn1009

Tonkonogy J, Goodglass H (1981) Language function, foot of the third frontal gyrus, and rolandic operculum. Arch Neurol 38:486–490

Tourville JA, Reilly KJ, Guenther FH (2008) Neural mechanisms underlying auditory feedback control of speech. Neuroimage 39:1429–1443

Veroude K, Norris DG, Shumskaya E, Gullberg M, Indefrey P (2010) Functional connectivity between brain regions involved in learning words of a new language. Brain Lang 113:21–27. https://doi.org/10.1016/j.bandl.2009.12.005

Vigneau M, Beaucousin V, Hervé PY, Duffau H, Crivello F, Houdé O, Mazoyer B, Tzourio-Mazoyer N (2006) Meta-analyzing left hemisphere language areas: phonology, semantics, and sentence processing. Neuroimage 30:1414–1432. https://doi.org/10.1016/j.neuroimage.2005.11.002

Vigneau M, Beaucousin V, Hervé P-Y, Jobard G, Petit L, Crivello F, Mellet E, Zago L, Mazoyer B, Tzourio-Mazoyer N (2011) What is right-hemisphere contribution to phonological, lexico-semantic, and sentence processing? Insights from a meta-analysis. Neuroimage 54:577–593

Wildgruber D, Ackermann H, Klose U, Kardatzki B, Grodd W (1996) Functional lateralization of speech production at primary motor cortex: a fMRI study. Neuroreport 7:2791–2795

Wilson SM, Iacoboni M (2006) Neural responses to non-native phonemes varying in producibility: evidence for the sensorimotor nature of speech perception. Neuroimage 33:316–325. https://doi.org/10.1016/j.neuroimage.2006.05.032

Wilson SM, Saygin AP, Sereno MI, Iacoboni M (2004) Listening to speech activates motor areas involved in speech production. Nat Neurosci 7:701–702. https://doi.org/10.1038/nn1263

Yue Q, Martin RC, Hamilton AC, Rose NS (2018) Non-perceptual regions in the left inferior parietal lobe support phonological short-term memory: evidence for a buffer account? Cereb Cortex (1991). https://doi.org/10.1093/cercor/bhy037

Zatorre RJ, Belin P (2001) Spectral and temporal processing in human auditory cortex. Cereb Cortex (1991) 11:946–953

Zago L, Petit L, Turbelin MR, Andersson F, Vigneau M, Tzourio-Mazoyer N (2008) How verbal and spatial manipulation networks contribute to calculation: an fMRI study. Neuropsychologia 46(9):2403–2414

Partie III

Mise au point d'une méthode pour l'étude de la variabilité interindividuelle des réseaux du repos : prise en compte du caractère tridimensionnel des données

1. SIMS : une nouvelle méthode de détection des réseaux cérébraux instables et de sous-populations utilisant la classification ascendante hiérarchique

---

Le travail présenté ci-dessous a été exposé dans le cadre des 51es Journées de Statistique 2019 de la Société Française de Statistiques à Vandœuvre-lès-Nancy sur le Campus des Aiguillettes de l'Université de Lorraine. Il fait également l'objet de l'article ci-après qui constitue l'intégralité de ce premier chapitre de la Partie III :

Labache L., Joliot M., Doucet G., Saracco J. (2020). Study of inter-individual variability of three-dimensional data table: detection of unstable variables and samples. Submitted to *Computational Statistics*.

Computational Statistics manuscript No.
(will be inserted by the editor)

Study of inter-individual variability of three-dimensional data table

Detection of unstable variables and samples

Loïc Labache · Marc Joliot · Gaëlle E. Doucet · Jérôme Saracco

Received: date / Accepted: date

Abstract We propose two methodologies in order to better understand the inter-individual variability of resting-state functional Magnetic Resonance Imaging (fMRI) brain data. The aim of the study was to quantify whether the average dendrogram is representative of the initial population and to identify its possible sources of instability. The average dendrogram is based on the Pearson correlation between resting-state networks. The first method identifies networks that can lead to unstable partitions of the average dendrogram. The second method identified homogeneous sub-samples of participants for whom their associated average dendrograms were more stable than that of the whole sample. The two suggested methods have shown significant quantifiable behavioral data results with regards to detecting an unstable network or presence of subpopulations when the noise level does not conceal the structure of the data. These two methods have been successfully applied to establish a cerebral atlas for late adulthood. The first method made it clear that there was no unstable network among the atlas networks. The second method highlighted the presence of two distinct sub-populations with different age-related brain organizations.

Keywords hierarchical clustering, inter-individual variability, detection of sources of instability, fMRI

Loïc Labache · Marc Joliot
Groupe d'Imagerie Neurofonctionnelle – CEA & IMN, UMR 5293 – Centre Broca Nouvelle-Aquitaine, 146 rue Léo Saignat, 33000 Bordeaux, France
E-mail: loic.labache@u-bordeaux.fr E-mail: marc.joliot@u-bordeaux.fr

Gaelle E. Doucet
Boys Town National Research Hospital, Omaha, NE, USA
E-mail: gaelle.doucet@boystown.org

Jérôme Saracco · Loïc Labache
Inria Bordeaux Sud Ouest & Institut de Mathématiques de Bordeaux, UMR CNRS 5251 & ENSC Bordeaux INP, 109 Avenue Roul, 33400 Talence, France
E-mail: jerome.saracco@math.u-bordeaux.fr

1 Introduction

The analysis of the partitions stability of a dendrogram is a crucial issue in order to check the replicability of the selected partitions.

For classical two-dimensional data, it is possible to obtain a measure of the stability of the clusters (obtained from a given partition) using the approximately unbiased p-value (AU-value) obtained with a multiscale bootstrap resampling method (MBR: [1]) available via the `pvclust` function of the R library of the same name [2]. The AU-value then indicates the unbiased frequency of occurrence of a cluster across the reference population of the dendrogram.

There is currently no counterpart to this method for three-dimensional data. This paper thus develops a similar method to `pvclust` that is adapted to any kind of three-dimensional data and, in particular, for resting-state functional Magnetic Resonance Imaging (rs-fMRI) data.

fMRI allows to obtain regional brain electrical activity ([3], [4]) by monitoring relative fluctuations in the Blood Oxygen Level Dependent (BOLD) signal.

The study of human brains' resting state functional organization consists in analyzing the synchronicity between the BOLD signals of different brain areas or networks. Commonly, the synchronicity study is performed using the calculation of Pearson correlation coefficients between the BOLD signals of all network pairs, resulting in correlation matrices of dimension $K \times K$ for K brain networks. There are databases of several hundred individuals containing 3D structures (of dimension $K \times K$) that gather all of the correlation matrices $M_s,\ s = 1, ..., S$ of the S individuals in the database.

For a some databases, in this case, the BIL&GIN database, [5]), the first work consisted of a agglomerative hierarchical clustering of K brain networks. The second step was to find an optimal number of clusters reflecting the best resting state cerebral organisation [6]. The methodology consisted of averaging all the Fisher transformations of the matrices M in the following way:

$$M_m = \tanh\left(\frac{\sum_{s=1}^{S} \operatorname{arctanh}(M_s)}{S}\right) \tag{1}$$

This matrix is then transformed into a dissimilarity matrix $D_m : D_m = (1 - M_m)/2$.. Then m the aggregation of the K brain networks is accomplished via agglomerative hierarchical clustering(according to Ward' method)based on D_m.

Taking into account the inter-individual variability, [6] adapted a procedure called `pvclust` [7] which allows researchers to assess the uncertainty associated with the different partitions of the hierarchical clustering through a p-value obtained by bootstrapping. The previous methodology provides a Bootstrap Probability p-value (called BP-value) and after correction, an Approximately Unbiased p-value (denoted AU-value). The AU-values are calculated using the bootstrap values recommended in [2] by using anywhere from 50% to 140%

of the sample. These p-values indicate how well the different partitions are supported by the data.

To illustrate this methodology, let us consider a population of 439 subjects. The optimal number of clusters was determined using the R library `NbClust` [8]. This package provides 30 statistical indices for determining the optimal number of clusters and offers the best clustering scheme from the different results obtained by varying all combinations of the number of clusters for the chosen method, in this case, hierarchical clustering with Ward's criterion. We selected the number of clusters that satisfied a maximum of indices and found it to be equal to 3. For the corresponding three optimal clusters the associated BP and AU-values are equal to 100% (Fig. 1). [2] recommends using AU-values, these 3 retained clusters were perfectly represented by our data. However, the AU-values represent the stability of the M_m based clusters and not on the empirical frequency of appearance through these clusters across the S subjects, called individual frequencies below. Fig. 1 illustrates this event. We can see the evolution of the BP-values as a function of the proportion of subjects used in the bootstrap sampling, as well as the actual value of the individual frequencies of cluster occurrence. For example, for the considered partition of 3 clusters, the corresponding three BP-values are 100%, whereas the individual frequencies of appearance are respectively 5% , 4% and 12% for these 3 clusters. The individual frequencies of occurrence correspond to the number of times a cluster appears among the individual dendrograms of the population. In the study of intrinsic brain organization, these proportions are unreliable and, in a general framework, this shows that the `pvclust` algorithm cannot be used for three-dimensional data; the BP-values do not reflect the individual frequencies.

In this paper, two methodologies are proposed to better understand the inter-individual variability of partitions from M_m :

- the first one allows the identification of networks that can lead to unstable partitions from M_m;
- the second one allows the identification of homogeneous subpopulations of subjects across the population by maximizing the individual frequency of appearance of clusters from the partitions built on their associated M_m matrices.

In the first part of this paper, we will present how to calculate the empirical frequency Q_k through a network R_k based on the comparison of its position in the average dendrogram with respect to the individual dendrograms. We will present how to use it to identify an unstable network at the population level. Finally, from the individual frequency of a cluster, we show how to extract, from the initial population, subpopulations that are, on average, more stable.

2 Presentation of the proposed approaches

Consider $M_s,\ s = 1, ..., S$, the S individual correlation matrices of dimension $K \times K$.

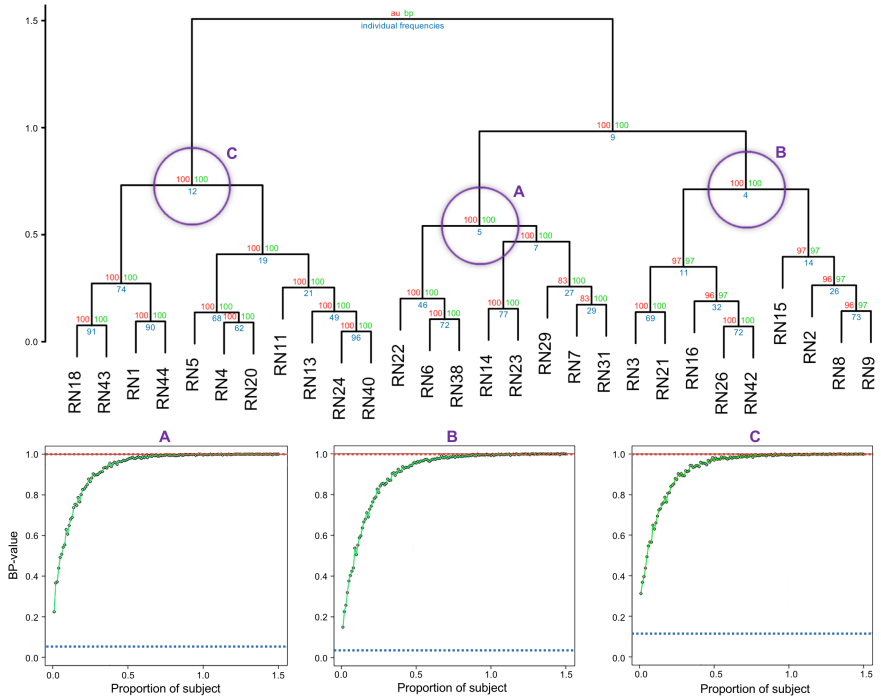

Fig. 1 Agglomerative hierarchical clustering from M_m (top). Evolution of BP-value as a function of the proportion of individuals sampled in the bootstrap (below). The individual frequency of the clusters are in blue. The BP-values are in green. The AU-values are in red.

Starting from the hierarchical ascendant clustering based on the mean matrix M_m defined in the introduction, K nested partitions$P_m^j,\ j = 1, \ldots, K$ can be obtained and summarized by vectors of size K defined as follows: for the partition (also called pattern afterwards) into j clusters, the k^{th} component of P_m^j is equal to 1 if the network R_k appears in the new cluster created by switching from a partition into $(j+1)$ clusters to a partition into j clusters . In the following, we will note:

$$P_m = \{P_m^1, \ldots, P_m^j, \ldots, P_m^K\} \tag{2}$$

with $P_m^1 = (1, \ldots, 1)$ and $P_m^K = (0, \ldots, 0)$ by convention.

In the same way, for each subject s, the corresponding K nested partitions can be constructed from the M_s matrices:

$$P_s = \{P_s^1, \ldots, P_s^j, \ldots, P_s^K\} \quad \text{for } s = 1, \ldots, S \tag{3}$$

For each non-trivial1e[1] partition from M_m , we will search, among the $(K-2)$ non-trivial partitions of each subject s, the element of P_s closest to P_m^j based on the Sorensen-Dice index defined as follows:

[1] Partitioning into one cluster (respectively into K clusters) is considered as trivial.

$$C_s^j = 1 - \min_{l=2,\ldots,K-1} \frac{2(P_m^j)' P_s^l}{(P_m^j)' P_m^j + (P_s^l)' P_s^l} \tag{4}$$

where the notation v' denotes the transpose of the vector v. A zero index C_s^j (respectively equal to 1) indicates that the vectors P_m^j and P_s^j are equal (respectively, do not share a common network).

In the following, we call *alternative pattern* to P_m^j, denoted by $\tilde{P}^j$ hereafter, the pattern(s) of P_s closest to P_m^j in the sense of the index C_s^j (if this pattern is not equal to the average pattern P_m^j).

From the set of the $\tilde{P}^j$, it is then possible to calculate a Q_k score of participations for each network R_k . This score Q_k represents the empirical frequency (expressed in %) that the network R_k is constituted of an alternative pattern, whatever the average pattern. For an average pattern P_m^j, let us define F^j as the number of single subjects expressing the alternative pattern $\tilde{P}^j$, and let F_k^j be the number of single subjects expressing the alternative pattern $\tilde{P}^j$ containing the network k. The empirical frequency Q_k of a network R_k is then defined as follows:

$$Q_k = \frac{\sum_{j=1}^{K-2} F_k^j}{\sum_{j=1}^{K-2} F^j} \tag{5}$$

Note that an alternative pattern of P_m^j can never be equal to an average pattern P_m^j of another level than $l \neq j$.

2.1 Method for identifying an unstable network

From the participation score Q_k of each network R_k, it is possible to identify the one that will be said to be *unstable* among the K networks (i.e. a network that will not be stable with respect to Pm across the subjects). Typically, a network R_{k^*} that "roams" on the dendrogram associated with P_m without having a fixed attachment within the S individual dendrograms P_s leads to an unstable mean tree. The network showing the most marked instability is obtained by :

$$k^* = \arg \max_{k=1,\ldots,K} Q_k \tag{6}$$

By convention, if $Q_1 = \ldots = Q_K$, it is considered that there are no unstable networks.

2.2 Method for identifying subpopulations of subjects

Let us first define the individual frequencies of the *average* dendrogram patterns P_m^j denoted F_m^j as the number of single subjects expressing P_m^j.

First, the methodology consists of iteratively selecting the subjects belonging to the pattern $P_m^{j^*}$ such that $j^* = \arg\min_{j=2,\ldots,K-1} F_j$. At each iteration, the selected subjects then form a new subpopulation, and the new current population is composed of the unselected subjects. The stopping criterion is to obtain a tree in the current subpopulation such that $\forall j, F_m^j = 1$.

In order to counteract the presence of noise in the data, the cophenetic correlation d [9] between each of the dendrograms obtained from the mean matrix of each identified subpopulation is then calculated. This allows to group subjects belonging to the same subpopulations based on cophenetic correlations above a fixed threshold t. The choice of t is left to the user: however it should be noted that: 1) the threshold t directly influences the creation of subpopulations and 2) it allows the reduction of noise in the tridimensional data, if noise is present. A high value of t (i.e. close to 1) will be recommended if similar populations in the three-dimensional data is suspected, close to 0.5 otherwise. To do this, we set up the following iterative procedure. Initially, we calculate the matrix of cophenetic correlations between the mean dendrograms of the subpopulations obtained at the end of the first step. Thereafter, we threshold this matrix according to t (i.e. correlations lower than t are set to 0). From this matrix, we construct the d-weighted graph G, where each node represents a subpopulation. Thanks to the Louvain method [10], an optimal partition number is obtained by maximizing the modularity of the G graph. Subsequently, the subpopulations are grouped together according to the Louvain partitioning, then a new cophenetic correlation matrix is computed from the mean dendrograms of these new subpopulations. Louvain partitioning procedure is then repeated until G has only one node.

This procedure (Algorithm 1) leads to iteratively extracting the most stable subjects from the *average* current $P_m^{current}$ dendrogram. It should be noted that by construction, $P_m^{current}$ will vary in terms of the arrangement and composition of its scores.

Finally, this procedure is able to identify the existence of a subpopulation of subjects with a pattern that differs constantly within it, or identify the existence of a subpopulation that does not have a strong structure in terms of dendrogram.

Algorithm 1: Identification of subpopulations

Input: $F_m^j, individuals, P_m^j$
while $\forall j, F_m^j = 1$ **do**
  $group_i \leftarrow individuals \in P_m^{j^*}, j^* = \arg\min_{j=2,...,K-1} F^j$;
  $curentPopulation \leftarrow individuals \notin group_t$;
  $(F_m^j, P_m^j, Dend_i) \leftarrow frequency\_extraction(curentPopulation)$;
end
while $|graphFromMatriceD| == 1$ **do**
  $matriceD \leftarrow cophenetic(Dend_i)$;
  $matriceD < t \leftarrow 0$;
  $modules \leftarrow Louvain(graphFromMatriceD)$;
  $subPopulation \leftarrow individuals \in modules$;
end
Output: *subPopulation*

where *frequency_extraction* is the implemented algorithm described in Sect. 2 in order to extract the individual frequencies of the average dendrogram partitions, *cophenetic* is the function that computes the matrix of cophenetic correlations between all the dendrograms two by two of a list of dendrograms, *Louvain* is the implemented Louvain algorithm for identifying modules from a weighted graph G (here each node of the graph is a dendrogram composed of s individuals), and *dendrograms* is the function computing the dendrogram from M_m.

3 Study of numerical behavior

The numerical behaviour of the two proposed methodologies is illustrated on simulated *fMRI-type* data.

- In the first simulation study, we consider a population of S subjects whose correlation matrices $M_s, s = 1, ..., S$ are *close* (in terms of *mean* dendrogram), except for a network R^{k^*} which is randomly permuted for each subject. The objective here is to detect this unstable network which makes the *mean* dendrogram P_m not very representative of the population of S subjects.
- In the second simulation study, the population of S subjects is composed of two subpopulations of homogeneous subjects (in terms of the *average* dendrogram). The objective here is to identify these two subpopulations.

Data generation. In order to create subjects *close to each other* in the population (or subpopulation), we introduce a correlation matrix M that we will *noise* with a Gaussian random error ε centered with a standard deviation σ as follows: for $1 \leq i < l \leq K$,

$$M_{(i,l)} = \tanh(\text{arctanh}(M_{(i,l)}) + e_{i,l}) \quad \text{et} \quad M_{(l,i)} = M_{(i,l)} \tag{7}$$

where $M_{(i,l)}$ denotes the element (i, j) of the matrix M and $e_{(i,l)}$ is a realization of the noise ε. Different noise levels σ were considered in the simulation study. Naturally, the higher the noise level, the less homogeneous the population (or subpopulation) generated. To make the simulation study interesting, we consider σ values such that the *mean* dendrogram is similar to the un-noised *mean* dendrogram.

Thereafter, we will work with data similar to those presented in the introduction (i.e. correlation matrices consisting of $K = 28$ resting-state networks R_k).

3.1 Simulation 1: identification of the unstable network

In this first simulation, we will generate for a noise level of $0 \leq \sigma \leq 1$ with a step of 0.1, with K groups of $S = 500$ subjects from one of the individual M matrices presented in the introduction. For each noise level and each network, we have randomly permuted[2] a network R_k, i.e: for a given noise level σ, we have $K = 28$ groups of $S = 500$ subjects. The objective is to detect, for each noise level and for each permutation, the targeted network R_k (i.e. the permuted network) as the unstable network using the proposed methodology.

Using the methodology proposed for a noise level $\sigma = 0$, we can see in Fig. 2 that we manage in 89.3% of the cases to detect the permuted network as the one with the highest Q score. Looking more closely, we can see on the average dendrogram of the group before permutation (Fig. 3), that for the permutations of the networks R_k (`RN11`, `RN23` and `RN29`), the network R^{k*} is detected each time the one which is directly linked to R_k (`RN22`, `RN14` and `RN7` respectively) instead of R_k itself.

Taking the `RN38` network as an example, when we look at the power of the method across all the different noise levels σ (Fig. 4), we can see that we are able to detect the correct permuted network (i.e. R_{k^*} = `RN38`) regardless of the noise level applied to the population of 500 subjects whose network has been permuted. In this example, although RN38 (in green in Fig. 4) is always the network with the highest Q score, the network `RN6` (in yellow in Fig. 4) is very close behind. By removing the `RN38` network from the whole population, we can see that the new mean dendrogram is much more stable with only a few alternative *non-dominant* patterns (due to the different noise level); leading to a much higher individual frequency of the mean P_m^k patterns, which is a very low standard deviation of the Q_k score without a k^* ever actually being detected.

Globally, for 11 different noise levels from 0 to 1 (step of 0.1), out of the 28 possible permutations, we detect the correct $k*$ (i.e. the permuted network R_k) 95.1% of the time. The 4.9% error corresponds each time to the identification of the network directly linked to the network R_k initially swapped for the simulation.

[2] i.e. switch the values of the corresponding row/column in the correlation matrix

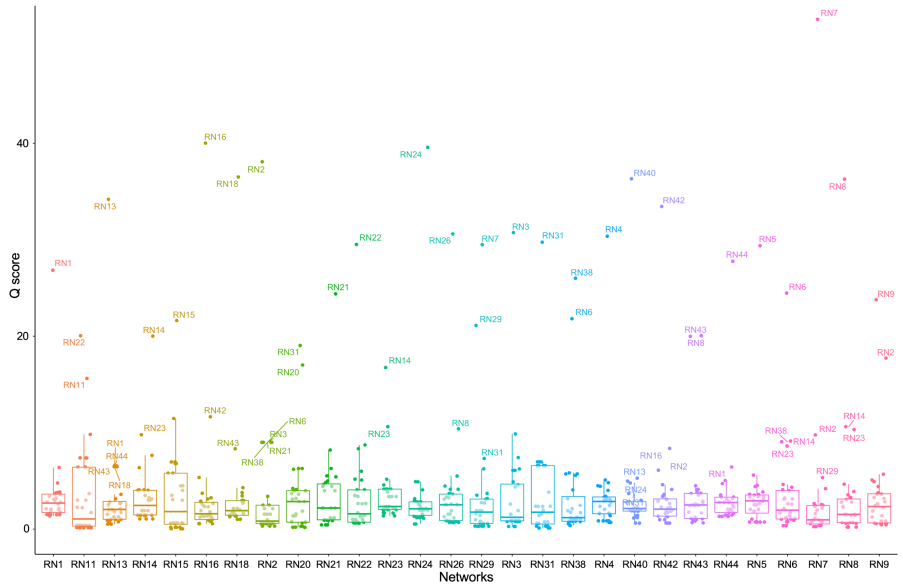

Fig. 2 Boxplot of the Q_k score at $\sigma = 0$ for each permutation of K.

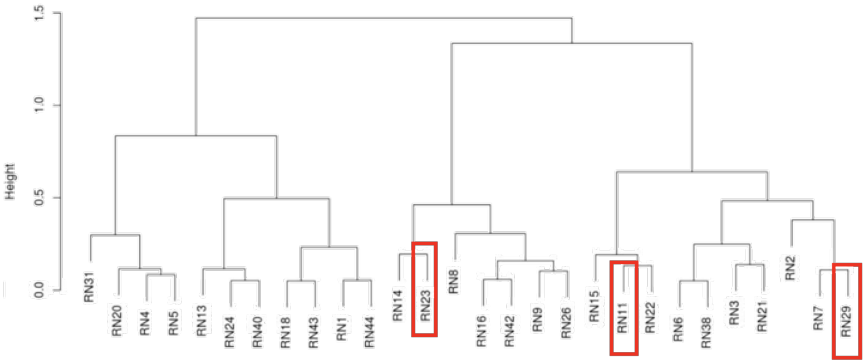

Fig. 3 *Average* dendrogram (constructed from M_m) of the population of $S = 500$ subjects before the permutation of any network R_k. In the red box, permuted R_k networks not detected as $k*$ at noise level $\sigma = 0$.

Our methodology allows us to detect the permuted R_{k*} network leading to the instability of the mean dendrogram and those regardless of the noise level injected in the data. Note that when σ increases, (there is no more information / common structure in the data), all Q_k scores will converge to $1/k$, i.e. each network participates in many alternative patterns or none of the networks participate in alternative patterns.

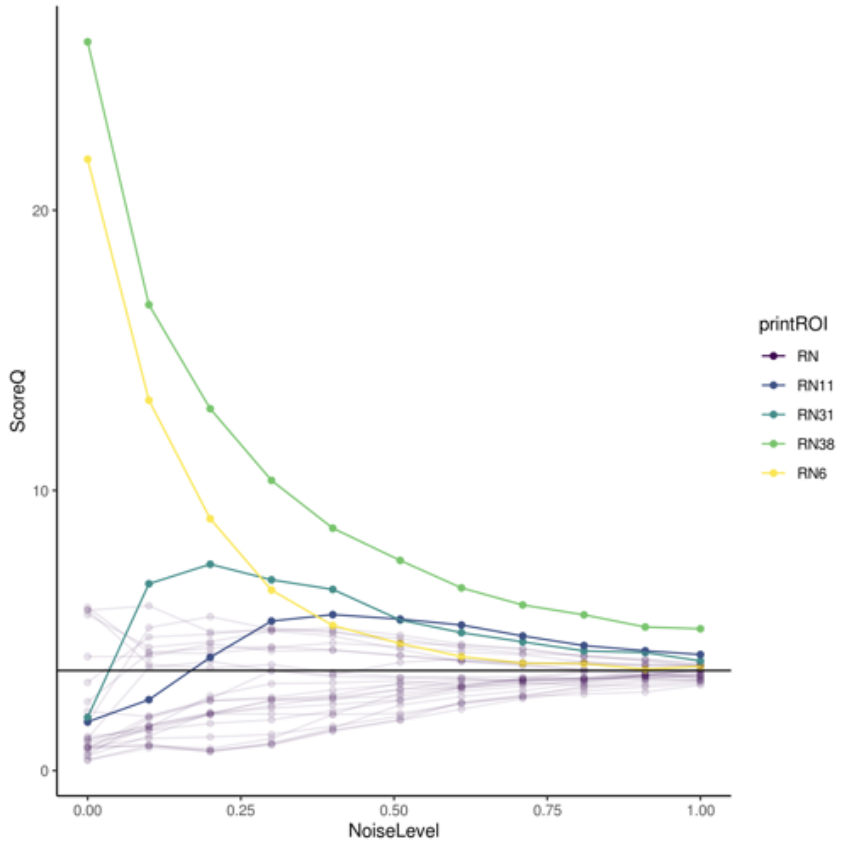

Fig. 4 Example of the evolution of the Q_k score of the permuted network R_k = `RN38` as a function of the noise level σ in a population of $S = 500$ subjects. The colored curves correspond to the 4 R_k being most often detected as R_{k^*}. In green the target network `RN38`, in yellow the network `RN6` directly linked to `RN38` in the initial dendrogram (see Fig. 3)

3.2 Simulation 2: identification of homogeneous subpopulations

3.2.1 Detection of equidistributed population

In this part, we will consider two populations (G_{50}^1 and G_{50}^2) of $S = 500$ subjects. In each population, the subjects are equally divided into two subpopulations A and B of 250 subjects each. For G_{50}^1, the proximity between the mean dendrogram of A and B is measured by the cophenetic correlation is 0.18 (i.e. subpopulation A is very distant from subpopulation B in terms of the brain organization of their resting-state networks R_k). For G_{50}^2, the cophenetic correlation between A and B is 0.95, which means they are two subpopulations whose brain organization is very close to each other.

Table 1 Evolution of the detection of subpopulations A and B according to the evolution of the noise level σ in Group 1 ($G1$) and 2 ($G2$). Equidistributed population: Group G^1_{50}, cophenetic correlation between A and B of 0.18, 50% of subjects of each subpopulation A and B. Group G^2_{50}, cophenetic correlation between A and B of 0.95, 50% of subjects of each subpopulation A and B. Not equidistributed population: Group G^1_{75}, cophenetic correlation between A and B of 0.18, 75% of subjects of the subpopulation A and 25% of B. Group G^2_{75}, cophenetic correlation between A and B of 0.95, 75% of subjects of the subpopulation A and 25% of B.

Equitably distributed population (50% A & 50% B)								
	Subpopulation A				Subpopulation B			
	$\sigma = 0$	$\sigma = 0.12$	$\sigma = 0.25$	$\sigma = 0.50$	$\sigma = 0$	$\sigma = 0.12$	$\sigma = 0.25$	$\sigma = 0.50$
Group 1	50	44	28	11	50	36	12	0
Group 2	50	24	1	0	50	17	8	11
Not equitably distributed population (75% A & 25% B)								
	Subpopulation A				Subpopulation B			
	$\sigma = 0$	$\sigma = 0.12$	$\sigma = 0.25$	$\sigma = 0.50$	$\sigma = 0$	$\sigma = 0.12$	$\sigma = 0.25$	$\sigma = 0.50$
Group 1	75	65	64	0	25	11	0	0
Group 2	75	58	33	10	25	0	21	0

Finally, for G^1_{50} and G^2_{50}, we will consider different cases with a noise level σ ranging from 0 to 0.5.

These two case studies, represented by G^1_{50} and G^2_{50}, will allow us to evaluate the subpopulation detection power of our algorithm in addition to the presence of noise. Concerning the grouping threshold for the part of the method using the Louvain method; $t = 0.8$ for G^1_{50} and $t = 0.99$ for G^2_{50}. Note that the threshold is more restrictive for G^2_{50} since A and B are more similar in this population.

The results for the G^1_{50} study are provided in Tab. 1. For a null noise level, the algorithm perfectly identifies individuals as belonging to subpopulation A or B. For a noise level $\sigma = 0.12$, the algorithm is able to identify 44% of the individuals belonging to subpopulation A and 36% belonging to population B. For a noise level $\sigma = 0.25$, the algorithm finds more than 50% of the individuals belonging to subpopulation A (28% of individuals identified belonging to this subpopulation), but less than 25% of the individuals belonging to subpopulation B. At the maximum noise level $\sigma = 0.50$, the algorithm finds 11% of individuals from subpopulation A and none from subpopulation B.

The results for the G^2_{50} study are shown in Tab. 1. In contrast to G^1, the mean dendrograms of subpopulations A and B are here similarly closer to each other according to their cophenetic distance (equal to 0.95 for G^2, 0.18 for G^1). This has a direct impact on the algorithm's ability to identify individuals as belonging to subpopulation A or B. Concerning subpopulation A, the algorithm identifies correctly the individuals for a zero noise level, but the identification drops to 24, 1 and 0% as it increases, which is worse than for G^1. There were the same results for the identification of subpopulation B, with results half as good as for G^1.

For a noise level σ multiplied by 2, the proportion of individuals identified as belonging to subpopulation A or B tends to be divided by 2. Moreover, in view of the results, subpopulation B of G^1_{50} seems less stable on average than subpopulation A; the opposite is true for G^2_{50}.

3.2.2 Detection of not equidistributed population

In this part we will consider two populations (G^{1bis} and G^{2bis}) of $S = 500$ subjects. In each of the populations the subjects are equally divided into two subpopulations A and B; of 375 subjects for A and 125 for B. For G^1, the proximity between the mean dendrogram of A and B is the same as in the previous part, as the grouping threshold for the part of the method using the Louvain method.

Finally, for G^{1bis} and G^{2bis}, we simulated different cases with a noise level σ ranging from 0 to 0.5.

The simulation results are available in Tab. 1. Concerning subpopulation A for G^{1bis} and G^{2bis}, the algorithm identifies more than 85% of its individuals up to a noise level $\sigma = 0.25$. As for the equitably distributed subpopulations, the algorithm manages to identify 100% of the individuals belonging to the different subpopulations when the noise level is zero, and 0% when $\sigma = 0.50$ (there is an exception for G^{2bis} where 10% of the individuals of subpopulation A are correctly identified).

Again, we can note that the more noise increases one group disappears, either the A group or the B group. The more the number of subjects belonging neither to A nor to B increases up to a rate of 100%.

We alos note from Tab. 1 that: first the subjects detected as belonging to group A or B are initially subjects belonging to these groups (very low noise error rate). Secondly, it is interesting to note that the category of subjects neither belonging to group A or B is composed of similar proportions to the one we initially injected during the creation of the simulation.

4 A real case study

An example of the application of the method may be found in [11]. There is currently no brain atlas of the intrinsic organization of the brain constructed from populations whose individuals are over 40 years of age. However, the brain, and thus the brain networks that compose it, undergo continuous reconfiguration throughout adult life ([12], [13]). The absence of brain atlases from older populations therefore directly influences the results related to the different properties of intrinsic networks. In this context, the objective of the study was to construct a reliable brain atlas derived only from healthy older participants. Doucet et al. [11] analyzed resting-state fMRI data from 184 individuals aged 55-80 years from the `SALD` cohort (Southwest University Lifespan Dataset, [14]). Using a multi-step independent component analysis approach they identified 24 Resting-state Networks (`RNs`, Fig. 5 - A.).

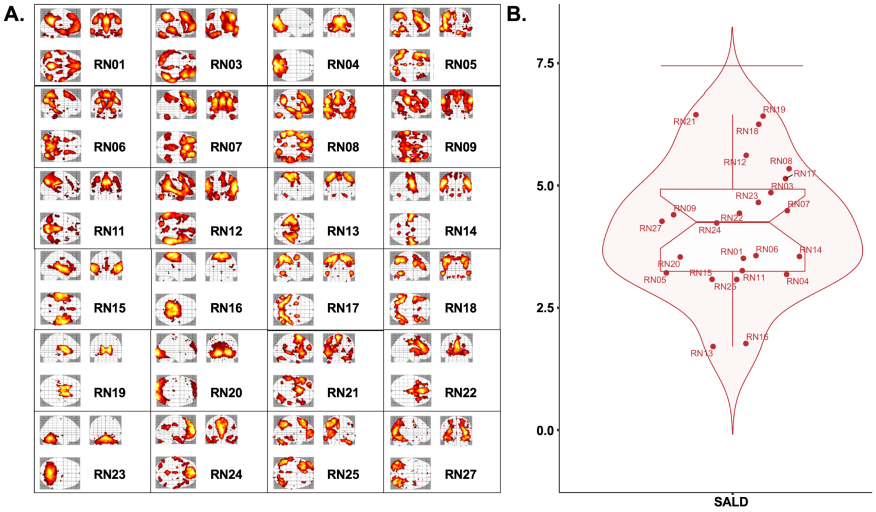

Fig. 5 Presentation of the Resting-state Networks (`RNs`) of the `SALD` cohort and their stability. **A.** Spatial map of the `RNs` obtained from the multi-step independent component analysis on the intrinsic connectivity data of the `SALD` cohort. **B.** Tukey box of the stability Q_k score for each network in the `SALD` cohort. The horizontal red line represents the limit at which a `RN` is considered unstable (extremum).

In this framework, our method was used to verify: 1) the stability of the identified intrinsic networks (`RNs`) and 2) the presence of subpopulations in the data (the cophenetic threshold was fixed at 0.85).

We found that no `RNs` in the `SALD` sample of individuals aged 55 or older were unstable (Fig. 5 - B.).

In addition, two subpopulations were identified in the `SALD` cohort Fig. 6. The first one (Subpopulation 1 in Fig. 6) is composed of 85 individuals and has a mean age of 62.5 years old. The second one (Subpopulation 2 in Fig. 6) is composed of 94 individuals and has a mean average age of 64.5 years old. A two-tailed Student's t-test revealed no difference between the 2 subpopulations in terms of demographics variables (Edinburgh test: $p = 0.8$, sexe: $p = 0.15$, Pearson's chi-squared test), neither in anatomical variables (Total Intracranial Volume: $p = 0.81$) or in quality control variable (all $p > 0.2$). A one-tailed t-test revealed a significant inferior average age in the first subpopulation than in second one ($p = 0.032$).

A comparison of the average dendrograms of the two subpopulations highlights the existence of 2 partitions in each subpopulation. The first one includes `RNs` related to the extrinsic system (blue rectangles in Fig. 6): which is a system driven by external inputs and activated during sensory stimulations, including the attentional and the sensory-motor network. The second partition corresponds to the intrinsic system (Red rectangle in Fig. 6) that is used in inner-oriented mental activity.

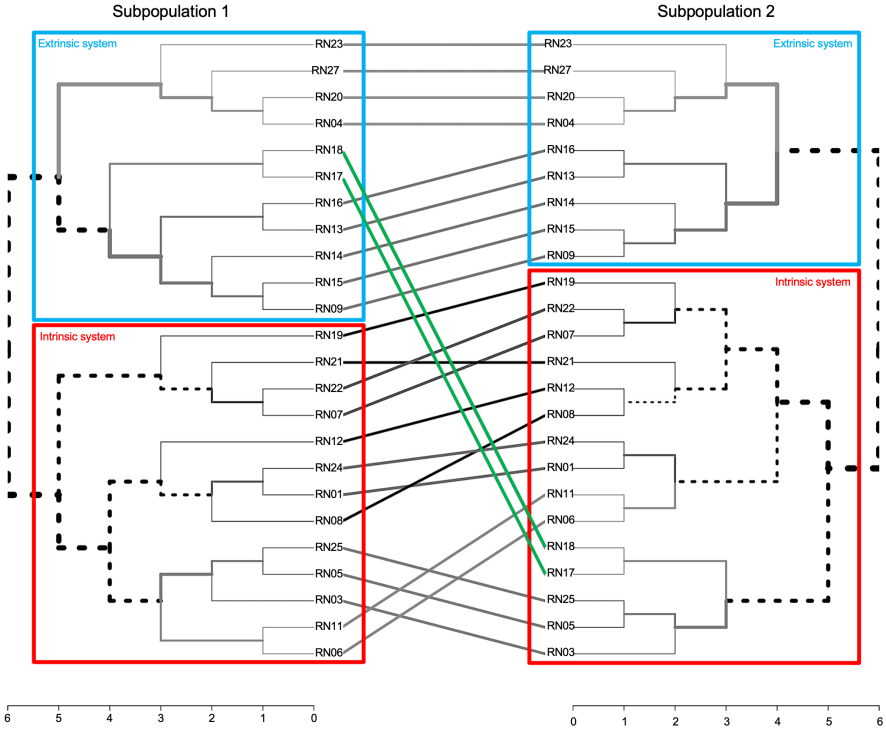

Fig. 6 Tanglegram between subpopulations in the `SALD` cohort. The red rectangle represents the intrinsic system; in blue the extrinsic system. The green lines correspond to the two `RNs` whose positioning in the mean dendrogram differs from one subpopulation to another.

This organization of resting-state brain processes corresponds well to the organization highlighted in [6]. The calculation of the cophenetic distance between the two means dendrograms of the two subpopulations was 0.76, revealing two slightly different organizations. The main difference between the two subpopulations (Fig. 6 comes from the networks `RN18` and `RN17`, which in the case of subpopulation 1, belongs to the extrinsic system whereas these `RNs` belong to the intrinsic system in the second. The `RN18` corresponds to one of the fronto-temporo-parietal network involved during the executive processes of selecting and monitoring our behaviours. The `RN17` corresponds to the spatial attention network. These two `RNs` are grouped together very early in the two dendrograms, thus we can tentatively identify this couple as being a marker of the resting state activity either turned towards the outside, or towards oneself.

This organizational difference, possibly related to age, compared to young subjects [6], deserves to be addressed more in-depth study with complementary neuroscientific approach, such as the resting state questionnaire for evaluation of inner experience during the conscious resting state [15].

5 Concluding remarks

In this study, we introduced two statistical approches allowing: 1) to analyze the stability of the constituent features of an average dendrogram produced from three-dimensional data, which is the Q_k score, and 2) to extract homogeneous subpopulations in terms of individual dendrograms from three-dimensional data.

The first one is based on the new reliability Q_k score introduced in Section 2. This core represents the relative position of the network k across the individual dendrograms, relative to the average dendrogram. The simulation study provided good numerical performance of the proposed methodology.

Furthermore, the second proposed approach is able to identify the existence of a subpopulation of subjects with a pattern of features that differs constantly within it, or the existence of a subpopulation that does not have a strong structure in terms of dendrogram.

Concerning the capacities of the algorithm to identify subpopulations, the similarity between subpopulations, the proportion of each subpopulation directly influences the performance of the algorithm. A subpopulation which is small in number of individuals and whose mean dendrogram is not singular: i.e. whose cophenetic distance is high in relation to the mean dendrogram of the other subpopulations, will be difficult to identify. In contrast, a large subpopulation with a singular dendrogram will be easy to identify. The modulation of the threshold value t comes into play here, a t value close to 1 allowing a better distinction between two similar dendrograms according to the cophenetic distance.

These two new methods will soon be available via a library called `SIMS` (*Similarity of Individual MatriceS*) on `GitHub`, on `CRAN`, and it can also be directly requested from the first author.

Funding

Gaelle E. Doucet was supported by the National Institute of Aging (R03AG064001) and the National Institute of General Medical Sciences (P20GM130447).

Conflict of interest

The authors declare that they have no conflict of interest.

References

1. Efron, B., Bootstrap confidence intervals for a class of parametric problems, Biometrika, 72(1), 45-58 (1985).
2. Suzuki, R., Shimodaira, H., Pvclust: an R package for assessing the uncertainty in hierarchical clustering, Bioinformatics, 22(12), 1540-1542 (2006).

3. Logothetis, N. K., Pauls, J., Augath, M., Trinath, T., Oeltermann, A., Neurophysiological investigation of the basis of the fMRI signal, Nature, 412(6843), 150-157 (2001).
4. Schummers, J., Yu, H., Sur, M., Tuned responses of astrocytes and their influence on hemodynamic signals in the visual cortex, Science, 320(5883), 1638-1643 (2008).
5. Mazoyer, B., Mellet, E., Perchey, G., Zago, L., Crivello, F., Jobard, G., Delcroix, N., Leroux, G., Petit, L., Joliot, M., Tzourio-Mazoyer, N., BIL&GIN: A neuroimaging, cognitive, behavioral, and genetic database for the study of human brain lateralization, Neuroimage, 124, 1225-1231 (2016).
6. Doucet, G., Naveau, M., Petit, L., Delcroix, N., Zago, L., Crivello, F., Jobard, G., Tzourio-Mazoyer, N., Mazoyer, B., Mellet, E., Joliot, M., Brain activity at rest: a multiscale hierarchical functional organization. Journal of Neurophysiology, 105(6), 2753-2763 (2011).
7. Suzuki, R., Shimodaira, H., An application of multiscale bootstrap resampling to hierarchical clustering of microarray data: How accurate are these clusters. The Fifteenth International Conference on Genome Informatics, 34 (2004).
8. Charrad, M., Ghazzali, N., Boiteau, V., Niknafs, A., NbClust: An R Package for determining the relevant number of clusters in a data set, Journal of Statistical Software, 61(6), 1-36 (2014).
9. Sokal, R. R., Rohlf, F. J., The comparison of dendrograms by objective methods, Taxon, 11(2), 33-40 (1962).
10. Blondel, V. D., Guillaume, J. L., Lambiotte, R., Lefebvre, E., Fast unfolding of communities in large networks. Journal of statistical mechanics: theory and experiment, 2008(10), P10008 (2008).
11. Doucet, G. E., Labache, L., Thompson, P. M., Joliot, M., Frangou, S., Atlas55+: brain functional atlas of resting-state networks for late adulthood, BioRxiv 2020.07.13.200824 (2020); doi: https://doi.org/10.1101/2020.07.13.200824.
12. Damoiseaux, J. S., Effects of aging on functional and structural brain connectivity. Neuroimage, 160, 32-40 (2017).
13. Yaple, Z.A., Stevens, W.D., Arsalidou, M., Meta-analyses of the n-back working memory task: fMRI evidence of age-related changes in prefrontal cortex involvement across the adult lifespan, Neuroimage, 196, 16-31 (2019).
14. Wei, D., Zhuang, K., Ai, L., Chen, Q., Yang, W., Liu, W., Wang, K., Sun, J., Qiu, J., Structural and functional brain scans from the cross-sectional Southwest University adult lifespan dataset, Scientific data, 5, 180134 (2018).
15. Delamillieure, P., Doucet, G., Mazoyer, B., Turbelin, M. R., Delcroix, N., Mellet, E., Zago, L., Crivello, F., Petit, L., Tzourio-Mazoyer, N., Joliot, M., The resting state questionnaire: An introspective questionnaire for evaluation of inner experience during the conscious resting state. Brain research bulletin, 81(6), 565-573 (2010).

2. Librairie R de SIMS

La librairie *SIMS* (*Similarity of Individual MatriceS*) implémente la méthodologie présentée au chapitre précédent permettant d'étudier la stabilité de données tridimensionnelles via la détection de variables instables et/ou de sous-populations dans l'échantillon. *SIMS* est développé sous R (version 3.6.3, [RCT20]). Je présente ici les principales fonctions permettant de détecter une variable instable dans un jeu de données, ainsi que celles permettant de détecter la présence de sous-populations dans l'échantillon de départ.

Dans ce cadre, j'utiliserai le jeu de données tridimensionnelles que nous avons utilisé comme exemple dans la dernière partie du chapitre précédent : *i.e.* les 184 individus, âgés de 55 à 80 ans, de la cohorte SALD (*Southwest University Lifespan Dataset*, [WEI17]). Doucet & al. ont mis en avant la présence de 24 RNs[75] (*Resting-state Network*) dans cette cohorte [DOU20]. Chaque individu est alors défini par sa matrice de connectivité intrinsèque. Une matrice représente les corrélations paire par paire des 24 RNs.

La fonction `weighingVariable` implémente l'algorithme qui permet de calculer la stabilité de chaque variable d'intérêt, à travers les dendrogrammes individuels : ici les RNs. Les dendrogrammes individuels sont construits en utilisant la méthode de Ward à partir de la matrice des distances $D_{i,j} = (1 - M_{i,j})/2$, ($i,j = 1, 2, ..., n$ avec $n = 24$). Toutes les partitions individuelles sont comparées entre les individus à l'aide de l'indice de Sorensen-Dice. L'unique argument de la fonction est le tableau tridimensionnel `T` de taille $184 * 24 * 24$ contenant l'ensemble des données. La fonction renvoie une variable contenant le score `Q` attribué à chaque RN, ainsi qu'un graphique (boîte de Tukey) permettant de déterminer visuellement la présence d'extrema parmi les variables (Figure 29).

[75] Les RNs sont numérotés "RNX", X étant le numéro attribué au réseau.

```
dim(Q) ; summary(T)
[1] 184  24  24
    Min.  1st Qu.   Median     Mean  3rd Qu.     Max.
-0.78304 -0.07808  0.13945  0.17595  0.39509  1.00000
Q <- weighingVariable(T)
plot(Q) # affiche la boîte de Tukey
```

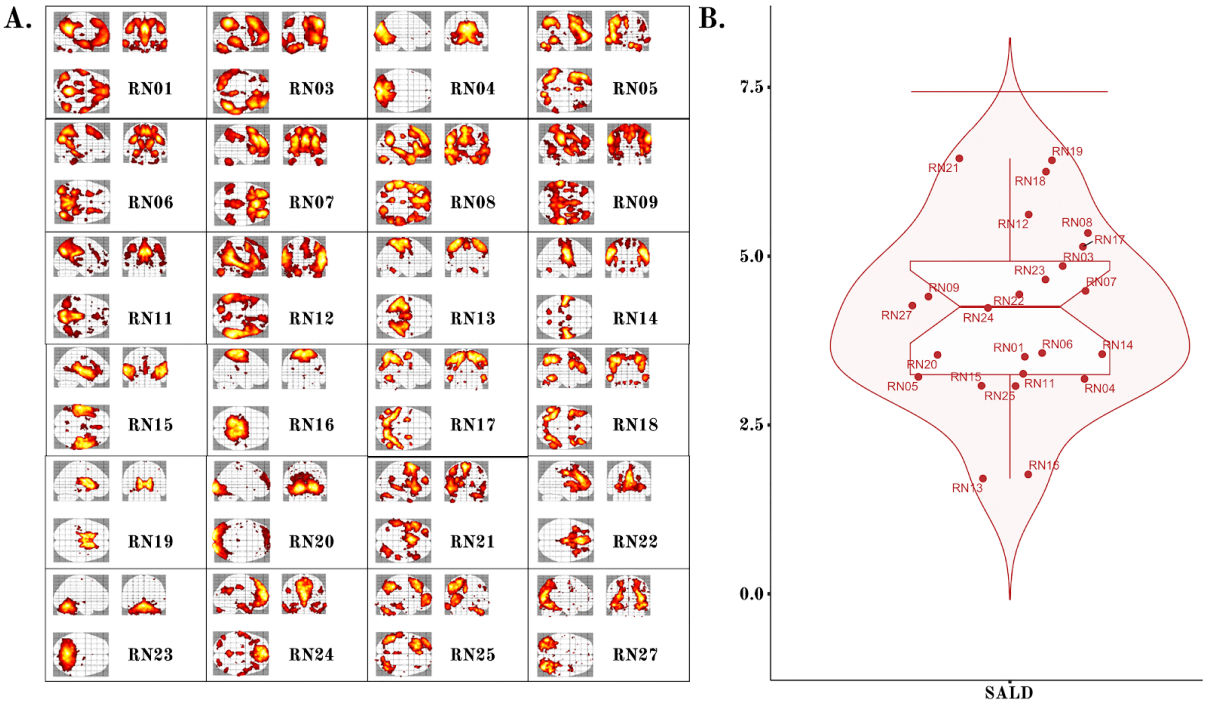

Figure 29 : Présentation des réseaux intrinsèques de la cohorte SALD et de leur stabilité. **A.** *Carte spatiale des composantes obtenues à partir de l'algorithme de [NAV12] sur les données de connectivité intrinsèque de la cohorte SALD. Figure adaptée de [DOU20].* **B.** *Boîte de Tukey du score Q de stabilité pour chaque réseau de la cohorte SALD. La ligne rouge horizontale représente la limite à partir de laquelle un réseau est considéré comme instable (extremum). Graphique réalisé à l'aide de la librairie R ggplot2 [WIC16].*

La fonction `subPopulation` implémente la méthode permettant d'identifier la présence ou non de sous-populations dans la population d'origine, à savoir ici parmi les 184 individus de la cohorte SALD. Les arguments de la fonction sont ici :

- le tableau tridimensionnel `T` de taille $184 * 24 * 24$ contenant l'ensemble des données,
- le seuil de la distance cophénétique `coph` au-dessus duquel les groupes d'individus identifiés sont regroupés, car jugés trop similaires par l'utilisateur, afin d'obtenir les sous-populations finales.

La fonction `subPopulation` retourne une liste `P` contenant K éléments, K étant égal au nombre de sous-populations identifiées, chaque élément de `P` contient :

- un vecteur `v` de la liste des individus formant la sous-population,
- leur dendrogramme moyen `d`,
- un vecteur contenant le score `Q` de la stabilité de chaque variable pour cette sous-population,
- une matrice `c` contenant les distances cophénétiques entre chaque dendrogramme des K sous-populations.

La fonction permet également de visualiser la différence d'organisation des dendrogrammes de chaque sous-population à l'aide d'un *tanglegram* (Figure 30).

```
P <- subPopulation(T, coph = 0.85)
length(P)
[1] 2
head(P[[1]]$v, 3) ; length(P[[1]]$v)
[1] "t0123" "t0012" "t0034"
[1] 71
head(P[[1]]$Q, 3)
[1] 1.5 2.7 3.9
P[[1]]$c
[1] 0.76
plot(P) # affiche le tanglegram entre chaque élément n de P
```

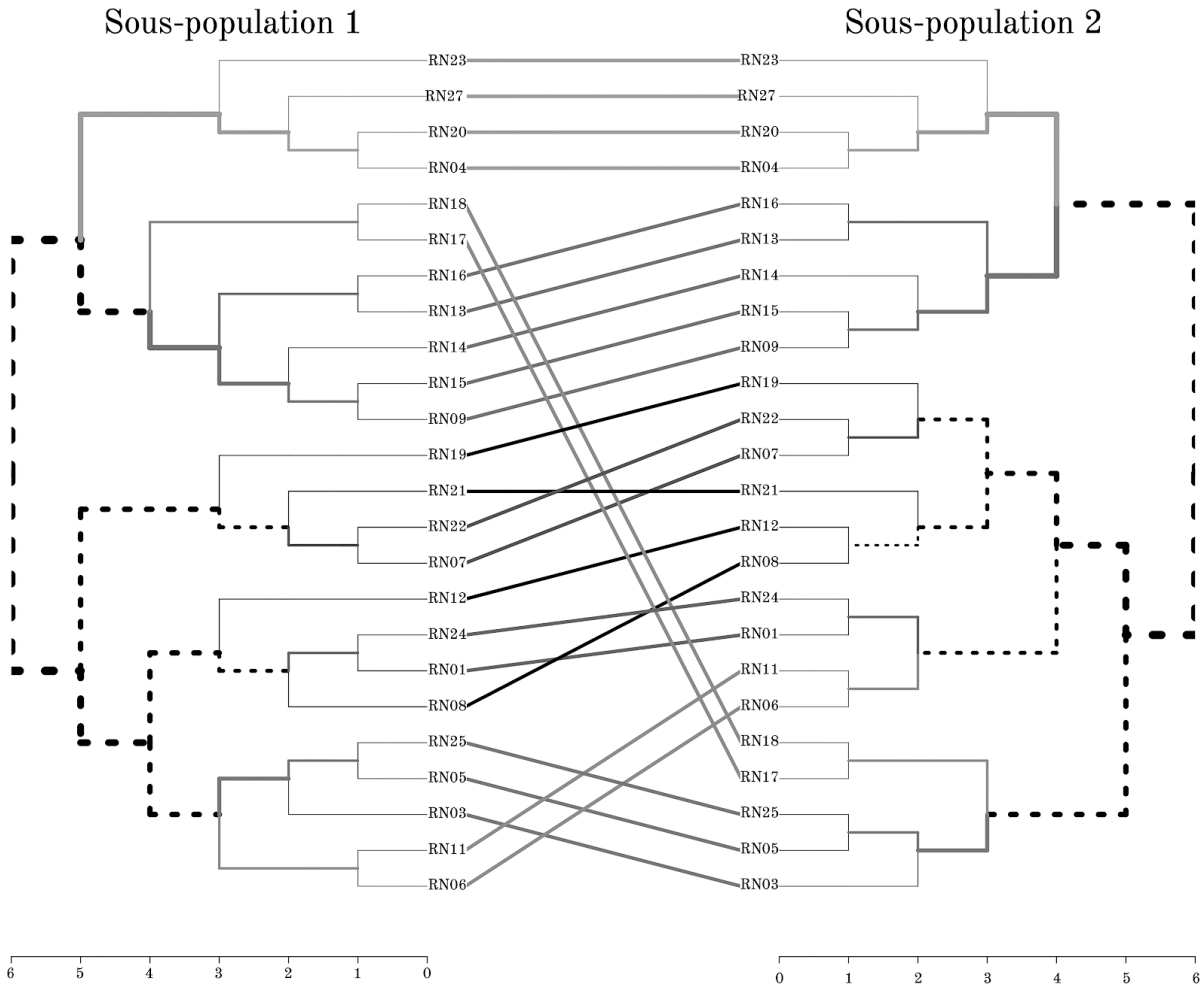

Figure 30 : *Tanglegram* entre les sous-populations présentes dans la cohorte SALD.

Partie IV

Conclusion et perspectives

J'ai développé au cours de cette thèse plusieurs méthodes statistiques fructueuses permettant dans un premier temps d'élaborer des atlas des réseaux cérébraux sous-tendant les fonctions cognitives latéralisées, puis dans un second temps, d'évaluer et caractériser la variabilité inter-individuelle.

La méthodologie combinant l'analyse par conjonction, la classification ascendante hiérarchique et la théorie des graphes a conduit à la publication de deux articles concernant les bases anatomo-fonctionnelles des réseaux supportant le traitement de la phrase : l'atlas SENSAAS, et du mot : l'atlas WMCA. Le travail réalisé concernant l'étude de la variabilité interindividuelle a conduit au développement d'une nouvelle méthodologie d'évaluation de la variabilité interindividuelle basée sur la classification hiérarchique : la méthode SIMS.

Dans la continuité du travail commencé, j'ai utilisé SENSAAS afin d'étudier l'atypicalité de la latéralisation du langage via une classification hiérarchique multitâche et multimodale. Je présenterai par la suite un bref résumé d'une sélection de travaux réalisés par d'autres équipes de recherche qui ont utilisé SENSAAS dans leurs études. De plus, j'ai élaboré deux atlas supplémentaires concernant le support anatomique du contrôle sensorimoteur de la main, ainsi que du support anatomo-fonctionnel de l'attention visuo-spatiale. SIMS a également permis d'évaluer la stabilité des réseaux intrinsèques identifiés au cours du développement d'un nouvel atlas cérébral global adapté aux individus de plus de 55 ans, ainsi que d'évaluer l'homogénéité des 3 cohortes utilisées pour son élaboration.

Ces travaux sont présentés dans les chapitres qui suivent et sont suivis d'idées prospectives concernant les suites possibles à donner aux recherches développées au cours de cette thèse.

1. Applications de l'atlas SENSAAS

1.1. Etude de l'organisation typique et atypique de l'organisation cérébrale du langage

J'ai utilisé l'atlas des aires supramodales de la phrase (SENSAAS, [LAB19]) afin d'étudier la variabilité interindividuelle de la latéralisation hémisphérique du langage ([LAB20], Partie I - chapitre 3.2.3.). Ce travail identifie trois groupes

d'individus caractérisés par différentes organisations inter- et intra-hémisphériques du réseau du langage : deux groupes de sujets typiques et un groupe de sujets atypiques. Il nous a également permis de caractériser dans ces 3 groupes la variabilité de l'intégration de l'information au repos dans les régions de SENSAAS, d'analyser l'occurrence des dissociations de latéralisation au cours des différentes modalités langagières et de montrer des différences d'organisation anatomique et de compétences cognitives. En conclusion, l'organisation cérébrale atypique du langage, révélée par une asymétrie droite induite par les tâches langagières, est soutenue au repos par des réseaux homotopiques connectés bilatéralement pour le langage (Figure 31) et par une forte connectivité intrinsèque grâce à un large corps calleux. L'article correspondant est disponible en Annexes : 2.

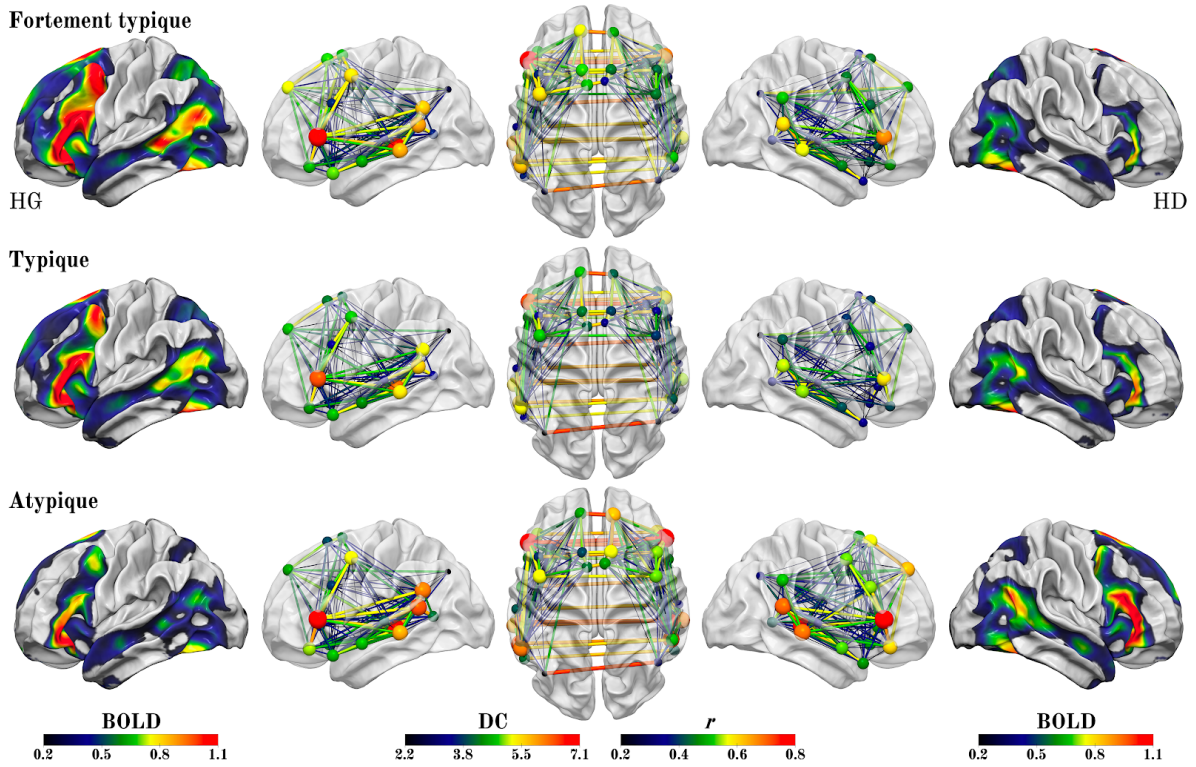

Figure 31 : Figure de synthèse illustrant les différentes organisations du langage intra- et inter-hémisphériques observées dans les 3 groupes identifiés dans [LAB20]. *La colonne de gauche montre la carte d'activation moyenne de l'hémisphère gauche des groupes lors de la tâche de production de phrase (l'amplitude d'activation du signal BOLD est donnée par l'échelle de couleurs) et la colonne de droite la carte d'activation moyenne de l'hémisphère droit superposée au gabarit de la BIL&GIN dans l'espace MNI réalisée à l'aide du logiciel Surf Ice. Les deuxième, troisième et quatrième colonnes montrent les vues latérales gauche, supérieure et droite du réseau de connectivité intrinsèque du langage, chaque région du réseau étant représentée par une sphère située au centre de masse de ses coordonnées MNI. Pour chaque région, une sphère colorée indique la centralité de degré (DC) moyenne du groupe (la valeur de DC est donnée par l'échelle de couleurs, et la taille de la sphère est proportionnelle à la valeur). Les lignes colorées indiquent la valeur du coefficient de corrélation de Pearson r entre deux régions (la valeur est indexée par l'échelle de couleurs, et l'épaisseur de la ligne est proportionnelle à la valeur).*

1.2. Applications de SENSAAS par d'autres équipes de recherche

SENSAAS a déjà utilisé dans le cadre de l'étude des bases génétiques de la dominance atypique de l'hémisphère droit pour le langage. Carrion-Castillo & al. ont notamment mis en évidence chez les individus atypiques une mutation des gènes impliqués dans le cytosquelette de l'actine[76] [CAR19]. Cette découverte offre pour la première fois un aperçu des influences génétiques moléculaires sur les mécanismes conduisant à la mise en place de la dominance hémisphérique pour les processus langagiers.

Un second exemple concerne l'étude du réseau du langage et de la mémoire chez des individus souffrant d'épilepsie du lobe temporal médian. Ici, Roger & al. ont montré une hyperconnectivité des aires limbiques avec le reste du réseau, alors que cette zone est atrophiée chez les patients. La réorganisation du réseau en termes de force de connectivité intrinsèque n'est pourtant pas associée avec de meilleurs performances cognitives [ROG20].

2. Elaboration de nouveaux atlas cérébraux

2.1. Mise au point d'atlas des régions de la préférence manuelle et de l'attention visuo-spatiale

2.1.1. HAMOTA : *Hand Atlas of MOTor Areas*

Comme présenté dans la Partie I - chapitre 3.1., nous avons identifié un ensemble de 13 hROIs sous-tendant le contrôle sensorimoteur de la main (Figure 24). Cet ensemble inclut des régions motrices primaires, prémotrices, somatosensorielles primaires et secondaires, le thalamus et le putamen dorsal, ainsi que le 4ème lobe cérébelleux. Une analyse descriptive des variations du signal BOLD au cours des tâches de RFTT et LFTT dans les 13 ROIs a mis en évidence[77], et ce dans les deux groupes, de fortes activations controlatérales et désactivations ipsilatérales dans les

[76] L'actine est une protéine jouant un rôle important dans l'architecture et les mouvements cellulaires.

[77] Ces observations sont évidemment inversées pour le cervelet.

aires motrices et somatosensorielles primaires, conduisant à de larges asymétries en faveur de la main préférée.

HAMOTA a non seulement permis d'identifier les aires recrutées pour le mouvement de la main, mais a également mis en évidence, pour la première fois et de manière originale, le support anatomo-fonctionnel de la préférence manuelle en expliquant 81% de sa distribution. En effet, l'examen des profils des différences controlatérales et ipsilatérales entre les mouvements de la main préférée et non préférée dans les 11 hROIs incluses dans le modèle révèle que de plus fortes activations controlatérales et des désactivations ipsilatérales des hROIs motrices sont liées au côté de la main utilisée, tandis que dans les autres hROIs, de plus fortes activations controlatérales et des désactivations ipsilatérales sont reliées à la latéralisation de la main (main préféremment utilisée).

2.1.2. ALANs : *Atlas of Lateralized Attention Networks*

Comme présenté dans la Partie I - chapitre 3.1., nous avons identifié un ensemble de 66 hROIs significativement activées et asymétriques droites durant la tâche de JBL dans un groupe de 130 individus droitiers (Figure 23, [ZAG20]). Nous avons dans un second temps caractérisé ces hROIs en fonction d'une tâche attentionnelle de bas niveau : SGV. Une analyse de la connectivité intrinsèque de l'ensemble de 66 hROIs, telle que réalisée dans [LAB19], nous a ainsi permis d'identifier 4 réseaux sous-tendant la dominance des fonctions attentionnelles spatiales. Il s'avère que les sous-ensembles obtenus à partir de l'analyse par conjonction des tâches de JBL et SGV se répartissent de manière graduelle au sein des 4 réseaux de connectivité intrinsèque. Ce résultat permet de mettre en évidence une spécialisation des réseaux du repos : 1- les 4 réseaux possèdent environ 25% de hROIs impliquées dans les 2 tâches attentionnelles, 2- un réseau occipital spécialisé dans les processus attentionnel de bas niveau (67% de hROIs également activées au cours de SGV), 3- un réseau pariéto-frontal spécialisé dans les processus attentionnels de haut niveau (80% des hROIs étant spécifiques à la tâche de JBL), 4- un réseau temporo-frontal et occipito-pariétal médian intermédiaire impliqué à part égale à la fois dans l'attention de bas et de haut niveau.

2.2. Application de SIMS à l'élaboration d'un atlas de la connectivité intrinsèque

La nouvelle méthode SIMS développée au cours de ma thèse permet de prendre en compte la variabilité inter-individuelle lors de la classification et de questionner l'existence de sous-populations au sein d'une population. Elle a été utilisée afin d'étudier la stabilité des réseaux de connectivité intrinsèque obtenus chez des individus âgés de plus de 55 ans, ainsi que la stabilité des données utilisées [DOU20]. Les 5 réseaux intrinsèques forment ainsi un atlas fonctionnel des réseaux du repos pour la fin de l'âge adulte. Doucet & al. ont ainsi montré que les réseaux intrinsèques chez les individus âgés diffèrent significativement de ceux identifiés chez le jeune adulte.

3. Perspectives de recherches

Une première piste de recherche directement inspirée des différents travaux présentés est l'élaboration d'un atlas intégrant l'ensemble des réseaux de la spécialisation hémisphérique : à partir des atlas SENSAAS, WMCA, HAMOTA et ALANs. Le DMN sera également intégré du fait de la mise en évidence récente de son rôle dans l'organisation atypique du langage [RAE18] et dans la centralisation de l'information provenant des réseaux attentionnels et langagiers ([FOX20] et [GOR20]).

Cet atlas multimodal et multi-échelle permettra de caractériser la topologie globale des fonctions étudiées sous l'influence de la spécialisation hémisphérique chez les individus typiques et d'étudier régionalement les patterns de dominance. La caractérisation topologique sera multimodale intégrant les caractéristiques fonctionnelles (IRMf), mais également anatomiques (épaisseur corticale, myélinisation du cortex, surfaces) et psycho-comportementales (performances cognitives).

D'un point de vue méthodologique, la construction d'un atlas intégré de la spécialisation hémisphérique permettra d'attribuer à chaque région un ou plusieurs rôles via l'utilisation des techniques de la théorie des réseaux multi-couches [BET17]. La théorie des réseaux multi-couches permet d'empiler les atlas individuels les uns au

dessus des autres en les reliant via leurs régions communes. Jusqu'ici l'étude topologique des réseaux fonctionnels a été réalisée de manière statique, l'utilisation d'une méthode dynamique telle que la théorie du contrôle [JU20] permettrait d'étudier la reconfiguration des réseaux au cours de différents états cognitifs [SAL20], mais également au cours de la réhabilitation pour les patients.

Un tel atlas permettra de caractériser, de manière longitudinale, les régions et les mécanismes supports du rétablissement des fonctions langagières et attentionnelles chez des patients ayant subi des lésions cérébrales sur la base de l'hypothèse du phénomène de *degeneracy*. Le phénomène de *degeneracy*, introduit en neurobiologie par le Pr. Gerald Edelman, est défini comme "la capacité d'élément structurellement différent permettant de remplir la même fonction ou de produire le même résultat" [EDE01]. Pour ce qui nous concerne, cela signifie qu'un processus cognitif particulier peut être sous-tendu par plus d'un ensemble de régions cérébrales [PRI02]. L'étude de patients ayant subi des lésions cérébrales permettrait alors d'identifier un ensemble de régions support de la récupération. Cet ensemble de région pourra être mis en parallèle avec l'ensemble des régions clés de la spécialisation hémisphérique et de la répartition inter-hémisphérique de la dominance pour différentes fonctions cognitives identifié chez les individus non pathologiques, afin d'établir une possible correspondance entre ces deux mécanismes [VIN19].

Concernant les perspectives de SIMS, le développement du cadre théorique supportant la méthode pourrait être envisagé, à l'image du cadre théorique supportant *pvclust* [SUZ06]. De plus, la méthode est applicable dès que des données tridimensionnelles se présenteront. L'utilisation de SIMS afin de mettre en relation les questionnaires du repos et l'interaction entre les réseaux intrinsèques est envisageable et offre des perspectives intéressantes sur la caractérisation de l'état mental des individus au cours de l'état de repos conscient.

Bibliographie

[ABD14] Abdollahi, R. O., Kolster, H., Glasser, M. F., Robinson, E. C., Coalson, T. S., Dierker, D., ... & Orban, G. A. (2014). Correspondences between retinotopic areas and myelin maps in human visual cortex. *Neuroimage*, *99*, 509-524.

[ALL14] Allen, E. A., Damaraju, E., Plis, S. M., Erhardt, E. B., Eichele, T., & Calhoun, V. D. (2014). Tracking whole-brain connectivity dynamics in the resting state. *Cerebral cortex*, *24*(3), 663-676.

[ALV19] Alves, P. N., Foulon, C., Karolis, V., Bzdok, D., Margulies, D. S., Volle, E., & de Schotten, M. T. (2019). An improved neuroanatomical model of the default-mode network reconciles previous neuroimaging and neuropathological findings. *Communications biology*, *2*(1), 1-14.

[AMU10] Amunts, K. (2010). Structural indices of asymmetry. *The two halves of the brain*, 145-176.

[AMU13] Amunts, K., Lepage, C., Borgeat, L., Mohlberg, H., Dickscheid, T., Rousseau, M. É., ... & Shah, N. J. (2013). BigBrain: an ultrahigh-resolution 3D human brain model. *Science*, *340*(6139), 1472-1475

[AND95] Andreasen, N. C., O'Leary, D. S., Cizadlo, T., Arndt, S., Rezai, K., Watkins, G. L., ... & Hichwa, R. D. (1995). Remembering the past: two facets of episodic memory explored with positron emission tomography. *American Journal of Psychiatry*, *152*(11), 1576-1585.

[AND10a] Andrews-Hanna, J. R., Reidler, J. S., Sepulcre, J., Poulin, R., & Buckner, R. L. (2010). Functional-anatomic fractionation of the brain's default network. *Neuron*, *65*(4), 550-562.

[AND10b] Andrews-Hanna, J. R., Reidler, J. S., Huang, C., & Buckner, R. L. (2010). Evidence for the default network's role in spontaneous cognition. *Journal of neurophysiology*, *104*(1), 322-335.

[AND12] Andrews-Hanna, J. R. (2012). The brain’s default network and its adaptive role in internal mentation. *The Neuroscientist*, *18*(3), 251-270.

[ARI96] Arieli, A., Sterkin, A., Grinvald, A., & Aertsen, A. D. (1996). Dynamics of ongoing activity: explanation of the large variability in evoked cortical responses. *Science, 273*(5283), 1868-1871.

[ARI17] Aria, M., & Cuccurullo, C. (2017). bibliometrix: An R-tool for comprehensive science mapping analysis. *Journal of Informetrics, 11*(4), 959-975.

[ASH99] Ashburner, J., & Friston, K. J. (1999). Nonlinear spatial normalization using basis functions. *Human brain mapping, 7*(4), 254-266.

[AUZ13] Auzias, G., Lefevre, J., Le Troter, A., Fischer, C., Perrot, M., Régis, J., & Coulon, O. (2013). Model-driven harmonic parameterization of the cortical surface: HIP-HOP. *IEEE transactions on medical imaging, 32*(5), 873-887.

[AUZ16] Auzias, G., Coulon, O., & Brovelli, A. (2016). MarsAtlas: A cortical parcellation atlas for functional mapping. *Human brain mapping, 37*(4), 1573-1592.

[BAN01] Bandettini, P. A., & Ungerleider, L. G. (2001). From neuron to BOLD: new connections. *Nature neuroscience, 4*(9), 864-866.

[BAN20] Bandettini, P. A. (2020). fMRI. *MIT Press*.

[BAS95] Basser, P. J., Pierpaoli, C. (1995). Diffusion Tensor MRI: a new tool to elucidate brain microstructure and nerve fiber organization. In Proceedings of the First International Conference for Functional Mapping of the Human Brain, Paris P (Vol. X, p.Y).

[BAS08] Bassett, D. S., Bullmore, E., Verchinski, B. A., Mattay, V. S., Weinberger, D. R., & Meyer-Lindenberg, A. (2008). Hierarchical organization of human cortical networks in health and schizophrenia. *Journal of Neuroscience, 28*(37), 9239-9248.

[BAS12] Bassett, D. S., Nelson, B. G., Mueller, B. A., Camchong, J., & Lim, K. O. (2012). Altered resting state complexity in schizophrenia. *Neuroimage, 59*(3), 2196-2207.

[BAS17a] Bassett, D. S., & Sporns, O. (2017). Network neuroscience. *Nature neuroscience, 20*(3), 353-364.

[BAS17b] Bassett, D. S., & Bullmore, E. T. (2017). Small-world brain networks revisited. *The Neuroscientist, 23*(5), 499-516.

[BEC05] Beckmann, C. F., DeLuca, M., Devlin, J. T., & Smith, S. M. (2005). Investigations into resting-state connectivity using independent component analysis.

Philosophical Transactions of the Royal Society B: Biological Sciences, 360(1457), 1001-1013.

[BEL91] Belliveau, J. W., Kennedy, D. N., McKinstry, R. C., Buchbinder, B. R., Weisskoff, R., Cohen, M. S., ... & Rosen, B. R. (1991). Functional mapping of the human visual cortex by magnetic resonance imaging. *Science, 254*(5032), 716-719.

[BEN01] Ben-Hur, A., Elisseeff, A., & Guyon, I. (2001). A stability based method for discovering structure in clustered data. In *Biocomputing 2002* (pp. 6-17).

[BER29] Berger, H. (1929). Über das elektroenkephalogramm des menschen. *Archiv für psychiatrie und nervenkrankheiten, 87*(1), 527-570.

[BER95] Berman, K. F., Ostrem, J. L., Esposito, G., Van Horn, J. D., Mattay, V. S., Kirkby, B. S., Weinberger, D. R (1995). Heritability of cognitively-related regional cerebral blood flow: a PET study comparing normal monozygotic and dizygotic twins. In Proceedings of the First International Conference for Functional Mapping of the Human Brain, Paris P (Vol. X, p. Y).

[BER20] Bertolero, M. A., & Bassett, D. S. (2020). On the nature of explanations offered by network science: A perspective from and for practicing neuroscientists. *Topics in Cognitive Science*.

[BET17] Betzel, R. F., & Bassett, D. S. (2017). Multi-scale brain networks. *Neuroimage, 160*, 73-83.

[BIJ19] Bijsterbosch, J. D., Beckmann, C. F., Woolrich, M. W., Smith, S. M., & Harrison, S. J. (2019). The relationship between spatial configuration and functional connectivity of brain regions revisited. *Elife, 8*, e44890.

[BIN09] Binder, J. R., Desai, R. H., Graves, W. W., & Conant, L. L. (2009). Where is the semantic system? A critical review and meta-analysis of 120 functional neuroimaging studies. Cerebral cortex, 19(12), 2767-2796.

[BIN11] Binder, J. R. (2011). Functional MRI is a valid noninvasive alternative to Wada testing. *Epilepsy & behavior, 20*(2), 214-222.

[BIS95] Biswal, B., Yetkin, F. Z., Haughton, V. M., & Hyde, J. S. (1995). Functional connectivity in the motor cortex of resting human brain using echo-planar MRI. *Magnetic resonance in medicine, 34*(4), 537–541.

[BIS12] Biswal, B. B. (2012). Resting state fMRI: a personal history. *Neuroimage, 62*(2), 938-944.

[BON36] Bonferroni, C. (1936). Teoria statistica delle classi e calcolo delle probabilita. Pubblicazioni del *R Istituto Superiore di Scienze Economiche e Commericiali di Firenze, 8*, 3-62.

[BOS92] Boser, B. E., Guyon, I. M., & Vapnik, V. N. (1992, July). A training algorithm for optimal margin classifiers. In *Proceedings of the fifth annual workshop on Computational learning theory* (pp. 144-152).

[BOY96] Boynton, G. M., Engel, S. A., Glover, G. H., & Heeger, D. J. (1996). Linear systems analysis of functional magnetic resonance imaging in human V1. *Journal of Neuroscience, 16*(13), 4207-4221.

[BRO12] Brodmann, K. (1912). Neue Ergebnisseuber die vergleichen de histologische Localisationder Grosshirnrindemitbesonderer Berücksichtigung des Stirnhirns. *Anat. Anz, 41*, 157-216.

[BRO20] Brodoehl, S., Gaser, C., Dahnke, R., Witte, O. W., & Klingner, C. M. (2020). Surface-based analysis increases the specificity of cortical activation patterns and connectivity results. *Scientific reports, 10*(1), 1-13.

[BUC07] Buckner, R. L., & Vincent, J. L. (2007). Unrest at rest: default activity and spontaneous network correlations. *Neuroimage, 37*(4), 1091-1096.

[BUC08] Buckner, R. L., Andrews-Hanna, J. R., & Schacter, D. L. (2008). The brain's default network: anatomy, function, and relevance to disease. *Annals of the New York Academy of Sciences*, 1124, 1–38.

[BUC09] Buckner, R. L., Sepulcre, J., Talukdar, T., Krienen, F. M., Liu, H., Hedden, T., ... & Johnson, K. A. (2009). Cortical hubs revealed by intrinsic functional connectivity: mapping, assessment of stability, and relation to Alzheimer's disease. *Journal of neuroscience, 29*(6), 1860-1873.

[BUC11] Buckner, R. L., Krienen, F. M., Castellanos, A., Diaz, J. C., & Yeo, B. T. (2011). The organization of the human cerebellum estimated by intrinsic functional connectivity. *Journal of neurophysiology, 106*(5), 2322-2345.

[BUC13a] Buckner, R. L., & Krienen, F. M. (2013). The evolution of distributed association networks in the human brain. *Trends in cognitive sciences, 17*(12), 648-665.

[BUC13b] Buckner, R. L., Krienen, F. M., & Yeo, B. T. (2013). Opportunities and limitations of intrinsic functional connectivity MRI. *Nature neuroscience*, *16*(7), 832.

[BUC19a] Buckner, R. L., & Margulies, D. S. (2019). Macroscale cortical organization and a default-like apex transmodal network in the marmoset monkey. *Nature communications*, *10*(1), 1-12.

[BUC19b] Buckner, R. L., & DiNicola, L. M. (2019). The brain's default network: updated anatomy, physiology and evolving insights. *Nature Reviews Neuroscience*, *20*(10), 593-608.

[BUL09] Bullmore, E., & Sporns, O. (2009). Complex brain networks: graph theoretical analysis of structural and functional systems. *Nature reviews neuroscience*, *10*(3), 186-198.

[BUL11] Bullmore, E. T., & Bassett, D. S. (2011). Brain graphs: graphical models of the human brain connectome. *Annual review of clinical psychology*, *7*, 113-140.

[CAR19] Carrion-Castillo, A., Van der Haegen, L., Tzourio-Mazoyer, N., Kavaklioglu, T., Badillo, S., Chavent, M., ... & Francks, C. (2019). Genome sequencing for rightward hemispheric language dominance. *Genes, Brain and Behavior*, *18*(5), e12572.

[COH08] Cohen, A. L., Fair, D. A., Dosenbach, N. U., Miezin, F. M., Dierker, D., Van Essen, D. C., ... & Petersen, S. E. (2008). Defining functional areas in individual human brains using resting functional connectivity MRI. *Neuroimage*, *41*(1), 45-57.

[CHA14] Charrad, M., Ghazzali, N., Boiteau, V., & Niknafs, A. (2014). NbClust: An R Package for determining the relevant number of clusters in a data set. *Journal of Statistical Software*, *61*(6), 1-36.

[CHO12] Choi, E. Y., Yeo, B. T., & Buckner, R. L. (2012). The organization of the human striatum estimated by intrinsic functional connectivity. *Journal of neurophysiology*, *108*(8), 2242-2263.

[CLA99] Clark DD, Sokoloff L. 1999. Circulation and energy metabolism of the brain. In *Basic Neurochemistry: Molecular, Cellular and Medical Aspects*, ed. GJ

Siegel, BW Agranoff, RW Albers, SK Fisher, MD Uhler, pp. 637–70. Philadelphia: Lippincott-Raven.

[COH83] Cohen, J., Cohen, P., West, S. G., & Aiken, L. S. (1983). Applied multiple regression. *Correlation Analysis for the Behavioral Sciences*, 2.

[COI05] Coifman RR, et al. (2005) Geometric diffusions as a tool for harmonic analysis and structure definition of data: Diffusion maps. *Proc Natl Acad Sci USA 102*(21):7426–7431.

[COL94] Collins, D. L., Neelin, P., Peters, T. M., & Evans, A. C. (1994). Automatic 3D intersubject registration of MR volumetric data in standardized Talairach space. *Journal of computer assisted tomography, 18*(2), 192-205.

[COL12] Cole, M. W., Yarkoni, T., Repovš, G., Anticevic, A., & Braver, T. S. (2012). Global connectivity of prefrontal cortex predicts cognitive control and intelligence. *Journal of Neuroscience, 32*(26), 8988-8999.

[COL13] Cole, M. W., Reynolds, J. R., Power, J. D., Repovs, G., Anticevic, A., & Braver, T. S. (2013). Multi-task connectivity reveals flexible hubs for adaptive task control. *Nature neuroscience, 16*(9), 1348.

[COL14] Cole, M. W., Bassett, D. S., Power, J. D., Braver, T. S., & Petersen, S. E. (2014). Intrinsic and task-evoked network architectures of the human brain. *Neuron, 83*(1), 238-251.

[COM94] Comon, P. (1994). Independent component analysis, a new concept?. S*ignal processing, 36*(3), 287-314.

[COR20] Cornblath, E. J., Ashourvan, A., Kim, J. Z., Betzel, R. F., Ciric, R., Adebimpe, A., ... & Gur, R. C. (2020). Temporal sequences of brain activity at rest are constrained by white matter structure and modulated by cognitive demands. *Communications biology, 3*(1), 1-12.

[CRA12] Craddock, R. C., James, G. A., Holtzheimer III, P. E., Hu, X. P., & Mayberg, H. S. (2012). A whole brain fMRI atlas generated via spatially constrained spectral clustering. *Human brain mapping, 33*(8), 1914-1928.

[CSA06] Csardi G, Nepusz T: The igraph software package for complex network research, *InterJournal, Complex Systems 1695*. 2006. http://igraph.org

[DAD20] Dadi, K., Varoquaux, G., Machlouzarides-Shalit, A., Gorgolewski, K. J., Wassermann, D., Thirion, B., & Mensch, A. (2020). Fine-grain atlases of functional modes for fMRI analysis. *Neuroimage*, 117126.

[DAM06] Damoiseaux, J. S., Rombouts, S. A. R. B., Barkhof, F., Scheltens, P., Stam, C. J., Smith, S. M., & Beckmann, C. F. (2006). Consistent resting-state networks across healthy subjects. *Proceedings of the national academy of sciences, 103*(37), 13848-13853.

[DEH17] Dehaene, S., Lau, H., & Kouider, S. (2017). What is consciousness, and could machines have it?. Science, 358(6362), 486-492.

[DEL10] Delong, A., Osokin, A., Isack, H. N., & Boykov, Y. (2012). Fast approximate energy minimization with label costs. *International journal of computer vision, 96*(1), 1-27.

[DES06] Desikan, R. S., Ségonne, F., Fischl, B., Quinn, B. T., Dickerson, B. C., Blacker, D., ... & Albert, M. S. (2006). An automated labeling system for subdividing the human cerebral cortex on MRI scans into gyral based regions of interest. *Neuroimage, 31*(3), 968-980.

[DES10] Destrieux, C., Fischl, B., Dale, A., & Halgren, E. (2010). Automatic parcellation of human cortical gyri and sulci using standard anatomical nomenclature. *Neuroimage, 53*(1), 1-15.

[DIE15] Diez, I., Bonifazi, P., Escudero, I., Mateos, B., Muñoz, M. A., Stramaglia, S., & Cortes, J. M. (2015). A novel brain partition highlights the modular skeleton shared by structure and function. *Scientific reports, 5*, 10532.

[DIJ10] Van Dijk, K. R., Hedden, T., Venkataraman, A., Evans, K. C., Lazar, S. W., & Buckner, R. L. (2010). Intrinsic functional connectivity as a tool for human connectomics: theory, properties, and optimization. *Journal of neurophysiology, 103*(1), 297-321.

[DIJ12] Van Dijk, K. R., Sabuncu, M. R., & Buckner, R. L. (2012). The influence of head motion on intrinsic functional connectivity MRI. *Neuroimage, 59*(1), 431-438.

[DOH20] Dohmatob, E., Dumas, G., & Bzdok, D. (2020). Dark control: The default mode network as a reinforcement learning agent. *Human Brain Mapping*.

[DOU11] Doucet, G., Naveau, M., Petit, L., Delcroix, N., Zago, L., Crivello, F., ... & Joliot, M. (2011). Brain activity at rest: a multiscale hierarchical functional organization. *Journal of neurophysiology, 105*(6), 2753-2763.

[DOU19] Doucet, G. E., Lee, W. H., & Frangou, S. (2019). Evaluation of the spatial variability in the major resting-state networks across human brain functional atlases. *Human brain mapping, 40*(15), 4577-4587.

[DOU20] Doucet G., Labache L., Joliot M., Frangou S. (2020). Atlas55+: Brain Functional Atlas of Resting-state Networks for Healthy Late Adulthood. *Cerebral Cortex*, sous presse.

[DRO04] Dronkers, N., & Ogar, J. (2004). Brain areas involved in speech production.

[DYM01] Dym, R. J., Burns, J., Freeman, K., & Lipton, M. L. (2011). Is functional MR imaging assessment of hemispheric language dominance as good as the Wada test?: a meta-analysis. *Radiology, 261*(2), 446-455.

[EDE01] Edelman, G. M., & Gally, J. A. (2001). Degeneracy and complexity in biological systems. *Proceedings of the National Academy of Sciences, 98*(24), 13763-13768.

[EIC18a] Eickhoff, S. B., Constable, R. T., & Yeo, B. T. (2018). Topographic organization of the cerebral cortex and brain cartography. *Neuroimage, 170*, 332-347.

[EIC18b] Eickhoff, S. B., Yeo, B. T., & Genon, S. (2018). Imaging-based parcellations of the human brain. *Nature Reviews Neuroscience, 19*(11), 672-686.

[EFR96] Efron, B., Halloran, E., & Holmes, S. (1996). Bootstrap confidence levels for phylogenetic trees. Proceedings of the National Academy of Sciences, 93(23), 13429-13429.

[ENG13] Engel, A. K., Gerloff, C., Hilgetag, C. C., & Nolte, G. (2013). Intrinsic coupling modes: multiscale interactions in ongoing brain activity. *Neuron, 80*(4), 867-886.

[ESS98] Van Essen, D. C., Drury, H. A., Joshi, S., & Miller, M. I. (1998). Functional and structural mapping of human cerebral cortex: solutions are in the surfaces. *Proceedings of the National Academy of Sciences, 95*(3), 788-795.

[ESS12] Van Essen, D. C., Glasser, M. F., Dierker, D. L., Harwell, J., & Coalson, T. (2012). Parcellations and hemispheric asymmetries of human cerebral cortex analyzed on surface-based atlases. *Cerebral cortex*, *22*(10), 2241-2262.

[EVA93] Evans, A. C., Collins, D. L., Mills, S. R., Brown, E. D., Kelly, R. L., & Peters, T. M. (1993, October). 3D statistical neuroanatomical models from 305 MRI volumes. In 1993 IEEE conference record nuclear science symposium and medical imaging conference (pp. 1813-1817). IEEE.

[EVA12] Evans, A. C., Janke, A. L., Collins, D. L., & Baillet, S. (2012). Brain templates and atlases. *Neuroimage*, *62*(2), 911-922.

[FAI08] Fair, D. A., Cohen, A. L., Dosenbach, N. U., Church, J. A., Miezin, F. M., Barch, D. M., ... & Schlaggar, B. L. (2008). The maturing architecture of the brain's default network. *Proceedings of the National Academy of Sciences*, *105*(10), 4028-4032.

[FAN16] Fan, L., Li, H., Zhuo, J., Zhang, Y., Wang, J., Chen, L., ... & Fox, P. T. (2016). The human brainnetome atlas: a new brain atlas based on connectional architecture. *Cerebral cortex*, *26*(8), 3508-3526.

[FEI10] Feinberg, D. A., Moeller, S., Smith, S. M., Auerbach, E., Ramanna, S., Glasser, M. F., ... & Yacoub, E. (2010). Multiplexed echo planar imaging for sub-second whole brain FMRI and fast diffusion imaging. *PloS one*, *5*(12).

[FIN07] Findeis, M. A. (2007). The role of amyloid β peptide 42 in Alzheimer's disease. *Pharmacology & therapeutics*, *116*(2), 266-286.

[FIN15] Finn, E. S., Shen, X., Scheinost, D., Rosenberg, M. D., Huang, J., Chun, M. M., ... & Constable, R. T. (2015). Functional connectome fingerprinting: identifying individuals using patterns of brain connectivity. *Nature neuroscience*, *18*(11), 1664-1671.

[FIS04a] Fiser, J., Chiu, C., & Weliky, M. (2004). Small modulation of ongoing cortical dynamics by sensory input during natural vision. *Nature*, *431*(7008), 573-578.

[FIS04b] Fischl, B., Van Der Kouwe, A., Destrieux, C., Halgren, E., Ségonne, F., Salat, D. H., ... & Caviness, V. (2004). Automatically parcellating the human cerebral cortex. *Cerebral cortex*, *14*(1), 11-22.

[FLO20] Floegel, M., Fuchs, S., & Kell, C. A. (2020). Differential contributions of the two cerebral hemispheres to temporal and spectral speech feedback control. *Nature Communications, 11*(1), 1-12.

[FOR12a] Fornito, A., Harrison, B. J., Zalesky, A., & Simons, J. S. (2012). Competitive and cooperative dynamics of large-scale brain functional networks supporting recollection. *Proceedings of the National Academy of Sciences, 109*(31), 12788-12793.

[FOR12b] Fornito, A., Zalesky, A., Pantelis, C., & Bullmore, E. T. (2012). Schizophrenia, neuroimaging and connectomics. *Neuroimage, 62*(4), 2296-2314.

[FOR16] Fornito, A., Zalesky, A., & Bullmore, E. (2016). *Fundamentals of brain network analysis*. Academic Press.

[FOX85] Fox, P. T., Perlmutter, J. S., & Raichle, M. E. (1985). A stereotactic method of anatomical localization for positron emission tomography. *Journal of computer assisted tomography, 9*(1), 141-153.

[FOX88] Fox, P. T., Mintun, M. A., Reiman, E. M., & Raichle, M. E. (1988). Enhanced detection of focal brain responses using intersubject averaging and change-distribution analysis of subtracted PET images. *Journal of Cerebral Blood Flow & Metabolism, 8*(5), 642-653.

[FOX05] Fox, M. D., Snyder, A. Z., Vincent, J. L., Corbetta, M., Van Essen, D. C., & Raichle, M. E. (2005). The human brain is intrinsically organized into dynamic, anticorrelated functional networks. *Proceedings of the National Academy of Sciences, 102*(27), 9673-9678.

[FOX20] Fox, K. C., Shi, L., Baek, S., Raccah, O., Foster, B. L., Saha, S., ... & Parvizi, J. (2020). Intrinsic network architecture predicts the effects elicited by intracranial electrical stimulation of the human brain. *Nature Human Behaviour*, 1-14.

[FRA07] Fransson, P., Skiöld, B., Horsch, S., Nordell, A., Blennow, M., Lagercrantz, H., & Åden, U. (2007). Resting-state networks in the infant brain. *Proceedings of the National Academy of Sciences, 104*(39), 15531-15536

[FRA13] Franco, A. R., Mannell, M. V., Calhoun, V. D., & Mayer, A. R. (2013). Impact of analysis methods on the reproducibility and reliability of resting-state networks. *Brain connectivity, 3*(4), 363-374.

[FRE11] French, L., & Pavlidis, P. (2011). Relationships between gene expression and brain wiring in the adult rodent brain. *PLoS Comput Biol*, *7*(1), e1001049.

[FRI93] Friston, K. J., Frith, C. D., Liddle, P. F., & Frackowiak, R. S. (1993). Functional connectivity: the principal-component analysis of large (PET) data sets. *Journal of cerebral blood flow and metabolism : official journal of the International Society of Cerebral Blood Flow and Metabolism*, *13*(1), 5–14.

[FRI03] Friston, K. J., Harrison, L., & Penny, W. (2003). Dynamic causal modelling. *Neuroimage*, *19*(4), 1273-1302.

[FRI19] Friston, K. J., Preller, K. H., Mathys, C., Cagnan, H., Heinzle, J., Razi, A., & Zeidman, P. (2019). Dynamic causal modelling revisited. *Neuroimage*, *199*, 730-744.

[FUK06] Fukunaga, M., Horovitz, S. G., van Gelderen, P., de Zwart, J. A., Jansma, J. M., Ikonomidou, V. N., ... & Duyn, J. H. (2006). Large-amplitude, spatially correlated fluctuations in BOLD fMRI signals during extended rest and early sleep stages. *Magnetic resonance imaging*, *24*(8), 979-992.

[FUL16] Fulcher, B. D., & Fornito, A. (2016). A transcriptional signature of hub connectivity in the mouse connectome. *Proceedings of the National Academy of Sciences*, *113*(5), 1435-1440.

[GAR04] Garfield, E. (2004). Historiographic mapping of knowledge domains literature. *Journal of Information Science*, *30*(2), 119-145.

[GEN17] Genon, S., Li, H., Fan, L., Müller, V. I., Cieslik, E. C., Hoffstaedter, F., ... & Moebus, S. (2017). The right dorsal premotor mosaic: organization, functions, and connectivity. *Cerebral Cortex*, *27*(3), 2095-2110.

[GEN18] Genon, S., Reid, A., Langner, R., Amunts, K., & Eickhoff, S. B. (2018). How to characterize the function of a brain region. *Trends in cognitive sciences*, *22*(4), 350-364.

[GEO95] George, J., Mosher, J., Schmidt, D., Aine, C., Wood, C., Lewine, J., ... & Belliveau, J. (1995). Functional neuroimaging by combined MRI, MEG and fMRI. In Proceedings of the First International Conference for Functional Mapping of the Human Brain, Paris P (Vol. 1, p. 89).

[GIR02] Girvan, M., & Newman, M. E. (2002). Community structure in social and biological networks. *Proceedings of the national academy of sciences, 99*(12), 7821-7826.

[GLA11] Glasser, M. F., & Van Essen, D. C. (2011). Mapping human cortical areas in vivo based on myelin content as revealed by T1-and T2-weighted MRI. *Journal of Neuroscience, 31*(32), 11597-11616.

[GLA13] Glasser, M. F., Sotiropoulos, S. N., Wilson, J. A., Coalson, T. S., Fischl, B., Andersson, J. L., ... & Van Essen, D. C. (2013). The minimal preprocessing pipelines for the Human Connectome Project. *Neuroimage, 80*, 105-124.

[GLA16] Glasser, M. F., Coalson, T. S., Robinson, E. C., Hacker, C. D., Harwell, J., Yacoub, E., ... & Smith, S. M. (2016). A multi-modal parcellation of human cerebral cortex. *Nature, 536*(7615), 171-178.

[GOR12] Gordon, E. M., Stollstorff, M., & Vaidya, C. J. (2012). Using spatial multiple regression to identify intrinsic connectivity networks involved in working memory performance. Human brain mapping, 33(7), 1536-1552.

[GOR16] Gordon, E. M., Laumann, T. O., Adeyemo, B., Huckins, J. F., Kelley, W. M., & Petersen, S. E. (2016). Generation and evaluation of a cortical area parcellation from resting-state correlations. *Cerebral cortex, 26*(1), 288-303.

[GOR17] Gordon, E. M., Laumann, T. O., Gilmore, A. W., Newbold, D. J., Greene, D. J., Berg, J. J., ... & Hampton, J. M. (2017). Precision functional mapping of individual human brains. *Neuron, 95*(4), 791-807.

[GOR20] Gordon, E. M., Laumann, T. O., Marek, S., Raut, R. V., Gratton, C., Newbold, D. J., ... & Petersen, S. E. (2020). Default-mode network streams for coupling to language and control systems. *Proceedings of the National Academy of Sciences, 117*(29), 17308-17319.

[GRE03] Greicius, M. D., Krasnow, B., Reiss, A. L., & Menon, V. (2003). Functional connectivity in the resting brain: a network analysis of the default mode hypothesis. *Proceedings of the National Academy of Sciences, 100*(1), 253-258.

[GRE18] Greene, A. S., Gao, S., Scheinost, D., & Constable, R. T. (2018). Task-induced brain state manipulation improves prediction of individual traits. *Nature communications, 9*(1), 1-13.

[GRI14] Griffanti, L., Salimi-Khorshidi, G., Beckmann, C. F., Auerbach, E. J., Douaud, G., Sexton, C. E., ... & Moeller, S. (2014). ICA-based artefact removal and accelerated fMRI acquisition for improved resting state network imaging. *Neuroimage, 95*, 232-247.

[GU15] Gu, S., Pasqualetti, F., Cieslak, M., Telesford, Q. K., Alfred, B. Y., Kahn, A. E., ... & Bassett, D. S. (2015). Controllability of structural brain networks. *Nature communications, 6*(1), 1-10.

[GUS01] Gusnard, D. A., & Raichle, M. E. (2001). Searching for a baseline: functional imaging and the resting human brain. Nature reviews neuroscience, 2(10), 685-694.

[HAG08] Hagmann, P., Cammoun, L., Gigandet, X., Meuli, R., Honey, C. J., Wedeen, V. J., & Sporns, O. (2008). Mapping the structural core of human cerebral cortex. *PLoS Biol, 6*(7), e159.

[HAR76] Harris, F. S., & Rhoton, A. L. (1976). Anatomy of the cavernous sinus: a microsurgical study. *Journal of neurosurgery, 45*(2), 169-180.

[HAX01] Haxby, J. V., Gobbini, M. I., Furey, M. L., Ishai, A., Schouten, J. L., & Pietrini, P. (2001). Distributed and overlapping representations of faces and objects in ventral temporal cortex. *Science, 293*(5539), 2425-2430.

[HAX12] Haxby, J. V. (2012). Multivariate pattern analysis of fMRI: the early beginnings. *Neuroimage, 62*(2), 852-855.

[HE08a] He, Y., Chen, Z., & Evans, A. (2008). Structural insights into aberrant topological patterns of large-scale cortical networks in Alzheimer's disease. *Journal of Neuroscience, 28*(18), 4756-4766.

[HE08b] He, B. J., Snyder, A. Z., Zempel, J. M., Smyth, M. D., & Raichle, M. E. (2008). Electrophysiological correlates of the brain's intrinsic large-scale functional architecture. *Proceedings of the National Academy of Sciences, 105*(41), 16039-16044.

[HER85] Hérault, J., Jutten, C., & Ans, B. (1985). Détection de grandeurs primitives dans un message composite par une architecture de calcul neuromimétique en apprentissage non supervisé. In *10ème Colloque sur le traitement du signal et des images*, FRA, 1985. GRETSI, Groupe d'Etudes du Traitement du Signal et des Images.

[HER13] Hervé, P. Y., Zago, L., Petit, L., Mazoyer, B., & Tzourio-Mazoyer, N. (2013). Revisiting human hemispheric specialization with neuroimaging. *Trends in cognitive sciences, 17*(2), 69-80.

[HES19] Hesling, I., Labache, L., Joliot, M., & Tzourio-Mazoyer, N. (2019). Large-scale plurimodal networks common to listening to, producing and reading word lists: an fMRI study combining task-induced activation and intrinsic connectivity in 144 right-handers. *Brain Structure and Function, 224*(9), 3075-3094.

[HEU10a] Van Den Heuvel, M. P., & Hulshoff Pol, H. E. (2010). Specific somatotopic organization of functional connections of the primary motor network during resting state. *Human brain mapping, 31*(4), 631-644.

[HEU10b] Van Den Heuvel, M. P., Mandl, R. C., Stam, C. J., Kahn, R. S., & Pol, H. E. H. (2010). Aberrant frontal and temporal complex network structure in schizophrenia: a graph theoretical analysis. *Journal of Neuroscience, 30*(47), 15915-15926.

[HIL10] Hill, J., Inder, T., Neil, J., Dierker, D., Harwell, J., & Van Essen, D. (2010). Similar patterns of cortical expansion during human development and evolution. *Proceedings of the National Academy of Sciences, 107*(29), 13135-13140.

[HOU73] Hounsfield, G. N. (1973). Computerized transverse axial scanning (tomography): Part 1. Description of system. *The British journal of radiology, 46*(552), 1016-1022.

[HOU02] Houdé, O., Mazoyer, B., Tzourio-Mazoyer, N., & Crivello, F. (2002). Cerveau et psychologie: Introduction à l'imagerie cérébrale anatomique et fonctionnelle. Presses universitaires de France.

[HOR95] Horwitz, B., McIntosh, A. R., Haxby, J. V., Furey, M., Salerno, J. A., Schapiro, M. B., ... & Grady, C. L. (1995). Network analysis of PET-mapped visual pathways in Alzheimer type dementia. In Proceedings of the First International Conference for Functional Mapping of the Human Brain, Paris P (Vol. X, p. Y).

[HUN18] Huntenburg, J. M., Bazin, P. L., & Margulies, D. S. (2018). Large-scale gradients in human cortical organization. *Trends in cognitive sciences, 22*(1), 21-31.

[HYD95] Hyde, J. S., Biswal, B., Yetkin, F. Z., & Haughton, V. M. (1995). Functional connectivity determined from analysis of physiological fluctuations in a

series of echo-planar images. In Proceedings of the First International Conference for Functional Mapping of the Human Brain, Paris P (Vol. X, p. Y).

[ICN09] International Commission on Non-Ionizing Radiation Protection. (2009). Amendment to the ICNIRP "Statement on medical magnetic resonance (MR) procedures: protection of patients". *Health Physics, 97*(3), 259-261.

[ING65] Ingvar, D. H., & Risberg, J. (1965). Influence of mental activity upon regional cerebral blood flow in man: a preliminary study. *Acta Neurologica Scandinavica, 41*(S14), 183-186.

[JAM90] James, W. (1890). *The principles of psychology* (Vol. 1). New York, Henry Holt and Company.

[JAM16] James, G. A., Hazaroglu, O., & Bush, K. A. (2016). A human brain atlas derived via n-cut parcellation of resting-state and task-based fMRI data. *Magnetic resonance imaging, 34*(2), 209-218.

[JOH08] Johnston, J. M., Vaishnavi, S. N., Smyth, M. D., Zhang, D., He, B. J., Zempel, J. M., ... & Raichle, M. E. (2008). Loss of resting interhemispheric functional connectivity after complete section of the corpus callosum. *Journal of Neuroscience, 28*(25), 6453-6458.

[JOL15] Joliot, M., Jobard, G., Naveau, M., Delcroix, N., Petit, L., Zago, L., ... & Tzourio-Mazoyer, N. (2015). AICHA: An atlas of intrinsic connectivity of homotopic areas. *Journal of neuroscience methods, 254*, 46-59.

[JOS19] Joseph Richards and Robrecht Cannoodt (2019). diffusionMap: Diffusion Map. R package version 1.2.0.

[JOU15] Jouen, A. L., Ellmore, T. M., Madden, C. J., Pallier, C., Dominey, P. F., & Ventre-Dominey, J. (2015). Beyond the word and image: characteristics of a common meaning system for language and vision revealed by functional and structural imaging. *NeuroImage, 106*, 72-85.

[JU20] Ju, H., & Bassett, D. S. (2020). Dynamic representations in networked neural systems. *Nature Neuroscience*, 1-10.

[KAI15] Kaiser, R. H., Andrews-Hanna, J. R., Wager, T. D., & Pizzagalli, D. A. (2015). Large-scale network dysfunction in major depressive disorder: a meta-analysis of resting-state functional connectivity. *JAMA psychiatry, 72*(6), 603-611.

[KAN13] *Principles of Neural Science*, Fifth Editon. (2013). Ed. by Kandel, E. R., Schwartz, J. H., Jessell, T. M., Siegelbaum, S. A., & Hudspeth, A. J.. McGraw-Hill Companies, Medical. LXVII-1709p.

[KEN03] Kenet, T., Bibitchkov, D., Tsodyks, M., Grinvald, A., & Arieli, A. (2003). Spontaneously emerging cortical representations of visual attributes. *Nature*, *425*(6961), 954-956.

[KEV97] Kevles, B. (1997). *Naked to the bone: medical imaging in the twentieth century*. Rutgers University Press.

[KIT15] Kitzbichler, M. G., Khan, S., Ganesan, S., Vangel, M. G., Herbert, M. R., Hämäläinen, M. S., & Kenet, T. (2015). Altered development and multifaceted band-specific abnormalities of resting state networks in autism. *Biological psychiatry*, *77*(9), 794-804.

[KLI19] Kliemann, D., Adolphs, R., Tyszka, J. M., Fischl, B., Yeo, B. T., Nair, R., ... & Paul, L. K. (2019). Intrinsic functional connectivity of the brain in adults with a single cerebral hemisphere. *Cell reports*, *29*(8), 2398-2407.

[KON19] Kong, R., Li, J., Orban, C., Sabuncu, M. R., Liu, H., Schaefer, A., ... & Yeo, B. T. (2019). Spatial topography of individual-specific cortical networks predicts human cognition, personality, and emotion. *Cerebral cortex*, *29*(6), 2533-2551.

[KWO92] Kwong, K. K., Belliveau, J. W., Chesler, D. A., Goldberg, I. E., Weisskoff, R. M., Poncelet, B. P., ... & Turner, R. (1992). Dynamic magnetic resonance imaging of human brain activity during primary sensory stimulation. *Proceedings of the National Academy of Sciences*, *89*(12), 5675-5679.

[LAB19] Labache, L., Joliot, M., Saracco, J., Jobard, G., Hesling, I., Zago, L., ... & Tzourio-Mazoyer, N. (2019). A SENtence Supramodal Areas AtlaS (SENSAAS) based on multiple task-induced activation mapping and graph analysis of intrinsic connectivity in 144 healthy right-handers. *Brain Structure and Function*, *224*(2), 859-882.

[LAB20] Labache, L., Mazoyer, B., Joliot, M., Crivello, F., Hesling, I., Tzourio-Mazoyer, N. (2020). Typical and atypical language brain organization according to intrinsic connectivity and multitasks functional asymmetries. *eLife*, sous presse.

[LAI13] Laird, A. R., Eickhoff, S. B., Rottschy, C., Bzdok, D., Ray, K. L., & Fox, P. T. (2013). Networks of task co-activations. *Neuroimage, 80*, 505-514.

[LAN55] Landau, W. H. (1955). The local circulation of the living brain; values in the unanesthetized and anesthetized cat. *Trans Amer Neurol Ass, 80*, 125-129.

[LAN79] Lance, G. N., & Williams, W. T. (1979). INVER: a program for the computation of distance-measures between attributes of mixed types. *Australian Computer Journal, 11*(1), 27-28.

[LAR09] Larson-Prior, L. J., Zempel, J. M., Nolan, T. S., Prior, F. W., Snyder, A. Z., & Raichle, M. E. (2009). Cortical network functional connectivity in the descent to sleep. *Proceedings of the National Academy of Sciences, 106*(11), 4489-4494.

[LAS63] Lassen, N. A., Høledt-Hasmussen, K., Søremen, S. C., Skinhøj, E., Cronquist, S., Bodforss, B., ... & Ingvar, D. H. (1963). Regional cerebral blood flow in man determined by krypton^{85}. *Neurology, 13*(9), 719-719.

[LAS10] Lashkari, D., Vul, E., Kanwisher, N., & Golland, P. (2010). Discovering structure in the space of fMRI selectivity profiles. *Neuroimage, 50*(3), 1085-1098.

[LAU73] Lauterbur, P. C. (1973). Image formation by induced local interactions: examples employing nuclear magnetic resonance. *Nature, 242*(5394), 190-191.

[LAU15] Laumann, T. O., Gordon, E. M., Adeyemo, B., Snyder, A. Z., Joo, S. J., Chen, M. Y., ... & Schlaggar, B. L. (2015). Functional system and areal organization of a highly sampled individual human brain. *Neuron, 87*(3), 657-670.

[LER16] Leriche MA, Le top-100 du CEA: Les 100 publications CEA les plus citées du Web of Science – *Panor@m'IST n°5*. Novembre 2016. CEA, Service Valorisation de l'information, Saclay, France.

[LIA13] Liang, X., Zou, Q., He, Y., & Yang, Y. (2013). Coupling of functional connectivity and regional cerebral blood flow reveals a physiological basis for network hubs of the human brain. *Proceedings of the National Academy of Sciences, 110*(5), 1929-1934.

[LIH09] Li, H., Handsaker, B., Wysoker, A., Fennell, T., Ruan, J., Homer, N., ... & Durbin, R. (2009). The sequence alignment/map format and SAMtools. *Bioinformatics, 25*(16), 2078-2079.

[LOG01] Logothetis, N. K., Pauls, J., Augath, M., Trinath, T., & Oeltermann, A. (2001). Neurophysiological investigation of the basis of the fMRI signal. *Nature, 412*(6843), 150-157.

[LU12] Lu, H., Zou, Q., Gu, H., Raichle, M. E., Stein, E. A., & Yang, Y. (2012). Rat brains also have a default mode network. *Proceedings of the National Academy of Sciences, 109*(10), 3979-3984.

[LUD10] Luders, E., Thompson, P. M., & Toga, A. W. (2010). The development of the corpus callosum in the healthy human brain. Journal of *Neuroscience, 30*(33), 10985-10990.

[LYN10] Lynall, M. E., Bassett, D. S., Kerwin, R., McKenna, P. J., Kitzbichler, M., Muller, U., & Bullmore, E. (2010). Functional connectivity and brain networks in schizophrenia. *Journal of Neuroscience, 30*(28), 9477-9487.

[MAN77] Mansfield, P. (1977). Multi-planar image formation using NMR spin echoes. *Journal of Physics C: Solid State Physics, 10*(3), L55.

[MAR11a] Markram, H., Meier, K., Lippert, T., Grillner, S., Frackowiak, R., Dehaene, S., ... & Grant, S. (2011). Introducing the human brain project. *Procedia Computer Science, 7*, 39-42.

[MAR11b] Mars, R. B., Jbabdi, S., Sallet, J., O'Reilly, J. X., Croxson, P. L., Olivier, E., ... & Behrens, T. E. (2011). Diffusion-weighted imaging tractography-based parcellation of the human parietal cortex and comparison with human and macaque resting-state functional connectivity. *Journal of Neuroscience, 31*(11), 4087-4100.

[MAR16] Margulies, D. S., Ghosh, S. S., Goulas, A., Falkiewicz, M., Huntenburg, J. M., Langs, G., ... & Jefferies, E. (2016). Situating the default-mode network along a principal gradient of macroscale cortical organization. *Proceedings of the National Academy of Sciences, 113*(44), 12574-12579.

[MAT78] Matsui T, Hirano A. *An atlas of the human brain for computerized tomography*. New York: Igaku-Shoin, 1978, 564 pp.

[MAZ93] Mazoyer, B. M., Tzourio, N., Frak, V., Syrota, A., Murayama, N., Levrier, O., ... & Mehler, J. (1993). The cortical representation of speech. *Journal of cognitive neuroscience, 5*(4), 467-479.

[MAZ01a] Mazziotta, J., Toga, A., Evans, A., Fox, P., Lancaster, J., Zilles, K., ... & Mazoyer, B. (2001). A probabilistic atlas and reference system for the human brain: International Consortium for Brain Mapping (ICBM). *Philosophical Transactions of the Royal Society of London. Series B: Biological Sciences*, *356*(1412), 1293-1322.

[MAZ01b] Mazoyer, B., Zago, L., Mellet, E., Bricogne, S., Etard, O., Houdé, O., ... & Tzourio-Mazoyer, N. (2001). Cortical networks for working memory and executive functions sustain the conscious resting state in man. *Brain research bulletin*, *54*(3), 287-298.

[MAZ08] Mazoyer, B. (2008). Jean Talairach (1911-2007): A life in stereotaxy. *Human brain mapping*, *29*(2), 250.

[MAZ14] Mazoyer, B., Zago, L., Jobard, G., Crivello, F., Joliot, M., Perchey, G., ... & Tzourio-Mazoyer, N. (2014). Gaussian mixture modeling of hemispheric lateralization for language in a large sample of healthy individuals balanced for handedness. *PloS one*, *9*(6), e101165.

[MAZ16] Mazoyer, B., Mellet, E., Perchey, G., Zago, L., Crivello, F., Jobard, G., ... & Joliot, M. (2016). BIL&GIN: a neuroimaging, cognitive, behavioral, and genetic database for the study of human brain lateralization. *Neuroimage*, *124*, 1225-1231.

[MCG83] McGilvery RW, Goldstein GW. 1983. Biochemistry: A Functional Approach. Philadelphia: Saunders.

[MCK98] McKeown, M. J., Makeig, S., Brown, G. G., Jung, T. P., Kindermann, S. S., Bell, A. J., & Sejnowski, T. J. (1998). Analysis of fMRI data by blind separation into independent spatial components. *Human brain mapping*, *6*(3), 160-188.

[MCK10] McKenna, A., Hanna, M., Banks, E., Sivachenko, A., Cibulskis, K., Kernytsky, A., ... & DePristo, M. A. (2010). The Genome Analysis Toolkit: a MapReduce framework for analyzing next-generation DNA sequencing data. *Genome research*, *20*(9), 1297-1303.

[MEL98] Mellet, E., Tzourio, N., Denis, M., & Mazoyer, B. (1998). Cortical anatomy of mental imagery of concrete nouns based on their dictionary definition. *Neuroreport*, *9*(5), 803-808.

[MEN11] Mennes, M., Zuo, X. N., Kelly, C., Di Martino, A., Zang, Y. F., Biswal, B., ... & Milham, M. P. (2011). Linking inter-individual differences in neural activation and behavior to intrinsic brain dynamics. Neuroimage, 54(4), 2950-2959.

[MEN12] Mennes, M., Kelly, C., Colcombe, S., Castellanos, F. X., & Milham, M. P. (2013). The extrinsic and intrinsic functional architectures of the human brain are not equivalent. *Cerebral cortex, 23*(1), 223-229.

[MEN13] Mennes, M., Kelly, C., Colcombe, S., Castellanos, F. X., & Milham, M. P. (2013). The extrinsic and intrinsic functional architectures of the human brain are not equivalent. *Cerebral cortex, 23*(1), 223-229.

[MER14] Merrien, J., Le Brun, D., Duval, B., & Le Brun, D. (2014). *Dictionnaire de la mer: savoir-faire, traditions, vocabulaire, techniques*. Omnibus.

[MES90] Mesulam, M. M. (1990). Large-scale neurocognitive networks and distributed processing for attention, language, and memory. *Annals of Neurology: Official Journal of the American Neurological Association and the Child Neurology Society*, *28*(5), 597-613.

[MES98] Mesulam, M. M. (1998). From sensation to cognition. *Brain: a journal of neurology, 121*(6), 1013-1052.

[MES00] Mesulam, M. M. (2000). Principles of behavioral and cognitive neurology. Oxford University Press.

[MES14] Mesulam, M. M., Rogalski, E. J., Wieneke, C., Hurley, R. S., Geula, C., Bigio, E. H., ... & Weintraub, S. (2014). Primary progressive aphasia and the evolving neurology of the language network. *Nature Reviews Neurology, 10*(10), 554.

[MES20] Messé, A. (2020). Parcellation influence on the connectivity-based structure–function relationship in the human brain. *Human Brain Mapping, 41*(5), 1167-1180.

[MIC12] Michel, V., Gramfort, A., Varoquaux, G., Eger, E., Keribin, C., & Thirion, B. (2012). A supervised clustering approach for fMRI-based inference of brain states. Pattern Recognition, 45(6), 2041-2049.

[MIL16] Miller, K. L., Alfaro-Almagro, F., Bangerter, N. K., Thomas, D. L., Yacoub, E., Xu, J., ... & Griffanti, L. (2016). Multimodal population brain imaging in the UK Biobank prospective epidemiological study. *Nature neuroscience, 19*(11), 1523.

[MOL19] Mollink, J., Smith, S. M., Elliott, L. T., Kleinnijenhuis, M., Hiemstra, M., Alfaro-Almagro, F., ... & Miller, K. L. (2019). The spatial correspondence and genetic influence of interhemispheric connectivity with white matter microstructure. *Nature neuroscience, 22*(5), 809-819.

[MOS80] Mosso A (1880) Sulla circolazione del sangue nel cervello dell'uomo. *Atti della R Acad Lincei Mem Cl Sci Fis Mat Nat III*:237–358

[MUE13] Mueller, S., Wang, D., Fox, M. D., Yeo, B. T., Sepulcre, J., Sabuncu, M. R., ... & Liu, H. (2013). Individual variability in functional connectivity architecture of the human brain. *Neuron, 77*(3), 586-595.

[NAK04] Nakagawa, S. (2004). A farewell to Bonferroni: the problems of low statistical power and publication bias. *Behavioral ecology, 15*(6), 1044-1045.

[NAS09] Naselaris, T., Prenger, R. J., Kay, K. N., Oliver, M., & Gallant, J. L. (2009). Bayesian reconstruction of natural images from human brain activity. *Neuron, 63*(6), 902-915.

[NAV12] Naveau, M., Doucet, G., Delcroix, N., Petit, L., Zago, L., Crivello, F., ... & Joliot, M. (2012). A novel group ICA approach based on multi-scale individual component clustering. application to a large sample of fMRI data. *Neuroinformatics, 10*(3), 269-285.

[NIU20] Niu, C., Cohen, A. D., Wen, X., Chen, Z., Lin, P., Liu, X., ... & Zhang, M. (2020). Modeling motor task activation from resting-state fMRI using machine learning in individual subjects. *Brain Imaging and Behavior*, 1-11.

[OCH16] Ochoa-Repáraz, J., & Kasper, L. H. (2016). The second brain: is the gut microbiota a link between obesity and central nervous system disorders?. *Current obesity reports, 5*(1), 51-64.

[OGA92] Ogawa, S., Tank, D. W., Menon, R., Ellermann, J. M., Kim, S. G., Merkle, H., & Ugurbil, K. (1992). Intrinsic signal changes accompanying sensory stimulation: functional brain mapping with magnetic resonance imaging. *Proceedings of the National Academy of Sciences, 89*(13), 5951-5955.

[OLS19] Olson, Eric T., "Personal Identity", The Stanford Encyclopedia of Philosophy (Fall 2019 Edition), Edward N. Zalta (ed.).

[OPS10] Opsahl, T., Agneessens, F., & Skvoretz, J. (2010). Node centrality in weighted networks: Generalizing degree and shortest paths. *Social networks*, *32*(3), 245-251.

[ORB15] Orban, P., Doyon, J., Petrides, M., Mennes, M., Hoge, R., & Bellec, P. (2015). The richness of task-evoked hemodynamic responses defines a pseudohierarchy of functionally meaningful brain networks. Cerebral cortex, 25(9), 2658-2669.

[PAR19] Parker, D. B., & Razlighi, Q. R. (2019). Task-evoked Negative BOLD Response and Functional Connectivity in the Default Mode Network are Representative of Two Overlapping but Separate Neurophysiological Processes. *Scientific reports, 9*.

[PAU36] Pauling, L., & Coryell, C. D. (1936). The magnetic properties and structure of hemoglobin, oxyhemoglobin and carbonmonoxyhemoglobin. *Proceedings of the National Academy of Sciences*, *22*(4), 210-216.

[PED11] Pedregosa, F., Varoquaux, G., Gramfort, A., Michel, V., Thirion, B., Grisel, O., ... & Vanderplas, J. (2011). Scikit-learn: Machine learning in Python. *Journal of machine learning research, 12*(Oct), 2825-2830.

[PEN11] Penny, W. D., Friston, K. J., Ashburner, J. T., Kiebel, S. J., & Nichols, T. E. (Eds.). (2011). *Statistical parametric mapping: the analysis of functional brain images*. Elsevier.

[PER15] Pernet, C. R., McAleer, P., Latinus, M., Gorgolewski, K. J., Charest, I., Bestelmeyer, P. E., ... & Belin, P. (2015). The human voice areas: Spatial organization and inter-individual variability in temporal and extra-temporal cortices. *Neuroimage, 119*, 164-174.

[PET78] Peters, M., & Durding, B. M. (1978). Handedness measured by finger tapping: A continuous variable. *Canadian Journal of Psychology/Revue canadienne de psychologie*, *32*(4), 257.

[PET88] Petersen, S. E., Fox, P. T., Posner, M. I., Mintun, M., & Raichle, M. E. (1988). Positron emission tomographic studies of the cortical anatomy of single-word processing. *Nature, 331*(6157), 585-589.

[PET96] Petit, L., Orssaud, C., Tzourio, N., Crivello, F., Berthoz, A., & Mazoyer, B. (1996). Functional anatomy of a prelearned sequence of horizontal saccades in humans. *Journal of Neuroscience, 16*(11), 3714-3726.

[PIN04] Pinault, D. (2004). The thalamic reticular nucleus: structure, function and concept. Brain research reviews, 46(1), 1-31.

[POL11] Poldrack, R. A., Mumford, J. A., & Nichols, T. E. (2011). Handbook of functional MRI data analysis. Cambridge University Press.

[POL18] Poldrack, R. A. (2018). The new mind readers: What neuroimaging can and cannot reveal about our thoughts. Princeton University Press.

[POP09] Popa, D., Popescu, A. T., & Paré, D. (2009). Contrasting activity profile of two distributed cortical networks as a function of attentional demands. *Journal of Neuroscience, 29*(4), 1191-1201.

[POS88] Posner, M. I., Petersen, S. E., Fox, P. T., & Raichle, M. E. (1988). Localization of cognitive operations in the human brain. *Science, 240*(4859), 1627-1631.

[POW10] Power, J. D., Fair, D. A., Schlaggar, B. L., & Petersen, S. E. (2010). The development of human functional brain networks. *Neuron, 67*(5), 735-748.

[POW11] Power, J. D., Cohen, A. L., Nelson, S. M., Wig, G. S., Barnes, K. A., Church, J. A., ... & Petersen, S. E. (2011). Functional network organization of the human brain. *Neuron, 72*(4), 665-678.

[PRI02] Price, C. J., & Friston, K. J. (2002). Degeneracy and cognitive anatomy. *Trends in cognitive sciences, 6*(10), 416-421.

[PUL16] Pulvermüller, F., & Fadiga, L. (2016). Brain language mechanisms built on action and perception. In *Neurobiology of Language* (pp. 311-324). Academic Press.

[RAD17] Radon, J. (1917). Über die Bestimmung von Funktionen durch ihre Integralwerte längs gewisser Mannigfaltigkeiten. *Berichte über die Verhandlungen der Königlich-Sächsischen Akademie der Wissenschaften zu Leipzig, Mathematisch-Physische Klasse, Leipzig: Teubner, 69*: 262–277.

[RAE18] Raemaekers, M., Schellekens, W., Petridou, N., & Ramsey, N. F. (2018). Knowing left from right: asymmetric functional connectivity during resting state. *Brain Structure and Function, 223*(4), 1909-1922.

[RAI98] Raichle, M. E. (1998). Behind the scenes of functional brain imaging: a historical and physiological perspective. *Proceedings of the National Academy of Sciences, 95*(3), 765-772.

[RAI01] Raichle, M. E., MacLeod, A. M., Snyder, A. Z., Powers, W. J., Gusnard, D. A., & Shulman, G. L. (2001). A default mode of brain function. *Proceedings of the National Academy of Sciences, 98*(2), 676-682.

[RAI05] Raichle, M. E., & Gusnard, D. A. (2005). Intrinsic brain activity sets the stage for expression of motivated behavior. *Journal of Comparative Neurology, 493*(1), 167-176.

[RAI06a] Raichle, M. E., & Mintun, M. A. (2006). Brain work and brain imaging. Annu. Rev. Neurosci., 29, 449-476.

[RAI06b] Raichle, M. E. (2006). The brain's dark energy. *Science, 314*(5803), 1249-1250.

[RAI09] Raichle, M. E. (2009). A brief history of human brain mapping. *Trends in neurosciences, 32*(2), 118-126.

[RAI14] Raichle, M. E., & Shepherd, G. M. (2014). Angelo Mosso's circulation of blood in the human brain. Oxford University Press.

[RCT20] R Core Team (2020). R: A language and environment for statistical computing. *R Foundation for Statistical Computing*, Vienna, Austria. URL https://www.R-project.org/.

[ROG20] Roger, E., Pichat, C., Torlay, L., David, O., Renard, F., Banjac, S., ... & Baciu, M. (2020). Hubs disruption in mesial temporal lobe epilepsy. A resting-state fMRI study on a language-and-memory network. *Human brain mapping, 41*(3), 779-796.

[ROL77] Roland, P. E., Skinhoj, E., Larsen, B., Lassen, N. A., & Ingvar, D. H. (1977). Cerebral Function, Metabolism and Circulation. *Acta Neurol Scand, 56*(suppl 64), 542-543.

[ROL85] P.E. Roland, Application of imaging of brain blood flow to behavioral neurophysiology: The cortical field activation hypothesis, in: L. Sokoloff ŽEd.., *Brain Imaging and Brain Function*, Raven, New 77. York, 1985, pp. 87–106.

[ROL98] Roland, P. E., & Zilles, K. (1998). Structural divisions and functional fields in the human cerebral cortex. *Brain research reviews, 26*(2-3), 87-105.

[ROS08] Rosvall, M., & Bergstrom, C. T. (2008). Maps of random walks on complex networks reveal community structure. *Proceedings of the National Academy of Sciences, 105*(4), 1118-1123.

[ROS09] Rosvall, M., Axelsson, D., & Bergstrom, C. T. (2009). The map equation. *The European Physical Journal Special Topics, 178*(1), 13-23.

[ROY90] Roy, C. S., & Sherrington, C. S. (1890). On the regulation of the blood-supply of the brain. *The Journal of physiology, 11*(1-2), 85-158.

[RUB10] Rubinov, M., & Sporns, O. (2010). Complex network measures of brain connectivity: uses and interpretations. *Neuroimage, 52*(3), 1059-1069.

[RUB11] Rubinov, M., & Sporns, O. (2011). Weight-conserving characterization of complex functional brain networks. *Neuroimage, 56*(4), 2068-2079.

[SAL20] Salehi, M., Karbasi, A., Barron, D. S., Scheinost, D., & Constable, R. T. (2020). Individualized functional networks reconfigure with cognitive state. *NeuroImage, 206*, 116233.

[SAN14] Santarnecchi, E., Galli, G., Polizzotto, N. R., Rossi, A., & Rossi, S. (2014). Efficiency of weak brain connections support general cognitive functioning. *Human brain mapping, 35*(9), 4566-4582.

[SCH08] Schummers, J., Yu, H., & Sur, M. (2008). Tuned responses of astrocytes and their influence on hemodynamic signals in the visual cortex. *Science, 320*(5883), 1638-1643.

[SCH13] Schrödel, T., Prevedel, R., Aumayr, K., Zimmer, M., & Vaziri, A. (2013). Brain-wide 3D imaging of neuronal activity in Caenorhabditis elegans with sculpted light. *Nature methods, 10*(10), 1013.

[SCH18] Schaefer, A., Kong, R., Gordon, E. M., Laumann, T. O., Zuo, X. N., Holmes, A. J., ... & Yeo, B. T. (2018). Local-global parcellation of the human cerebral cortex from intrinsic functional connectivity MRI. *Cerebral Cortex, 28*(9), 3095-3114.

[SEJ14] Sejnowski, T. J., Churchland, P. S., & Movshon, J. A. (2014). Putting big data to good use in neuroscience. *Nature neuroscience, 17*(11), 1440.

[SHE88] Shepherd, G. M. (1988). Neurobiology. *Oxford University Press*.

[SHE10] Sheline, Y. I., Price, J. L., Yan, Z., & Mintun, M. A. (2010). Resting-state functional MRI in depression unmasks increased connectivity between networks via the dorsal nexus. *Proceedings of the National Academy of Sciences, 107*(24), 11020-11025.

[SHE13] Shen, X., Tokoglu, F., Papademetris, X., & Constable, R. T. (2013). Groupwise whole-brain parcellation from resting-state fMRI data for network node identification. *Neuroimage, 82*, 403-415.

[SHI00] Shi, J., & Malik, J. (2000). Normalized cuts and image segmentation. *IEEE Transactions on pattern analysis and machine intelligence, 22*(8), 888-905.

[SHI12] Shirer, W. R., Ryali, S., Rykhlevskaia, E., Menon, V., & Greicius, M. D. (2012). Decoding subject-driven cognitive states with whole-brain connectivity patterns. *Cerebral cortex, 22*(1), 158-165.

[SHU97] Shulman, G. L., Fiez, J. A., Corbetta, M., Buckner, R. L., Miezin, F. M., Raichle, M. E., & Petersen, S. E. (1997). Common blood flow changes across visual tasks: II. Decreases in cerebral cortex. *Journal of cognitive neuroscience, 9*(5), 648-663.

[SHU04] Shulman, R. G., Rothman, D. L., Behar, K. L., & Hyder, F. (2004). Energetic basis of brain activity: implications for neuroimaging. *Trends in neurosciences, 27*(8), 489-495.

[SJØ20] Sjøgård, M., Bourguignon, M., Costers, L., Dumitrescu, A., Coolen, T., Roshchupkina, L., ... & Van Schependom, J. (2020). Intrinsic/extrinsic duality of large-scale neural functional integration in the human brain. *bioRxiv*.

[SMI04] Smith, S. M., Jenkinson, M., Woolrich, M. W., Beckmann, C. F., Behrens, T. E., Johansen-Berg, H., ... & Niazy, R. K. (2004). Advances in functional and structural MR image analysis and implementation as FSL. *Neuroimage, 23*, S208-S219.

[SMI09] Smith, S. M., Fox, P. T., Miller, K. L., Glahn, D. C., Fox, P. M., Mackay, C. E., ... & Beckmann, C. F. (2009). Correspondence of the brain's functional

architecture during activation and rest. *Proceedings of the National Academy of Sciences, 106*(31), 13040-13045.

[SMI13] Smith, S. M., Beckmann, C. F., Andersson, J., Auerbach, E. J., Bijsterbosch, J., Douaud, G., ... & Kelly, M. (2013). Resting-state fMRI in the human connectome project. *Neuroimage, 80*, 144-168.

[SNE73] Sneath PH, Sokal RR (1973) *Numerical taxonomy*. The principles and practice of numerical classification (a series of books in biology), vol 573. WF Freeman and Co., San Francisco.

[SPE18] Spencer, N. J., Hibberd, T. J., Travis, L., Wiklendt, L., Costa, M., Hu, H., ... & Sorensen, J. (2018). Identification of a rhythmic firing pattern in the enteric nervous system that generates rhythmic electrical activity in smooth muscle. *Journal of Neuroscience, 38*(24), 5507-5522.

[SPO05] Sporns, O., Tononi, G., & Kötter, R. (2005). The human connectome: a structural description of the human brain. *PLoS Comput Biol, 1*(4), e42.

[SPO07] Sporns, O., Honey, C. J., & Kötter, R. (2007). Identification and classification of hubs in brain networks. *PloS one, 2*(10), e1049.

[SPO11] Sporns, O. (2011). The human connectome: a complex network. *Annals of the New York Academy of Sciences, 1224*(1), 109-125.

[SPRE10] Spreng, R. N., Stevens, W. D., Chamberlain, J. P., Gilmore, A. W., & Schacter, D. L. (2010). Default network activity, coupled with the frontoparietal control network, supports goal-directed cognition. *Neuroimage, 53*(1), 303-317.

[STA08] Stark, D. E., Margulies, D. S., Shehzad, Z. E., Reiss, P., Kelly, A. C., Uddin, L. Q., ... & Milham, M. P. (2008). Regional variation in interhemispheric coordination of intrinsic hemodynamic fluctuations. *Journal of Neuroscience, 28*(51), 13754-13764.

[STA14] Stafford, J. M., Jarrett, B. R., Miranda-Dominguez, O., Mills, B. D., Cain, N., Mihalas, S., ... & Fryer, J. D. (2014). Large-scale topology and the default mode network in the mouse connectome. *Proceedings of the National Academy of Sciences, 111*(52), 18745-18750.

[STE56] Steinhaus, H. (1956). Sur la division des corp matériels en parties. *Bull. Acad. Polon. Sci, 1*(804), 801.

[STE10] Stephan, K. E., Penny, W. D., Moran, R. J., den Ouden, H. E., Daunizeau, J., & Friston, K. J. (2010). Ten simple rules for dynamic causal modeling. *Neuroimage, 49*(4), 3099-3109.

[SUP08] Supekar, K., Menon, V., Rubin, D., Musen, M., & Greicius, M. D. (2008). Network analysis of intrinsic functional brain connectivity in Alzheimer's disease. *PLoS Comput Biol, 4*(6), e1000100.

[SUZ06] Suzuki, R., & Shimodaira, H. (2006). Pvclust: an R package for assessing the uncertainty in hierarchical clustering. *Bioinformatics, 22*(12), 1540-1542.

[TAL49] Talairach, J., Hecaen, H., David, M., Monnier, M., & Deajuriaguerra, J. (1949). Recherches sur la coagulation thérapeutique des structures sous-corticales chez lhomme. *Revue neurologique, 81*(1), 4-24.

[TAL52] Talairach J, De Ajuriaguerra J, David M (1952) Etudes stéréotaxiques des structures encephaliques profondes chez l'homme. Technique - Intérêt physiopathologique et thérapeutique. *La Presse Médicale 60*:605-609.

[TAL67] Talairach, J., Szikla, G., Tournoux, P., Prossalentis, A., Bordas-Ferrer, M., & Covella, L. lacob M, Mempel E (1967) Atlas d'anatomie stéréotaxique du télencéphale. (Cie M&, eds). Paris.

[TAV16] Tavor, I., Jones, O. P., Mars, R. B., Smith, S. M., Behrens, T. E., & Jbabdi, S. (2016). Task-free MRI predicts individual differences in brain activity during task performance. *Science, 352*(6282), 216-220.

[TER75] Ter-Pogossian, M. M., Phelps, M. E., Hoffman, E. J., & Mullani, N. A. (1975). A positron-emission transaxial tomograph for nuclear imaging (PETT). *Radiology, 114*(1), 89-98.

[THO14] Thompson, P. M., Stein, J. L., Medland, S. E., Hibar, D. P., Vasquez, A. A., Renteria, M. E., ... & Wright, M. J. (2014). The ENIGMA Consortium: large-scale collaborative analyses of neuroimaging and genetic data. Brain imaging and behavior, 8(2), 153-182.

[TOG03] Toga, A. W., & Thompson, P. M. (2003). Mapping brain asymmetry. *Nature Reviews Neuroscience, 4*(1), 37-48.

[TOM13] Tomasi, D., Wang, G. J., & Volkow, N. D. (2013). Energetic cost of brain functional connectivity. *Proceedings of the National Academy of Sciences, 110*(33), 13642-13647.

[TON12] Tong, F., & Pratte, M. S. (2012). Decoding patterns of human brain activity. *Annual review of psychology, 63*, 483-509.

[TUR11] Turken AU, Dronkers, NF (2011). The neural architecture of the language comprehension network: converging evidence from lesion and connectivity analyses. *Frontiers in systems neuroscience, 5*:1.

[TZO97] Tzourio, N., El Massioui, F., Crivello, F., Joliot, M., Renault, B., & Mazoyer, B. (1997). Functional anatomy of human auditory attention studied with PET. *Neuroimage, 5*(1), 63-77.

[TZO02] Tzourio-Mazoyer, N., Landeau, B., Papathanassiou, D., Crivello, F., Etard, O., Delcroix, N., ... & Joliot, M. (2002). Automated anatomical labeling of activations in SPM using a macroscopic anatomical parcellation of the MNI MRI single-subject brain. *Neuroimage, 15*(1), 273-289.

[TZO16a] Tzourio-Mazoyer, N. (2016). Intra-and inter-hemispheric connectivity supporting hemispheric specialization. In *Micro-, meso-and macro-connectomics of the brain* (pp. 129-146). Springer, Cham.

[TZO16b] Tzourio-Mazoyer, N. (2016). Intra-and inter-hemispheric connectivity supporting hemispheric specialization. In *Micro-, meso-and macro-connectomics of the brain* (pp. 129-146). Springer, Cham.

[TZO20] Tzourio-Mazoyer N., Labache L., Zago L., Hesling I., Mazoyer B. (2020). Neural support of manual preference based on right and left during right and left finger-tapping induced activations and resting-state connectivity in 287 healthy adults balanced for handedness. Submitted to *Laterality*.

[UGU13] Uğurbil, K., Xu, J., Auerbach, E. J., Moeller, S., Vu, A. T., Duarte-Carvajalino, J. M., ... & Strupp, J. (2013). Pushing spatial and temporal resolution for functional and diffusion MRI in the Human Connectome Project. *Neuroimage, 80*, 80-104.

[UHR18] Uhrig, L., Sitt, J. D., Jacob, A., Tasserie, J., Barttfeld, P., Dupont, M., ... & Jarraya, B. (2018). Resting-state dynamics as a cortical signature of anesthesia in monkeys. *Anesthesiology, 129*(5), 942-958.

[URC19] Urchs, S., Armoza, J., Moreau, C., Benhajali, Y., St-Aubin, J., Orban, P., & Bellec, P. (2019). MIST: A multi-resolution parcellation of functional brain networks. *MNI Open Research, 1*(3), 3.

[VEN80] Venn, J. (1880). I. On the diagrammatic and mechanical representation of propositions and reasonings. *The London, Edinburgh, and Dublin philosophical magazine and journal of science, 10*(59), 1-18.

[VIN07] Vincent, J. L., Patel, G. H., Fox, M. D., Snyder, A. Z., Baker, J. T., Van Essen, D. C., ... & Raichle, M. E. (2007). Intrinsic functional architecture in the anaesthetized monkey brain. *Nature, 447*(7140), 83-86.

[VIN19] Vingerhoets, G. (2019). Phenotypes in hemispheric functional segregation? Perspectives and challenges. *Physics of life reviews, 30*, 1-18.

[WAD60] Wada, J., & Rasmussen, T. (1960). Intracarotid injection of sodium amytal for the lateralization of cerebral speech dominance: experimental and clinical observations. *Journal of neurosurgery, 17*(2), 266-282.

[WAE20] Weaverdyck, M. E., Lieberman, M. D., & Parkinson, C. (2020). Multivoxel pattern analysis in fMRI: A practical introduction for social and affective neuroscientists. *Social Cognitive and Affective Neuroscience*.

[WAN15] Wang, D., Buckner, R. L., Fox, M. D., Holt, D. J., Holmes, A. J., Stoecklein, S., ... & Baker, J. T. (2015). Parcellating cortical functional networks in individuals. *Nature neuroscience, 18*(12), 1853.

[WAR63] Ward Jr, J. H. (1963). Hierarchical grouping to optimize an objective function. *Journal of the American statistical association, 58*(301), 236-244.

[WED95] Wedeen, V. J., Davis, T. L., Weisskoff, R. M., Tootell, R., Rosen, B. R., & Belliveau, J. W. (1995). White matter connectivity explored by MRI. In Proceedings of the First International Conference for Functional Mapping of the Human Brain, Paris P (Vol. 1, p. 69).

[WEI17] Wei, D., Zhuang, K., Chen, Q., Yang, W., Liu, W., Wang, K., ... & Qiu, J. (2017). Structural and functional MRI from a cross-sectional Southwest University Adult lifespan Dataset (SALD). *BioRxiv*, 177279.

[WIC16] H. Wickham. ggplot2: Elegant Graphics for Data Analysis. *Springer-Verlag New York*, 2016.

[WOL11] Wolf, L., Goldberg, C., Manor, N., Sharan, R., & Ruppin, E. (2011). Gene expression in the rodent brain is associated with its regional connectivity. *PLoS computational biology,* 7(5), e1002040.

[YEO11] Thomas Yeo, B. T., Krienen, F. M., Sepulcre, J., Sabuncu, M. R., Lashkari, D., Hollinshead, M., ... & Fischl, B. (2011). The organization of the human cerebral cortex estimated by intrinsic functional connectivity. *Journal of neurophysiology, 106*(3), 1125-1165.

[YEO13] Yeo, B. T., Krienen, F. M., Chee, M. W., & Buckner, R. L. (2014). Estimates of segregation and overlap of functional connectivity networks in the human cerebral cortex. *Neuroimage, 88*, 212-227.

[YEO16] Yeo, B. T., & Eickhoff, S. B. (2016). Systems neuroscience: A modern map of the human cerebral cortex. *Nature, 536*(7615), 152-154

[ZAG16] Zago, L., Petit, L., Mellet, E., Jobard, G., Crivello, F., Joliot, M., ... & Tzourio-Mazoyer, N. (2016). The association between hemispheric specialization for language production and for spatial attention depends on left-hand preference strength. *Neuropsychologia, 93*, 394-406.

[ZAG17] Zago, L., Hervé, P. Y., Genuer, R., Laurent, A., Mazoyer, B., Tzourio-Mazoyer, N., & Joliot, M. (2017). Predicting hemispheric dominance for language production in healthy individuals using support vector machine. *Human Brain Mapping, 38*(12), 5871-5889.

[ZAG20] Zago L., Labache L., Tzourio-Mazoyer N., Mazoyer B. (2020). Atlas of Lateralized Attention Networks (ALANs) in right-handers. *BioRxiv.*

[ZAL10] Zalesky, A., Fornito, A., Harding, I. H., Cocchi, L., Yücel, M., Pantelis, C., & Bullmore, E. T. (2010). Whole-brain anatomical networks: does the choice of nodes matter? *Neuroimage, 50*(3), 970-983.

[ZAL12] Zalesky, A., Cocchi, L., Fornito, A., Murray, M. M., & Bullmore, E. D. (2012). Connectivity differences in brain networks. *Neuroimage, 60*(2), 1055-1062.

[ZHA10] Zhang, D., & Raichle, M. E. (2010). Disease and the brain's dark energy. *Nature Reviews Neurology, 6*(1), 15.

[ZHO10] Zhou, J., Greicius, M. D., Gennatas, E. D., Growdon, M. E., Jang, J. Y., Rabinovici, G. D., ... & Seeley, W. W. (2010). Divergent network connectivity

changes in behavioural variant frontotemporal dementia and Alzheimer's disease. *Brain, 133*(5), 1352-1367.

[ZHU12] Zhu, D., Li, K., Faraco, C. C., Deng, F., Zhang, D., Guo, L., ... & Liu, T. (2012). Optimization of functional brain ROIs via maximization of consistency of structural connectivity profiles. *NeuroImage, 59*(2), 1382-1393.

[ZHU13] Zhu, D., Li, K., Guo, L., Jiang, X., Zhang, T., Zhang, D., ... & Wee, C. Y. (2013). DICCCOL: dense individualized and common connectivity-based cortical landmarks. *Cerebral cortex, 23*(4), 786-800.

[ZIL15] Zilles, K., Bacha-Trams, M., Palomero-Gallagher, N., Amunts, K., & Friederici, A. D. (2015). Common molecular basis of the sentence comprehension network revealed by neurotransmitter receptor fingerprints. *Cortex, 63*, 79-89.

[ZUO10a] Zuo, X. N., Di Martino, A., Kelly, C., Shehzad, Z. E., Gee, D. G., Klein, D. F., ... & Milham, M. P. (2010). The oscillating brain: complex and reliable. *Neuroimage, 49*(2), 1432-1445.

[ZUO10b] Zuo, X. N., Kelly, C., Adelstein, J. S., Klein, D. F., Castellanos, F. X., & Milham, M. P. (2010). Reliable intrinsic connectivity networks: test–retest evaluation using ICA and dual regression approach. *Neuroimage, 49*(3), 2163-2177.

[ZUO12] Zuo, X. N., Ehmke, R., Mennes, M., Imperati, D., Castellanos, F. X., Sporns, O., & Milham, M. P. (2012). Network centrality in the human functional connectome. *Cerebral cortex, 22*(8), 1862-1875.

Annexes

1. Construction du référentiel stéréotaxique

La construction de l'espace proportionnel de Talairach (Figure 32) pour un individu repose sur la localisation et l'alignement de deux repères anatomiques (amers[78] ou points remarquables communs) [TAL52] ; la commissure antérieure (CA, origine de l'espace 3D) et la commissure postérieure (CP). Ces deux points sont des faisceaux de fibres blanches reliant les deux hémisphères. Le choix de ces faisceaux est justifié par leur proximité avec les noyaux gris centraux, structures ayant la plus faible variabilité interindividuelle.

L'établissement des amers permet de définir un plan bicommissural (plan CA-CP, axe z, coupe axiale) perpendiculaire au plan inter-hémisphérique (axe y, coupe sagittale) défini à partir de la scissure longitudinale (Figure 32). Deux plans verticaux supplémentaires sont ensuite définis (axe x, coupe coronale) ; l'un passant par la CA (VCA), l'autre par la CP (VCP). Les limites de l'espace tridimensionnel de Talairach sont ensuite fixées par les points ; le plus haut du cortex pariétal, le plus postérieur du cortex occipital, le plus bas du cortex temporal, le plus antérieur du cortex frontal et le plus latéral du cortex pariéto-temporal, la boîte de l'espace stéréotaxique est ainsi construite.

Le volume total est ensuite divisé par 8 au-dessus de la ligne CA-CP, en 4 en dessous, en 4 antérieurement et postérieurement à la ligne VCA et VCP respectivement. L'espace restant entre VCA et VCP est ensuite divisé par 3. Un espace proportionnel est ainsi construit et permet par la suite de normaliser tout individu par un jeu de transformations incluant une réorientation suivie d'un "*morphing*" permettant de ramener chacune de ces dimensions dans cet espace (largeur, hauteur, longueur), afin qu'une même structure anatomique apparaisse au même endroit pour un

[78] En écho à la navigation maritime, un amer est un point de repère fixe et sans ambiguïté utilisé pour naviguer à vue [MER14]. Dans l'espace de Talairach, les amers sont les deux commissures (CA et CP), l'occiput, le pôle frontal, le pôle occipital, et la voûte crânienne.

même triplet de coordonnées chez chaque individu. Pour se situer dans cet espace, il faut par la suite se référer à l'atlas de Talairach [TAL67] qui contient un template dont les structures cérébrales anatomiques et cytoarchitectoniques (d'après les aires de Brodmann) sont entièrement labellisées. La localisation de ces structures est en réalité probabiliste, Talairach faisant déjà à l'époque référence à une forte variabilité inter-individuelle du cortex [TAL67] ; il préconise d'ailleurs, en plus de cette approche indirecte de localisation, d'avoir recours à une approche directe permettant une meilleure localisation des structures cérébrales (telle que l'IRM). De plus, cet atlas se base uniquement sur l'hémisphère gauche (longtemps conservé dans le formol) d'une femme de 60 ans, faisant fi de la variabilité anatomique liée au sexe, à l'âge, à l'hémisphère et aux individus.

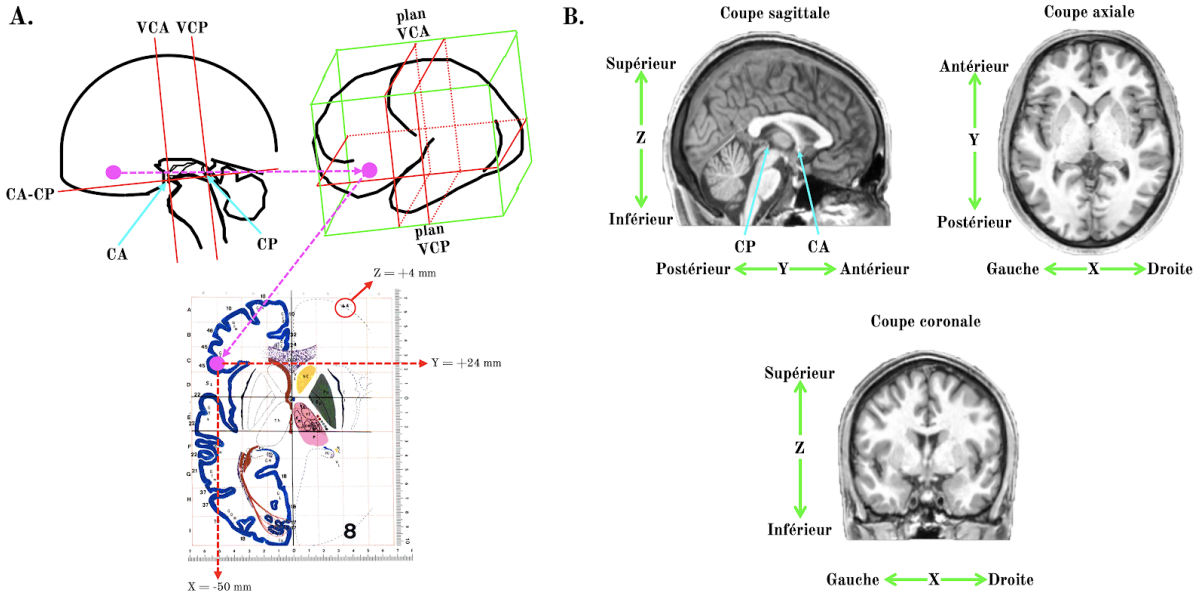

Figure 32 : A. Illustration de l'espace commun stéréotaxique de Talairach. *Après détection des commissures antérieure (CA) et postérieure (CP) permettant d'orienter le cerveau dans un plan horizontal perpendiculaire au plan inter-hémisphérique passant par la ligne CA-CP (en haut à gauche), et de la délimitation des plans verticaux de CA (VCA) et de CP (VCP) on peut appliquer les transformations proportionnelles afin de positionner le cerveau dans la boîte de l'espace stéréotaxique de Talairach (en haut à droite en vert). En bas au centre, coupe Z = 4 de l'atlas de référence de l'espace stéréotaxique de Talairach [TAL67], le rond rose illustre la localisation à partir d'un triplet de coordonnées stéréotaxiques du gyrus frontal inférieur gauche (X = -50 mm, Y = +24 mm, Z = +4 mm). Figure adaptée de [HOU02].* **B.** Système de référence en anatomie cérébrale. *Représentation des trois axes principaux utilisés dans l'espace de coordonnées stéréotaxique standard pour l'IRM. Vue T1 de la coupe sagittale, axiale et coronale d'un individu acquis sur un IRM 3T Siemens PRISMA.*

2. Etude de l'organisation cérébrale typique et atypique du langage

---

Labache, L., Mazoyer, B., Joliot, M., Crivello, F., Hesling, I., Tzourio-Mazoyer, N. (2020). Typical and atypical language brain organization according to intrinsic connectivity and multitasks functional asymmetries. *eLife*, sous presse.

RESEARCH ARTICLE

Typical and atypical language brain organization based on intrinsic connectivity and multitask functional asymmetries

Loïc Labache[1,2,3,4,5,6], Bernard Mazoyer[1,2,3,7]*, Marc Joliot[1,2,3], Fabrice Crivello[1,2,3], Isabelle Hesling[1,2,3], Nathalie Tzourio-Mazoyer[1,2,3]

[1]Université de Bordeaux, Institut des Maladies Neurodégénératives, UMR 5293, Groupe d'Imagerie Neurofonctionnelle, Bordeaux, France; [2]CNRS, Institut des Maladies Neurodégénératives, UMR 5293, Groupe d'Imagerie Neurofonctionnelle, Bordeaux, France; [3]CEA, Institut des Maladies Neurodégénératives, UMR 5293, Groupe d'Imagerie Neurofonctionnelle, Bordeaux, France; [4]Université de Bordeaux, Institut de Mathématiques de Bordeaux, UMR 5251, Bordeaux, France; [5]Bordeaux INP, Institut de Mathématiques de Bordeaux, UMR 5251, Bordeaux, France; [6]INRIA Bordeaux Sud-Ouest, Institut de Mathématiques de Bordeaux, UMR 5251, Contrôle de Qualité et Fiabilité Dynamique, Talence, France; [7]Centre Hospitalier Universitaire de Bordeaux, Bordeaux, France

Abstract Based on the joint investigation in 287 healthy volunteers (150 left-Handers (LH)) of language task-induced asymmetries and intrinsic connectivity strength of the sentence-processing supramodal network, we show that individuals with atypical rightward language lateralization (N = 30, 25 LH) do not rely on an organization that simply mirrors that of typical leftward lateralized individuals. Actually, the resting-state organization in the atypicals showed that their sentence processing was underpinned by left and right networks both wired for language processing and highly interacting by strong interhemispheric intrinsic connectivity and larger corpus callosum volume. Such a loose hemispheric specialization for language permits the hosting of language in either the left and/or right hemisphere as assessed by a very high incidence of dissociations across various language task-induced asymmetries in this group.

***For correspondence:** bernard.mazoyer@u-bordeaux.fr

Competing interests: The authors declare that no competing interests exist.

Funding: See page 26

Received: 08 May 2020
Accepted: 16 October 2020
Published: 16 October 2020

Reviewing editor: Ingrid S Johnsrude, University of Western Ontario, Canada

Introduction

Hemispheric specialization, and more particularly hemispheric specialization for language, can be defined as *"... a hemisphere-dependent relationship between a cognitive, sensory, or motor function and a set of brain structures. It includes both the hosting by a given hemisphere of specialized networks that have unique functional properties and mechanisms that enable the inter-hemispheric coordination necessary for efficient processing"* (***Hervé et al., 2013***). Major issues on the topic of hemispheric functional segregation have been listed in a recent review article (***Vingerhoets, 2019***). Highlighting the importance of in-depth investigations of individuals exhibiting atypical hemispheric lateralization for language production, several burning questions related to this atypical phenotype were identified including the characterization of its regional pattern, its relationship with handedness, its structural underpinnings, whether such atypicality holds for other cognitive functional phenotypes, and whether it is associated with variations in behavior and/or cognitive abilities.

To comprehensively understand typical and atypical hemispheric organization for high-order language processing, it is necessary to examine the functional organization of the language network in

the dominant hemisphere together with its interhemispheric coordination with the mirroring network in the opposite hemisphere. Such an approach can be completed by integrating different and complementary neuroimaging information provided by resting-state and task-induced activation investigations.

Task-induced functional asymmetries are reliable markers for assessing individuals' hemispheric specialization for language, as attested by the very good concordance between fMRI asymmetries measured during language tasks and Wada testing, which is considered the gold standard to measure dominance (**Dym et al., 2011**). This methodology makes it possible to revisit the incidence of atypical organization in healthy individuals in relationship with handedness. The earliest research on this topic reported that rare individuals presenting a shift in lateralization—having rightward asymmetry during language tasks—can be found in left-handers (**Hund-Georgiadis et al., 2002**; **Pujol et al., 1999**; **Szaflarski et al., 2002**). This last observation is consistent with previous aphasia studies (**Hécaen and Sauguet, 1971**) and investigations of epileptic patients with Wada testing (**Isaacs et al., 2006**), but the very low incidence of atypical individuals coupled with the low incidence of left handedness is a difficulty in the assessment of language lateralization variability in healthy individuals. To overcome this issue, we gathered a database of healthy volunteers specifically enriched in left-handers (BIL and GIN; **Mazoyer et al., 2016**) and measured the Hemispheric Functional Lateralization index (HFLI; **Wilke and Schmithorst, 2006**) for sentence production in 297 of its participants. We thereby uncovered 3 patterns of language lateralization, namely, 10 strong-atypical individuals with strong rightward lateralization that included only left-handers, 37 ambilateral individuals, including 23 left-handers, with weak or no lateralization and 250 typical individuals with strong leftward lateralization, including 120 left-handers (**Mazoyer et al., 2014**). In a subsequent investigation of regional asymmetries in these same participants, we provided evidence that there were no differences between typical right- and left-handers in terms of regional patterns of asymmetry. In contrast, left-handed ambilaterals were not lateralized unlike right-handed ambilaterals who showed a modest leftward asymmetry (**Tzourio-Mazoyer et al., 2016**). Left-handed ambilaterals were also characterized by higher connectivity at rest across homotopic language regions suggesting that enhanced interhemispheric cooperation at rest is a marker of increased interhemispheric cooperation associated with decreased asymmetries during sentence minus list production contrast (**Tzourio-Mazoyer et al., 2016**).

This last result highlights the importance of resting-state fMRI for the investigation of language network organization, as it makes it possible to measure the functional intrinsic connectivity of networks within each hemisphere and the differences in connectivity between the hemispheres. **Raemaekers et al., 2018** showed a significant association across individuals between the asymmetry in functional connectivity scores and the asymmetries in language task lateralization scores measured in language regions located along the longitudinal fissure in 423 healthy volunteers. Consistent with the Raemaekers et al. report, we have recently shown that in the left hemisphere, the resting-state degree centrality (Rs_DC), or strength of connectivity, was significantly correlated with task-induced activations in the supramodal network of regions dedicated to sentence processing (SENT_CORE; **Labache et al., 2019**). Moreover, the Reynolds' study involving 117 children demonstrated that asymmetry in the strength of connectivity between language areas followed the same developmental pattern of increases in asymmetry between 2 and 7 years old (**Reynolds et al., 2019**) as that reported with task-induced activations (**Friederici et al., 2011**; **Perani et al., 2011**). Finally, such asymmetries in within-hemisphere intrinsic connectivity at rest are modified in individuals with rightward lateralization for language production (**Joliot et al., 2016**). Taken together, these studies demonstrate that language network intrinsic connectivity and its asymmetry are important markers to characterize the variability in language organization in the brain.

A key issue that remains unresolved regarding the typical and atypical organization for language in healthy individuals is that of dissociation. Actually, there is very little knowledge on homogeneity in lateralization across different language components in healthy individuals. Neuropsychological studies such as the seminal study conducted by Hécaen in left-handers (**Hécaen and Sauguet, 1971**; **Hécaen et al., 1981**) have shown that hemispheric dominance is not a property of a given hemisphere but rather that the dominant hemisphere may shift for different language functions in some individuals. After left hemisphere lesions, left-handed aphasic patients can show rare deficits in comprehension, while deficits in production are constant, indicating a dissociation of these two language components (**Hécaen et al., 1981**). PET studies with healthy volunteers have provided evidence of

dissociations between production and comprehension in rare left-handers, with a leftward asymmetry during production and a rightward asymmetry during comprehension (for example, **Tzourio-Mazoyer et al., 2004**). In pathological states, particularly epilepsy, several studies have reported dissociations between asymmetries for language production and those for listening (**Baciu et al., 2003**; **Kurthen et al., 1994**; **Kurthen et al., 1992**; **Lee et al., 2008**), and the results of a longitudinal study of Wada testing in four of these patients suggested that language production was more likely to shift hemispheres than speech comprehension (**Lee et al., 2008**).

The occurrence of dissociation, particularly in some healthy individuals, suggests a potential independence of different language components in terms of hemispheric dominance, which calls for the search for factors in brain organization that could allow different language components to be hosted in different hemispheres. One hypothesis could be that a loose organization in terms of lateralization, marked by some bilateral involvement of language areas and strong interhemispheric connectivity, would make it possible for different language components to be lateralized in different hemispheres. In such a case, one should observe an increased occurrence of dissociations in atypicals, and a better knowledge of the characteristics of the individuals who are more likely to host dissociations will make it possible to optimize the neuroimaging paradigm used to determine language lateralization. For example, as implemented in presurgical evaluations of epileptic patients (**Baciu et al., 2003**; **Baciu et al., 2005**), a paradigm that includes a battery of language tasks in addition to production could be designed for this subpopulation.

Regarding these matters, the present study, which includes measures of lateralization during production, listening and reading tasks in the same participants, is an opportunity to refine the understanding of dissociations. Reading is the last language function acquired through development, since the emergence of this language component relies on strong interactions between speech, eye motor systems, and preorthographic processing by visuospatial attentional areas whose lateralization is located in different hemispheres (**Lobier et al., 2012**; **Petit et al., 2015**). One might suggest that dissociations between the lateralization of speech comprehension and production could occur from two different sources of variability: speech perception (**Zatorre et al., 2002**) and motor control of speech (**Lieberman et al., 2007**), respectively. Nevertheless, examining reading lateralization, which is established later on the basis of comprehension and production lateralization, will allow us to enlarge the question of the possible sources of interindividual variability in language lateralization to that of the relationships between rightward lateralized visuospatial functions and leftward lateralized language functions.

Hemispheric asymmetries in gray and white matter have been used to investigate variability in hemispheric specialization for language, although these measures mainly provide information on inherited gross anatomical differences between the two hemispheres, which are observable at the whole brain level as a global torsion of the brain (i.e. the Yakovlevian torque; **Toga and Thompson, 2003**). In areas related to language processing, such as the *planum temporale* close to the sylvian fissure, leftward asymmetries of fissure depth are seen in utero (**Habas et al., 2012**), and these asymmetries are of the same amplitude at birth as in adults (**Hill et al., 2010**), showing no subsequent modifications during development (**Li et al., 2014**). Notably, in adults, the gross leftward asymmetry of the *planum temporale* does not have the characteristics of a marker of hemispheric dominance at the individual level (**Tzourio-Mazoyer et al., 2018**). Even if some local relationships were found between gray matter and language task-induced functional asymmetries during word-listening, they explain only a small fraction of the interindividual variability of local functional asymmetries (**Josse et al., 2009**). The *corpus callosum,* made of fibers connecting both hemispheres, has also been investigated as it is the main anatomical support for interhemispheric connectivity. The *corpus callosum* surface or volume has thus been measured as a potential anatomical marker of this interhemispheric connectivity. Actually, during the course of phylogenesis, increasing brain volumes go along with decreasing corpus callosum volumes relative to brain size (review in **Hopkins and Cantalupo, 2008**). On this basis, one should expect that a strong lateralization would be associated with a smaller corpus callosum volume, as previously observed in males for anatomical hemispheric asymmetries (**Dorion et al., 2000**). To date, no studies have investigated the direct relationships between the interindividual variability in hemispheric specialization for language and anatomical hemispheric asymmetries or *corpus callosum* volume, so there is still no evidence of a direct association between anatomical and functional asymmetries.

This survey of previous findings can be summarized in the following way: leftward lateralized typical individuals can be right- or left-handers, they have leftward anatomical asymmetries both at the hemispheric level and at the regional level, they are leftward asymmetrical during language production and leftward asymmetrical for Rs_DC at rest, and they show lower intrinsic interhemispheric connectivity than individuals who are symmetrical during language production. In contrast, the type of organization in individuals who are not leftward lateralized is difficult to summarize because of the low incidence of atypical language lateralization and its heterogeneity. For instance, either a rightward asymmetry or an absence of asymmetry during language production can be observed in atypical individuals, corresponding either to a shift in the dominant hemisphere or to bilateral dominant or nondominant hemispheres, as we have previously shown using support vector machine (***Zago et al., 2017***). Moreover, to our knowledge, there is a lack of information on the lateralization of language comprehension and reading and the occurrence of dissociations in relation to typical or atypical language organization.

Another open question is the relationship between typical and atypical hemispheric specialization for language and cognitive performance that can be envisioned within different frameworks. Some authors have proposed that the decreased verbal performance observed in language developmental disorders may be related to a lack of lateralization (***Bishop, 2013***; ***Tallal, 1981***; ***Tallal and Schwartz, 1981***). In healthy volunteers, there is some evidence of such a relationship but with a moderate impact on performance not specific to verbal abilities (***Mellet et al., 2014b***). A larger framework would be the possible association between defects in complementary specialization and nonoptimal cognitive functioning (reviewed in ***Vingerhoets, 2019***), with such an abnormal setting of complementary specialization being expected to occur in individuals with atypical hemispheric specialization for language brain organization.

To address these important questions regarding the interindividual variability in language organization in healthy individuals, we investigated 287 participants from the BIL and GIN who completed both resting-state fMRI and task-related fMRI during sentence-production, sentence-listening and sentence-reading tasks. These participants were also mapped for their anatomical hemispheric asymmetries and completed a battery of seven verbal and four visuospatial tests (***Mazoyer et al., 2016***).

Results

Descriptive statistics of the groups identified by hierarchical clustering

The agglomerative hierarchical procedure resulted in the identification of 3 clusters; three clusters were found to be optimal by 14 R statistical indices (from over 30 that were used to assess the quality of the classification). Hereafter, we will refer to these clusters as groups varying in their 'language organization'. These three clusters were labeled according to their task-induced mean asymmetries: a first cluster including 125 participants with strong leftward asymmetries in the three language tasks was named strong typical (TYP_STRONG; see ***Table 1*** and ***Figure 1***), a second cluster of 132 participants exhibiting moderate leftward asymmetry was labeled mild typical (TYP_MILD), while the third cluster included the remaining 30 participants showing rightward mean asymmetry in the three tasks was labeled atypical (ATYP). Whenever needed, the TYP_STRONG and TYP_MILD groups were pooled and referred to as the TYP group.

Task performance

Response time in each of the three tasks did not depend on 'language organization' (***Table 2***), when age, handedness and sex were taken into account (all $p>0.49$). The mean number of words generated per sentence was 12.4 (SD = 2.0), was also independent of 'language organization' classification, when age, handedness and sex were taken into account ($p=0.97$). Note that the average number of recalled sentences was 9.42 (SD = 0.96) for a maximum of 10.

Demography and handedness

A significant difference was observed in the proportion of left-handers among the 3 'language organization' groups ($p=0.0007$) due to a larger proportion of left-handers in the ATYP (83.3%) than in either the TYP_MILD (49.3%) or TYP_STRONG (46.4%) groups. The differences in the proportion of left-handers were significant between the ATYP and TYP_MILD groups ($p=0.0007$) and ATYP and

Table 1. Characteristics of the three groups after hierarchical clustering on the variables that served at the classification and also on absolute values of task-induced asymmetries.

SENT_CORE network asymmetry (left minus right) was calculated as the volumetric mean of the 18 hROIs in each contrast while hub asymmetry was calculated as the volumetric mean of the 3 hROIs classified as hubs in 145 right-handers (RH)(inferior frontal gyrus: F3t, and two regions of the superior temporal sulcus: STS3 and STS4). mIHHC corresponds to the averaged resting-state Inter Hemispheric Homotopic Correlation across the 18hROIs composing SENT_CORE (Rs_mIHHC). Resting-state Degree Connectivity (Rs_DC) was calculated in the SENT_CORE network in each hemisphere. Mean Rs_DC corresponds to the mean of the left and right SENT_CORE Rs_DC. The standard deviations are between brackets.

	TYP_STRONG N = 125	TYP_MILD N = 132	ATYP N = 30
Task-induced variables			
SENT_CORE asymmetry			
$PROD_{SENT\text{-}WORD}$	0.557 (0.17)	0.296 (0.12)	−0.114 (0.19)
$LISN_{SENT\text{-}WORD}$	0.299 (0.13)	0.167 (0.09)	−0.155 (0.17)
$READ_{SENT\text{-}WORD}$	0.351 (0.18)	0.217 (0.14)	−0.177 (0.15)
SENT_HUBS asymmetry			
$PROD_{SENT\text{-}WORD}$	0.80 (0.23)	0.391 (0.18)	−0.119 (0.30)
$LISN_{SENT\text{-}WORD}$	0.42 (0.19)	0.210 (0.15)	−0.291 (0.28)
$READ_{SENT\text{-}WORD}$	0.51 (0.29)	0.287 (0.23)	−0.358 (0.30)
SENT_CORE absolute asymmetry			
$PROD_{SENT\text{-}WORD}$	0.557 (0.17)	0.295 (0.12)	0.190 (0.12)
$LISN_{SENT\text{-}WORD}$	0.300 (0.12)	0.168 (0.08)	0.169 (0.12)
$READ_{SENT\text{-}WORD}$	0.351 (0.18)	0.221 (0.13)	0.189 (0.13)
SENT_HUBS absolute asymmetry			
$PROD_{SENT\text{-}WORD}$	0.803 (0.23)	0.393 (0.17)	0.250 (0.20)
$LISN_{SENT\text{-}WORD}$	0.430 (0.19)	0.214 (0.14)	0.318 (0.25)
$READ_{SENT\text{-}WORD}$	0.515 (0.30)	0.307 (0.20)	0.370 (0.28)
Resting-state variables			
Rs_mIHHC	0.571 (0.07)	0.578 (0.07)	0.610 (0.06)
mean Rs_DC	8.670 (1.42)	7.949 (1.24)	9.460 (1.60)
Rs_DC asymmetry	0.500 (0.77)	0.478 (0.64)	−0167 (0.78)

The online version of this article includes the following source data for Table 1:

Source data 1. Data Source for ***Table 1***.

Source data 2. Detailed information concerning the ***Table 1*** data Source file.

TYP_STRONG groups (p=0.0001), while no difference was observed between the TYP_MILD and TYP_STRONG groups (p=0.48).

The proportion of women differed among the three groups (p=0.006, chi-square test); the proportion was significantly higher in the TYP_MILD group (58%) than in the TYP_STRONG group (38%; p=0.0013, t-test) but was not different between the ATYP group (50%) and either the TYP_MILD (p=0.41) or TYP_STRONG (p=0.25) groups.

Note that there were no significant differences in age or cultural levels between the three groups (p>0.29 in both cases).

Profile of task-induced lateralization according to 'language organization'

A significant 'task' by 'language organization' interaction on the absolute values of task-induced asymmetry was found for both the SENT_CORE and the SENT_HUBS set of regions of interest

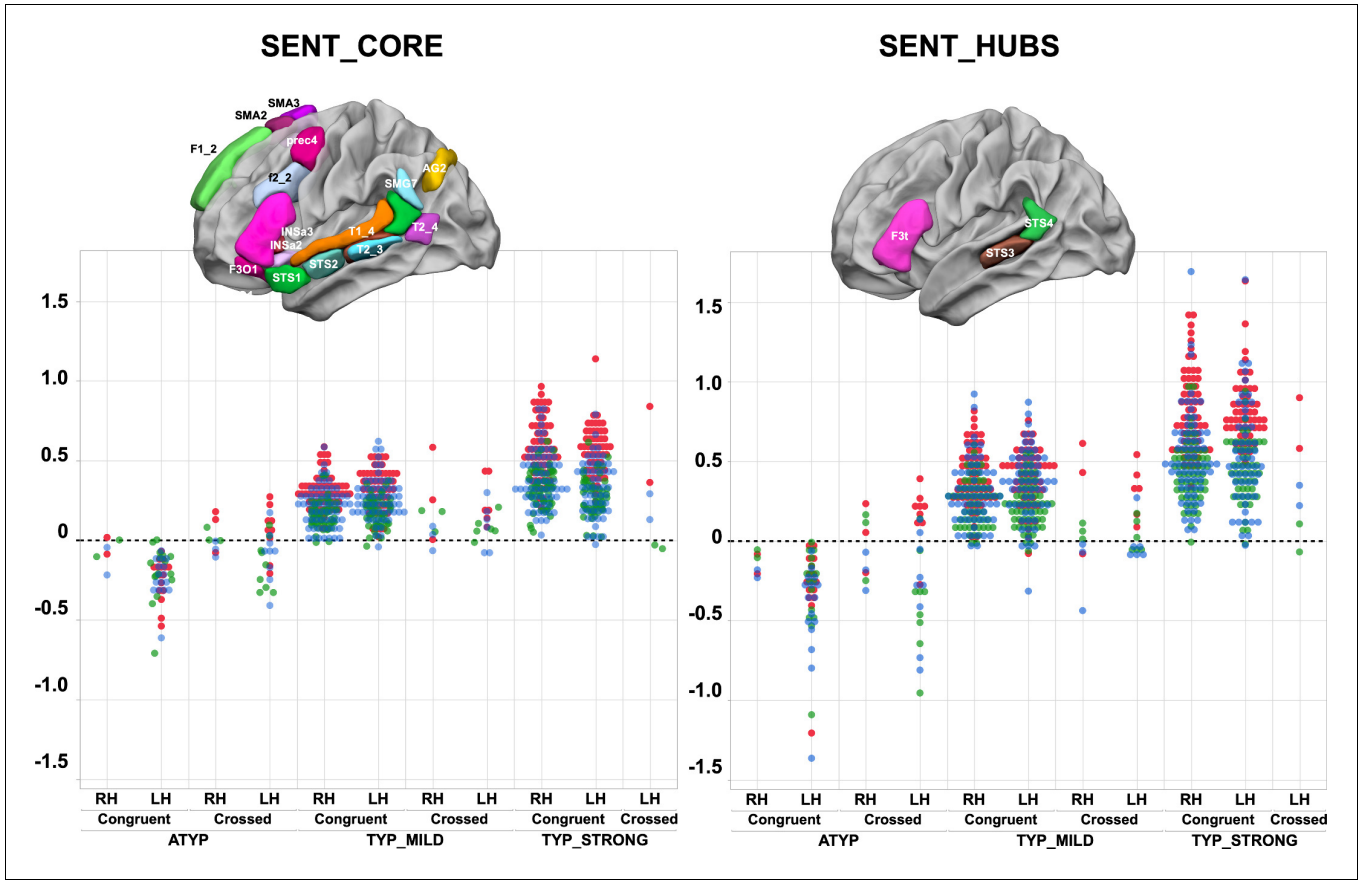

Figure 1. Scatterplots of individual asymmetry values in each task measured as the mean of SENT_CORE and as the mean of the three hubs (SENT_HUBS) for the three groups clustered by hierarchical clustering and stratified according to their status as CONGRUENT or CROSSED and their handedness (right-handers: RH, left-handers: LH) . The first row depicts the location of the 18 hROIs constituting the SENT_CORE network (left) and the 3 hROIs constituting SENT_HUBS (right). Atypicals (ATYP), typicals with moderate asymmetries (TYP_MILD) and typicals with strong asymmetries (TYP_STRONG) correspond to the three groups resulting from multitask and multimodal hierarchical agglomerative clustering. ($PROD_{SENT\text{-}WORD}$: red, $LISN_{SENT\text{-}WORD}$: green and $READ_{SENT\text{-}WORD}$: blue).
The online version of this article includes the following source data for figure 1:

Source data 1. Data source for ***Figure 1***.
Source data 2. Detailed information concerning the ***Figure 1*** data source file.

(ROIs) (MANOVA analyses, $p<10^{-4}$ for both cases; see ***Figure 1*** and ***Table 1***). Indeed, in contrast to the two other groups, the ATYP group did not show any difference in asymmetry across the language tasks in either SENT_CORE (all $p>0.99$) or SENT_HUBS ($p>0.83$). In contrast, there were significant differences between tasks for both the TYP_STRONG or TYP_MILD groups in both SENT_CORE and SENT_HUBS, with a stronger asymmetry during the $PROD_{SENT\text{-}WORD}$ than during the $READ_{SENT\text{-}WORD}$ task (all $p<0.001$), with the asymmetry during the latter being larger than that during the $LISN_{SENT\text{-}WORD}$ task (all $p<0.017$). Note that the 'task' main effect was significant for both SENT_CORE and SENT_HUBS ($p<10^{-4}$).

There was a significant 'language organization' by 'handedness' interaction on SENT_CORE ($p=10^{-4}$), although the interaction did not reach significance on SENT_HUBS ($p=0.12$). In SENT_CORE, this interaction was because the right-handed individuals in the TYP_STRONG group had higher asymmetry strength than the left-handers ($p=0.03$), while the opposite pattern was observed in the ATYP group: left-handers had stronger asymmetry strength than right-handers (uncorrected $p=0.0075$). Note that there were no differences between right-handers and left-handers in the

Table 2. Measures related to task execution in the three groups varying in hemispheric lateralization.
Mean (SD) of response times and self-reports of task difficulty rated on a 1 to 5 scale are shown for each fMRI run (Sentence production: PROD, sentence listening: LISN, sentence reading: READ). In addition, sample mean (SD) of the average number of words per sentence recalled during the debriefing of the PROD run is shown.

	TYP_STRONG N = 125	TYP_MILD N = 132	ATYP N = 30
Task difficulty			
LISN	1.12 (0.40)	1.14 (0.45)	1.25 (0.80)
READ	1.17 (0.40)	1.23 (0.55)	1.20 (0.43)
PROD	2.74 (1.07)	2.69 (1.06)	2.88 (1.10)
Response time (ms)			
LISN	388.8 (134)	386.3 (126)	396.9 (96)
READ	3733.3 (579)	3731.8 (560)	3755.8 (552)
PROD	5600.0 (850)	5631.2 (968)	5645.5 (1095)
Number of words per sentence			
PROD	12.36 (2.03)	12.37 (1.87)	12.36 (2.55)

The online version of this article includes the following source data for Table 2:
Source data 1. Data Source for ***Table 2***.
Source data 2. Detailed information concerning the ***Table 2*** data Source file.

TYP_MILD (p=0.64) and ATYP (p=0.08) groups. A similar pattern, although not reaching the significance threshold, was found in SENT_HUBS.

There was no main effect of 'handedness' on the absolute values of asymmetries with SENT_HUBS (p=0.94), but there was a significant effect with SENT_CORE (p=0.0023). Finally, there was no significant 'language organization' by 'handedness' by 'task' triple interaction (SENT_CORE: p=0.29; SENT_HUBS: p=0.57).

Intrinsic connectivity

In contrast to previous findings, there was no 'handedness' main effect or 'handedness' by 'language organization' interaction on any of the SENT_CORE intrahemispheric and interhemispheric intrinsic connectivity variables (p>0.52).

A significant main effect of 'language organization' was observed on the mean resting-state interhemispheric homotopic correlation (Rs_mIHHC, p=0.0077) due to significantly lower Rs_mIHHC in the TYP_STRONG group than in the ATYP group (p=0.01, see ***Table 1***), while there were no significant differences between the TYP_STRONG and TYP_MILD groups (p=0.12) or between the ATYP and TYP_MILD groups (p=0.20).

A significant main effect of 'language organization' was observed on the average of the left and right intrahemispheric degree centrality (Rs_DC, $p<10^{-4}$): the ATYP group showed a significantly higher average Rs_DC than either the TYP_MILD ($p<10^{-4}$) or TYP_STRONG (p=0.013) groups, while the TYP_STRONG group had a significantly higher average Rs_DC than the TYP_MILD group ($p<10^{-4}$).

A 'language organization' by 'side' interaction was also found to be significant on Rs_DC ($p<10^{-4}$): the ATYP group showed no leftward asymmetry (asymmetry not significantly different from 0: p=0.80), in contrast to both the TYP_STRONG and TYP_MILD groups (significant leftward asymmetry: both $p<10^{-4}$), leading to significant differences between the ATYP group and the two other groups (both $p<10^{-4}$), while Rs_DC leftward asymmetry was not different between the TYP_MILD and TYP_STRONG groups (p=0.96).

Inspection of the right and left Rs_DC values in the three groups showed two different patterns depending on the considered hemisphere (***Figure 2*** and ***Table 1***). In the left hemisphere, the TYP_MILD group had a significantly lower Rs_DC than the TYP_STRONG group (p=0.0018) but was not different from the ATYP group (p=0.063), and the TYP_STRONG group was not different from the ATYP group (p=1). In the right hemisphere (***Figure 2***), the ATYP group had very strong Rs_DC

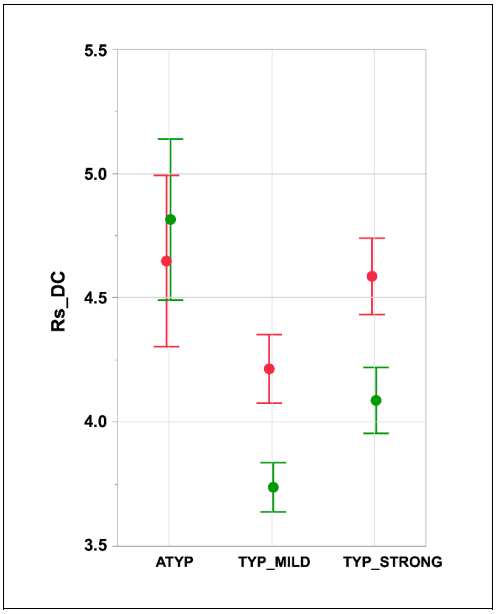

Figure 2. Intrahemispheric mean intrinsic connectivity strength of the SENT_CORE network in the three groups differing in language organization. Right (green) and left (red) values of the mean resting-state degree connectivity (Rs_DC) of SENT_CORE in the three groups. Significant leftward DC asymmetry is only present in TYP groups (Tukey's HSD test $p<10^{-4}$, N TYP_MILD = 132, N TYP_STRONG = 125) and right Rs_DC is higher in the ATYP group (N = 30) than in the TYP_STRONG and TYP_MILD groups ($p<10^{-4}$, Tukey's HSD test). Error bars correspond to the 95% confidence intervals.

The online version of this article includes the following source data for figure 2:

Source data 1. Data source for ***Figure 2***.
Source data 2. Detailed information concerning the ***Figure 2*** data source file.

values, which were larger than those in both the TYP_MILD ($p<10^{-4}$) and TYP_STRONG ($p<10^{-4}$) groups, whereas the TYP_STRONG group showed significantly larger Rs_DC values than the TYP_MILD group (p=0.0044).

Dissociations in asymmetry direction across tasks

Descriptive statistics

Twenty-three individuals exhibited dissociation in their asymmetries induced by the three language tasks. These 23 individuals will be referred to as 'CROSSED' and the others as 'CONGRUENT'. The occurrence of CROSSED individuals within each lateralization group was higher in the ATYP group (N = 12, 40%) than in either the TYP_MILD (N = 9, 6.82%, $p<10^{-4}$) or TYP_STRONG (N = 2, 1.6% $p<10^{-4}$) groups, while the difference in the occurrence of dissociation between the TYP_MILD and TYP_STRONG groups failed to reach significance (p=0.057).

Seventeen of the 23 (74%) CROSSED participants were left-handed, a proportion significantly larger than that in the rest of the sample (p=0.02). Meanwhile, the gender ratio was not different from the rest of the sample (10 women, 43%; p=0.60).

Dissociations in the CROSSED_ATYP individuals mostly corresponded to leftward asymmetry during $PROD_{SENT\text{-}WORD}$ together with rightward asymmetry during $READ_{SENT\text{-}WORD}$ and $LISN_{SENT\text{-}WORD}$, and this pattern held for both SENT_CORE and SENT_HUBS (***Figure 3***). Only 3 of the 12 CROSSED_ATYP individuals showed the reverse pattern of rightward asymmetry during $PROD_{SENT\text{-}WORD}$ together with leftward asymmetry during $READ_{SENT\text{-}WORD}$ and/or $LISN_{SENT\text{-}WORD}$ (see ***Figure 3***).

The picture was very different for dissociations in TYP_MILD individuals who were characterized by small rightward asymmetries mainly observed with $READ_{SENT\text{-}WORD}$ (only one participant had a strong negative asymmetry with $READ_{SENT\text{-}WORD}$ in SENT_HUBS). Finally, the two dissociations observed in the TYP_STRONG group were very weak negative asymmetries during $LISN_{SENT\text{-}WORD}$ regardless of the considered set of ROIs (see ***Figure 3***).

There was a main effect of 'dissociation' on the task-induced strength of asymmetry restricting the analysis to the ATYP and TYP_MILD groups, where DISSOCIATED had lower asymmetry strength than CONGRUENT in both SENT_CORE and SENT_HUBS (both p<0.013), without any interaction with"task' or"language organization' (all p>0.20).

Dissociation and resting-state organization

Considering the TYP individuals as a single group because they did not show any difference in Rs_DC (i.e. the TYP_MILD and TYP_STRONG groups were merged), there was a significant 'language organization' by 'dissociation' interaction on the mean Rs_DC value (p=0.049) due, in

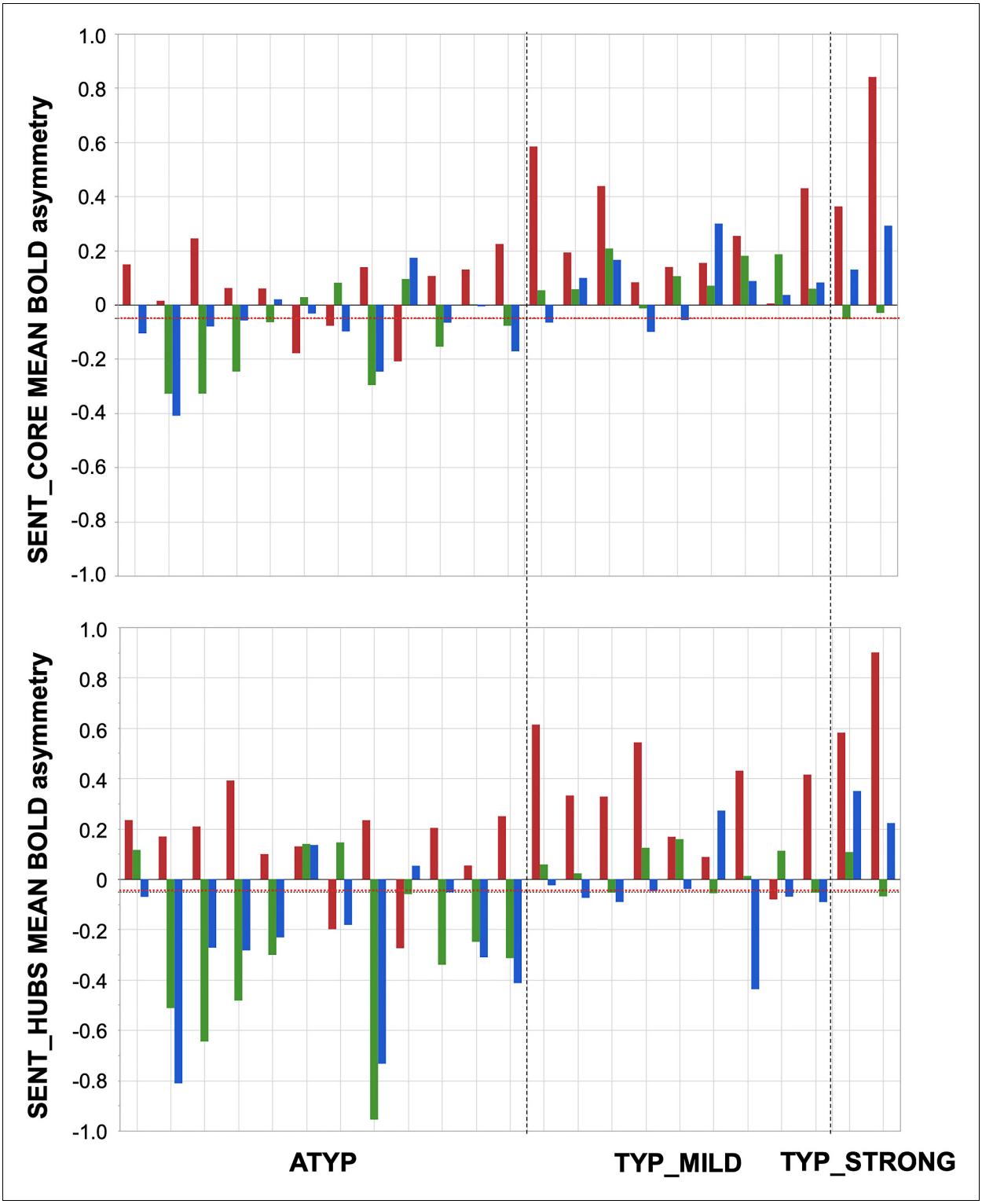

Figure 3. Participants showing dissociations between their three task-related functional asymmetries in each of the three groups classified by language organization. Individual values of left minus right blood oxygen level-dependent (BOLD) asymmetries measured during $PROD_{SENT\text{-}WORD}$ (red), $LISN_{SENT\text{-}WORD}$ (green) and $READ_{SENT\text{-}WORD}$ (blue) in SENT_CORE regions (top) and in SENT_HUBS (bottom). The red dotted line corresponds to the arbitrary threshold of 0.05 in asymmetry strength that was applied to define a rightward asymmetry.

Figure 3 continued on next page

Figure 3 continued

The online version of this article includes the following source data for figure 3:

Source data 1. Data source for ***Figure 3***.
Source data 2. Detailed information concerning the ***Figure 3*** data source file.

particular, to significantly higher mean Rs_DC in the CROSSED_ATYP individuals than in the CROSSED and CONGRUENT TYP individuals ($p<0.0027$, for all post hoc tests corrected for multiple comparisons). The CONGRUENT_ATYP individuals did not differ from the CROSSED or CONGRUENT TYP individuals (all $p>0.15$), and there was no difference between the CROSSED_TYP and CONGRUENT_TYP individuals ($p=0.92$). Note that there was no 'dissociation' main effect (all $p>0.18$) and no 'language organization' by 'dissociation' by 'side' interaction (p interaction = 0.60).

In contrast, there was a significant 'language organization' by 'dissociation' interaction on Rs_mIHHC ($p=0.02$, see ***Figure 4***) due, in particular, to significantly higher Rs_mIHHC in the CROSSED_ATYP individuals than in the CROSSED_TYP individuals (merging TYP_MILD and TYP_STRONG) that were not different in Rs_mIHHC whether CROSSED or CONGRUENT ($p<0.016$ for all, post hoc tests corrected for multiple comparisons). The CONGRUENT_ATYP individuals did not differ from the CROSSED or CONGRUENT TYP individuals (both $p>0.43$), nor did the CROSSED_TYP and CONGRUENT_TYP individuals differ ($p=0.91$).

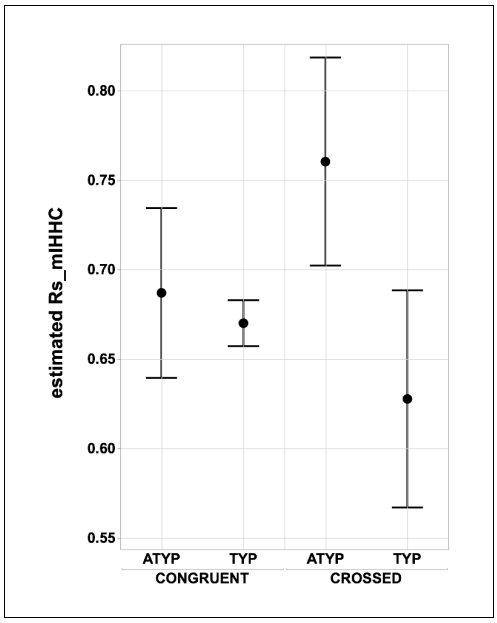

Figure 4. Interhemispheric intrinsic connectivity strength across homotopic regions (Rs_mIHHC) in SENT_CORE in the CONGRUENT and CROSSED TYP and ATYP groups. The estimated mean interhemispheric homotopic correlation expressed as the Fisher z-transformation of Rs_mIHHC is higher in the CROSSED atypicals group (N = 12) than in the TYP group (merging TYP_MILD and TYP_STRONG, N CROSSED = 11, N CONGRUENT = 246), regarding of whether they are CONGRUENT or CROSSED (both $p<0.016$, Tukey's HSD test).
The online version of this article includes the following source data for figure 4:

Source data 1. Data source for ***Figure 4***.
Source data 2. Detailed information concerning the ***Figure 4*** data source file.

Hemispheric anatomical asymmetries and corpus callosum volume

The tissue compartment values for the four groups (TYP or ATYP by CROSSED or CONGRUENT) are provided in ***Table 3***. Repeated measures MANCOVA of the GMasym and WMasym residuals (after adjusting these variables for sex, handedness, age, and total intracranial volume) showed a significant main effect of 'language organization' ($p=0.02$). Post hoc t-tests showed that both GMasym and WMasym were smaller in the ATYP group than in the TYP group ($p=0.03$). There was no effect of 'dissociation' ($p=0.99$) and no significant 'language organization' by 'dissociation' interaction ($p=0.36$). There was no interaction between 'tissue compartment' (gray or white matter) and 'language organization' ($p=0.92$) or between 'tissue compartment' and 'dissociation' ($p=0.26$), and there was no 'tissue compartment' by 'language organization' by 'dissociation' triple interaction ($p=0.15$).

ANOVA of the CCvol residuals (after adjustment for the same covariates as for GMasym and WMasym) showed a significant 'language organization' by 'dissociation' interaction ($p=0.049$). Post hoc analyses showed that the CROSSED_ATYP individuals had a larger CCvol volume than the CROSSED_TYP individuals (uncorrected post hoc t-test: $p=0.037$, HSD correction: $p=0.16$; see ***Table 1***).

Cognitive abilities

Results of principal component analysis (PCA) of the 11 scores on the verbal and visuospatial tests

The average scores for the 11 completed tests are presented for each group in ***Table 4***. PCA applied to the residuals of the scores (after adjustment for age, sex, cultural level and handedness) uncovered four components that explained 49% of the total variance. The first component, which we will refer to as spatial (SPA), aggregated residuals of the mental rotation test, the Corsi block test, the maze test, and the Raven matrices (loadings: 0.62, 0.39, 0.60, and 0.68, respectively). The second component, labeled phonological (PHONO), mainly included the pseudoword and rhyming test residuals (loadings: 0.48 and 0.72, respectively) and, marginally, the vocabulary test (loading: 0.36). The third component was mostly an auditory verbal memory component (MEM), including the auditory verbal word and pseudoword learning test residuals (loadings: 0.77 and 0.49, respectively). The fourth component was a verbal component (VERB) including all the verbal test residuals except those of the two learning tests, with the strongest loading being for the verb fluency test (0.64) and comparable loadings for each of the others (reading span test: 0.34, listening span test: 0.31, and vocabulary test: 0.31).

Cognitive skills and language organization

Repeated measures MANOVA of the four PCA components (SPA, MEM, PHONO, and VERB) revealed a significant 'language organization' by 'cognitive component' interaction (p=0.0003; ***Figure 5***), while the 'language organization' main effect was not significant (p=0.21).

Post hoc analyses showed that the 'language organization' by 'cognitive component' interaction was due to the difference in variation in SPA and MEM. The SPA scores were significantly higher in the TYP_STRONG group than in the two other groups, but the scores were not significantly different between the latter (TYP_STRONG: 0.29 ± 0.15; TYP_MILD: −0.19 ± 0.14; ATYP: −0.41 ± 0.29; uncorrected p<0.0063; TYP_MILD vs. ATYP, p=0.39). Meanwhile, the MEM scores were significantly lower in the ATYP group than in the two other groups (ATYP: −0.57 ± 0.23; TYP_MILD: 0.19 ± 0.11; TYP_STRONG: 0.05 ± 0.11; p<0.043). In addition, there was no effect of the 'language organization' on the other two verbal components, namely, VERB and PHONO (p>0.18 and p>0.13, respectively).

Finally, there was no relationship between dissociations and cognitive performance in either the ATYP or TYP_MILD individuals (p=0.17).

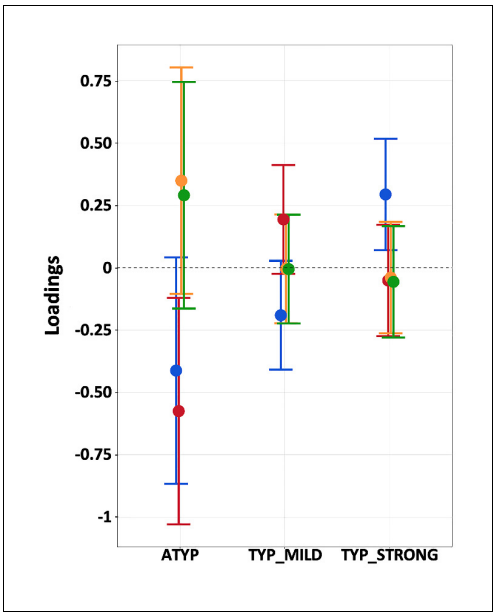

Figure 5. Estimated loadings of the four main principal components of cognitive abilities in the three groups having different language lateralization. The color code for the components is as follows: SPA: blue, MEM: red, PHONO: light orange, and VERB: green. Error bars represent 95% confidence intervals.

The online version of this article includes the following source data for figure 5:

Source data 1. Data source for ***Figure 5***.

Source data 2. Detailed information concerning the ***Figure 5*** data source file.

Comparison of different classifications for language lateralization

We compared the outcome of the present multitask multimodal hierarchical classification applied to the sample of 287 participants to those previously obtained with two different classifications based on the $PROD_{SENT\text{-}WORD}$ contrast only; these classifications included (1) a Gaussian mixture modeling of the HFLI observed for this contrast (***Mazoyer et al., 2014***) and (2) support

vector machine classification of each hemisphere dominance based on the pattern of its voxels in the $PROD_{SENT\text{-}WORD}$ contrast maps (***Zago et al., 2017***). The outcomes of the multitask multimodal hierarchical classification, Gaussian mixture modeling, and support vector machine classifications applied to the same sample of 287 participants are presented in ***Figure 6***.

Multitask multimodal hierarchical classification vs. Gaussian mixture modeling

There was a high concordance of classification of typicals with the two methods (98% of Gaussian mixture modeling typicals were classified as TYP_MILD or TYP_STRONG).

Gaussian mixture modeling identified 10 rightward lateralized LH (strong atypicals; GMM-SA in ***Figure 6***), among whom nine completed the resting-state acquisition and were thus included in the present study. These nine individuals were all clustered in the ATYP group as defined by the multitask multimodal hierarchical classification. We also found that 15 other individuals in the multitask multimodal hierarchical classification ATYP group actually belonged to the ambilateral group identified by Gaussian mixture modeling (GMM-AMB in ***Figure 6***) according to their weak $PROD_{SENT\text{-}WORD}$ HFLI. The remaining six individuals in the multitask multimodal hierarchical classification ATYP group were classified by Gaussian mixture modeling as typicals (GMM-TYP in ***Figure 6***) because of their leftward HFLI during $PROD_{SENT\text{-}WORD}$.

The multitask multimodal hierarchical classification did not individualize any cluster resembling the group of 37 ambilaterals as defined by Gaussian mixture modeling in the ***Mazoyer et al., 2014*** study. Rather, aside from the 15 aforementioned ambilaterals clustered in the ATYP group in the present study, the 22 other ambilaterals as defined by Gaussian mixture modeling were here classified either as TYP_MILD (N = 16) or TYP_STRONG (N = 6).

Note that whereas all Gaussian mixture modeling-SA were left-handers, 5 among the 135 right-handers (3.7%) were classified as atypical with multitask multimodal hierarchical classification: two among these were dissociated with leftward lateralization during language production in SENT_CORE and the SENT_HUBS, leaving only three right-handers with atyical organization in the three tasks (2%). These three right-handers were not classified as strong-atypical by Gaussian mixture

Table 3. Gray and white matter hemispheric volumes and their left minus right asymmetry (mean and (SD), in cc) as well as midsagittal corpus callosum volume (mean and (SD), in cc), in subgroups of individuals according to their multitask multimodal hierarchical classification and the absence/presence of dissociated task-related functional asymmetries.

TYP: participants classified with multitask multimodal hierarchical classification as either TYP_STRONG or TYP_MILD, that is showing TYP left functional lateralization; ATYP: participants classified with multitask multimodal hierarchical classification as ATYPICAL, that is showing atypical right functional lateralization. CROSSED: participants with at least one dissociation of functional lateralization among the three language tasks; CONGRUENT: participants with no dissociation.

	TYP		ATYP	
	Congruent N = 246	**Crossed N = 11**	**Congruent N = 18**	**Crossed N = 12**
Gray Matter				
Left	327.00 (32)	337.59 (47)	337.42 (35)	317.30 (16)
Right	315.64 (32)	325.72 (48)	327.77 (33)	306.48 (15)
Asymmetries	11.35 (4.00)	11.87 (4.50)	9.65 (5.03)	10.82 (3.82)
White Matter				
Left	216.67 (26)	221.92 (36)	222.43 (26)	208.61 (15)
Right	213.38 (25)	217.82 (35)	220.22 (25)	206.38 (14)
Asymmetries	3.33 (2.19)	4.11 (1.74)	2.22 (2.41)	2.23 (2.03)
Corpus Callosum	5.31 (0.85)	5.21 (0.67)	5.45 (0.90)	5.48 (0.74)

The online version of this article includes the following source data for Table 3:

Source data 1. Data Source for ***Table 3***.

Source data 2. Detailed information concerning the ***Table 3*** data Source file.

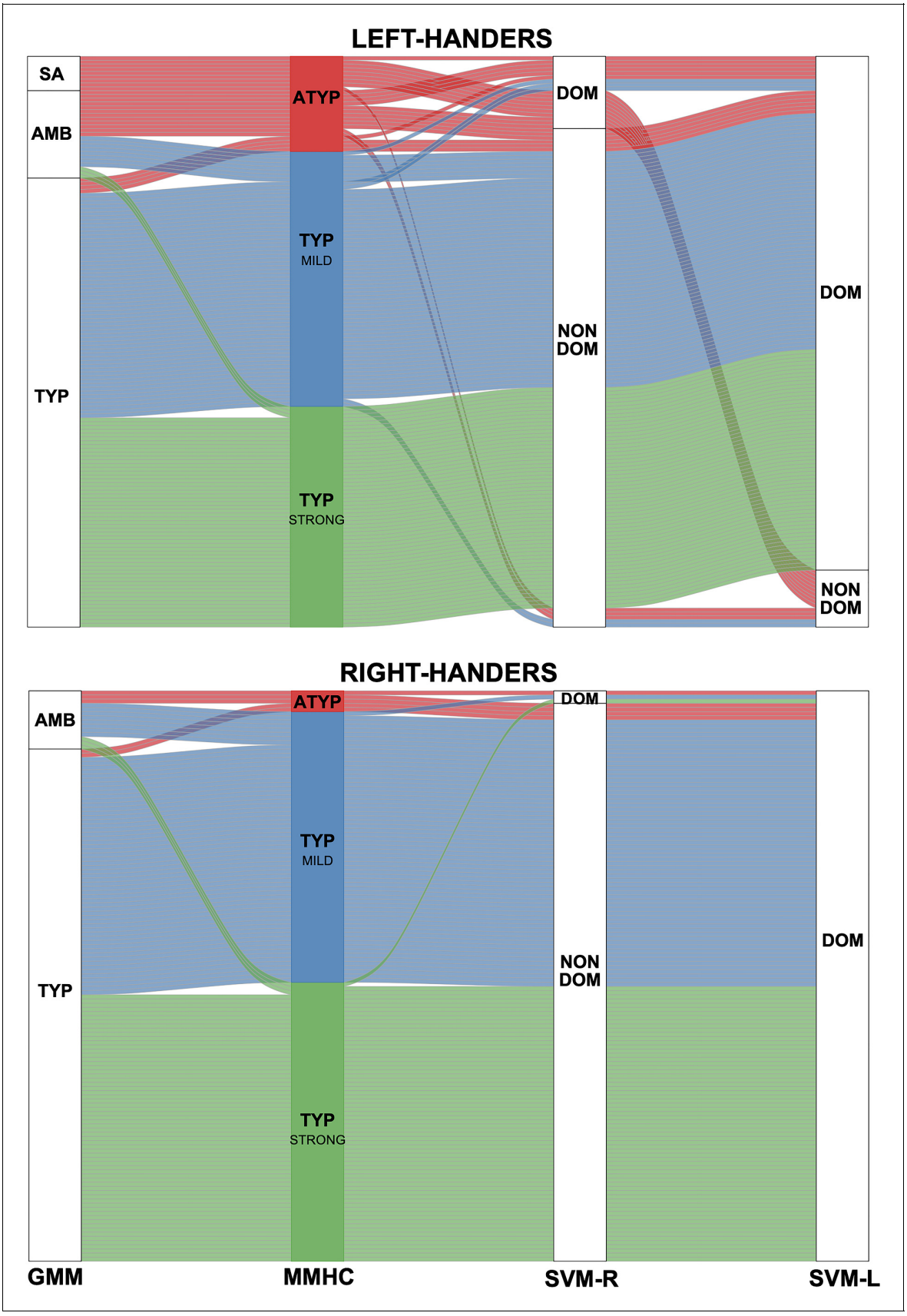
LEFT-HANDERS
SA
AMB
TYP
ATYP
TYP
MILD
TYP
STRONG
DOM
NON
DOM
DOM
NON
DOM
RIGHT-HANDERS
AMB
TYP
ATYP
TYP
MILD
TYP
STRONG
DOM
NON
DOM
DOM
GMM
MMHC
SVM-R
SVM-L

Figure 6. Alluvial plots comparing the present Multitask Multimodal Hierarchical Classification (MMHC) with two previous classifications only based on the functional asymmetry during production of sentences minus word-list in the same sample of participants: Gaussian Mixture Modeling (GMM) classification on Hemispheric Functional Lateralization Index (HFLI, ***Mazoyer et al., 2014***) and Support Vector Machine (***Zago et al., 2017***) classification in the right (SVM-R) and left hemisphere (SVM-L). Each line corresponds to a participant with the following color code: red for multitask multimodal hierarchical classification-atypical (ATYP), blue for multitask multimodal hierarchical classification-TYP_MILD, and green for multitask multimodal hierarchical classification-TYP_STRONG. The Gaussian mixture modeling method identified each individual as either strong_atypical (SA), ambilateral (AMB), or typical (TYP). identified the voxel-based pattern of each hemisphere of an individual as either dominant (DOM) or nondominant (NON DOM).

The online version of this article includes the following source data for figure 6:

Source data 1. Data source for ***Figure 6***.

Source data 2. Detailed information concerning the ***Figure 6*** data source file.

modeling but rather as ambilaterals because their HFLI for $PROD_{SENT-WORD}$, albeit negative, was above the threshold (−50) used for segregating strong atypicals from ambilaterals.

Multitask multimodal hierarchical classification vs. support vector machine

Seventeen of the 30 atypical individuals as defined by multitask multimodal hierarchical classification (57%) had a right-hemisphere labeled dominant by support vector machine. Conversely, the multitask multimodal hierarchical classification atypical cluster aggregated 77% of the 22 participants labeled as having a dominant right hemisphere. One should also note that 41% (7 among 17) of these right-hemisphere dominant ATYP individuals also had a left dominant hemisphere (i.e. were codominant), whereas the ATYP cluster aggregated 77% of the 12 participants labeled as having a codominant hemisphere. Notably, the eight ambilaterals as defined by Gaussian mixture modeling left-handers classified as having a dominant right-hemisphere pattern were classified as atypical by multitask multimodal hierarchical classification (***Zago et al., 2017***).

Table 4. Mean (SD, in cc) of scores at the different tests of the cognitive battery in the three groups differing in their language organization as defined by a multitask multimodal hierarchical classification.

	TYP_STRONG N = 125	TYP_MILD N = 132	ATYP N = 30
Verbal tests			
Rey: word learning	65.98 (7.57)	65.07 (7.51)	64.73 (7.57)
Pseudo-words learning	36.52 (10.44)	34.64 (11.16)	34.47 (9.68)
Verbal fluency	48.19 (9.82)	46.55 (10.01)	47.63 (8.85)
Reading span test	4.07 (1.08)	3.91 (1.11)	4.25 (1.11)
Listening span test	4.85 (1.06)	4.57 (1.14)	4.63 (1.21)
Vocabulary	28.39 (3.78)	27.80 (3.74)	28.07 (4.42)
Rhyming	68.38 (4.56)	67.17 (6.11)	65.93 (5.62)
Visuo-spatial tests			
Mental Rotation Test	11.08 (4.27)	10.70 (4.60)	10.17 (4.63)
Corsi block	5.99 (1.06)	5.72 (1.04)	5.73 (0.94)
Maze	6.68 (2.66)	6.09 (2.32)	4.42 (2.39)
Raven matrix	111.78 (9.70)	109.82 (10.47)	106.00 (9.48)

The online version of this article includes the following source data for Table 4:

Source data 1. Data Source for ***Table 4***.

Source data 2. Detailed information concerning the ***Table 4*** data Source file.

Summary of the results

In a sample of 287 healthy adults that included over 50% left-handers, a hierarchical classification based both on language task-induced asymmetries and on resting-state organization within the SENT_CORE network identified three clusters of individuals with different intra- and interhemispheric organization for sentence processing. Two clusters of similar sizes aggregated 257 (90% of the sample) leftward lateralized individuals. The 132 TYP_STRONG individuals (of which 46.4% were left-handers) were highly leftward lateralized for both task-induced asymmetry and intrahemispheric intrinsic connectivity, while showing low interhemispheric connectivity. This pattern of language organization was associated with strong leftward asymmetry of gray and white matter hemispheric volumes and with high visuospatial performance. The 125 TYP_MILD individuals (including 50.7% left-handers) differed from the TYP_STRONG individuals by their moderate leftward task-induced asymmetries, lower left hemisphere degree of connectivity and larger interhemispheric homotopic connectivity. The moderate leftward language organization in the TYP_MILD individuals was more frequent in women and was associated with a larger occurrence of dissociations than in the TYP_STRONG individuals (7% compared to 1.6%). Visuospatial cognitive abilities were lower in the TYP_MILD group than in the TYP_STRONG group. The third (ATYP) cluster of 30 individuals included the highest proportion of left-handers (83%). Mean asymmetry in the ATYP group was rightward lateralized during the three language tasks, with a striking lack of differences in asymmetry strengths across tasks, in contrast to the two groups of typicals. Organization at rest in the ATYP group was marked by bilateral high intrahemispheric connectivity and strong interhemispheric connectivity. Such a low hemispheric specialization pattern was associated with a high occurrence of dissociations among the functional asymmetries in the three language tasks (40%), lower leftward asymmetries of gray and white matter hemispheric volumes, and when dissociated, larger corpus callosum volumes. Finally, the ATYP cluster showed lower verbal memory abilities than the two other clusters. Comparison of the present classification to previous classifications based only on $PROD_{SENT\text{-}WORD}$ revealed the importance of the multitask approach conjointly with resting-state measures of Rs_DC in the language network to segregate the atypicals within the individuals with low $PROD_{SENT\text{-}WORD}$ hemispheric asymmetries.

Discussion

A multimodal multitask classification provides an enhanced definition of atypical language organization

Compared to the high consistency of the classification of individuals having typical language organization, the definition of atypicality for language lateralization based on neuroimaging investigations is complex, and the type of brain organization supporting language functions in atypical individuals is still not comprehensively understood.

All individuals having a rightward hemispheric lateralization of language production as measured with Gaussian mixture modeling were classified into the ATYP group in the present study, suggesting that having a rightward lateralization for production is a clear criterion of atypicality, as already validated by Wada studies (***Dym et al., 2011***). However, the present classification did not individualize a cluster resembling the group of 37 ambilaterals identified in ***Mazoyer et al., 2014***, which indicated that not being clearly lateralized by production was not sufficient to ascertain atypicality. The difficulty in asserting language dominance in individuals with little fMRI lateralization during production is consistent with Bauer et al.'s meta-analysis showing that fMRI is more accurate in assessing language dominance in cases of strong leftward asymmetry (***Bauer et al., 2014***). However, the Bauer study involved patients suffering from epilepsy and thus likely to have language network reorganization.

To identify the discriminative variables that split the 37 ambilaterals into the 3 'language organization' groups, we conducted an additional analysis entering the nine variables we used for the multitask multimodal hierarchical classification as repeated measures, and we found in the 37 individuals classified ambilaterals in ***Mazoyer et al., 2014*** a very significant 'language organization' main effect and interaction with the repeated measures (both $p<0.0001$). Post hoc analyses revealed that among these 37 ambilaterals, the 12 individuals classified as ATYP had significantly lower task-induced asymmetry in SENT_HUBS and SENT_CORE (all $p<0.001$) and a significantly lower Rs_DC asymmetry

(p=0.002) than those classified as TYP_MILD or TYP_STRONG. In contrast, there was no difference in averaged Rs_DC or Rs_mIHHC values. These findings thus confirmed that, in order to comprehensively describe the dominance for language in individuals having low HFLI during language production, it is useful to apply a multitask battery as has been proposed by some authors (**Baciu et al., 2005**; **Niskanen et al., 2012**), which particularly allows the detection of individuals with dissociations as demonstrated by **Baciu et al., 2003**. Importantly, the present study also demonstrated that resting-state connectivity variables, measured at the language network level, particularly Rs_DC asymmetry, in association with task-induced asymmetry, are of interest for the identification of atypical individuals.

In left-handers, a weak functional asymmetry during language production makes atypical organization with rightward asymmetry for other language components highly probable (80%), whereas the same weak functional asymmetry in right-handed individuals is associated with a TYP leftward lateralization in most cases (86%). Such observations are consistent with the classification by support vector machine showing that all ambilateral right-handers had a left hemisphere with a dominant pattern (**Zago et al., 2017**), whereas the eight left-handed ambilaterals as classified with Gaussian mixture modeling and who had a dominant right-hemisphere pattern with support vector machine, were classified into the ATYP group by the present method.

The fact that 80% of the ATYP individuals were left-handed is consistent with previous research showing that reverse lateralization is mainly seen in left-handers, whether in adults (**Króliczak et al., 2016**; **Somers et al., 2015a**) or in children (**Szaflarski et al., 2012**). Here, a right shift in hemisphere dominance for language was found in 12% of left-handers (when taking into account the different language components, as done in the present study), compared to only 6% when considering their HFLI for production only (**Mazoyer et al., 2014**). The difference between these two proportions provides an estimate of the decreased sensitivity when detection of atypicals among left-handersLH is performed using a production task only rather than a multitask multimodal approach as we implemented in the present study. The present multimodal classification identified five right-handed ATYP individuals (3.6%, compared to 16.7% of left-handers), a phenomenon as rare as the published case reports of crossed aphasia in right-handers (**Alexander and Annett, 1996**; **Hindson et al., 1984**), raising the question of whether this is a pathological state rather than part of interindividual variability of language organization (**Coppens et al., 2002**). Among these five right-handed ATYP individuals, three had been previously classified as ambilaterals and two as typicals by Gaussian mixture modeling of the $PROD_{SENT\text{-}WORD}$ HFLI, with the latter two individuals having negative asymmetries during $LISN_{SENT\text{-}WORD}$ and $READ_{SENT\text{-}WORD}$. It is noticeable that these five right-handers had lower task-induced asymmetry strength than the 25 left-handed ATYP individuals, independent of the task, leaving open the question of whether right- and left-handed ATYP individuals are actually comparable.

Finally, the present classification sheds some light on the brain organization for language in individuals as defined by the support vector machine approach (**Zago et al., 2017**). Actually, the ATYP cluster aggregated 77% of the 22 participants labeled as having a right dominant hemisphere by support vector machine. This is very consistent with the high Rs_DC found for the right SENT_CORE network of the ATYP individuals. One should also note that 41% (7 among 17) of these right-hemisphere dominant ATYP individuals also had a dominant left hemisphere (i.e. were codominant), whereas the ATYP cluster aggregated 77% of the 12 participants labeled as having a codominant hemisphere. This strong association between atypicality and codominance is also consistent with the finding that ATYP individuals were characterized by high bilateral connectivity of their SENT_CORE network, which is likely to reduce the bias toward the dominance of a given hemisphere and attest to a more bilateral organization for language.

Organization of intrinsic connectivity in atypical individuals: although they show rightward task-induced asymmetries, their left hemisphere is also wired for language

In a previous study, we noted that the 10 left-handers with strong rightward HFLI exhibited a pattern of regional asymmetries that was the reverse of the pattern observed in typical individuals (**Tzourio-Mazoyer et al., 2016**), a result in line with cortical stimulation findings suggesting that individuals shifting their dominant hemisphere actually have a reverse regional organization (**Chang et al., 2011**; **Drane et al., 2012**). The present study results, although consistent with this view in terms of

task-induced asymmetries, demonstrated that, by contrast, the SENT_CORE network intrinsic connectivity properties of ATYP individuals did not mirror those of individuals with leftward task-induced asymmetries. Although the mean of the group was strongly rightward asymmetrical in the three tasks, the ATYP individuals showed high and symmetrical Rs_DC values, meaning that the SENT_CORE network was highly connected in both hemispheres, and it is remarkable that their left hemisphere Rs_DC value was not different from that of the TYP_STRONG individuals, whereas their right hemisphere Rs_DC value was higher than that of the TYP_STRONG individuals (***Figure 7***). The ATYP individuals thus had a significantly larger mean Rs_DC value of SENT_CORE in both hemispheres, making them highly connected individuals and suggesting that their left hemisphere could be organized in a way similar to that of the TYP individuals, that is as a potentially dominant hemisphere for language. In addition, the ATYP individuals showed the highest interhemispheric connectivity across SENT_CORE homotopic areas, constituting a highly efficient network for sentence processing that straddled the two hemispheres. The fact that even in individuals shifting their task-induced lateralization to the right, the left hemisphere is wired for high-order language processing leads to the hypothesis that the left hemisphere is the language hemisphere by default.

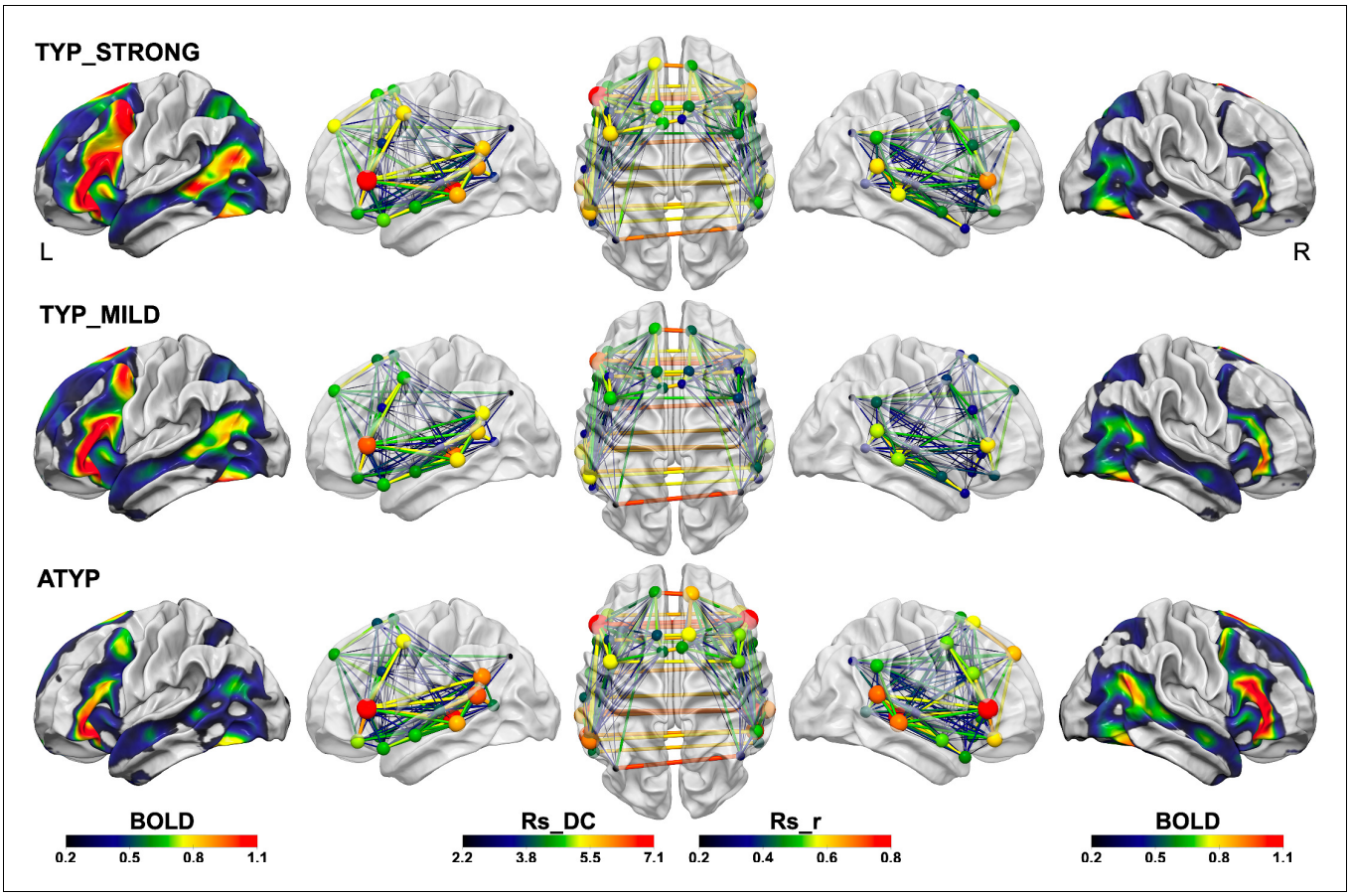

Figure 7. Summary figure illustrating the different SENT_CORE intra- and inter-hemispheric organizations observed in the three groups identified by hierarchical clustering. The left column shows the group mean activation maps during $PROD_{SENT\text{-}WORD}$ (BOLD activation amplitude is given by color scale) of the left hemisphere and the right column the mean activation map of the right hemisphere superimposed on the white matter surface rendering of the BIL and GIN template obtained with the Surf Ice software (https://www.nitrc.org/projects/surfice/). The second, third and fourth columns show the left lateral, superior and right lateral views of the SENT_CORE intrinsic connectivity network, each region of the network being represented by a sphere located at the mass center of its MNI coordinates. For each SENT_CORE region, a colored sphere indicate the group average region degree centrality of intrinsic connectivity (the Rs_DC value is given by color scale, and sphere size is proportional to value), whereas a colored line indicates the strength of the Pearson intrinsic correlation coefficient between two SENT_CORE regions (the Rs_r value is given by color scale, and line thickness is proportional to value).

A trace of how ATYP individuals overcome the left hemisphere default-mode organization for language can be found in the loss of congruence in the sentence network at rest and during sentence processing. In right-handers, we observed a positive correlation across individuals between asymmetries of activations and Rs_DC (***Labache et al., 2019***), while the ATYP group showed an absence of mean Rs_DC asymmetry but mean rightward task-induced symmetries. Notably, both the CROSSED and CONGRUENT ATYP individuals had a left hemisphere Rs_DC as strong as that in the TYP_STRONG individuals, meaning that their left SENT_CORE network connectivity was not different from that of strong leftward lateralized individuals (***Figure 7***) supporting the hypothesis that ATYP left hemisphere is wired for language as it is for typical individuals. Actually, ATYP differed from typicals in their right-hemisphere organization at rest that exhibited a high strength of intrinsic connectivity, in agreement with their task-induced rightward activations (***Figure 7***).

The pattern of ATYP individual network intrinsic organization is thus a networking of both hemispheres profiled for the processing of high-order language, combined with strong anatomical and functional underpinning of interhemispheric interactions as evidenced by higher correlations across homotopic regions of SENT_CORE and larger corpus callosum in the DISSOCIATED_ATYP individuals. The ATYP group also showed a more bilateral anatomical organization with decreased leftward gray and white matter hemispheric asymmetries likely to result in more flexibility in the side hosting the different language tasks and therefore allowing dissociations. In fact, the ATYP group hosted the largest proportion of participants showing dissociations and thus relying on one or the other hemisphere as the dominant hemisphere depending on the language component, which may be related to their stronger interhemispheric connectivity. Such a hypothesis was partly confirmed by the comparison of individuals with dissociations in the three groups that demonstrated that CROSSED ATYP individuals had significantly higher interhemispheric connectivity and more variation in the strength of asymmetries when DISSOCIATED than the two other groups. These strong between-task differences in asymmetry strengths reflect an important shift in hemispheric control, which were particularly seen between $PROD_{SENT\text{-}WORD}$ and the two other tasks underpinned by the strong interhemispheric connectivity allowing for cooperation across the bilaterally located task-dependent dominant language networks.

Two types of leftward organization for language, with an overrepresentation of women but not of left-handers in mildly lateralized typical individuals

The present segregation of leftward lateralized individuals in the two groups is consistent with the two Gaussian components of the $PROD_{SENT\text{-}WORD}$ HFLI distribution in typical individuals observed in our previous work (***Mazoyer et al., 2014***). However, these two Gaussian components showed too much overlap to allow a clear separation of the two groups of typical individuals. One original observation of the present study is thus the evidence of differences in terms of functional connectivity between two groups of typical individuals. Although leftward lateralized and showing the same gradient of asymmetry across the three tasks, the TYP_MILD individuals exhibited significant particularities in their inter- and intrahemispheric—although typical—intrinsic connectivity organization with lower asymmetries of task-induced activations but also lower Rs_DC and higher Rs_mIHHC within SENT_CORE. In other words, their decreased strength in task-induced functional asymmetries was associated with an intra- vs. interhemispheric intrinsic connectivity pattern showing less differentiation across hemispheres together with increased connection between them. Such a pattern of looser hemispheric specialization for language in the TYP_MILD group is consistent with a higher occurrence of dissociations than in the TYP_STRONG group, although those dissociations were of moderate intensity and mainly observed for the reading task.

The proportion of women was larger in the TYP_MILD cluster (58%) than in either of the two other clusters (38% in the TYP_STRONG and 50% in the ATYP clusters), as well as in the whole sample (49%), consistent with previous reports of reduced language lateralization in women (***Levy and Reid, 1978***; ***McGlone and Davidson, 1973***). Interestingly, gender differences in cluster constitution in the present work were present only in the two groups of typicals but not in the ATYP group. Such a subtle association between sex and language lateralization may explain the inconsistency in the reports of a sex effect in hemispheric specialization for language (***Sommer et al., 2004***) since, in contrast to handedness, it is not associated with the occurrence of critical changes in language lateralization. Actually, the proportion of left-handers was not increased in the TYP_MILD group

(compared to the TYP_STRONG group), confirming that the relationship between handedness and language lateralization is better grounded in the large occurrence of left-handers among rightward lateralized individuals rather than by a decreased lateralization for language in left-handers (*Mazoyer et al., 2014*).

Dissociations of lateralization across language components are of different natures in typical and atypical individuals with a particular status for the lateralization of reading

Dissociations were detected with higher sensitivity when considering the SENT_HUBS hROIs rather than the whole set of SENT_CORE area ROIs. This is the reason why we considered a participant dissociated if they had opposed asymmetry across tasks on either one or both variables.

The low incidence of dissociations that we observed in the TYP individuals and, in particular, in the TYP right-handers (4%) was consistent with the literature that reports rare cases of dissociations of production and comprehension in healthy right-handed participants (*Jansen et al., 2006*; *Tzourio-Mazoyer et al., 2004*). A point of interest was the occurrence of dissociation between the lateralization for reading and the lateralization for production and listening, which, to our knowledge, has not yet been reported. In leftward lateralized TYP individuals, dissociations were mainly observed in the TYP_MILD individuals for whom, as in the TYP_STRONG individuals, reading was on average more lateralized than listening (although less than production).

Dissociations in this TYP_MILD cluster more often involved reading (5 out of 9 in SENT_HUBS; see *Figure 3*). Such a larger occurrence of dissociations involving reading may be related to the late acquisition of this language function. Indeed, the first phase of language development is perceptual, as revealed by studies showing that the auditory system of the fetus at 30-week gestation is mature enough to detect complex sounds (*McMahon et al., 2012*) and to differentiate phonemes (*Hepper and Shahidullah, 1994*). After only a few hours of postnatal exposure, newborns respond specifically to speech (*Dehaene-Lambertz et al., 2002*). Then, because of maturation of the vocal tract, the second phase is production (*Mowrer, 1980*). From the second half of the first year of life, the child enters the babbling phase proper and begins to make choices specific to the structures of his or her mother tongue at the prosodic, phonetic and syllabic levels (*Oller, 1980*). These first steps toward articulation are an essential step that reflects the existence of a functional link between the processes of perception and the production of vocal sounds and gives the child the opportunity to receive proprioperceptive feedback (*Rodgon, 1976*).

While speech perception and production tightly codevelop very early in the establishment of language, reading is based on both the ability to hear and segment words into phonemes and then to associate these phonemes with graphemes, with the mapping of orthographic to phonological representations during reading being intrinsically cross-modal (*McNorgan et al., 2014*). In fact, reading develops in interaction with object recognition in the left fusiform gyrus (*Kassuba et al., 2011*) and rightward lateralized visuospatial and visuomotor processes such as the saccadic system supporting eye movement during reading (*Petit et al., 2009*). More particularly, during reading, eye movements are not only an oculomotor ability but also the integration of visual and language processes at the word level and at the syntactic level (*Richards et al., 2017*). In fact, reading depends on an alternation of fixations and saccades, the latter being defined as forward progressions or backward regressions. Even if forward progressions are the most common eye movements, backward regressions have been revealed to be correlated with the syntactic complexity of sentences, suggesting that these eye regressions depend on the relationships that the words making up the statement have to each other (*Lopopolo et al., 2019*). Thus, reading ability involves both visuospatial and language processes. Such a late specialization could lead to the possibility that different factors could intervene in the establishing of reading lateralization, with these factors being different from those acting during the first stages of language development.

The picture was very different for ATYP individuals, whose predominant dissociation pattern was a leftward lateralization for production and a rightward lateralization for both reading and listening (*Figure 3*, left). Considering the developmental timing of language components mentioned above, this could be an indication that ATYP lateralization for language perception and production is established early in different hemispheres. The second observation is that in the ATYP individuals, the lateralization of heteromodal areas during reading follows that of auditory sentence comprehension, demonstrating the prevalence of sensory integration over action in these individuals, which is

different from the lateralization organization in the TYP_MILD individuals. The fact that reading lateralization has different relationships with production and listening according to the sentence lateralization organization can provide new insight into the variability in the establishing of reading dominance and, potentially, a possible relationship between atypicality and dyslexia, since there is still a great debate between lateralization and reading impairments (***Wilson and Bishop, 2018***). Assessing the type of dissociations would be of great interest for shedding new light on language impairments.

The more frequent rightward lateralization during LISN than during PROD in the ATYP left-handers was consistent with the observation of Hécaen of a high occurrence of production deficits after left-hemisphere lesions in left-handers, while comprehension deficits were rare (***Hécaen et al., 1981***). Such a dissociation corresponds to that of action vs. perception as defined by ***Fuster, 2009***, with sentence reading and listening being colateralized. It is remarkable that, when compared to both TYP groups, the ATYP group showed a decrease in (absolute value) asymmetry strength that was larger for production than for the other tasks, leading to an absence of a difference between the asymmetries in production, listening, and reading. Such a diminished asymmetry during production is striking because of the link existing between hand preference and language production, with both functions being on the action side and being localized in close frontal areas. One should have expected left-handers to have stronger rightward asymmetry during language production than during the other tasks in relation to their left-hand dominance. This was not the case, even when considering only the CONGRUENT_ATYP individuals. However, handedness was associated with a stronger mean rightward asymmetry in the left-handed ATYP individuals and stronger leftward asymmetry in the right-handed TYP_STRONG individuals, independent of the task, as if the hemisphere controlling the dominant hand is a slight attractor for language lateralization. This modest effect of handedness is consistent with the observation that patients who had suffered from right plexus brachial injury at birth, therefore disabled in the use of their right hand, present a shifting of their language production asymmetries toward the right hemisphere, although without a complete shift (***Auer et al., 2009***).

Are different language organizations associated with differences in cognitive abilities?

Better visuospatial performance was present in the TYP_STRONG individuals, who had the largest between-hemisphere differences and lower interhemispheric connectivity. Such a result suggests that the better spatial abilities reported in RHright-handers in a meta-analysis (***Somers et al., 2015b***) might have been related to the fact that the TYP_STRONG group hosted the highest proportion of right-handers. The present results suggest that strong leftward lateralization of both language task-induced and resting-state connectivity asymmetries in the core language network is associated with better visuospatial performance, as if less involvement of the right hemisphere in sentence processing was facilitating visuospatial processing. Such an observation can be viewed as an argument in favor of the 'crowding effect' theory stating that an optimal split of functions across the two hemispheres facilitates cognitive functioning (review in ***Vingerhoets, 2019***). Of course, further exploration of the relationships between the different aspects of visuospatial cognitive abilities and the strength of both leftward lateralization for language and rightward lateralization for visuospatial functions, as well as their interindividual variability, is needed to confirm this hypothesis.

Decreased verbal memory abilities in the ATYP group suggest that the reorganization occurring on top of the language organization by default in this group is at the cost of suboptimal cognitive functioning, while mild, although leftward, lateralization for language appears to be as efficient for language processing as strong leftward lateralization. Considering that the ATYP group included 15 of the ambilateral individuals defined in ***Mazoyer et al., 2014***, the present observation is consistent with those of Mellet et al reporting lower performance in ambilaterals (***Mellet et al., 2014b***) concerning both verbal memory and visuospatial abilities.

Conclusions

The joint investigation of language task-induced asymmetries and intrinsic connectivity strength in the sentence-processing supramodal network, showed that individuals with atypical rightward language lateralization do not rely on an organization that simply mirrors that of typical leftward

lateralized individuals but rather is associated with a loose hemispheric specialization for language. The fact that these individuals had lower leftward gross macroscopical hemispheric anatomy than typical individuals suggests that such organization was supported, at least in part, by early developmental events resulting from a different trajectory or from the occurrence of plastic changes. Support for the hypothesis of the early establishment of this atypical organization comes from the coinvestigation of the lateralization of production and comprehension with reading. In atypicals, dissociations were observed between sentence production and comprehension (whether read or listened to), two functions known to be tightly coupled and early developing. By contrast, the rare dissociations found in typicals occurred for reading, a later acquired competence. Moreover, atypical organization occurring mainly in left-handers has a cost in terms of language abilities with less efficient verbal memory. Finally, the present results argue for multitask measures of language lateralization for evaluating hemispheric specialization for language in individuals with low lateralization for language production, especially if they are left-handed.

Materials and methods

Participants

The study sample was part of the BIL and GIN database that has been fully described elsewhere (***Mazoyer et al., 2016***). Briefly, 287 healthy participants of the BIL and GIN (150 left-handed, 140 women, 72 left-handed women) who completed the fMRI battery, including several language tasks and a resting-state acquisition, were included in the present work. The sample mean age was 25.8 years (SD = 6.5 years). The mean educational level of the participants was 15.6 years corresponding to almost 5 years education after the French baccalaureate (SD = 2.3 years).

For each participant, we recorded self-reported handedness and manual preference (MP) strength assessed with the Edinburgh inventory (***Oldfield, 1971***). Left-handed participants had an Edinburgh score of −63.2 (SD = 39.9).

Participants' cognitive evaluation

Participants' verbal abilities were evaluated with the following battery of seven tests: (1) a supraspan recall test of an 18-word-list (***Van der Elst et al., 2005***) for verbal memory evaluation; (2) a supraspan recall test of a list of 15 pseudo-words for verbal memory evaluation with minimal semantic associations; (3) a verb generation test for semantic verbal fluency exploration; (4) a synonym finding test for estimating vocabulary extent ***Binois and Pichot, 1956***; (5) a listening span test based on spoken sentences; (6) a reading span test based on read sentences for verbal working memory assessment (***Daneman and Carpenter, 1980***; ***Desmette et al., 1995***) and (7) a rhyming test on 80 visually presented pairs of pseudo-words for evaluation of graphophonemic conversion ability.

Visuospatial abilities were assessed with the following four tests: (1) The Mental Rotation Test (MRT), which estimates the ability to rotate and spatially manipulate mental images ***Vandenberg and Kuse, 1978***; (2) the Corsi Block test, which evaluates visuospatial short-term memory abilities ***Della Sala et al., 1999***; (3) a home-made 3D maze test for evaluating topographic orientation skills; and (4) the Raven matrix for assessing non-verbal reasoning.

Language tasks completed during fMRI

The language fMRI paradigm has been fully described elsewhere (***Labache et al., 2019***). In short, three fMRI runs were completed by the participants, each including a sentence-level task and a word-list reference task corresponding to randomized alternation of event-related trials. Within each trial, the participant was shown for 1 s either a line drawing (taken from the 'Le Petit Nicolas' comic strip series) or a scrambled drawing, that was immediately followed by a central fixation crosshair. While fixating the cross, the participant performed either the sentence task or the word-list reference task.

During the production run (PROD), after seeing a line drawing, the participant was instructed to covertly generate a sentence beginning with a subject and a complement, followed by a verb describing the action taking place and ending with an additional complement of a place or a manner. When a scrambled drawing was displayed, the subject was asked to covertly generate the list of the months of the year.

During the listening run (LISN), whenever a Petit Nicolas line drawing was displayed, the subject was instructed to carefully listen to a sentence dealing with the line drawing and to click at the end of the sentence. When a scrambled drawing was displayed, he/she was instructed to listen to the list of the months, days of the week and/or seasons and click at the end of the list.

During the reading run (READ), like in the two other tasks, whenever a line drawing was displayed, the subject was instructed to read a sentence based on the outline drawing. When a scrambled drawing was displayed, he/she was instructed to read the list of months, days of the week and/or seasons.

Task execution and performance

The response times corresponding to the end of the sentence production, sentence listening and sentence reading were recorded for each participant during the fMRI session, and right after the fMRI session, the participants were asked to rate the difficulty of each of the tasks on a 5-level scale (1:easy to 5:very difficult). For the production run, each participant was asked to recall and write down, whenever possible, the sentence he/she elaborated when presented with each image, the average number of words per (recalled) sentence being then computed.

Image acquisition and processing

Image acquisition

Imaging was performed on a Philips Achieva 3 Tesla MRI scanner (Philips, Erlangen, The Netherlands).

The structural MRI protocol consisted of a localizer scan, a high resolution three-dimensional T1-weighted volume (sequence parameters: TR 20 ms; TE 4.6 ms; flip angle 10˚; inversion time 800 ms; turbo field echo factor 65; sense factor 2; field of view 256 × 256×180 mm^3; 1 × 1 x 1 mm^3 isotropic voxel size) and a T2*-weighted multi-slice acquisition (T2*-weighted fast field echo (T2*-FFE), sequence parameters:TR = 3,500 ms; TE = 35 ms; flip angle = 90 deg; sense factor = 2; 70 axial slices; 2 x 2 x 2 mm^3 isotropic voxel size).

Language task-related functional volumes were acquired using a T2*-weighted echo-planar imaging (EPI) sequence (TR = 2 s; TE = 35 ms; flip angle = 80˚; 31 axial slices with a 240 × 240 mm^2 field of view and 3.75 × 3.75 × 3.75 mm^3 isotropic voxel size). In the three runs, 192, 194, and 194 T2*-weighted volumes were acquired for the production, listening, and reading sentence tasks, respectively.

Resting-state functional volumes (N = 240) were acquired as a single 8 min long run using the same T2*-weighted EPI sequence. Immediately prior to scanning, the participants were instructed to 'keep their eyes closed, to relax, to refrain from moving, to stay awake and to let their thoughts come and go'.

Processing of structural images

For each participant, (1) the T2*-FFE volume was rigidly registered to the T1-MRI; (2) the T1-MRI was segmented into three brain tissue classes (gray matter, white matter, and cerebrospinal fluid) and normalized to the BIL and GIN template including 301 volunteers from the BIL and GIN database using the SPM12 'segment' procedure (http://www.fil.ion.ucl.ac.uk/spm/) with otherwise default parameters. Whole volumes of these three compartments were extracted and brain volume calculated as their sum. In addition, hemispheric volumes (left and right) of gray and white matter were extracted to compute their asymmetries (***Table 3***).

A semi-automated in-house *corpus callosum* segmentation procedure was then applied to extract individual masks of corpus callosum obtained from 10 consecutive mid-sagittal slices of 1 mm width on individual white matter maps in the MNI stereotactic space. An additional processing step to remove the fornix, which was sometimes segmented and connected along with the corpus callosum, was added. Quality control of corpus callosum segmentation was achieved by visual inspection of all slices, and, when needed, manual corrections for minor segmentation error was applied using FSL software. Each individual *corpus callosum* mask was then applied to each participant's normalized and modulated white matter partition images to estimate individual corpus callosum volume (***Table 3***).

Pre-processing of task-related and resting-state functional volumes

Functional data were corrected for slice timing differences. To correct for subject motion during the runs, all T2*-weighted volumes were realigned using a 6-parameter rigid-body registration. The EPI-BOLD scans were then registered rigidly to the structural T2*-FFE image. The combination of all registration matrices allowed for warping the EPI-BOLD functional scans from the subject acquisition space to the standard space ($2 \times 2 \times 2$ mm^3 sampling size) with a single interpolation.

Time series of BOLD signal variations in white matter and cerebrospinal fluid (individual average time series of voxels that belonged to each tissue class) as well as temporal linear trends were removed from the rs-fMRI data series using a regression analysis. Additionally, rs-fMRI data were bandpass filtered (0.01 Hz - 0.1 Hz) using a least-squares linear-phase finite impulse response filter design.

Language task-fMRI processing

Language task contrast maps

Statistical parametric mapping (SPM12, http://www.fil.ion.ucl.ac.uk/spm/) was used for processing the task-related fMRI data. First, a 6 mm full width at half maximum (FWHM) gaussian filter was applied to volumes acquired during each run. For each participant, differences between BOLD signal volumes corresponding to sentence and list belonging to the same run were computed, namely sentence minus word-list production ($PROD_{SENT\text{-}WORD}$), sentence minus word-list reading ($READ_{SENT\text{-}WORD}$), and sentence minus word-list listening ($LISN_{SENT\text{-}WORD}$).

Regions of interest analysis using the SENSAAS atlas

BOLD signal variations during the three language tasks and resting-state and their asymmetries were then computed for the set of 18 pairs of homotopic frontal and temporal regions of interests (hROIs) that we previously identified in the subgroup of 144 right-handers as constituting a core network of language areas (SENT_CORE, ***Figure 1*** [***Labache et al., 2019***]). These 18 hROI-pairs were selected as activated and leftward asymmetrical in these same three tasks and as constituting at rest a network with strong positive correlations across the hROIS. Note that SENT_CORE areas contain the antero-posterior high-order language areas, consistent with language meta-analyses of healthy individuals (***Price, 2010***; ***Price, 2012***; ***Vigneau et al., 2006***), including three intrinsic connectivity hubs corresponding to the inferior frontal gyrus (F3t) and two regions of the superior temporal sulcus (STS: STS3 and STS4 ***Figure 1***).

Here, for each participant, each of the three contrast maps, and each of these 18 hROIs, left and right BOLD signal variations were computed by averaging the contrast BOLD values of all voxels located within the hROI volume. Then, for each participant and each contrast map, mean left and right BOLD variations and asymmetry for the whole network were also computed as a weighted (by volume) average of the corresponding 18 hROIs values (SENT_CORE), as well as the mean of the three hubs (SENT_HUBS).

Resting-state organization of SENT_CORE network

For each individual and each hROI composing the SENT_CORE network, we computed a degree centrality (Rs_DC) in each hemisphere. The Rs_DC in each participant and each hROI of each hemisphere was calculated as the sum of the positive correlations existing between one hROI and all the other hROIs of the SENT_CORE network. Rs_DC values were then averaged across the 18 hROIs of the same hemisphere and the resulting left and right averaged Rs_DC values were summed and divided by two so as to provide a SENT_CORE intra-hemispheric Rs_DC characterizing the strength of within hemisphere intrinsic connectivity for this network. We also computed the left minus right difference of the averaged Rs_DC values as a measure of the asymmetry in intra-hemispheric connectivity strengths for the SENT_CORE network.

Interhemispheric connectivity strength was estimated in each individual by the average across the 18 hROIs pairs constituting the SENT_CORE network of the z-transformed intrinsic correlation coefficient between homotopic ROIs (mean Inter-Hemispheric Homotopic Correlations, Rs_mIHHC).

Statistical analysis

Identification of groups of individuals with different brain organization for language through hierarchical clustering

In a previous work (**Mazoyer et al., 2014**), we have shown that the distribution of lateralization for sentence production, although of continuous nature, could be used to classify individuals into three discrete categories. So, we believe it was justified to try to categorize individuals taking into account not solely production but reading, listening and resting-state, as well. It is important to realize that we did not a priori decide that the number of categories for this multivariate classification would be 3 (as it was when using production only). Rather, the optimal number of clusters for this multivariate classification was obtained using a fully unsupervised methodology and a combination of 30 statistical criteria (see below).

The study sample was segregated in groups varying in their intra- and interhemispheric organization in SENT_CORE using an agglomerative hierarchical clustering procedure. The variables entered in this procedure were both functional asymmetries induced by each of the three language tasks and intra- and interhemispheric SENT_CORE intrinsic connectivity metrics.

Task-induced functional asymmetries were obtained both at the SENT_CORE level, because of the low intersubject variability that results from averaging over the whole set of 18 ROIs, and at the SENT_HUBS level (i.e. when averaging asymmetries over three hubs: F3t, STS3, and STS4) because, although more variable across individuals, this hub-averaged asymmetry involves supramodal regions having a key role in the sentence core network (see **Labache et al., 2019**). There were thus six variables for task-induced activation: the SENT_CORE and SENT_HUBS asymmetries for $LISN_{SENT\text{-}WORD}$, $PROD_{SENT\text{-}WORD}$ and $READ_{SENT\text{-}WORD}$.

To investigate both the intrahemispheric integration in the language networks and the interhemispheric differences, we included in the hierarchical classification the sum of the two hemisphere Rs_DC values (left Rs_DC + right Rs_DC) and the Rs_DC asymmetry (left Rs_DC – right Rs_DC) calculated in SENT_CORE. To account for interhemispheric intrinsic connectivity strength, we included the mean of the interhemispheric SENT_CORE homotopic correlation (Rs_mIHHC).

These nine variables were standardized before being jointly entered into an agglomerative hierarchical classification (**Sneath and Sokal, 1973**) that used the Euclidean distance for computing the dissimilarity matrix and the Ward distance (**Ward, 1963**) to aggregate the different participants into clusters using the '*hclust*' function provided by default in R. The optimal number of clusters was determined using the R library '*NbClust*' (**Charrad et al., 2014**). This package provides 30 statistical indices for determining the optimal number of clusters and offers the best clustering scheme from the different results obtained by varying all combinations of the number of clusters for the chosen method, in this case, hierarchical clustering with Ward's distance. We selected the number of clusters that satisfied a maximum of indices and found it to be equal to 3.

Hierarchical classification was completed with R (R version 3.5.1; **R Development Core Team, 2013**), while other statistical analyses were performed using JMP15 (http://www.jmp.com, SAS Institute Inc, 2018).

Identification of individuals with dissociations of lateralization across tasks

In a second step, we identified individuals exhibiting at least one dissociation in their lateralization among the three language tasks, which means those who exhibited SENT_CORE functional asymmetries larger than 0.05 in amplitude in the opposite direction in one task compared to the others. We also searched for individuals exhibiting a dissociation in their SENT_HUB asymmetries, which led to the definition of two categories of individuals: 1. those exhibiting a dissociation for either SENT_CORE or SENT_HUB or both, who were named 'CROSSED'; 2. those showing either leftward lateralization for all tasks for both SENT_CORE and SENT_HUBS or right lateralization for all tasks for both SENT_CORE and SENT_HUBS, who were named 'CONGRUENT'.

Pearson's chi-square tests were conducted to compare the proportion of 'dissociation' across the clusters identified by the classification.

Characterization of the groups provided by the classification with different brain organization of the language network

Task performance, demography and handedness

To ensure that potential differences in the asymmetries measured during the language tasks were not related to group differences in task execution time that was recorded during the task-induced fMRI session, response times were compared across 'language organization' groups (corresponding to the clusters of the hierarchical classification) taking into account sex, age, and brain volume. In addition, within each 'language organization' group, we compared the groups of 'CONGRUENT' and 'CROSSED' individuals.

The different 'language organization' groups were compared with variables known to be associated with variability in language lateralization, namely, handedness, sex, age, and brain volume. To complete these analyses, Pearson's chi-square tests were applied for discrete variables (handedness and sex) and ANOVA with Tukey's HSD post hoc tests for continuous variables (age and brain volume).

Task-induced and resting-state organization of the SENT_CORE network in groups varying in their language network organization

We first comprehensively described the different types of organization of the sentence networks in the groups issued from the hierarchical classification.

We used two repeated measures MANOVA to examine the task-induced asymmetries within SENT_CORE and SENT_HUBS in the three language tasks searching for 'task' (three levels), 'language organization' (three levels, that is, a number of levels corresponding to the number of identified clusters) and 'handedness' main effects and their interactions.

Note that to ensure that this between-group difference was not due to a difference in the occurrences of dissociations across 'language organization' groups, the statistical analysis was completed on the absolute values of asymmetries within SENT_CORE and SENT_HUBS. We also examined in the ATYP and TYP_MILD groups the effect of 'dissociation' and its interactions with 'task' on the strength of task-induced asymmetries. The TYP_STRONG group was not considered in this analysis because there were only 2 DISSOCIATED individuals in this group.

In the same way, we examined the resting-state variables, that is the Rs_DC asymmetries, Rs_DC mean and Rs_mIHHC. For Rs_mIHHC, we performed the Fisher z-transformation to conduct the analysis.

Finally, using repeated measures MANOVA, we searched whether there was a difference in resting-state organization with the occurrence of 'dissociations' depending on 'language organization' (restricted to two factors ATYP and TYP, as the TYP_STRONG and TYP_MILD groups that were not different for Rs_DC and Rs_mIHHC were merged) by comparing their mean Rs_DC values and asymmetries (including a main effect of 'side' in the MANOVA), and SENT_CORE Rs_mIHHC.

All post hoc analyses were conducted using Tukey's HSD test for multiple comparisons.

Anatomical variables

To investigate the brain structural differences in groups with different functional organization of language lateralization, we compared *corpus callosum* volume (CCvol) and asymmetries (left *minus* right) in gray matter (GMasym) and white matter (WMasym) hemispheric volumes. In this analysis, 'CROSSED' or 'CONGRUENT' was studied in interaction with the 'language organization' main effect restricted to two factors ('TYP' and 'ATYP').

First, to take into account variables that were found to covary with GMasym, WMasym and CCvol, we computed the residuals of MANCOVAs that included age, sex, total brain volume and handedness. These residuals of GMasym and WMasym were then entered in repeated measures ANOVA including a 'language organization' main effect restricted to two factors ('TYP' and 'ATYP') and dissociation ('CROSSED' or 'CONGRUENT') and their interaction as fixed factors and their interaction with the anatomical compartment (gray matter or white matter).

The residuals of CCvol were entered in ANOVA searching for an effect of a 'language organization' main effect restricted to two factors ('TYP' and 'ATYP'), an effect of dissociation with two factors ('CROSSED' or 'CONGRUENT') and their interaction.

Cognitive variables

First, we performed a multiple linear regression analysis of the scores of the 11 tests of the cognitive battery, including sex, manual preference, age, education level and total intracranial volume as predictors since these variables have been shown to partly explain the variance in these scores (**Mellet et al., 2014a**). Residuals of the 11 regression analyses were then entered into PCA with a promax rotation. We used the *scree* criterion to determine the number of components to be retained.

The 'language organization' groups were compared with regard to their cognitive abilities through repeated measures MANCOVA including the four components of the PCA obtained from the residuals of the 11 scores. Finally, an impact of 'dissociation' on cognitive abilities was also tested in the ATYP and TYP_MILD groups (only two dissociations in TYP_STRONG).

Post hoc analyses were conducted using uncorrected Student's t-tests.

Comparison of the different classifications for language lateralization

We also compared the present classification based on a multitask and multimodal approach to two other classifications that were previously applied to the same group of individuals, namely, the Gaussian mixture modeling classification on the HFLI obtained with the $PROD_{SENT\_WORD}$ contrast (**Mazoyer et al., 2014**) and an support vector machine approach applied at the voxel level, allowing us to classify the dominant and nondominant hemispheres of each participant according to their spatial pattern of activation during $PROD_{SENT\_WORD}$ (**Zago et al., 2017**).

To compare these three different classifications obtained in the 287 subjects, we used the '*ggalluvial*' R library to make an alluvial plot (**Brunson, 2020**). The alluvial plot allowed us to visualize, for each subject, their classification as TYP_STRONG TYP_MILD or ATYP issued from the present work, as typical, ambilateral (AMB), or strong-atypical (SA) based on HFLI (**Mazoyer et al., 2014**), and the classification of each of the hemispheres as dominant or nondominant obtained with support vector machine (**Zago et al., 2017**). Two plots were made, which included one for right-handed people and another for left-handers.

Acknowledgements

The authors thank their colleagues Laure Zago and Emmanuel Mellet for their careful reading of the manuscript and Violaine Veraccia for expert technical assistance, supported by Ginesislab, a joint (University Bordeaux/CEA/CNRS and Fealinx) laboratory supported by the French government agency (ANR 16-LCV2-0006-01).

Additional information

Funding

Funder	Grant reference number	Author
Agence Nationale de la Recherche	ANR 16-LCV2-0006-01	Marc Joliot

The funders had no role in study design, data collection and interpretation, or the decision to submit the work for publication.

Author contributions

Loïc Labache, Conceptualization, Data curation, Software, Formal analysis, Visualization, Methodology, Writing - original draft, Writing - review and editing; Bernard Mazoyer, Conceptualization, Resources, Formal analysis, Supervision, Methodology, Writing - original draft, Writing - review and editing; Marc Joliot, Data curation, Funding acquisition, Methodology, Writing - review and editing; Fabrice Crivello, Data curation, Visualization, Methodology, Writing - review and editing; Isabelle Hesling, Writing - original draft, Writing - review and editing; Nathalie Tzourio-Mazoyer, Conceptualization, Data curation, Formal analysis, Supervision, Validation, Methodology, Writing - original draft, Project administration, Writing - review and editing

Author ORCIDs

Loïc Labache https://orcid.org/0000-0002-5733-0743
Bernard Mazoyer https://orcid.org/0000-0003-0970-2837
Marc Joliot http://orcid.org/0000-0001-7792-308X
Fabrice Crivello https://orcid.org/0000-0001-6950-984X
Isabelle Hesling https://orcid.org/0000-0002-3719-983X
Nathalie Tzourio-Mazoyer https://orcid.org/0000-0002-6236-4390

Ethics

Human subjects: The Comité pour la Protection des Personnes dans la Recherche Biomédicale de Basse-Normandie approved the study protocol. All participants gave their informed, written consent, and received an allowance for their participation.

Decision letter and Author response

Decision letter https://doi.org/10.7554/eLife.58722.sa1
Author response https://doi.org/10.7554/eLife.58722.sa2

Additional files

Supplementary files

- Transparent reporting form

Data availability

All data generated or analysed during this study are included in the manuscript and supporting files. Source data files have been provided for all figures and tables.

The following dataset was generated:

Author(s)	Year	Dataset title	Dataset URL	Database and Identifier
Labache, Mazoyer, Joliot, Crivello, Tzourio-Mazoyer	2020	BIL&GIN Sentence and Rest asymmetries - eLife	https://doi.org/10.5061/dryad.ht76hdrcf	Dryad Digital Repository, 10.5061/dryad.ht76hdrcf

References

Alexander MP, Annett M. 1996. Crossed aphasia and related anomalies of cerebral organization: case reports and a genetic hypothesis. *Brain and Language* **55**:213–239. DOI: https://doi.org/10.1006/brln.1996.0102

Auer T, Pinter S, Kovacs N, Kalmar Z, Nagy F, Horvath RA, Koszo B, Kotek G, Perlaki G, Koves M, Kalman B, Komoly S, Schwarcz A, Woermann FG, Janszky J. 2009. Does obstetric brachial plexus injury influence speech dominance? *Annals of Neurology* **65**:57–66. DOI: https://doi.org/10.1002/ana.21538, PMID: 19194880

Baciu MV, Watson JM, McDermott KB, Wetzel RD, Attarian H, Moran CJ, Ojemann JG. 2003. Functional MRI reveals an interhemispheric dissociation of frontal and temporal language regions in a patient with focal epilepsy. *Epilepsy & Behavior* **4**:776–780. DOI: https://doi.org/10.1016/j.yebeh.2003.08.002, PMID: 14698719

Baciu MV, Watson JM, Maccotta L, McDermott KB, Buckner RL, Gilliam FG, Ojemann JG. 2005. Evaluating functional MRI procedures for assessing hemispheric language dominance in neurosurgical patients. *Neuroradiology* **47**:835–844. DOI: https://doi.org/10.1007/s00234-005-1431-3, PMID: 16142480

Bauer PR, Reitsma JB, Houweling BM, Ferrier CH, Ramsey NF. 2014. Can fMRI safely replace the wada test for preoperative assessment of language lateralisation? A meta-analysis and systematic review. *Journal of Neurology, Neurosurgery & Psychiatry* **85**:581–588. DOI: https://doi.org/10.1136/jnnp-2013-305659

Binois R, Pichot P. 1956. *Test De Vocabulaire* Paris, France:: Éditions Du Centre De Psychologie.

Bishop DV. 2013. Cerebral asymmetry and language development: cause, correlate, or consequence? *Science* **340**:1230531. DOI: https://doi.org/10.1126/science.1230531, PMID: 23766329

Brunson JC. 2020. *ggalluvial: Alluvial Plots in 'ggplot2'*.https://CRAN.R-project.org/package=ggalluvial

Chang EF, Wang DD, Perry DW, Barbaro NM, Berger MS. 2011. Homotopic organization of essential language sites in right and bilateral cerebral hemispheric dominance. *Journal of Neurosurgery* **114**:893–902. DOI: https://doi.org/10.3171/2010.11.JNS10888, PMID: 21235314

Charrad M, Ghazzali N, Boiteau V, Niknafs A. 2014. NbClust: anrpackage for determining the relevant number of clusters in a data set. *Journal of Statistical Software* **61**:1–36. DOI: https://doi.org/10.18637/jss.v061.i06

Coppens P, Hungerford S, Yamaguchi S, Yamadori A. 2002. Crossed aphasia: an analysis of the symptoms, their frequency, and a comparison with left-hemisphere aphasia symptomatology. *Brain and Language* **83**:425–463. DOI: https://doi.org/10.1016/S0093-934X(02)00510-2, PMID: 12468397

Daneman M, Carpenter PA. 1980. Individual differences in working memory and reading. *Journal of Verbal Learning and Verbal Behavior* **19**:450–466. DOI: https://doi.org/10.1016/S0022-5371(80)90312-6

Dehaene-Lambertz G, Dehaene S, Hertz-Pannier L. 2002. Functional neuroimaging of speech perception in infants. *Science* **298**:2013–2015. DOI: https://doi.org/10.1126/science.1077066, PMID: 12471265

Della Sala S, Gray C, Baddeley A, Allamano N, Wilson L. 1999. Pattern span: a tool for unwelding visuo-spatial memory. *Neuropsychologia* **37**:1189–1199. DOI: https://doi.org/10.1016/S0028-3932(98)00159-6, PMID: 10509840

Desmette D, Hupet M, Schelstraete M-A, Van der Linden M. 1995. Adaptation en langue française Du « Reading Span Test » de Daneman et Carpenter (1980). *L'année Psychologique* **95**:459–482. DOI: https://doi.org/10.3406/psy.1995.28842

Dorion AA, Chantôme M, Hasboun D, Zouaoui A, Marsault C, Capron C, Duyme M. 2000. Hemispheric asymmetry and corpus callosum morphometry: a magnetic resonance imaging study. *Neuroscience Research* **36**:9–13. DOI: https://doi.org/10.1016/S0168-0102(99)00102-9

Drane DL, Roraback-Carson J, Hebb AO, Hersonskey T, Lucas T, Ojemann GA, Lettich E, Silbergeld DL, Miller JW, Ojemann JG. 2012. Cortical stimulation mapping and wada results demonstrate a normal variant of right hemisphere language organization. *Epilepsia* **53**:1790–1798. DOI: https://doi.org/10.1111/j.1528-1167.2012.03573.x, PMID: 22780099

Dym RJ, Burns J, Freeman K, Lipton ML. 2011. Is functional MR imaging assessment of hemispheric language dominance as good as the wada test?: a meta-analysis. *Radiology* **261**:446–455. DOI: https://doi.org/10.1148/radiol.11101344, PMID: 21803921

Friederici AD, Brauer J, Lohmann G. 2011. Maturation of the language network: from inter- to intrahemispheric connectivities. *PLOS ONE* **6**:e20726. DOI: https://doi.org/10.1371/journal.pone.0020726, PMID: 21695183

Fuster JM. 2009. Cortex and memory: emergence of a new paradigm. *Journal of Cognitive Neuroscience* **21**:2047–2072. DOI: https://doi.org/10.1162/jocn.2009.21280, PMID: 19485699

Habas PA, Scott JA, Roosta A, Rajagopalan V, Kim K, Rousseau F, Barkovich AJ, Glenn OA, Studholme C. 2012. Early folding patterns and asymmetries of the normal human brain detected from in utero MRI. *Cerebral Cortex* **22**:13–25. DOI: https://doi.org/10.1093/cercor/bhr053, PMID: 21571694

Hécaen H, De Agostini M, Monzon-Montes A. 1981. Cerebral organization in left-handers. *Brain and Language* **12**:261–284. DOI: https://doi.org/10.1016/0093-934X(81)90018-3, PMID: 7214131

Hécaen H, Sauguet J. 1971. Cerebral dominance in left-handed subjects. *Cortex* **7**:19–48. DOI: https://doi.org/10.1016/S0010-9452(71)80020-5, PMID: 5567814

Hepper PG, Shahidullah BS. 1994. Development of fetal hearing. *Archives of Disease in Childhood - Fetal and Neonatal Edition* **71**:F81–F87. DOI: https://doi.org/10.1136/fn.71.2.F81

Hervé PY, Zago L, Petit L, Mazoyer B, Tzourio-Mazoyer N. 2013. Revisiting human hemispheric specialization with neuroimaging. *Trends in Cognitive Sciences* **17**:69–80. DOI: https://doi.org/10.1016/j.tics.2012.12.004, PMID: 23317751

Hill J, Dierker D, Neil J, Inder T, Knutsen A, Harwell J, Coalson T, Van Essen D. 2010. A surface-based analysis of hemispheric asymmetries and folding of cerebral cortex in term-born human infants. *Journal of Neuroscience* **30**:2268–2276. DOI: https://doi.org/10.1523/JNEUROSCI.4682-09.2010, PMID: 20147553

Hindson DA, Westmoreland DE, Carroll WA, Bodmer BA. 1984. Persistent broca's aphasia after right cerebral infarction in a right-hander. *Neurology* **34**:387. DOI: https://doi.org/10.1212/WNL.34.3.387, PMID: 6538284

Hopkins WD, Cantalupo C. 2008. Theoretical speculations on the evolutionary origins of hemispheric specialization. *Current Directions in Psychological Science* **17**:233–237. DOI: https://doi.org/10.1111/j.1467-8721.2008.00581.x

Hund-Georgiadis M, Lex U, Friederici AD, von Cramon DY. 2002. Non-invasive regime for language lateralization in right- and left-handers by means of functional MRI and dichotic listening. *Experimental Brain Research* **145**:166–176. DOI: https://doi.org/10.1007/s00221-002-1090-0, PMID: 12110956

Isaacs KL, Barr WB, Nelson PK, Devinsky O. 2006. Degree of handedness and cerebral dominance. *Neurology* **66**:1855–1858. DOI: https://doi.org/10.1212/01.wnl.0000219623.28769.74, PMID: 16801650

Jansen A, Deppe M, Schwindt W, Mohammadi S, Sehlmeyer C, Knecht S. 2006. Interhemispheric dissociation of language regions in a healthy subject. *Archives of Neurology* **63**:1344. DOI: https://doi.org/10.1001/archneur.63.9.1344, PMID: 16966524

Joliot M, Tzourio-Mazoyer N, Mazoyer B. 2016. Intra-hemispheric intrinsic connectivity asymmetry and its relationships with handedness and language lateralization. *Neuropsychologia* **93**:437–447. DOI: https://doi.org/10.1016/j.neuropsychologia.2016.03.013, PMID: 26988116

Josse G, Kherif F, Flandin G, Seghier ML, Price CJ. 2009. Predicting language lateralization from gray matter. *Journal of Neuroscience* **29**:13516–13523. DOI: https://doi.org/10.1523/JNEUROSCI.1680-09.2009, PMID: 19864564

Kassuba T, Klinge C, Hölig C, Menz MM, Ptito M, Röder B, Siebner HR. 2011. The left fusiform gyrus hosts trisensory representations of manipulable objects. *NeuroImage* **56**:1566–1577. DOI: https://doi.org/10.1016/j.neuroimage.2011.02.032, PMID: 21334444

Króliczak G, Piper BJ, Frey SH. 2016. Specialization of the left supramarginal gyrus for hand-independent Praxis representation is not related to hand dominance. *Neuropsychologia* **93**:501–512. DOI: https://doi.org/10.1016/j.neuropsychologia.2016.03.023, PMID: 27020138

Kurthen M, Helmstaedter C, Linke DB, Solymosi L, Elger CE, Schramm J. 1992. Interhemispheric dissociation of expressive and receptive language functions in patients with complex-partial seizures: an amobarbital study. *Brain and Language* **43**:694–712. DOI: https://doi.org/10.1016/0093-934X(92)90091-R, PMID: 1483198

Kurthen M, Helmstaedter C, Linke DB, Hufnagel A, Elger CE, Schramm J. 1994. Quantitative and qualitative evaluation of patterns of cerebral language dominance an amobarbital study. *Brain and Language* **46**:536–564. DOI: https://doi.org/10.1006/brln.1994.1030, PMID: 8044676

Labache L, Joliot M, Saracco J, Jobard G, Hesling I, Zago L, Mellet E, Petit L, Crivello F, Mazoyer B, Tzourio-Mazoyer N. 2019. A SENtence supramodal Areas AtlaS (SENSAAS) based on multiple task-induced activation mapping and graph analysis of intrinsic connectivity in 144 healthy right-handers. *Brain Structure and Function* **224**:859–882. DOI: https://doi.org/10.1007/s00429-018-1810-2, PMID: 30535758

Lee D, Swanson SJ, Sabsevitz DS, Hammeke TA, Scott Winstanley F, Possing ET, Binder JR. 2008. Functional MRI and wada studies in patients with interhemispheric dissociation of language functions. *Epilepsy & Behavior* **13**: 350–356. DOI: https://doi.org/10.1016/j.yebeh.2008.04.010, PMID: 18504162

Levy J, Reid M. 1978. Variations in cerebral organization as a function of handedness, hand posture in writing, and sex. *Journal of Experimental Psychology: General* **107**:119–144. DOI: https://doi.org/10.1037/0096-3445.107.2.119

Li G, Nie J, Wang L, Shi F, Lyall AE, Lin W, Gilmore JH, Shen D. 2014. Mapping longitudinal hemispheric structural asymmetries of the human cerebral cortex from birth to 2 years of age. *Cerebral Cortex* **24**:1289–1300. DOI: https://doi.org/10.1093/cercor/bhs413, PMID: 23307634

Lieberman P, Fecteau S, Théoret H, Garcia RR, Aboitiz F, MacLarnon A, Lieberman P. 2007. The evolution of human speech: its anatomical and neural bases. *Current Anthropology* **48**:39–66. DOI: https://doi.org/10.1086/509092

Lobier M, Peyrin C, Le Bas JF, Valdois S. 2012. Pre-orthographic character string processing and parietal cortex: a role for visual attention in reading? *Neuropsychologia* **50**:2195–2204. DOI: https://doi.org/10.1016/j.neuropsychologia.2012.05.023, PMID: 22659111

Lopopolo A, Frank SL, van den Bosch A, Willems R. 2019. Dependency parsing with your eyes. Dependency Structure Predicts Eye Regressions During Reading. DOI: https://doi.org/10.31234/osf.io/kusxb

Mazoyer B, Zago L, Jobard G, Crivello F, Joliot M, Perchey G, Mellet E, Petit L, Tzourio-Mazoyer N. 2014. Gaussian mixture modeling of hemispheric lateralization for language in a large sample of healthy individuals balanced for handedness. *PLOS ONE* **9**:e101165. DOI: https://doi.org/10.1371/journal.pone.0101165, PMID: 24977417

Mazoyer B, Mellet E, Perchey G, Zago L, Crivello F, Jobard G, Delcroix N, Vigneau M, Leroux G, Petit L, Joliot M, Tzourio-Mazoyer N. 2016. BIL&GIN: a neuroimaging, cognitive, behavioral, and genetic database for the study of human brain lateralization. *NeuroImage* **124**:1225–1231. DOI: https://doi.org/10.1016/j.neuroimage.2015.02.071, PMID: 25840118

McGlone J, Davidson W. 1973. The relation between cerebral speech laterality and spatial ability with special reference to sex and hand preference. *Neuropsychologia* **11**:105–113. DOI: https://doi.org/10.1016/0028-3932(73)90070-5, PMID: 4694772

McMahon E, Wintermark P, Lahav A. 2012. Auditory brain development in premature infants: the importance of early experience. *Annals of the New York Academy of Sciences* **1252**:17–24. DOI: https://doi.org/10.1111/j.1749-6632.2012.06445.x, PMID: 22524335

McNorgan C, Awati N, Desroches AS, Booth JR. 2014. Multimodal lexical processing in auditory cortex is literacy skill dependent. *Cerebral Cortex* **24**:2464–2475. DOI: https://doi.org/10.1093/cercor/bht100, PMID: 23588185

Mellet E, Jobard G, Zago L, Crivello F, Petit L, Joliot M, Mazoyer B, Tzourio-Mazoyer N. 2014a. Relationships between hand laterality and verbal and spatial skills in 436 healthy adults balanced for handedness. *Laterality* **19**:383–404. DOI: https://doi.org/10.1080/1357650X.2013.796965, PMID: 23745714

Mellet E, Zago L, Jobard G, Crivello F, Petit L, Joliot M, Mazoyer B, Tzourio-Mazoyer N. 2014b. Weak language lateralization affects both verbal and spatial skills: an fMRI study in 297 subjects. *Neuropsychologia* **65**:56–62. DOI: https://doi.org/10.1016/j.neuropsychologia.2014.10.010, PMID: 25455569

Mowrer DE. 1980. Phonological development during the first year of life. *Speech and Language* **4**:99–142. DOI: https://doi.org/10.1016/B978-0-12-608604-1.50008-2

Niskanen E, Könönen M, Villberg V, Nissi M, Ranta-Aho P, Säisänen L, Karjalainen P, Aikiä M, Kälviäinen R, Mervaala E, Vanninen R. 2012. The effect of fMRI task combinations on determining the hemispheric dominance of language functions. *Neuroradiology* **54**:393–405. DOI: https://doi.org/10.1007/s00234-011-0959-7, PMID: 21932015

Oldfield RC. 1971. The assessment and analysis of handedness: the edinburgh inventory. *Neuropsychologia* **9**: 97–113. DOI: https://doi.org/10.1016/0028-3932(71)90067-4, PMID: 5146491

Oller DK. 1980. The emergence of the sounds of speech in infancy. *Child Phonology* **5**:93–112. DOI: https://doi.org/10.1016/B978-0-12-770601-6.50011-5

Perani D, Saccuman MC, Scifo P, Anwander A, Awander A, Spada D, Baldoli C, Poloniato A, Lohmann G, Friederici AD. 2011. Neural language networks at birth. *PNAS* **108**:16056–16061. DOI: https://doi.org/10.1073/pnas.1102991108, PMID: 21896765

Petit L, Zago L, Vigneau M, Andersson F, Crivello F, Mazoyer B, Mellet E, Tzourio-Mazoyer N. 2009. Functional asymmetries revealed in visually guided saccades: an FMRI study. *Journal of Neurophysiology* **102**:2994–3003. DOI: https://doi.org/10.1152/jn.00280.2009, PMID: 19710382

Petit L, Zago L, Mellet E, Jobard G, Crivello F, Joliot M, Mazoyer B, Tzourio-Mazoyer N. 2015. Strong rightward lateralization of the dorsal attentional network in left-handers with right sighting-eye: an evolutionary advantage. *Human Brain Mapping* **36**:1151–1164. DOI: https://doi.org/10.1002/hbm.22693, PMID: 25409934

Price CJ. 2010. The anatomy of language: a review of 100 fMRI studies published in 2009. *Annals of the New York Academy of Sciences* **1191**:62–88. DOI: https://doi.org/10.1111/j.1749-6632.2010.05444.x, PMID: 20392276

Price CJ. 2012. A review and synthesis of the first 20 years of PET and fMRI studies of heard speech, spoken language and reading. *NeuroImage* **62**:816–847. DOI: https://doi.org/10.1016/j.neuroimage.2012.04.062, PMID: 22584224

Pujol J, Deus J, Losilla JM, Capdevila A. 1999. Cerebral lateralization of language in normal left-handed people studied by functional MRI. *Neurology* **52**:1038. DOI: https://doi.org/10.1212/WNL.52.5.1038, PMID: 10102425

R Development Core Team. 2013. R: A language and environment for statistical computing. Vienna, Austria: R Foundation for Statistical Computing. http://www.r-project.org

Raemaekers M, Schellekens W, Petridou N, Ramsey NF. 2018. Knowing left from right: asymmetric functional connectivity during resting state. *Brain Structure and Function* **223**:1909–1922. DOI: https://doi.org/10.1007/s00429-017-1604-y, PMID: 29299691

Reynolds JE, Long X, Grohs MN, Dewey D, Lebel C. 2019. Structural and functional asymmetry of the language network emerge in early childhood. *Developmental Cognitive Neuroscience* **39**:100682. DOI: https://doi.org/10.1016/j.dcn.2019.100682, PMID: 31376589

Richards T, Askren K, Mestre Z, Beers S, Abbott R. 2017. Relationships between eye movements during sentence reading comprehension, word spelling and reading, and DTI and fMRI connectivity in students with and without dysgraphia or dyslexia. *Journal of Systems and Integrative Neuroscience* **3**:1000150. DOI: https://doi.org/10.15761/JSIN.1000150

Rodgon MM. 1976. *Single-Word Usage Cognitive Development and the Beginnings of Combinatorial Speech* . Cambridge University Press.

Sneath PHA, Sokal RR. 1973. *Numerical Taxonomy*. W H Freeman and Company.

Somers M, Aukes MF, Ophoff RA, Boks MP, Fleer W, de Visser KC, Kahn RS, Sommer IE. 2015a. On the relationship between degree of hand-preference and degree of language lateralization. *Brain and Language* **144**:10–15. DOI: https://doi.org/10.1016/j.bandl.2015.03.006, PMID: 25880901

Somers M, Shields LS, Boks MP, Kahn RS, Sommer IE. 2015b. Cognitive benefits of right-handedness: a meta-analysis. *Neuroscience & Biobehavioral Reviews* **51**:48–63. DOI: https://doi.org/10.1016/j.neubiorev.2015.01.003, PMID: 25592981

Sommer IE, Aleman A, Bouma A, Kahn RS. 2004. Do women really have more bilateral language representation than men? A meta-analysis of functional imaging studies. *Brain* **127**:1845–1852. DOI: https://doi.org/10.1093/brain/awh207, PMID: 15240433

Szaflarski JP, Binder JR, Possing ET, McKiernan KA, Ward BD, Hammeke TA. 2002. Language lateralization in left-handed and ambidextrous people: fmri data. *Neurology* **59**:238–244. DOI: https://doi.org/10.1212/WNL.59.2.238, PMID: 12136064

Szaflarski JP, Rajagopal A, Altaye M, Byars AW, Jacola L, Schmithorst VJ, Schapiro MB, Plante E, Holland SK. 2012. Left-handedness and language lateralization in children. *Brain Research* **1433**:85–97. DOI: https://doi.org/10.1016/j.brainres.2011.11.026, PMID: 22177775

Tallal P. 1981. Language disabilities in children: perceptual correlates. *International Journal of Pediatric Otorhinolaryngology* **3**:1–13. DOI: https://doi.org/10.1016/0165-5876(81)90014-8, PMID: 7009462

Tallal P, Schwartz J. 1981. Hemispheric specialization for language processes. *Science* **211**:961. DOI: https://doi.org/10.1126/science.211.4485.961, PMID: 17819043

Toga AW, Thompson PM. 2003. Mapping brain asymmetry. *Nature Reviews Neuroscience* **4**:37–48. DOI: https://doi.org/10.1038/nrn1009, PMID: 12511860

Tzourio-Mazoyer N, Josse G, Crivello F, Mazoyer B. 2004. Interindividual variability in the hemispheric organization for speech. *NeuroImage* **21**:422–435. DOI: https://doi.org/10.1016/j.neuroimage.2003.08.032, PMID: 14741679

Tzourio-Mazoyer N, Joliot M, Marie D, Mazoyer B. 2016. Variation in Homotopic Areas' activity and inter-hemispheric intrinsic connectivity with type of language lateralization: an FMRI study of covert sentence generation in 297 healthy volunteers. *Brain Structure and Function* **221**:2735–2753. DOI: https://doi.org/10.1007/s00429-015-1068-x, PMID: 26013303

Tzourio-Mazoyer N, Crivello F, Mazoyer B. 2018. Is the planum temporale surface area a marker of hemispheric or regional language lateralization? *Brain Structure & Function* **223**:1217–1228. DOI: https://doi.org/10.1007/s00429-017-1551-7, PMID: 29101522

Van der Elst W, van Boxtel MP, van Breukelen GJ, Jolles J. 2005. Rey's verbal learning test: normative data for 1855 healthy participants aged 24-81 years and the influence of age, sex, education, and mode of presentation. *Journal of the International Neuropsychological Society* **11**:290–302. DOI: https://doi.org/10.1017/S1355617705050344, PMID: 15892905

Vandenberg SG, Kuse AR. 1978. Mental rotations, a group test of three-dimensional spatial visualization. *Perceptual and Motor Skills* **47**:599–604. DOI: https://doi.org/10.2466/pms.1978.47.2.599, PMID: 724398

Vigneau M, Beaucousin V, Hervé PY, Duffau H, Crivello F, Houdé O, Mazoyer B, Tzourio-Mazoyer N. 2006. Meta-analyzing left hemisphere language Areas: phonology, semantics, and sentence processing. *NeuroImage* **30**:1414–1432. DOI: https://doi.org/10.1016/j.neuroimage.2005.11.002, PMID: 16413796

Vingerhoets G. 2019. Phenotypes in hemispheric functional segregation? perspectives and challenges. *Physics of Life Reviews* **30**:1–18. DOI: https://doi.org/10.1016/j.plrev.2019.06.002, PMID: 31230893

Ward JH. 1963. Hierarchical grouping to optimize an objective function. *Journal of the American Statistical Association* **58**:236–244. DOI: https://doi.org/10.1080/01621459.1963.10500845

Wilke M, Schmithorst VJ. 2006. A combined bootstrap/histogram analysis approach for computing a lateralization index from neuroimaging data. *NeuroImage* **33**:522–530. DOI: https://doi.org/10.1016/j.neuroimage.2006.07.010, PMID: 16938470

Wilson AC, Bishop DVM. 2018. Resounding failure to replicate links between developmental language disorder and cerebral lateralisation. *PeerJ* **6**:e4217. DOI: https://doi.org/10.7717/peerj.4217, PMID: 29333343

Zago L, Hervé PY, Genuer R, Laurent A, Mazoyer B, Tzourio-Mazoyer N, Joliot M. 2017. Predicting hemispheric dominance for language production in healthy individuals using support vector machine. *Human Brain Mapping* **38**:5871–5889. DOI: https://doi.org/10.1002/hbm.23770, PMID: 28868791

Zatorre RJ, Belin P, Penhune VB. 2002. Structure and function of auditory cortex: music and speech. *Trends in Cognitive Sciences* **6**:37–46. DOI: https://doi.org/10.1016/S1364-6613(00)01816-7, PMID: 11849614